JOURNAL OF THE

Electrochemical Society

ol. 105, No. 11 November 1958

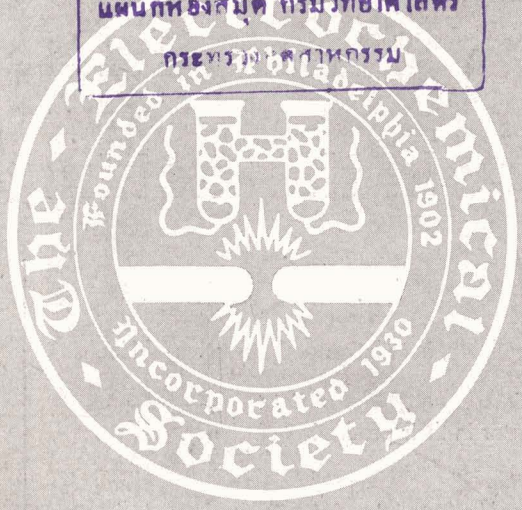

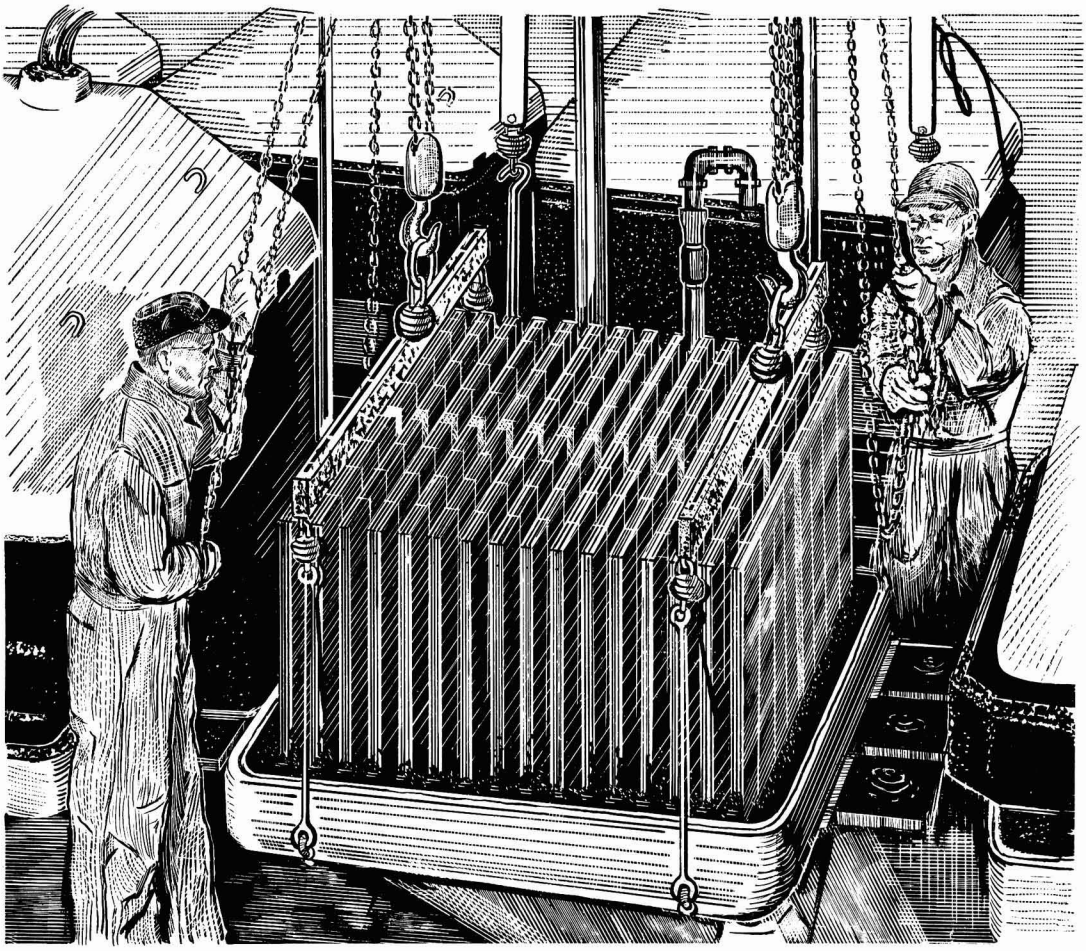

Efficiency in the making

Depth of experience in the building, installation and operation of Hooker cells is a highly important factor in their production efficiency.

High efficiency is also a characteristic of **GLC Anodes,** which are "custom made" to individual cell requirements.

FREE—*This illustration of cell renewal has been handsomely reproduced with no advertising text. We will be pleased to send you one of these reproductions with our compliments. Simply write to Dept. J-11.*

ELECTRODE GLC® DIVISION

GREAT LAKES CARBON CORPORATION

18 EAST 48TH STREET, NEW YORK 17, N.Y. OFFICES IN PRINCIPAL CITIES

Journal of the Electrochemical Society

NOVEMBER 1958 **VOL. 105 • NO. 11**

CONTENTS

Published monthly by The Electrochemical Society, Inc., from Manchester, N. H., **Executive Offices, Editorial Office** and **Circulation Dept.,** and **Advertising Office** at 1860 Broadway, New York 23, N. Y., combining the JOURNAL and TRANSACTIONS OF THE ELECTROCHEMICAL SOCIETY. Statements and opinions given in articles and papers in the JOURNAL OF THE ELECTROCHEMICAL SOCIETY are those of the contributors, and The Electrochemical Society assumes no responsibility for them. Nondeductible subscription to members $5.00; subscription to nonmembers $18.00. Single copies $1.25 to members, $1.75 to nonmembers. Copyright 1958 by The Electrochemical Society, Inc. Entered as second-class matter at the Post Office at Manchester, N. H., under the act of August 24, 1912.

Editorial

Electrochemistry in Japan

ABOUT 100 years ago Japan inaugurated its long march toward modern industrialization, so necessary now to support an ever-increasing population. Students were sent abroad to learn Western science and technology, and great efforts were made to adapt the new ideas and techniques to the development of Japan's resources. The first electric lights were turned on in 1886, and in the course of time a flourishing electrochemical industry became an important factor in the nation's economy. Establishment of the Bunsengesellschaft in 1894 and of The Electrochemical Society in 1902 stimulated interest in research and development at home. After World War I, the demand for electric power grew rapidly, and numerous hydroelectric plants were built.

Japan's electrochemical industry developed in a style peculiar to the country. A series of mountain ranges runs throughout the middle of the long and narrow Japanese archipelago. Many rather short rivers run down the mountains to the Pacific Ocean and the Sea of Japan, providing many sites for hydroelectric stations. However, the water flow is highly seasonal, and power plants which supply continuous users the year round have great surplus capacity in spring and summer. Electrochemical manufacture has been organized in such a way as to take advantage of this surplus power in making intermediates, which are stored and worked-up later. Naturally, the trend today is to build larger reservoirs so that power output can be spread over the year, and to supplement hydro with thermal power.

The Electrochemical Society of Japan was established in 1933, so is celebrating its 25th birthday. It is now more than two-thirds as large as our own Society, with some 2000 individual members and an additional 150 electrochemical manufacturing companies as supporting members. Its journal is published in Japanese and consequently it is not widely read abroad; the society has some 60 overseas members and the journal has 160 foreign subscribers. From its start in 1933 the journal printed a brief abstract of each article in English, and in 1956 this was increased to a full-page English abstract.

This year the society has started to publish an English-language edition of the journal, which is to appear quarterly and contain full translations of part of the articles from the preceding three-month period (see the announcement in *This Journal,* p. 194C, Sept. 1958). Overseas membership in the society remains at $5.00 per year, which will now include the new journal in English instead of the Japanese edition with English abstracts as formerly. A free sample copy will be sent on request to the Electrochemical Society of Japan at 3,1-chome, Yuraku-cho, Chiyoda-ku Tokyo. The society hopes that the new English edition will attract more foreign members and result in wider interest and knowledge of electrochemical research and advances in Japan.

—CVK

ANODE UNIFORMITY

...that really pays-off!

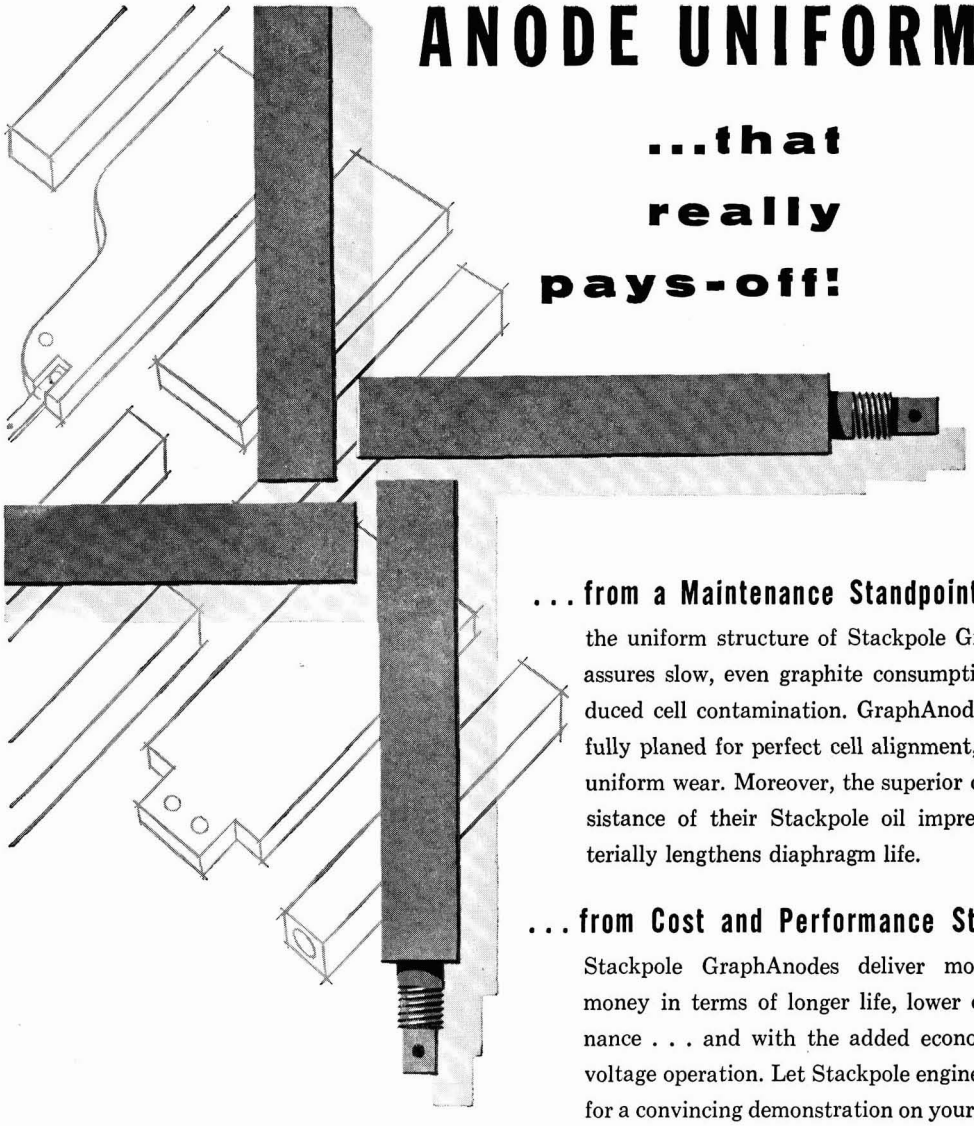

. . . from a Maintenance Standpoint

the uniform structure of Stackpole GraphAnodes assures slow, even graphite consumption with reduced cell contamination. GraphAnodes are carefully planed for perfect cell alignment, longer life, uniform wear. Moreover, the superior chemical resistance of their Stackpole oil impregnants materially lengthens diaphragm life.

. . . from Cost and Performance Standpoints

Stackpole GraphAnodes deliver more for the money in terms of longer life, lower cell maintenance . . . and with the added economy of low-voltage operation. Let Stackpole engineers arrange for a convincing demonstration on your equipment.
Stackpole Carbon Company, St. Marys, Penna.

STACKPOLE

GRAPHANODES

graphite anodes in grades, sizes and shapes for all electrolytic cells

TUBE ANODES • CATHODIC PROTECTION ANODES • FLUXING & DE-GASSING TUBES • BRUSHES for all rotating electrical equipment • ELECTRICAL CONTACTS • VOLTAGE REGULATOR DISCS • "CERAMAGNET"® CERAMIC MAGNETS • ROCKET NOZZLES • BEARINGS • SALT BATH RECTIFICATION RODS • SEAL RINGS • FRICTION RINGS • ELECTRODES & HEATING ELEMENTS • MOLDS & DIES • WELDING CARBONS • POROUS CARBON • and many other carbon, graphite, and electronic components.

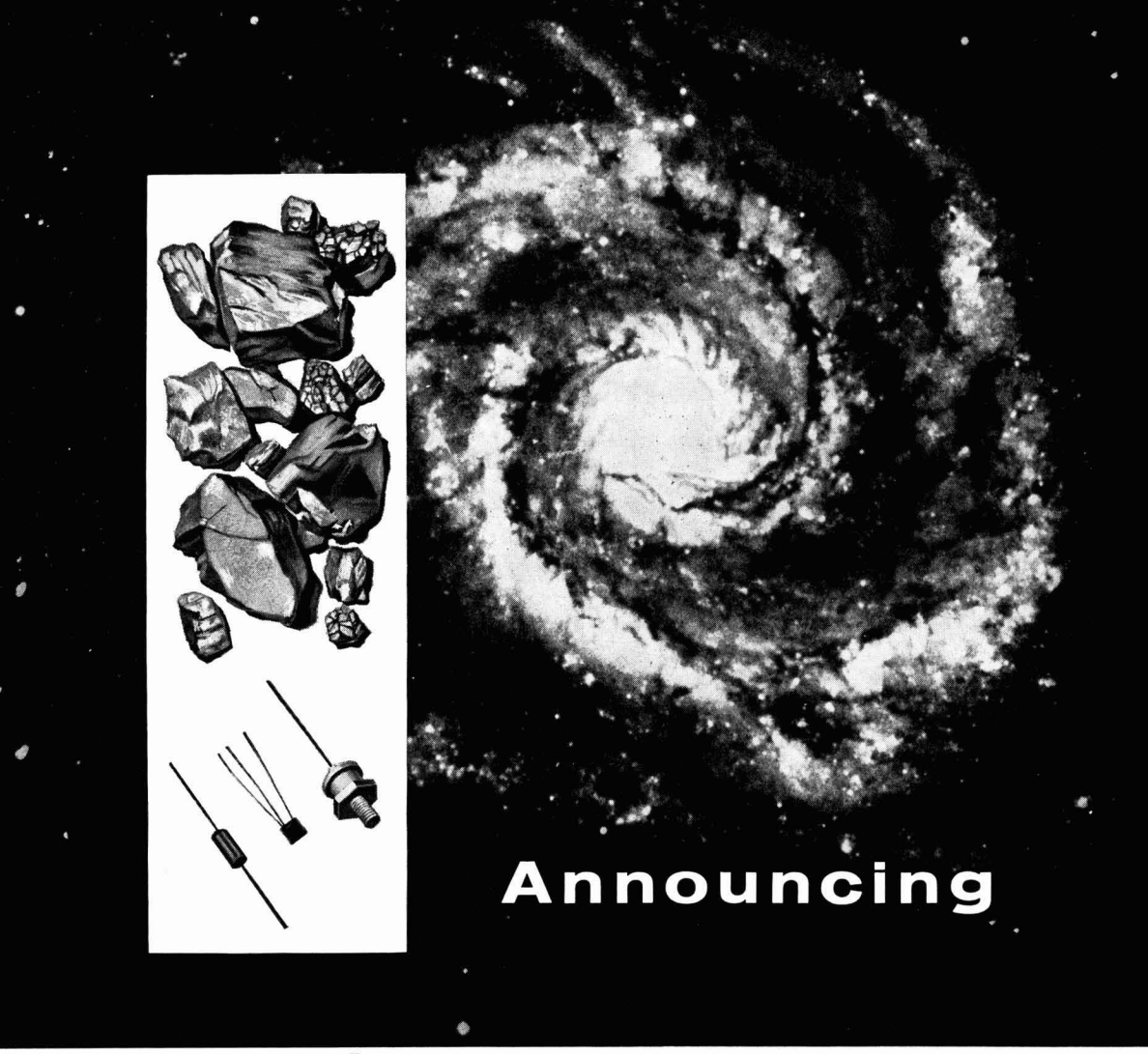

GRACE SILICON

(ultra-high purity)

Whether you make or use silicon devices, a new standard of quality is now available to you through Grace — leader in chemical research and development.

Grace Silicon, manufactured by the Pechiney process, has an extremely low boron content as well as over-all ultra-high purity. Other characteristics of Grace Silicon include uniform quality as verified by some of the nation's leading electronic manufacturers.

Wherever a semi-conductor of top quality is desired for rectifiers, transistors, diodes — get in touch with GRACE ELECTRONIC CHEMICALS, INC., at PLaza 2-7699 in Baltimore.

GRACE ELECTRONIC CHEMICALS, INC.

101 N. Charles St., Baltimore, Maryland

Subsidiary of W. R. GRACE & CO.

Investigation of Electrochemical Characteristics of Organic Compounds

II. Aromatic Nitroso Compounds

R. Glicksman and C. K. Morehouse

RCA Laboratories, Radio Corporation of America, Princeton, New Jersey

ABSTRACT

Aromatic C-nitroso compounds operate at higher potentials than the corresponding nitro compounds, as well as the various oximes, N-nitroso, and N-oxide organic compounds tested. In addition, the electrode potential during current flow is pH dependent and is affected by the type and position of the substituted group on the aromatic ring. Coulometric reduction studies of various p-nitrosophenol and p-nitrosodialkylamino compounds indicate reduction of these compounds takes place to the amino stage with a resultant 4-electron change per —NO group. The high theoretical ampere-minute capacity of the aromatic C-nitroso compounds, along with their high flat operating potentials, show these materials to have considerable promise for use as cathode materials in primary cells, when coupled with a magnesium anode.

Although the majority of oxidation-reduction processes involving organic compounds are not reversible from the thermodynamic standpoint, there are some notable exceptions. Conant and Lutz (1) examined nitrosobenzene and found it to be a reversible electrode, having an electrode potential of +0.605 v in a 0.2*N* HCl-acetone solution at 25°C, while Lutz and Lytton (2) determined the potentials of a series of substituted nitrosobenzene-phenylhydroxylamine systems and found them to be generally reversible.

The favorable potential of this reversible system, along with the high theoretical ampere-minute per gram capacities of nitroso compounds, suggests the use of these materials as cathodes in primary batteries. Previous studies of the electrochemical characteristics of aromatic nitro compounds (3) and their use as cathodes in primary cells (4) have demonstrated the practicability of organic materials as electrodes in galvanic cells.

In this paper the electrochemical properties of various nitroso compounds are presented, while a subsequent paper will deal with the use of the nitroso compounds as cathodes in actual primary cells.

Experimental

Because of the irreversible nature of the electrode reaction and polarization effects encountered during current flow, the electrochemical characteristics of many inorganic and organic compounds often cannot be predicted by thermodynamic calculations and a knowledge of their physical and chemical properties. A technique previously described by the authors (5) has been used to measure the operating potential during current flow and the coulombic capacity of various aromatic nitroso compounds. This technique consists in discharging at a constant current in a large volume of electrolyte a 0.5-g sample of the aromatic nitroso cathode material mixed with 10% Shawinigan acetylene black. The change in cathode potential with time was measured with a L&N Type K potentiometer using a saturated calomel reference electrode. The measured potentials were corrected for the *IR* drop associated with the apparatus and electrolyte by means of an oscillographic technique (6).

All half-cell potential data reported in this paper are referred to the normal hydrogen scale and include a liquid junction potential, which in most cases is small and can be neglected.

For most of the measurements an aqueous magnesium bromide electrolyte and a magnesium anode were used, while in studying the effect of *p*H on potential a zinc anode was employed with the acidic NH_4Cl-$ZnCl_2$-H_2O and basic NaOH-H_2O electrolytes.

General Cathode Half-Cell Potential Relationships of Nitroso and Related Organic Compounds

C-nitroso and nitrosamine compounds.—Nitroso compounds contain the nitroso group —N = O attached to a carbon atom, and have two properties which distinguish them from the nitrosamines, compounds in which the nitroso group is attached to a nitrogen atom. These are, first, the blue or green color of the true monomolecular nitroso compounds in all states of aggregation and, second, the tendency of the compounds to associate to colorless bimolecular complexes according to the nature of the other groups in the molecule.

Both the N-nitroso (nitrosamines) and C-nitroso compounds can be reduced electrolytically and by chemical means using Zn or Sn in dilute acetic acid solution to the substituted hydrazine and amine respectively (7, 8).

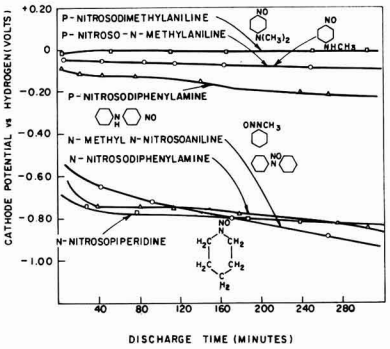

Fig. 1. Cathode half-cell potential of various C- and N-nitroso compounds discharged in 250 g/l $MgBr_2 \cdot 6H_2O$ electrolyte at a rate of 0.030 amp/g.

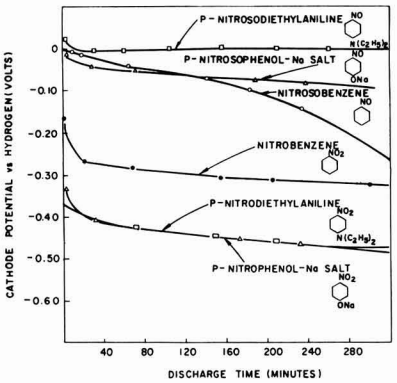

Fig. 2. Cathode half-cell potential of various C-nitroso compounds and their corresponding nitro compounds discharged in 250 g/l $MgBr_2 \cdot 6H_2O$ electrolyte at a rate of 0.030 amp/g.

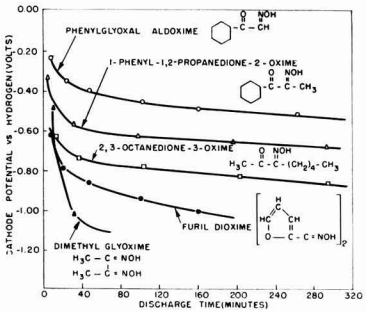

Fig. 3. Cathode half-cell potential of various oxime compounds discharged in 250 g/l $MgBr_2 \cdot 6H_2O$ electrolyte at a rate of 0.030 amp/g.

Presented in Fig. 1 are discharge data showing the change in half-cell potential with time as N-nitroso and C-nitroso compounds are discharged at a rate of 0.030 amp/g of material in an aqueous solution of 250 g/l of $MgBr_2 \cdot 6H_2O$. The N-nitroso compounds under these conditions of discharge operate at voltages of 0.6-0.7 v lower than their corresponding C-nitroso compounds. This relationship between the two types of nitroso compounds has been found to hold for all compounds tested.

Aromatic nitro and C-nitroso compounds.—Haber and Schmidt (9) showed that in the electrolytic reduction of nitrobenzene the basic steps of reduction are as follows:

$$C_6H_5NO_2 \rightarrow C_6H_5NO \rightarrow C_6H_5NHOH \rightarrow C_6H_5NH_2$$

The fact that nitrosobenzene was reduced to phenylhydroxylamine too readily to be capable of isolation as such indicated that nitrosobenzene was a stronger oxidizing agent than nitrobenzene.

Other evidence of the stronger oxidizing power of nitroso compounds has been reported by Glasstone and Hickling (10) who give depolarization potentials[1] of various organic compounds, which show that, as a class, nitroso compounds have potentials 0.2-0.3 v higher than nitro compounds. In addition, from polarographic studies of p-nitrosophenol and p-nitrophenol, Astle and McConnell (11) found that at a pH of 4 the half-wave potential of p-nitrosophenol is 0.48 v higher than that of the p-nitrophenol.

Presented in Fig. 2 are discharge data for various C-nitroso compounds and their corresponding nitro compounds. The C-nitroso compounds under these conditions of discharge operate at voltages of 0.2-0.4 v higher than the corresponding nitro compounds. These data show that C-nitroso compounds are stronger oxidizing agents than the corresponding nitro compounds and as cathode materials for primary batteries should operate at higher potentials during discharge.

Oximes and N-oxide compounds.—Aliphatic nitroso compounds RNO are known only when R is a tertiary radical;[2] consequently, reactions which would be expected to give primary or secondary nitroso compounds give oximes instead. Hence, these are sometimes called isonitroso compounds. The grouping $=CHNO$ becomes $-\overset{|}{C}=NOH$, a complete enolization.

Discharge data obtained on various oxime compounds are presented in Fig. 3. While a direct comparison cannot be made between nitroso and oxime type compounds, it is seen that the oximes operate at lower discharge potentials than the C-nitroso compounds tested under comparable conditions. It is significant that those compounds having a carbonyl group adjacent to the $-\overset{|}{C}=NOH$ group operate at higher cathode potentials than the other oximes tested. This is in agreement with the "electronegativity rule of reduction potentials" (12) which states that the organic compounds are more easily reduced as more electronegative groups are substituted in the same compound.

The amine oxides may be regarded as derivatives of the tautomeric form of hydroxylamine $H_3N \rightarrow O$. They are closely related to the tertiary amines from which they can be obtained by oxidation. Amine

[1] In the determination of "depolarization values," a definite quantity of the reducible substance is added to a given electrolyte containing a reversible hydrogen electrode, and the fall of potential of the latter is determined. The depolarization value so obtained gives an indication of the oxidizing power of the substance (10).

[2] An exception to this generalization is the compound 1-chloro-1-nitrosoethane, which exists as a colorless dimer.

Table I. Capacity data for various aromatic C-nitroso compounds

Cathode material	Ampere-minute per gram capacity: Theoretical	Ampere-minute per gram capacity: Obtained*	Efficiency (%)
Conventional inorganic cathodes			
Manganese dioxide	18.5	10.3	65.6†
Mercuric oxide	14.9	10.4	69.8
p-Nitrosophenol cathodes			
4-nitrosophenol	52.2	48.2	92.3
4-nitroso-3-methyphenol	46.9	40.0	85.3
5-nitroso-8-hydroxyquinoline	36.7	31.5	85.8
p-nitrosophenol-Na salt	44.3	23.8	53.7
p-Nitrosodialkylamino cathodes			
p-Nitrosodimethylaniline	42.9	37.4	87.2
4-nitroso-3-methyldimethylaniline	39.2	36.5	93.1
4-nitroso-3-hydroxyacetanilide	35.7	22.5	63.0
4-nitroso-3-hydroxydimethylaniline	38.7	30.8	79.6
Nitrosonaphthol cathodes			
4-nitroso-1-naphthol	37.1	18.4	49.6
2-nitroso-1-naphthol	37.1	9.8	26.4
1-nitroso-2-naphthol	37.1	9.6	25.9
1-nitroso-2-naphthol-3,6-disulfonic acid—disodium salt	17.1	11.8	69.0
Mononitroso cathodes			
nitrosobenzene	60.0	37.5	62.5
o-nitrosotoluene	53.1	24.2	45.6
4-nitrosoresorcinol	46.2	2.0	4.3
Dinitroso cathodes			
p-dinitrosobenzene	94.6	26.4	27.9
2,4-dinitrosoresorcinol	69.0	24.1	34.9
Nitronitroso cathodes			
m-nitronitrosobenzene	105.8	96.8	91.5
3-nitro-4-nitrosotoluene	96.9	77.1	79.6
Nitrosopyrimidine cathodes			
2,4,6-triamino-5-nitrosopyrimidine	41.8	28.8	68.9

* Computed from half-cell potential data in Fig. 5-11, using −0.40 v as cut off potential.
† Efficiency calculation based on 85% MnO_2 content.

oxides can be reduced to tertiary amines by reagents such as Sn and HCl. Ochiai (13) has shown that a number of pyridine-N-oxides and quinoline-N-oxides can be reduced polarographically with difficulty. Compounds of this type, such as pyridine-N-oxide and 2-piccoline-N-oxide, were found to be poor oxidizing agents and to operate at potentials too low to be measured by this experimental technique.

Effect of electrolyte composition on the cathode half-cell potential of C-nitroso compounds.—According to Latimer (14) the reaction involving the reduction of nitrosobenzene to phenylhydroxylamine can attain a reversible equilibrium, and the potential of the couple is as follows:

$$C_6H_5NO + 3H^+ + 2e^- = C_6H_5NH_2OH^+ \quad E^\circ = 0.60 \text{ v}$$

Phenylhydroxylamine, once formed, can react with the unreduced nitrosobenzene forming side products, or it can be reduced directly to aniline, in accordance with Haber and Schmidt's scheme.

$$C_6H_5NH_2OH^+ + 2H^+ + 2e^- = C_6H_5NH_3^+ + H_2O \quad E^\circ = 1.20 \text{ v}$$

It is seen from the above two reactions, that the electrode potential is influenced by the H^+ ion concentration.

Discharge data obtained on 2,4-dinitrosoresorcinol and p-nitrosodiethylaniline in three electrolytes of different *p*H are shown in Fig. 4. As expected, the discharge potentials of the nitroso compounds increase as the *p*H of the electrolyte is decreased. This behavior is typical of the aromatic C-nitroso compounds and the other N-nitroso and oxime compounds tested.

Half-Cell Potential Studies of Various C-Nitroso Compounds

Half-cell discharge data obtained on various aromatic C-nitroso compounds discharged continuously at a 0.005 amp/g rate in a $MgBr_2 \cdot 6H_2O$ (250 g/l) electrolyte are shown in Fig. 5-11 inclusive.

The capacities obtained to an arbitrary potential of −0.40 v (vs. S.H.E.) along with their electrode efficiencies are presented in Table I together with

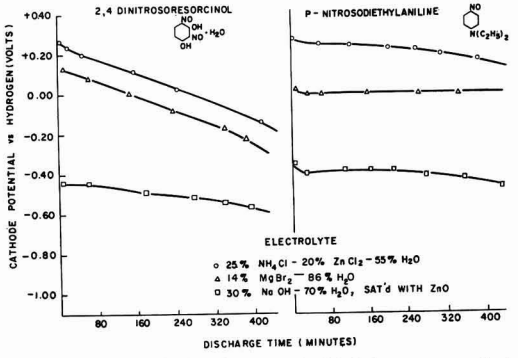

Fig. 4. Cathode half-cell potential of 2,4-dinitrosoresorcinol and p-nitrosodiethylaniline discharged in various electrolytes at a rate of 0.030 amp/g.

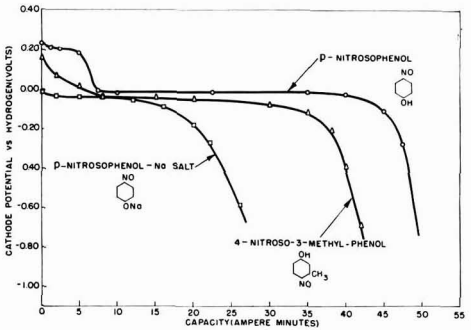

Fig. 5. Half-cell potential studies of various p-nitrosophenol derivatives discharged in 250 g/l $MgBr_2 \cdot 6H_2O$ electrolyte at a rate of 0.005 amp/g.

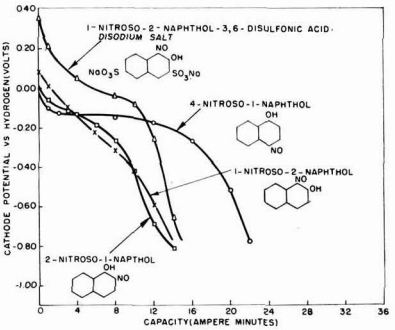

Fig. 6. Half-cell potential studies of various nitrosonaphthol derivatives discharged in 250 g/l $MgBr_2 \cdot 6H_2O$ electrolyte at a rate of 0.005 amp/g.

the theoretical capacities of these materials expressed in ampere-minutes per gram.

Nitrosophenols and related compounds.—Presented in Fig. 5 are half-cell discharge curves of various p-nitrosophenol derivatives. It is seen that, with the exception of the first 5-10 amp-min of discharge, these compounds have a flat operating potential throughout the course of their discharge. The high initial potential, which persists for a short time, appears to be characteristic of the hydroxyl group, as evidenced by the fact that other types of C-nitroso compounds, as well as p-nitrosophenol-Na salt, show no such behavior.

A possible explanation for this is that p-nitrosophenol is a tautomer of quinone monoxime

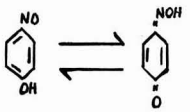

and in the free state the substance is actually present as the quinone monoxime while in the salts as derivatives of nitrosophenol, the phenolic H being more acidic than the oximic H atom. This being the case the initial potential would be due to the quinone monoxime; however, during the course of the discharge, hydroxide ion is formed and the solution becomes weakly basic, and at this stage the cathode potential would be that of the nitrosophenol salt.

The effect of adding a $—CH_3$ group to the 3 position of 4-nitrosophenol is to lower the operating potential of the parent compound by approximately 0.03 v. This type of behavior is consistent with that found for the aromatic nitro compounds (3), where the addition of an electron-repelling group to the benzene ring results in a compound having a lower discharge potential than its parent compound.

The effect of electron-attracting groups on the cathode potential is shown for the nitrosonaphthol compounds in Fig. 6. The addition of two $—SO_3Na$ groups to the naphthalene ring to form 1-nitroso-2-naphthol-3,6,-disulfonic acid disodium salt results in a compound having a discharge potential 0.2 v higher than the unsubstituted 1-nitroso-2-naphthol.

Presented in Fig. 7 are discharge curves for three types of aromatic hydroxy-nitroso compounds. It is seen that the greater the aromaticity of the ring

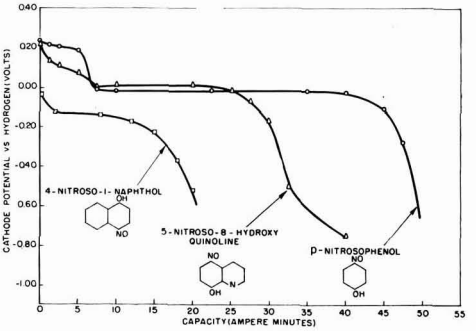

Fig. 7. Half-cell potential studies of various aromatic hydroxy-nitroso derivatives discharged in 250 g/l $MgBr_2 \cdot 6H_2O$ electrolyte at a rate of 0.005 amp/g.

structure, the higher is the cathode potential of the corresponding C-nitroso compound. This can be explained on the basis of a decreased electron density in the vicinity of the nitroso group as one goes to more aromatic ring structures. This decreased electron density results in a compound with an increased electron affinity and a higher discharge potential.

p-Nitrosodialkylamino compounds.—In Fig. 8, the half-cell discharge curves of various p-nitrosodialkylamino derivatives show both p-nitrosodimethylaniline and 4-nitroso-3-methyldimethylaniline to

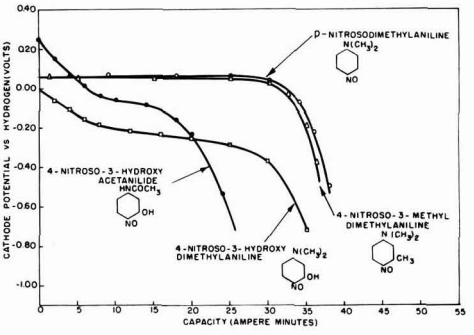

Fig. 8. Half-cell potential studies of various p-nitrosodialkylamino derivatives discharged in 250 g/l $MgBr_2 \cdot 6H_2O$ electrolyte at a rate of 0.005 amp/g.

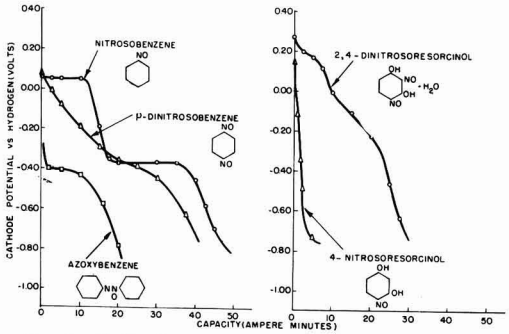

Fig. 9. Half-cell potential studies of various mono- and di-nitroso derivatives of benzene and resorcinol discharged in 250 g/l $MgBr_2 \cdot 6H_2O$ electrolyte at a rate of 0.005 amp/g.

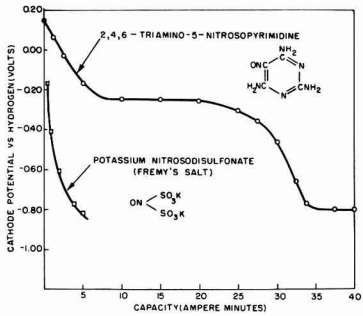

Fig. 10. Half-cell potential studies of various nitroso derivatives discharged in 250 g/l $MgBr_2 \cdot 6H_2O$ electrolyte at a rate of 0.005 amp/g.

have high, flat operating potentials throughout the course of their discharge. As with nitrosophenols, a $-CH_3$ group, ortho to the nitroso group, lowers the potential of the parent compound a very small amount. The effect of the more strongly electron-repelling —OH group in the 3 position is much more marked, resulting in a compound, 4-nitroso-3-hydroxydimethylaniline, which operates at a potential 0.3 v lower than p-nitrosodimethylaniline.

The high initial operating potential of the hydroxy compounds for the first 5-10 amp-min of discharge is again illustrated by the curves for 4-nitroso-3-hydroxyacetanilide and 4-nitroso-3-hydroxydimethylaniline. These o-nitrosophenol compounds exhibit the same type of discharge curve as the p-nitrosophenol compounds previously presented although they operate at considerably lower potentials.

Mono- and di-nitroso compounds.—In Fig. 9 are half-cell discharge curves of the mono and dinitroso derivatives of benzene and resorcinol. The reduction of nitrosobenzene is seen to take place stepwise, the first step occurring at a potential of +0.05 v, a value close to that of other p-hydroxy and p-dialkylamino nitroso compounds. The two step discharge may be explained by a 2 electron reduction to phenylhydroxylamine with subsequent reduction to aniline, or it can be attributed to the reduction of side products such as azoxybenzene, formed by the condensation of nitrosobenzene with phenylhydroxylamine. The discharge potential of azoxybenzene, shown in Fig. 9, is close to that of the second discharge step of nitrosobenzene, indicating the latter explanation is a distinct possibility. Additional half-cell discharge studies of azobenzene, another possible side product formed by the condensation of nitrosobenzene with aniline, indicate that this compound cannot be reduced under the experimental conditions, and it was therefore not considered further.

It was expected that the addition of another strongly electron attracting —NO group to nitrosobenzene would result in a dinitroso compound having a much higher operating potential than nitrosobenzene, similar to what one finds with the nitro and dinitrobenzene compounds (3). Actually, the potential of p-dinitrosobenzene is less than that of nitrosobenzene. For 4-nitrosoresorcinol, however, the addition of a —NO group to form 2,4-dinitrosoresorcinol results in a compound with a higher operating potential, a result in agreement with the behavior found in aromatic nitro compounds.

The apparent anomolous behavior of p-dinitrosobenzene could be due to the fact that this compound does not exhibit properties characteristic of a true nitroso compound[3] and the structure of the —NO group cannot be written as for a true nitroso compound (15).

Nitronitroso and other nitroso compounds.—Presented in Fig. 10 are discharge curves for potassium nitrosodisulfonate, an inorganic nitroso compound commonly known as Fremy's salt, and 2,4,6-triamino-5-nitrosopyrimidine, an example of a heterocyclic nitroso compound. Except for its high initial operating potential, the latter compound displays a flat voltage curve throughout the course of its discharge. The potassium nitrosodisulfonate gives little or no capacity under similar conditions of discharge. This is believed to be due to the instability of this compound which decomposes readily to ammonium sulfate, sulfur dioxide, and nitrous oxide (16).

Figure 11 shows discharge curves for m-nitronitrosobenzene and 3-nitro-4-nitrosotoluene. It is seen that these compounds operate at lower potentials than their corresponding mono nitroso compounds, again giving results in variance with what one would expect from the theory developed to ex-

[3] Of the three dinitrosobenzene compounds only the meta isomer has properties of a normal nitroso compound (15).

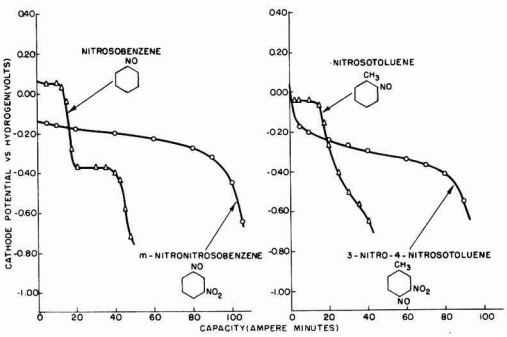

Fig. 11. Half-cell potential studies of various nitronitroso derivatives discharged in 250 g/l $MgBr_2 \cdot 6H_2O$ electrolyte at a rate of 0.005 amp/g.

plain the effect of group substitution on the operating potential of aromatic nitro compounds.

It is apparent that the type and position of the substituted group has an effect on the electrode potential of aromatic nitroso compounds. However from the data available, no definite correlations can be made, as in the case of the aromatic nitro compounds (3). The discharge data in Fig. 5-8 for various p-hydroxy and p-dialkylamino nitroso derivatives support the application of the above theory to aromatic C-nitroso compounds. However, data presented in Fig. 9 and 11 for nitrosobenzene, p-dinitrosobenzene, and m-nitronitrosobenzene cannot be explained by these theories.

The literature on the effect of group substitution on the potential of nitrosobenzene revealed some disagreement. Lutz and Lytton (2), studying the effect of added groups on the electrode potential of nitrosobenzene, contend that both electron-attracting and electron-repelling groups located ortho to the nitroso group raise the potential. In the para position, electron-repelling groups lower and electron-attracting groups raise the potential, while meta substituted groups have little or no effect on the potential regardless of the nature of the groups. The results presented in the present paper are in disagreement with those of Lutz and Lytton, whose results are difficult to understand in the light of the current theories dealing with the electron distribution in a molecule and its effect in determining the mechanism of organic reactions.

Hertel and Lebok (17) studied the electrolytic reduction of nitroso compounds and found that substitution on the ring normally increases the reactivity of the nitroso group in the order $—NO_2$, —Cl, —H, and $—N(CH_3)_2$. This is in agreement with what one finds for substituted nitrobenzene derivatives.

One of the difficulties associated with determining the effect of group substitution on the electrode potential of nitroso compounds is the tendency of these compounds to associate according to the nature of the other groups in the molecule to give bimolecular complexes. Solution favors depolymerization of these complexes, although it does not necessarily effect complete conversion to the monomeric form. As a result of this, complications may arise as with nitrosobenzene, in which the binitroso dimer is o-, p-directing, while in the monomeric form the nitroso group seems to be meta directing, as evidenced by the fact that o- and p-nitrosohalobenzenes undergo ready hydrolysis whereas the corresponding m-compounds are stable (18).

Another difficulty is the uncertainty about the exact structure of nitroso compounds, which information is necessary to develop a theory to explain the effect of structure on electrode potential during current flow.

Coulombic Capacity Studies of Aromatic C-Nitroso Compounds

Table I gives theoretical capacity data for the aromatic C-nitroso compounds presented in Fig. 5-11 compared with two of the cathode materials now used in commercial dry cells. The theoretical

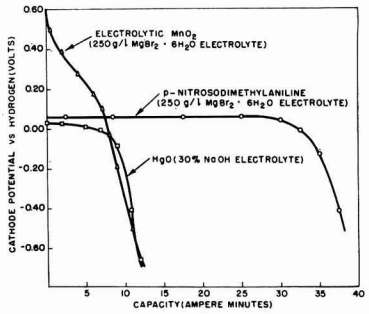

Fig. 12. Half-cell potential studies of various cathode materials discharged in compatible electrolytes at a rate of 0.005 amp/g.

capacities of the nitroso compounds were computed by means of Faraday's law, with the assumption that each nitroso group is reduced to the amino stage with a corresponding four electron change.

It is seen that most of the nitroso compounds listed have from 2 to 3 times greater theoretical ampere-minute capacity per unit of weight than manganese dioxide and mercuric oxide. However, because of the low density of the mononitroso compounds, the theoretical capacity in ampere-minutes per unit of volume is greater for the inorganic compounds.

Figure 12 shows discharge curves for p-nitrosodimethylaniline, one of the more attractive C-nitroso compounds, electrolytic manganese dioxide (85% MnO_2), and mercuric oxide. The p-nitrosodimethylaniline and electrolytic manganese dioxide were discharged at a rate of 0.005 amp/g in an aqueous solution of $MgBr \cdot 6H_2O$ (250 g/l), while the mercuric oxide was discharged at the same rate in a 30% solution of sodium hydroxide, saturated with zinc oxide.

On this test, to a half-cell potential of —0.4 v the manganese dioxide and mercuric oxide cathodes give capacities of 10.3 and 10.4 amp-min/g, corresponding to efficiencies of 65.6%[4] and 69.8%, respectively. At comparable conditions of discharge, p-nitrosodimethylaniline gives a capacity of 37.4 amp-min/g, corresponding to an efficiency of 87.2%. On this test, p-nitrosodimethylaniline gives more than three times the ampere-minute per gram capacity of electrolytic manganese dioxide and mercuric oxide, this capacity being greater than twice the theoretical limit of these inorganic cathode materials.

The high electrode efficiency of p-nitrosodimethylaniline is typical of that found for the p-nitrosodialkylamino and p-nitrosophenol compounds. However, poor efficiencies are also encountered among the aromatic nitroso compounds, as evidenced by the poor electrode efficiencies of the nitrosonaphthol compounds as well as of the two dinitroso compounds tested.

If the p-nitrosodimethylaniline cathode is coupled with a magnesium anode and a magnesium bromide electrolyte, it should result in a primary cell which would operate during current flow at constant volt-

[4] Efficiency calculation is 65.6% of 85% MnO_2 content.

age levels of 1.30-1.40 v. It is thus apparent that the aromatic C-nitroso compounds show considerable promise for use as cathode materials in primary cells, the most outstanding features of these compounds being their high constant operating potential, and their high theoretical capacity in ampere-minutes per gram.

Acknowledgment

The authors wish to express their appreciation to Mr. W. B. Hardy of American Cyanamid Co. for supplying some of the nitroso compounds.

Manuscript received March 24, 1958. This paper was prepared for delivery before the Buffalo Meeting, Oct. 6-10, 1957.

Any discussion of this paper will appear in a Discussion Section to be published in the June 1959 JOURNAL.

REFERENCES

1. J. B. Conant and R. E. Lutz, *J. Am. Chem. Soc.*, **45**, 1047 (1923).
2. R. E. Lutz and M. R. Lytton, *J. Org. Chem.*, **2**, 68 (1937).
3. R. Glicksman and C. K. Morehouse, *This Journal*, **105**, 299 (1958).
4. C. K. Morehouse and R. Glicksman, *ibid.*, **105**, 306 (1958).
5. C. K. Morehouse and R. Glicksman, *ibid.*, **103**, 94 (1956).
6. R. Glicksman and C. K. Morehouse, *ibid.*, **102**, 273 (1955).
7. S. Swann Jr., *Trans. Electrochem. Soc.*, **66**, 287 (1936).
8. S. Glasstone and A. Hickling, "Electrolytic Oxidation and Reduction," p. 164, D. Van Nostrand Co., Inc., New York (1936).
9. F. Haber and C. Schmidt, *Z. Physik. Chem.*, **32**, 271 (1900).
10. Ref. 8, pp. 32-33.
11. M. J. Astle and W. V. McConnell, *J. Am. Chem. Soc.*, **65**, 35 (1943).
12. M. Shikata and I. Tachi, *J. Chem. Soc. Japan*, **53**, 834 (1932); *Collection Czechoslov. Chem. Comm.*, **10**, 834 (1938).
13. E. Ochiai, *J. Pharm. Soc. Japan*, **69**, 1 (1949).
14. W. M. Latimer, "Oxidation Potentials," p. 136, Prentice Hall Inc., New York (1952).
15. G. A. Stoner, Ph.D. Thesis, Tulane University (1955).
16. Therald Moeller, "Inorganic Chemistry," p. 555, John Wiley & Sons, Inc., New York (1952).
17. E. Hertel and F. Lebok, *Z. Physik. Chem.*, (**B**)**47**, 315 (1940).
18. E. F. Degering, "Organic Nitrogen Compounds," p. 152, University Lithoprinters (1945).

Dry Cells Containing Various Aromatic C-Nitroso Compounds as Cathode Materials

C. K. Morehouse and R. Glicksman

RCA Laboratories, Radio Corporation of America, Princeton, New Jersey

ABSTRACT

Many aromatic C-nitroso compounds when coupled with a magnesium anode and a magnesium bromide electrolyte result in dry cells with practical features. The discharge characteristics of these cells are dependent on the particular aromatic C-nitroso compound used as a cathode. Magnesium-p-nitrosodimethylaniline dry cells operate at a flat voltage level between 1.3 and 1.4 v and give greater watt-minute capacities per unit of weight and volume than general purpose commercial Leclanché dry cells containing African manganese dioxide on a number of tests.

Previous work by the authors (1) showed that dry cells containing aromatic nitro compounds as cathodes coupled with a magnesium anode had many favorable performance characteristics. In addition, a study (2, 3) of the electrochemical properties of the reduction products of aromatic nitro and nitroso compounds indicated that the class of aromatic C-nitroso compounds also has many of the desirable properties of a cathode material for use in primary cells. For example, several of these compounds have high theoretical ampere-minute per gram capacities and flat potential-time discharge curves. These cathodes operate at high electrode efficiencies at potentials 0.2-0.4 v higher than their corresponding aromatic nitro cathode.

Arsem (4), the only reference found which refers to the use of nitroso compounds in primary cells, suggested coupling a zinc anode with an organic oxidizing agent such as p-nitrosodimethylaniline as the cathode. However, such a cell has an operating voltage of approximately 1.00 v and thus has practical limitations.

In this paper, the performance characteristics of dry cells containing a magnesium anode coupled with aromatic C-nitroso compounds as cathodes are presented.

Experimental

Dry cells containing various aromatic C-nitroso cathodes were assembled using an impact extruded AZ10A magnesium alloy can. The magnesium cans were lined with a piece of Nibroc salt-free paper, after which an extruded slug of cathode mix was inserted and consolidated in the lined can. A carbon rod with a brass cap fitted on one end was then inserted in the center of the cathode mix and the cells sealed in the conventional manner with a rosin base wax seal. The composition of a typical cathode mix used in this study is as follows:

p-Nitrosodimethylaniline	23.3% by weight
Shawinigan acetylene black	11.6% by weight
Barium chromate	1.1% by weight
Electrolyte (aqueous solution of 500 g/l $MgBr_2 : 6H_2O$ and 1.0 g/l $Li_2CrO_4 : 2H_2O$)	64.0% by weight

The AA-size cells contained approximately 5 g of this mix, the C-size 15-17 g, and the D-size cells 35-40 g.

Discharge characteristics and capacity data presented in the following sections were obtained by discharging the cells through fixed resistances and measuring the closed circuit voltage after various time intervals of discharge. All capacity data were gathered at 21.1° ± 1.1°C (70° ± 2°F) and 50 ± 5% R.H.

Voltage-Discharge Characteristics of Dry Cells Containing Various Aromatic C-Nitroso Compounds as Cathodes

Half-cell studies on various aromatic C-nitroso compounds showed that the type and position of the substituted group have an effect on their discharge potential. However, no definite correlations can be made, as in the case of the aromatic nitro compounds (2). Presented in Fig. 1-4 are discharge data obtained from AA-size dry cells containing various aromatic C-nitroso cathodes coupled with a magnesium anode. It is seen that the voltage discharge characteristics of these cells are similar to that found for the various aromatic nitroso cathodes in the half-cell studies (3).

Figure 1 shows 50- and 150-ohm continuous discharge data obtained on dry cells containing various p-nitrosodialkylamino cathodes. These cells operate at a flat voltage level above 1.30 v for most of their discharge life. The slight differences in voltage levels and capacities are attributed to variations associated with cell assembly and not to differences between structures of the cathode material.

Figure 2 gives data for some aromatic mono- and di-nitroso dry cells discharged continuously through 50- and 150-ohm resistances. It is seen that both the nitrosobenzene and o-nitrosotoluene cells have a two-step discharge curve with the nitrosobenzene cell operating at a higher voltage than the o-nitrosotoluene cells and for the first part of the discharge

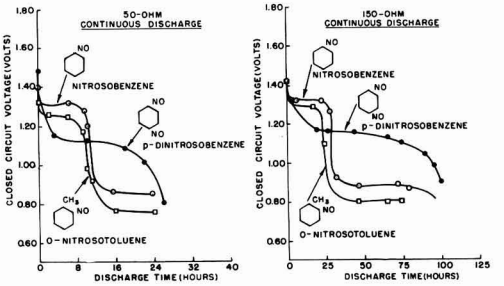

Fig. 2. Various AA-size magnesium-aromatic mono- and di-nitroso dry cells discharged continuously through 50- and 150-ohm resistances at 70° ± 2°F (50% R.H.).

at a potential close to that of the p-nitrosodialkylamino type of cells.

The p-dinitrosobenzene dry cells, although they have a higher initial closed circuit voltage, operate for most of their discharge period about 0.2 v lower than the nitrosobenzene cells. In addition, the capacity of the p-dinitrosobenzene cells is not markedly greater than that of the p-nitrosodialkylamino type cells, in spite of the greater theoretical ampere-minute capacity of the dinitroso compound.

As with the addition of the strongly electron attracting —NO group, the addition of a $—NO_2$ group to a mono nitroso compound results in a cathode with a lower operating potential. This relationship is shown by the cell discharge data in Fig. 2 and 3. The magnesium-m-nitronitrosobenzene AA-size cells operate between 1.1 and 1.2 v for most of their discharge life and give 50 and 160 hr of service to an end voltage of 0.90 v on the 50- and 150-ohm continuous discharge tests. These cells give comparable capacities to the magnesium-m-dinitrobenzene cells and are superior on these tests to the commercial general purpose Leclanché dry cells containing natural manganese dioxide and a starch-flour paste separator.

Figure 4 shows the discharge data for cells containing a magnesium anode and four aromatic hydroxynitroso compounds as cathodes. The magnesium-p-nitrosophenol cells operate for the first 6-7 amp-min of discharge between 1.40 and 1.50 v on these two tests, followed by a rapid drop to a voltage level between 1.20 and 1.30 v for most of the remaining discharge time. The second discharge

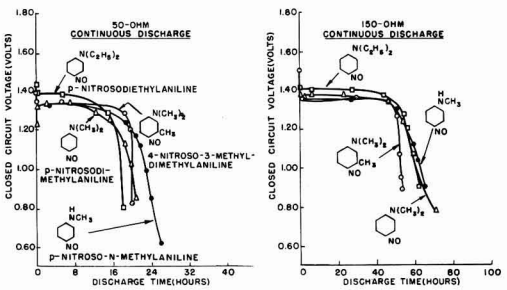

Fig. 1. Various AA-size magnesium-p-nitrosodialkylamino dry cells discharged continuously through 50- and 150-ohm resistances at 70° ± 2°F (50% R.H.).

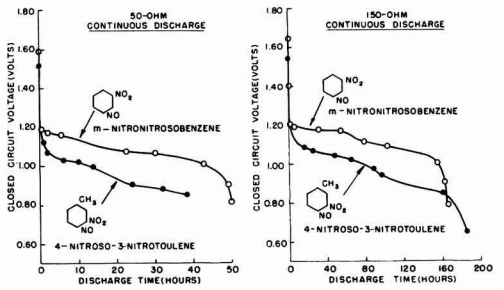

Fig. 3. Various AA-size magnesium-aromatic nitronitroso dry cells discharged continuously through 50- and 150-ohm resistances at 70° ± 2°F (50% R.H.).

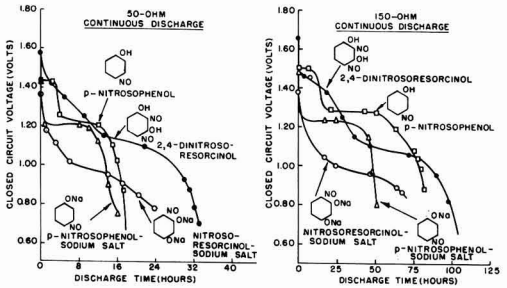

Fig. 4. Various AA-size magnesium-aromatic hydroxynitroso dry cells discharged continuously through 50- and 150-ohm resistances at 70° ± 2°F (50% R.H.).

step is close to that of the p-nitrosophenol-sodium salt. It is believed that a comparable compound is formed during discharge in a $MgBr_2$ electrolyte, as hydroxide ions are formed during discharge and neutralize the acidic phenolic H.

Figure 4 also shows the discharge characteristics of cells containing cathodes of 2,4-dinitrosoresorcinol and nitrosoresorcinol-sodium salt. As expected, the 2,4-dinitrosoresorcinol cells operate at a considerably higher voltage than the nitrosoresorcinol-sodium salt cells. It is also interesting to note that these dinitroso cells operate at a higher voltage than the mononitroso, p-dinitrosobenzene, and nitronitrosobenzene cells and exhibit a two-step voltage-discharge curve similar to the behavior found for aromatic dinitro cells.

Performance Characteristics of Magnesium-p-Nitrosodimethylaniline Dry Cells

The class of aromatic C-nitroso compounds includes many domestically available compounds which are stable solids and have theoretical ampere-minute capacities per unit of weight several times greater than the manganese dioxide and mercuric oxide cathodes used at present in commercial dry cells.

It is beyond the scope of this paper to characterize all types of magnesium-aromatic C-nitroso dry cells because of the large number of such electrochemical systems. Instead, the magnesium-p-nitrosodimethylaniline couple was selected for a more thorough study since this organic compound is more readily available, now being used as an intermediate in the production of a number of organic dyes. In the following sections, performance characteristics of these cells are compared with those of other dry cells.

Cell reactions.—Half-cell coulometric studies have shown that cathodes of p-nitrosodimethylaniline operate at efficiencies in excess of 85% (3). While the products formed during the discharge of a cell have not been analyzed, the experimentally obtained cathode ampere-minute capacities indicate that the electrode reactions during cell discharge are:

Cathode reaction

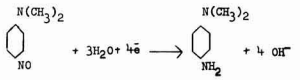

Anode reaction

$$Mg \rightarrow Mg^{++} + 2e^-$$

Over-all energy producing reaction

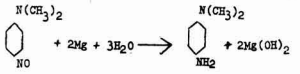

Cell discharge data.—From a cathode formulation study it was found that a higher ratio of carbon to p-nitrosodimethylaniline is required than is used in the manganese dioxide type of dry cells. A ratio of 2 parts of p-nitrosodimethylaniline to 1 part Shawinigan acetylene black by weight was found to give favorable results. The performance characteristics of cells of this formulation are discussed below.

Initial capacity data obtained on these cells discharged continuously through 4-, 50-, 150-, and 300-ohm resistances are shown in Fig. 5 and 6. The 4-ohm test represents a drain encountered in a flashlight application; the 150- and 300-ohm tests represent the current drains encountered in a B battery or a transistor radio receiver application. Included in Fig. 5 and 6 are discharged data for comparable size commercial Leclanché and magnesium-manganese dioxide dry cells. The commercial Leclanché dry cells were of the general purpose type and contained natural manganese dioxide and a starch-flour paste separator. The magnesium-manganese dioxide cells contained an impact ex-

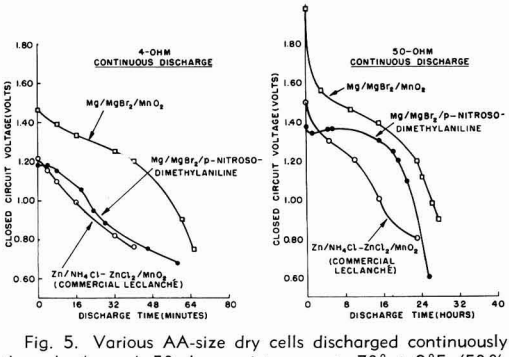

Fig. 5. Various AA-size dry cells discharged continuously through 4- and 50-ohm resistances at 70° ± 2°F (50% R.H.).

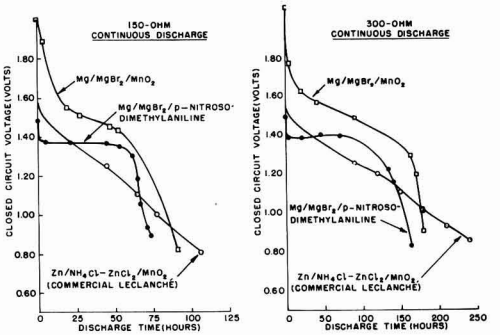

Fig. 6. Various AA-size dry cells discharged continuously through 150- and 300-ohm resistances at 70° ± 2°F (50% R.H.).

truded AZ10A magnesium alloy can, and were of the type under development by the Dow Chemical Company (5).

The 4-ohm continuous discharge test data show that the p-nitrosodimethylaniline cells have discharge characteristics comparable to the commercial Leclanché cells. On the 50-, 150-, and 300-ohm continuous discharge tests, it is seen that these organic cells have a flatter discharge curve than the two manganese dioxide dry cells and operate between 1.30 and 1.40 v for most of the discharge time.

Since performance requirements will vary depending on the application, the capacity data for the three types of AA-size cells obtained from the continuous discharge tests are summarized in several ways, as shown in Fig. 7-10 inclusive. In Fig. 7 the capacity in hours of service to 1.20 and 0.90 v end voltages are plotted against external load resistance. These data show that the p-nitrosodimethylaniline cells give more hours of service than the Leclanché cells to an end voltage of 1.20 v, but are inferior to both manganese dioxide cells to an end voltage of 0.90 v.

Since there are many applications which require maximum hours of service allowing a certain percentage voltage drop from initial closed-circuit voltage rather than maximum hours of service to specified end voltages, the capacity data are summarized in Fig. 8 in terms of hours of service vs. per cent voltage drop from initial closed-circuit voltage. The initial closed-circuit voltage was taken as the terminal voltage of the cell after 1 min of discharge through the respective resistance. The data in Fig. 8 illustrate one of the attractive properties of the p-nitrosodimethylaniline cells in that they give more hours of service than the manganese dioxide cells on the 50- and 150-ohm continuous discharge tests,

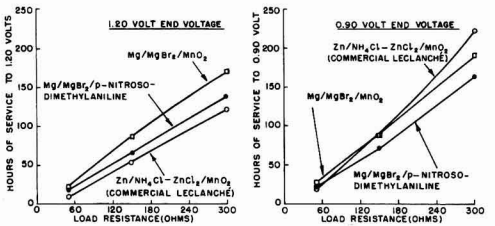

Fig. 7. Capacity in hours of service vs. load resistance of AA-size dry cells.

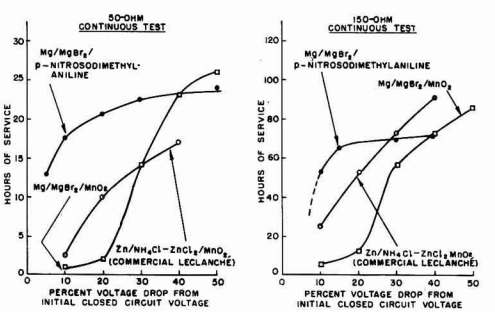

Fig. 8. Capacity in hours of service vs. per cent closed-circuit voltage drop of AA-size dry cells.

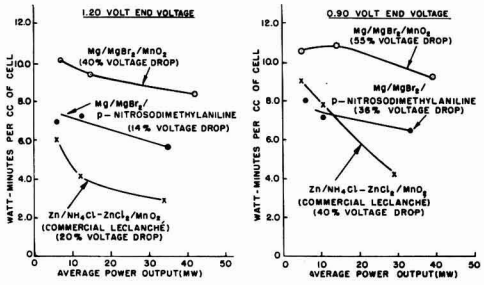

Fig. 9 Capacity in watt-minutes per cubic centimeter vs. average power output of AA-size dry cells.

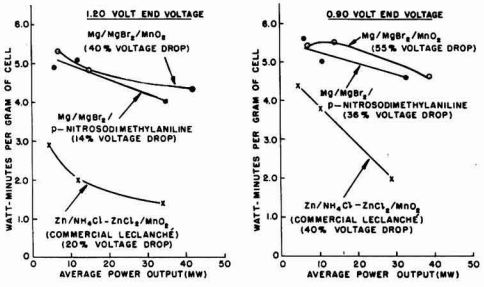

Fig. 10. Capacity in watt-minutes per gram vs. average power output of AA-size dry cells.

when the closed-circuit voltage of the cell is allowed to fall no more than 30%.

In order to normalize the voltage differences between the three cells, watt-minute capacities per unit of weight and volume to 1.20 and 0.90 v end voltages were plotted against average power output as shown in Fig. 9 and 10. The data in Fig. 9 show that the p-nitrosodimethylaniline cells give to an end voltage of 1.20 v watt-minute capacities per unit of volume between that obtained from the two manganese dioxide cells. To the lower 0.90 v end voltage the organic cells give higher capacities than the Leclanché at power output levels above 15 mw.

On the basis of watt-minute capacity per unit of weight, Fig. 10 shows that the p-nitrosodimethylaniline cells are comparable to the magnesium-manganese dioxide and superior to the Leclanché cells over a 10-40 mw range of continuous power output levels.

An additional analysis of the three cells, given in Table I, shows the approximate theoretical ampere-minute capacities and cathode efficiencies computed from their cell discharge data using a 0.90 v end voltage. These data were calculated with the assumption that the cathode material is the limiting cell component. It is seen that the p-nitrosodimethylaniline cathode becomes more efficient as the current drain is decreased, approaching its theoretical limit. In this respect it is comparable to the manganese dioxide cathodes.

Also included in Table I are comparable data obtained on p-nitrosodimethylaniline dry cells of an "inside-out construction." These cells contained a drawn steel cup coated on the inside with a conductive paint impermeable to the electrolyte. Ap-

Table I. Theoretical capacity and cathode efficiency of various AA-size dry cells

	Theoretical capacity/g of cathode material, amp-min	Approx wt of cathode material in cell, g	Approx theoretical cell capacity, amp-min	Cathode efficiency* of cells discharged continuously through following resistances, ohms			
				4	50	150	300
				(per cent)			
Zn/NH_4Cl-$ZnCl_2/MnO_2$ Commercial Leclanché	18.5	3.3	60.5	11.1	40.5	60.6	89.3
$Mg/MgBr_2/MnO_2$	18.5	3.9	72.2	25.6	62.9	72.6	71.9
$Mg/MgBr_2$/p-nitrosodimethylaniline (impact extruded can construction)	42.8	1.2	51.4	13.9	69.2	73.5	83.4
$Mg/MgBr_2$/p-nitrosodimethylaniline (inside-out construction)	42.8	1.8	77.0	—	54.5	69.3	96.0

* Data based on ampere-minute capacity to 0.90 v end voltage.

proximately 7 g of cathode mix of the previously described formulation were inserted into the steel cup, and then a magnesium rod (0.20 in. diameter) wrapped with Nibroc absorbent salt-free paper was inserted into the center of the cathode mix. The cell was next sealed in the conventional manner with a pitch seal. This construction offers the advantages of (*a*) lower cost and (*b*) larger volume of cathode mix which results in greater theoretical cell capacity over the impact extruded can design. Discharge data obtained from cells of this design are shown in Fig. 11. Included for comparison are data for a comparable size Leclanché cell and a p-nitrosodimethylaniline dry cell containing an impact extruded magnesium alloy can. Cells of the inside-out design have a greater theoretical capacity (Table I) and give more hours of service than the comparable size p-nitrosodimethylaniline cells of the impact extruded magnesium alloy can design. At the present stage of development these "inside-out" cells operate at a slightly lower voltage, due to *IR* losses associated with the design. It is believed that with further development these losses can be largely eliminated, and the cells will operate at a potential close to that obtained with the impact extruded can design.

Other size p-nitrosodimethylaniline dry cells have been assembled and found to have similar relationships to comparable size Leclanché and magnesium-manganese dioxide cells. Figure 12 gives capacity data obtained on D-size cells discharged continuously and intermittently through 4-ohm resistances simulating the discharge through a 0.25-amp flashlight bulb. It is seen that the p-nitrosodimethylaniline cell has a flatter discharge curve and gives more minutes of service to a 0.90 v end voltage than either of the manganese dioxide cells on the continuous test. On the intermittent test it gives more minutes of service than the Leclanché cell but less than the magnesium-manganese dioxide cell.

Conclusions

Many aromatic C-nitroso compounds have properties suitable for the design of improved dry cells when coupled with a magnesium anode and a magnesium bromide electrolyte. The discharge characteristics of these cells are dependent on the choice of aromatic C-nitroso cathode.

Dry cells containing various aromatic C-nitroso cathodes have been stored for 12 months at 70°F and have given 75-90% of initial capacity. However, at 113°F (90% R.H.) failure occurred after two months' storage.

The AA-size magnesium-p-nitrosodimethylaniline dry cells have been studied in greater detail. These cells have a flat voltage-discharge curve, operating for most of their discharge time above 1.30 v, and give greater watt-minute capacities per unit of weight and volume than the commercial Leclanché dry cells on a number of tests. Increased capacity can be obtained from this electrochemical system by using an inside-out construction instead of the impact extruded can design.

The magnesium-aromatic C-nitroso dry cells exhibit the same difficulties associated with other magnesium dry cells, namely, loss in capacity on light intermittent tests, "delayed action," and high impedance. It is believed that these problems can be overcome with further development.

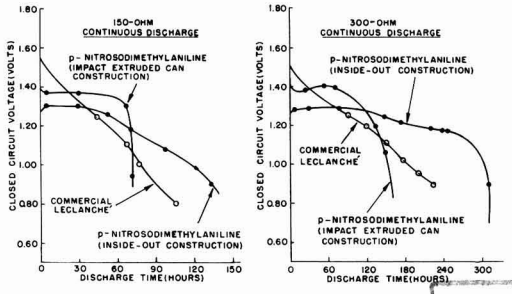

Fig. 11. Various AA-size dry cells discharged continuously through 150- and 300-ohm resistances at 70° ± 2°F (50% R.H.).

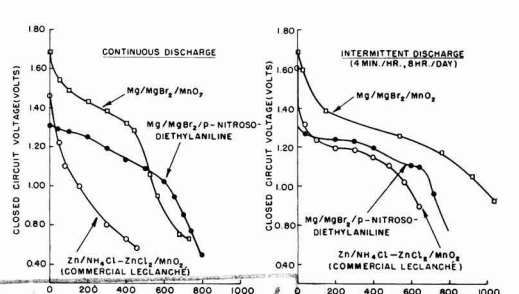

Fig. 12. Various D-size dry cells discharged through 4-ohm resistances at 70° ± 2°F (50% R.H.).

Acknowledgment

The authors wish to express their appreciation to Mr. G. R. Ganges and Dr. G. S. Lozier for assistance in gathering some of the cell data and their many helpful comments made during this study.

Manuscript received April 9, 1958. This paper was prepared for delivery before the Buffalo Meeting, Oct. 6-10, 1957.

Any discussion of this paper will appear in a Discussion Section to be published in the June 1959 JOURNAL.

REFERENCES

1. C. K. Morehouse and R. Glicksman, *This Journal*, **105**, 306 (1958).
2. R. Glicksman and C. K. Morehouse, *ibid.*, **105**, 299 (1958).
3. R. Glicksman and C. K. Morehouse, *ibid.*, **105**, 000 (1958).
4. W. C. Arsem, U. S. Pat. 2,306,927, Dec. 29, 1942.
5. R. C. Kirk, P. F. George, and A. B. Fry, *This Journal*, **99**, 323 (1952).

Textures of Electrodeposited Lead Dioxide

Yasuichi Shibasaki[1]

Department of Electrochemistry, Yokohama National University, Yokohama, Japan

ABSTRACT

Slightly coarse, dull smooth, bright smooth, fibrous, columnar, rough, granular, and porous textures were found for electrodeposited lead dioxide. Textures, relative strengths, and conditions of electrodeposition of lead dioxide are discussed. The bright, smooth lead dioxide was found to be the strongest.

It has been noticed in many experiments on electrodeposition of lead dioxide under different conditions that there is a close relation between strength and texture of the electrodeposited lead dioxide. This paper describes a study of the textures of various electrodeposits.

Experimental

Basis materials.—Mixture of finely powdered lead dioxide and polystyrene.—Finely powdered lead dioxide was passed through a 100-mesh screen and homogeneously mixed with polystyrene and benzene in the weight ratio of 100: (2 ~ 3): (8 ~ 20). This mixture was applied 5-10 mm thick onto a perforated hollow cylinder of stainless steel. The benzene was removed by evaporation and the mixture finished mechanically to a cylindrical rod. This rod was used as a substrate in the untreated condition or after the following treatment. The rod was made the anode for electrolysis of a 5-10% NaOH solution or a dilute H_2SO_4 solution at a current density of about 10 amp/dm^2 for 5-10 min, then washed with water, a dilute HNO_3 solution, and water successively. After electrodeposition the substrate could be removed easily from the electrodeposit by dissolving the polystyrene in a solvent such as benzene.

Mixture of powdered graphite and solid paraffin.—Powdered graphite (passed through a 100-mesh screen) and paraffin, (mp 50°-60°C) were mixed homogeneously in the weight ratio of 3.5:1 at temperatures higher than the melting point of paraffin. The mixture was applied 5-10 mm thick onto a perforated hollow cylinder of copper at the same temperatures. After cooling it was finished mechanically to a rod. The rod was cleaned by being made the anode or cathode for electrolysis of a 5-10% NaOH solution at a current density of about 10 amp/dm^2 until its surface was almost perfectly wet, then washed with water, a dilute HNO_3 solution, and water successively. The rod was used as a substrate for electrodeposition while the surface was wet. After electrodeposition it could be removed

[1] Present address: Department of Chemistry, The Ohio State University, Columbus, Ohio.

Table I. Samples of electrodeposited lead dioxide and electrodeposition conditions under which they were electrodeposited

Texture and No.	Electrodeposited lead dioxide Size (cm) When cylinder: Outside diameter	Length	Thickness	Weight (kg)
SC1	Rectangular plate	1.5 × 6	× 0.06	0.005
SC2	Rectangular plate	2 × 6.5	× 0.03	0.0035
DS	4	6	0.6	0.35
BS1	3	20	0.35	0.47
BS2	0.6	7.3	0.04	0.05
BS3	2.3	13	0.35	0.25
BS4	2.5	13.5	0.3	0.17
BS5	2.5	20	0.28	0.34
BS6	1.8	10.6	0.4	0.17
BS7	5.8	83	0.7	8.4
BS8	5.5	82	0.7	7.3
BS9	2.8	13.5	0.5	0.41
BS10	5	57	0.85	5.2
M(F,G)			0.8	
C			0.57	
G1	5.7	90	0.76	8.5
G2	6	90	0.9	10
G3	3.2	14	0.6	0.62
G(S)1			0.6	
G(S)2			0.6	
G(R)			0.6	
R1	Rectangular plate 2 × 5			
R2	Rectangular plate 2 × 5			
R3	Rectangular plate 2 × 5			
R4	Rectangular plate 2 × 5			
R5	1.9	12	0.4	0.18
P1			0.6	
P2			0.17	

SS, slightly coarse; DS, dull smooth; BS, bright smooth; M(F, G), (a), mixture of lead dioxide and polystyrene; (b), mixture of

easily from the electrodeposit by melting the paraffin or dissolving it in a solvent.

Nickel cylinder; nickel plated cylindrical lead tube; or 0.15 mm thick rectangular nickel plate covered except for one surface by applying a mixture of paraffin and vaseline.—The surfaces of these substrates were cleaned by being made the anode or cathode for electrolysis of a 5-10% NaOH solution at a current density of about 10 amp/dm^2 until their surfaces were almost perfectly wet, then washed with water, a dilute HNO_3 solution, and water successively. The tendency of electrodeposited lead dioxide to deform itself during and after electrodeposition depends on the conditions of electrodeposition (1). When lead dioxide is electrodeposited on a deformable substrate such as the nickel plate, it will deform itself and the substrate easily; stresses in the deposit will be lessened. Therefore, lead dioxide electrodeposited on a deformable substrate is usually less liable to cracking than that electrodeposited on a nondeformable substrate such as the first four substrates mentioned above. Consequently, when the tendency to crack was great, the nickel plate was used as a substrate. When there is little tendency to deformation, electrodeposited lead dioxide does not tend to crack, regardless of the type of substrate used.

If a thick layer of lead dioxide is deposited on the nickel plate, it tends to deposit not only on the over part of the substrate surface but also on the part which protrudes from the perimeter of the substrate in accordance with the progress of the electrodeposition. In this case it is quite difficult to maintain a constant current density during electrodeposition and, when the tendency is small, the other substrates are suitable.

Electrolysis cells and electrolytes.—Two cylindrical porcelain vessels of about 30^e x 30 cm and 70^e x 100 cm were used for the electrodeposition. When the substrate was cylindrical, it was placed vertically at the center of a copper cylindrical cathode which was, in turn, placed in contact with the inside of the vessel. The substrate was rotated primarily around its center axis. When the substrate was a plate, it was placed parallel to a copper plate cathode.

The electrolytes which were used for the electrodeposition are shown in Table I. Solutions were agitated. Powdery carbonates of lead and copper were dissolved in the electrolytes to control acidities and supply metal ions during electrodeposition.

Conditions for electrodeposition, such as composition and temperature of electrolyte, and current density, were maintained as constant as possible. Under extended periods, however, small fluctuations were unavoidable.

Table I. Samples of electrodeposited lead dioxide and electrodeposition conditions under which they were electrodeposited—continued

Conditions of electrodeposition							
Substrate		Composition of electrolyte		Temperature of electrolyte (°C)	Current density (A·dm^{-2})	Time of electrodeposition (hr)
Kind	Motion (rpm when cylinder)	Substances and their concentration in water [Pn: $Pb(NO_3)_2$, Cn: $Cu(NO_3)_2$] (m)	pH			
(c) iii)	Repose	Pn: 1, Cn: 0.1	2 ~ 4	20	0.1	115.5
					1	5.5
(b)	60		1 ~ 4	27 ~ 30	4	30
(c) ii)		Pn: 1	1 ~ 3	20 ~ 23	5.0 ~ 5.6	14
(c) i)	Repose	Pn: 1, Cn: 0.1	2 ~ 4	20	5.5	1.5
(b)	60	Pn: 1, $Al(NO_3)_3$: 0.1	1 ~ 2	14.5 ~ 18.5	4.5	17.5
(a)	60 ~ 100	Pn: 1, Cn: 0.1, $Mn(NO_3)_2$: 0.01	1.5 ~ 4	20	2	30
(b)		Pn: 1, Cn: 0.1, $Al(NO_3)_3$: 0.1, $CH_3(CH_2)_7CH{=}CH(CH_2)_7CH_2O(C_2H_4O)_{18}H$: 0.005	2 ~ 3	15	3.4	16
(a)		Pn: 1, Cn: 0.1, CH_3-<>-SO_2NH_2: 0.0065	2 ~ 4	14 ~ 16	3.2 ~ 3.6	24
				12 ~ 16	2.0 ~ 3.4	49
				13 ~ 15	2.3 ~ 3.4	50
(b)		Pb$(NH_2SO_3)_2$: 1, Cu$(NH_2SO_3)_2$: 0.1, $C_{12}H_{25}O(C_2H_4O)_6H$: 0.002		20	2	50
				20 ~ 25	1 ~ 2	95
(a), Reciprocation, 20 cm·sec^{-1}		Pn: 1, Cn: 0.1, $Al(NO_3)_3$: 0.3	1 ~ 3	23	5	31.5
				14	6	19
(a)	60 ~ 100	Pn: 1, Cn: 0.1	2 ~ 4	19 ~ 26	4.8 ~ 6.0	21
		Pn: 1, Cn: 0.1, CH_3-<>-SO_2NH_2: 0.003	1 ~ 4	11 ~ 18	2.7 ~ 4.9	52
(b)	50 ~ 100 (many stripes)		1 ~ 3	27 ~ 31	7	21
(b)	300 ~ 400	Pn: 1, Cn: 0.1	1 ~ 2	28 ~ 33	7.0 ~ 7.7	16
	500 ~ 600				20	0.43
(c) iii)	Repose			20	30	0.27
					40	0.08
			2 ~ 4		50	0.17
(a)		Pb$(NH_2SO_3)_2$: 1, Cu$(NH_2SO_3)_2$: 0.1, Powdery active carbon: 0.8		14 ~ 15	1.7 ~ 2	37
(b)	60 ~ 100	Pn: 1, Cn: 0.1	1 ~ 3	27 ~ 30	4	30
				20	5	6.5

mixture of fibrous and granular; C, columnar; G, granular; G(S), stripe-shape granular; G(R), ringe-shape granular; R, rough; P, porous. graphite and paraffin; (c) i), nickel cylinder; (c) ii), nickel plated cylindrical tube; (c) iii), nickel plate.

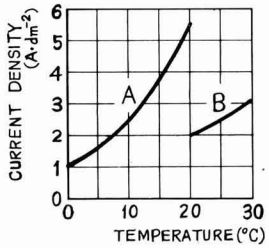

Fig. 1. Relation between current density and temperature of the electrolyte for the electrodeposition of bright, smooth lead dioxide. Curve A, 1 mole $Pb(NO_3)_2$ solution; Curve B, 1 mole $Pb(NH_2SO_3)_2$ solution.

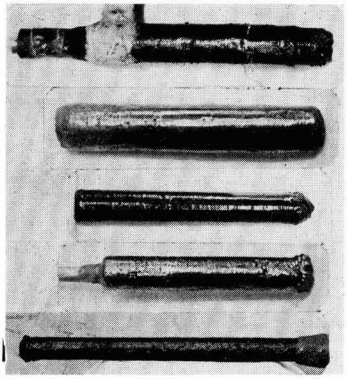

Fig. 2. Hollow cylinders of bright, smooth lead dioxide, from top to bottom: BS1, BS4, BS5, BS6, and BS7.

Results of Experiments

Slightly coarse textured lead dioxide, whose surface is similar in nature to the surface of a very fine grain sandpaper, is deposited under the conditions of low current density and ambient temperature. It is brittle and easily cracked (see SC in Table I).

Dull, smooth lead dioxide is frequently deposited when the current density is slightly low at room temperature or when the electrolyte contains one or more of certain impurities. It has comparatively large strengths (see DS in Table I).

Bright, smooth lead dioxide is compact, strong, and most suitable for an insoluble anode. Suitable conditions found for obtaining bright, smooth deposits are:

1. The surface of the substrate should be smooth; however, when other conditions are suitable, the roughness of the deposit is less than that of the substrate.

2. The relation between current density and temperature of the electrolyte is shown in Fig. 1. Lower temperatures give more suitable conditions.

3. It is desirable that one or more of the following substances be added to the electrolyte: Al^{3+}, Mn^{2+}, polyoxyethylenealkylether, paratoluenesulfonamide. However, the desirable relations between the current density and temperature are generally effected by the addition of these substances.

4. Iron and cobalt compounds should not be present in the electrolyte. If they are present in concentrations exceeding 0.0001 mole and 0.001 mole, then a rough, weak lead dioxide is apt to be electrodeposited (2).

5. It is desirable generally that the concentration of a lead salt be high, but it must not be so high that the salt may be deposited on the electrodeposition surface as a result of a fall in the temperature of the electrolyte, an increase of the H^+ activity in the electrolyte, etc. (see Fig. 2 and BS in Table I).

The fibrous texture consists of a group of fibers, and the columnar texture consists of a group of columns. Under conditions that fibers or columns tend to deposit, while the electrodeposited lead dioxide layer is thin, the layer generally consists of fine crystals; however, with the increase of layer thickness, fibers or columns tend to grow up along flow lines of the electric current.

Fibrous lead dioxide tends to electrodeposit when the current density is slightly high at room temperature. Strengths of the fibrous lead dioxide rank next to those of the dull, smooth lead dioxide (see Fig. 3 and M(F,G) in Table I).

Columnar lead dioxide tends to electrodeposit when the current density is high at room temperature. In general the column has an irregularly shaped polygonal cross section, the sides of the polygon being curved lines. The cross-sectional area is generally 0.1-50 mm^2.

Although the column appears to be connected to its neighboring part, it is actually in contact only with the layer of the first stage of electrodeposition. In the event that a group of columns crowd, as typified in Fig. 4, the layer electrodeposited during the first period, for example, the first electrodeposited layer which is generally 1-3 mm thick, consists of fine grains which are connected more firmly to their neighboring parts. However, the layer electrodeposited at a later period consists of columns which are not connected but are instead only in contact with their neighboring parts.

Although the columns themselves in the columnar texture are comparatively strong, they are easily separated by external forces. Therefore, the columnar lead dioxide is brittle and weak, and its life for use in electrolyses is short (see Fig. 4 and C in Table I).

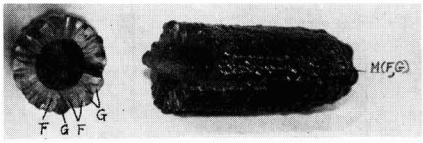

Fig. 3. Lead dioxide of the mixed texture of fiber and granule; F, fiber; G, granule.

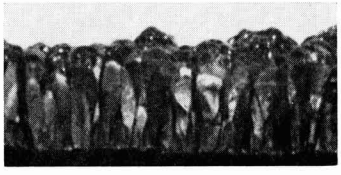

Fig. 4. Broken surface of columnar lead dioxide: C

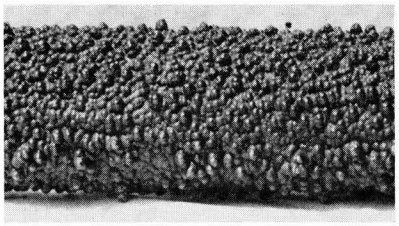

Fig. 5. Hollow cylindrical rod of granular lead dioxide: G2

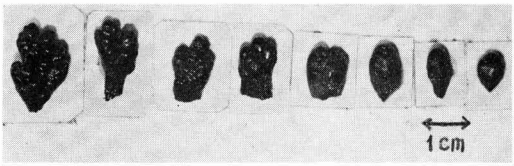

Fig. 6. Granules usually electrodeposited

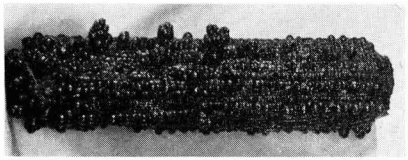

G3

Fig. 7. Electrodeposited lead dioxide whose granules were formed on projected points of the substrate. The substrate was shaped by hand with a knife to a cylindrical rod. There was many stripes parallel to the axis on the surface of the substrate.

The granular texture results from a grouping of granules (see Fig. 5 and G2 in Table I). An irregular cone or pyramid is the common shape of the granules encountered. The vertex lies near the substrate, and the base is a curved surface like a semi-sphere in the first stage and becomes a complex shape as electrodeposition progresses. For instance, some secondary granules may appear on this surface and, moreover, tertiary granules may appear on the secondary granules, etc. The granules ordinarily grow at an accelerated rate during the progress of electrodeposition. The types of granules usually electrodeposited are shown in Fig. 6.

In general, the major portion of a side of a granule appears to the naked eye to be connected to the neighboring part; however, the only connection is at the root (the part near the vertex), the remainder being merely in contact. For this reason the granule is easily removed by external forces, and the granular lead dioxide is brittle and weak.

The lead dioxide of this texture tends to be electrodeposited under one or more of the following conditions: (*a*) the surface of the substrate is rough; a granule is often formed on a projecting point on the surface of the substrate (see Fig. 7 and G3 in Table I); (*b*) high current density is at room temperature; (*c*) electrolyte composition suitable for the electrodeposition of this texture exhibits poor throwing power; (*d*) foreign particles are in the electrolyte.

If the electrolyte or electrode surface is in motion during electrodeposition, the shape of the granule is influenced. For instance, when the electrolyte flows past the electrodeposition surface during electrodeposition, the granule grows as shown in Fig. 8.

When the lead dioxide is electrodeposited on the surface of a cylinder which is rotating around its axis at high speed, the relative motion of the electrodeposition surface and the electrolyte results in the formation of stripe-shape or ring-shape protuberances in the circumferential direction instead of granules (see Fig. 9 and G(S) and G(R) in Table I).

The rough texture results from powders or fine granules which connect one another roughly. The rough lead dioxide is somewhat porous and weak. It tends to deposit under one or two of the following conditions: (*a*) current density is very high or the concentration of the Pb^{2+} is very low; rough lead dioxide is more easily electrodeposited when the current density is so high or the Pb^{2+} concentration is so low that oxygen is evolved simultaneously; (*b*) there are certain impurities in the electrolyte. Iron compounds, cobalt compounds, and finely powdered active carbon are examples of these (2) (see Fig. 10 and R1-R5 in Table I).

A porous texture is one that has many pits or pores. Porous lead dioxide is generally weak. This electrodeposits when gas bubbles adhere to the electrode surface and are not removed for a long time during electrodeposition or when the salt concentration of the electrolyte is so high that the salt crystallizes on the anode surface during electrodeposition. The adhering bubbles are apt to be re-

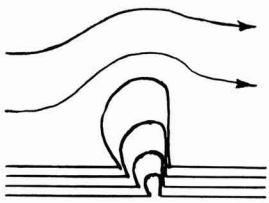

Fig. 8. Relation between growth of the granule and relative motion of the electrodeposition surface and electrolyte.

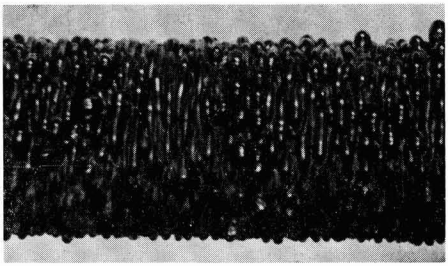

Fig. 9. Hollow cylindrical rod consisting of stripe-shape protuberances: G(S)1.

Fig. 10. Thin plate of rough lead dioxide: R4

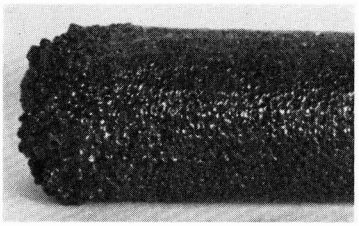

Fig. 11. Hollow cylinder of porous lead dioxide: P2

moved by adding a small quantity of a surface-active agent to the electrolyte or by brushing the surface with a nonconducting brush during electrolysis.

When the concentration of a salt in the electrolyte is high, crystals of the salt are likely to be deposited on the electrode surface, owing to the lowering of the temperature of the electrolyte or the decrease of the solubility of the salt, owing to the production of an acid on the anode surface. The crystallized salt is partly or entirely covered with the lead dioxide being electrodeposited, and pores are made when the partly covered salt is removed by washing with water (see Fig. 11 and P1 and P2 in Table I).

Conclusions

The textures of the electrodeposited lead dioxide and the relation among the textures, the strengths of the lead dioxide, and the conditions of the electrodeposition were obtained as shown in Table II.

Bright, smooth lead dioxide was the strongest. This was electrodeposited when the substrate was smooth, when the current densities were 1 amp/dm^2 at 0°C, 2.5 amp/dm^2 at 10°C, and 5.5 amp/dm^2 at 20°C with concentrated lead nitrate solution, and 2 amp/dm^2 at 20°C with concentrated lead sulfamate solution, when one or a combination of the following substances were present in the electrolyte: aluminum salts, manganese salts, polyoxyethelene-alkylether, paratoluenesulfonamide, or when the concentrations of iron or cobalt compounds present in the electrolyte were less than 0.0001 mole and 0.001 mole, respectively.

Table II. Textures and strengths of lead dioxide obtained under various conditions of electrodeposition

Texture of electrodeposited lead dioxide	Order of the strengths of lead dioxide	Conditions of electrodeposition: Current density of electrodeposition	Conditions of electrodeposition: Order of smoothness of the surface of substrate
Slightly coarse texture	7	Very low	
Dull, smooth texture	2	Slightly low	2
Bright, smooth texture	1	Medium	1
Fibrous texture	3	Slightly high	3
Columnar texture	4	Rather high	4
Granular texture	5	High	5
Rough texture	8	Very high	
Porous texture	6	Gas bubbles or crystals of a salt adhere to the surface of the electrodeposition	

Acknowledgment

This research was supported in part from scientific research funds granted by the Educational Department of the Japanese Government and in part by a grant from the Yokohama Battery Factory of Tohtetsu Industry Company Ltd.

Manuscript received Nov. 21, 1957. This paper was prepared for delivery before the Ottawa Meeting, Sept. 28-Oct. 2, 1958.

Any discussion of this paper will appear in a Discussion Section to be published in the June 1959 JOURNAL.

REFERENCES

1. Y. Shibasaki, *Bull. Faculty Eng. Yokohama Natl. Univ.*, **1**, 105 (1951); **2**, 69 (1953); **3**, 77 (1954); **4**, 85 (1955); **5**, 149 (1956); *J. Electrochem. Assoc. Japan*, **19**, 82 (1951); *J. Chem. Soc. Japan, Industrial Chem. Sec.*, **53**, 97 (1950); **54**, 205 (1951); **54**, 357 (1951); **54**, 713 (1951); **55**, 61 (1952); **55**, 558 (1952); **56**, 230 (1953); **56**, 398 (1953); **56**, 485 (1953); **57**, 341 (1954); **57**, 703 (1954); **57**, 794 (1954); **58**, 95 (1955); **58**, 179 (1955).
2. Y. Shibasaki, *J. Chem. Soc. Japan, Industrial Chem. Sec.*, **54**, 713 (1951); **58**, 95 (1955).

Galvanic Corrosion

II. Effect of pH and Dissolved Oxygen Concentration on the Aluminum-Steel Couple

M. J. Pryor[1] and D. S. Keir

Department of Metallurgical Research, Kaiser Aluminum & Chemical Corporation, Spokane, Washington

ABSTRACT

The effect of pH, dissolved gas composition, and deaeration on the galvanic characteristics of the aluminum-steel couple was investigated. High-purity aluminum cathodically protects steel completely in chloride solutions within the pH range 0.2-14.0. The galvanic currents and weight losses of the aluminum anodes are at a minimum from pH 4.0 to 10.0. Within this pH range the rate of galvanic corrosion is controlled by oxygen depolarization at the steel cathodes. The galvanic current fluctuates because the oxide film on the steel cathode is thickening with time in an erratic manner.

At higher and lower pH the rate of galvanic corrosion is much greater and is independent of the oxygen concentration in solution. The reaction occurring on the steel cathodes is the vigorous evolution of gaseous hydrogen. Any oxide films on the steel cathodes are subjected to rapid reductive dissolution to soluble ferrous ions. Consequently the galvanic current is extremely steady and reproducible.

In an earlier paper (1) the current flow and polarization characteristics of the aluminum-steel galvanic couple in sodium chloride solution were investigated. It was found that: (*a*) steel was cathodically protected by high-purity Al over a wide range of ratios of electrode areas, (*b*) both the galvanic current and Al weight loss were approximately proportional to the cathode area and independent of the anode area, and (c) the galvanic current was approximately proportional to the rate at which the solution was stirred. These results showed that the rate of galvanic corrosion in nearly neutral chloride solutions was controlled by oxygen depolarization at the steel cathodes. The Al anodes were corroded slightly more rapidly than was calculated from the galvanic current flow. This suggested that the local cathodes on active Al anodes were not completely suppressed under the conditions studied.

Experiments described in this paper represent an extension of the previous studies. The effect of pH, varying oxygen concentration in solution, and deaeration on galvanic current flow and on anodic weight loss has been investigated. The conditions under which the air-formed oxide film on the steel cathode is stable have been determined and have been correlated with the galvanic results.

Experimental

Materials.—The Al and mild steel used in this investigation were in the form of cold rolled sheet 0.088 cm thick and had the same compositions as described in a previous paper (1).

All solutions were made from analytical reagent chemicals and distilled water and were presaturated with the appropriate gas before the experiment.

Steel specimens were prepared as described previously (1). Aluminum specimens were etched in 1.0*N* NaOH for 10 min, rinsed in distilled water, dried, rinsed again in benzene, and stored in dry air for 24 hr.

Experimental Method

The closed galvanic cell used in this investigation had a solution capacity of 100 ml and is shown in Fig. 1. Two dissimilar metal electrodes (A and B) having dimensions 5 x 1 cm immersed in solution were held rigidly in place 2 cm apart by means of a small Lucite disk (C). The effective electrode area was 10 cm^2. The electrodes were connected to Pt wires (D) which passed out of the cell through glass seals to a zero resistance microammeter. The connections between (D) and the electrodes (A and B) were embedded in Lucite to prevent any galvanic corrosion. The cell was provided with a salt bridge (E) for measuring the potential of the couple by standard methods.

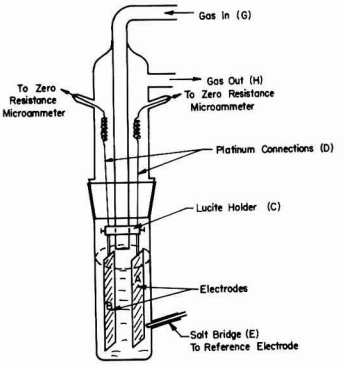

Fig. 1. Galvanic cell

[1] Present address: Metals Research Division, Olin Mathieson Chemical Corporation, New Haven, Conn.

Before any experiment, the appropriate solution was saturated in a separate vessel by prolonged bubbling with the particular gas or gas mixture under investigation. The solution was quickly transferred to the galvanic cell and the same gas, presaturated with water vapor, passed in through the tube (G) and out through (H). The rate at which the gas was passed through the galvanic cell was not critical provided the surface of the solution was not visibly agitated. The gases investigated were oxygen, air, air freed from CO_2, and helium.

Solutions having variable hydrogen ion concentration from $10^{-2}N$ to $10^{-12}N$ and having constant chloride ion concentration (±1%) were prepared by adjusting the pH of $1.0N$ NaCl with either HCl or NaOH. Normal HCl and NaOH, respectively, were used for pH values of 0.2 and 14.0; the latter contained no added chloride. The cell was contained in a water bath thermostatically controlled at 25° ± 0.05°C.

Current, potential, and weight loss measurements in the galvanic cells were made as described previously (1).

Results

Galvanic experiments at different pH values in solutions saturated with dissolved air.—Triplicate galvanic experiments were carried out at each pH value from 0.2 to 14.0. The duration of experiments within the pH range 6.0-10.0 was 96 hr. With the exception of measurements at pH 14.0 which were carried out for 4 hr, all other experiments were carried out for 24 hr. The purpose of employing these various times was to permit the use of one experimental method while still preventing significant (a change of less than 0.5 pH units) depletion of hydrogen ions. This experimental method was considered to be less objectionable than the use of buffered solutions since these introduce specific anion effects. Although this extrapolation does not take care of change in corrosion rate, the error introduced is small in comparison with the very large change in galvanic current and weight loss with pH.

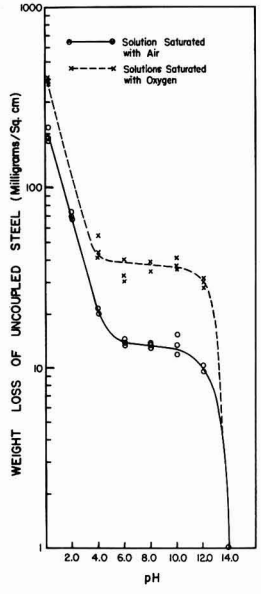

Fig. 2. Relationship between weight loss of uncoupled steel and pH of solutions saturated with air and oxygen. Calculations based on 96-hr run. Actual period for pH 14.0 was 4 hr; for pH 6.0-10.0, 96 hr; for all others, 24 hr.

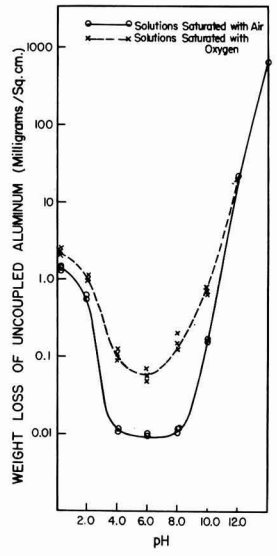

Fig. 3. Relationship between weight loss of uncoupled Al in 96 hr and pH of solutions saturated with air and oxygen at 25°C. See caption Fig. 2.

Figure 2 shows the relationship between weight loss in 96 hr and pH for uncoupled steel specimens in solutions saturated with air and with oxygen and maintained in equilibrium with these gases. The curves are of the type previously reported by Forrest, Roetheli, and Brown (2) for mild steel.

Figure 3 shows the relationship between weight loss in 96 hr and pH for uncoupled Al specimens in similar solutions. These curves exhibit minimum weight loss within the pH range of 4.0-8.0 as had been found previously by Edeleanu and Evans (3).

Steel specimens coupled to Al anodes in similar solutions were completely cathodically protected over the entire pH range studied. At the same time the weight losses of the Al anodes were increased (Fig. 4). Figure 5 shows the relation between the number of coulombs flowing and pH. The curve closely parallels the anodic weight loss vs. pH curve in Fig. 4. Table I shows the calculated anodic weight loss due to the galvanic current flow. At pH values up to 10.0 this comprises only 71-91% of the total anodic weight loss. At pH 14.0 the weight loss due to galvanic current flow is only 34-45% of the total weight loss. Evidently substantial proportions of the Al weight losses are due to local cell corrosion particularly at high pH.

Effect of gas atmosphere.—Figures 2-5 show experimental results on weight loss and current flow in solutions presaturated with air. Similar experiments were performed using air freed from CO_2.

Table I. Weight losses of Al anodes due to galvanic corrosion and local action at different pH in solutions saturated with air

pH	No. of coulombs flowing in 96 hr	Galvanic wt loss of Al anode, mg/cm²	Total Al wt loss, mg/cm²	Wt loss due to local action, mg/cm²	% local action wt loss
0.2	4916; 4270; 4870	45.9; 39.9; 45.4	53.2; 47.5; 53.7	7.3; 7.7; 8.3	14; 16; 15
2.0	276; 272; 256	2.6; 2.6; 2.4	3.2; 3.2; 2.9	0.6; 0.7; 0.5	20; 21; 18
4.0	72; 64	0.7; 0.6	1.0; 0.9	0.3; 0.2	29; 29
6.0	42; 41; 42	0.4; 0.4; 0.4	0.5; 0.5; 0.4	0.1; 0.1; 0.05	17; 19; 9
8.0	40; 40; 41	0.4; 0.4; 0.4	0.5; 0.5; 0.5	0.1; 0.1; 0.1	18; 18; 19
10.0	40; 44	0.4; 0.4	0.5; 0.5	0.1; 0.1	21; 18
14.0	23,600; 23,450	219; 220	643; 589	424; 368	66; 55

However, the removal of CO_2 in no way changed any of the results. Figures 2-5 also show that presaturation with oxygen and the maintenance of an oxygen atmosphere over the solution increase the rate of corrosion and galvanic corrosion of Al and the rate of corrosion of uncoupled steel. In the galvanic experiments the effect is only observed from pH 4.0-10.0. On uncoupled specimens of Al and steel the effect is observed over a somewhat broader pH range.

Figure 6 shows current-time curves, at zero external resistance, in normal NaCl (pH 6.0) presaturated with and maintained in atmospheres of air, oxygen, and helium. In solutions saturated with air the oxygen evidently becomes partly depleted quite rapidly and the galvanic current achieves a value of around 10 $\mu a/cm^2$ of cathode area. In solutions initially saturated with oxygen, the dissolved oxygen concentration is higher and so less depletion and higher galvanic currents are obtained. Only very small galvanic currents flow in solutions saturated with He. Table II shows the anodic weight losses of Al anodes and the number of coulombs flowing as a function of gas atmosphere.

Figure 7 shows the results of similar experiments in normal HCl and NaOH. Here, initial saturation of the solution with oxygen or helium (not shown in these curves) has no significant effect on the galvanic current flow or on the weight losses of Al anodes.

Potential measurements.—Potential measurements of the couple on closed circuit were carried out during all galvanic experiments as described previously (1). Figure 8 shows the potentials[2] of the galvanic couples at different pH values in solutions presaturated and remaining in contact with the air.

Oxide film stability.—The stability of the air-formed oxide film on a steel cathode has been shown to affect the current-potential relationship existing during cathodic protection (4). In order to determine whether a similar effect exists during galvanic corrosion, the stability of visible oxide films on steel cathodes coupled to Al anodes was determined at different pH values. Steel specimens were heat-tinted to the first order red interference color. A small portion of the oxide was autoreduced (5) by immersion in dilute HCl. The steel specimens were then coupled to Al anodes in solutions of different pH. The rate of reductive dissolution of the remaining red film could then be judged quite accurately

[2] Except in the first few minutes of the galvanic experiments, potentials were constant to within ±10 mv.

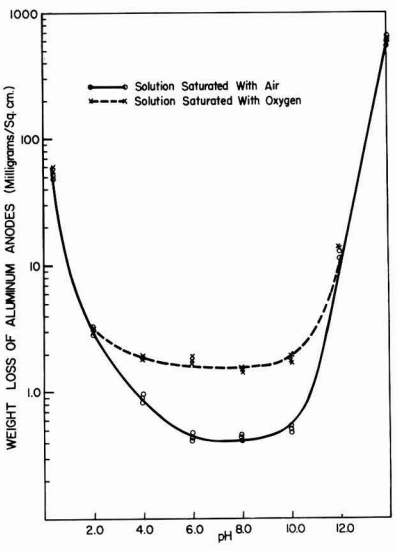

Fig. 4. Effect of pH on the weight loss in 96 hr of Al anodes in solutions saturated with air and oxygen at 25°C. See caption Fig. 2.

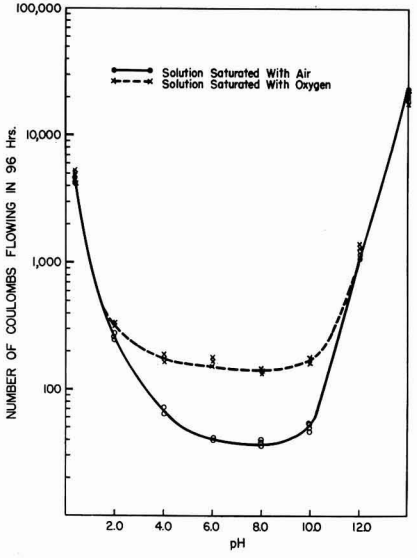

Fig. 5. Effect of pH on the number of coulombs flowing in 96 hr in solutions saturated with air and oxygen at 25°C. See caption Fig. 2.

Table II. Effect of saturation with different gases on galvanic corrosion of the Al-steel couple in 1.0*N* NaCl

Gas environment	pH	No. of coulombs flowing	Galvanic wt loss of Al anode, mg/cm²	Total Al wt loss, mg/cm²	Al wt loss due to local action, mg/cm²
Helium	6.0	6; 4	0.05; 0.04	0.07; 0.04	0; 0.02
Air	6.0	42; 41; 42	0.4; 0.4; 0.4	0.5; 0.4; 0.5	0.1; 0.1; 0.05
Oxygen	6.0	170; 166; 187	1.6; 1.6; 1.8	1.8; 1.8; 1.9	0.2; 0.2; 0.1

by observation of the time at which the boundary disappeared. The times required for reductive dissolution of the thermal oxide films at different *p*H values are shown in Table III.

Discussion

This investigation shows that steel is cathodically protected by coupling to high-purity Al, not only in nearly neutral chloride solutions as was shown previously (1), but over the entire *p*H range. The galvanic current flow (Fig. 5) and the weight losses of the Al anodes (Fig. 4) are strongly *p*H dependent and follow the same general trend as the weight loss variation of uncoupled Al specimens with *p*H (Fig. 3).

Neither the galvanic current flow nor the anodic weight losses are affected significantly by saturation with different gases at high and at low *p*H values (Fig. 4, 5, 7). Consequently the cathodic reaction occurring on the steel cathodes at these *p*H values must be primarily the evolution of gaseous hydrogen.

Within the *p*H range of 4.0-10.0 both galvanic current flow and anodic Al weight losses are strongly dependent on dissolved oxygen concentration. Saturation of the solutions with dissolved oxygen increases galvanic current flow by a factor of approximately five over that obtained in solutions saturated with dissolved air (Fig. 5 and 7). These results support the previous contention (1) that the primary cathodic reaction on steel cathodes in nearly neutral solutions is the reduction of dissolved oxygen in solution. The over-all galvanic corrosion within this *p*H range is controlled by the rate at which dissolved oxygen can diffuse from the bulk of the solution to the cathode surface. Clearly from Fig. 7 this is controlled to a considerable degree by the oxygen content of the gas above the solution.

Removal of most of the dissolved oxygen from nearly neutral solutions by saturation with He reduces the galvanic current flow virtually to zero (Fig. 6, Table I). Since the reduction of dissolved oxygen can no longer occur, the primary cathodic reaction must now be the evolution of hydrogen.

Table III. Effect of *p*H on time required for reductive dissolution of first order red oxide films on steel coupled to Al

*p*H	Time for reductive dissolution
0.20	1 sec
2.04	12 sec
4.00	1 day
6.15	Incomplete reduction after 4 days
7.95	Incomplete reduction after 4 days
9.95	2 days
12.00	1 day
14.00	5 sec

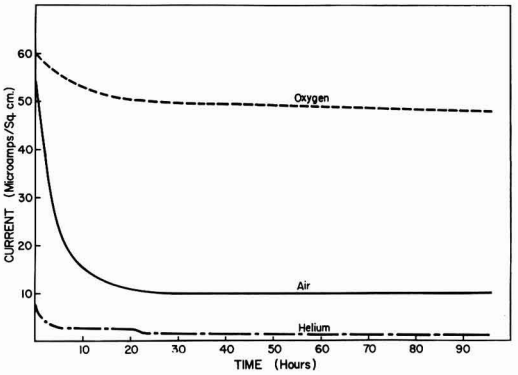

Fig. 6. Relationship between galvanic current flow and time in normal NaCl (pH 6.0) solution saturated with air, oxygen, and helium at 25°C.

Previous work (6) showed that, at potentials in the region of −0.5 to −0.6 v, the cathodic evolution of hydrogen from a steel surface is an extremely sluggish process and is highly polarized. High cathodic polarization of hydrogen evolution at potentials within the range −0.5 to −0.6 v therefore accounts for the very low values of galvanic current (Fig. 6) in nearly neutral solutions containing very little dissolved oxygen.

Figure 8 shows the relationship between the potential of the couple and *p*H. Potential is roughly constant up to *p*H 10. Consequently local action weight loss (Table I) is also roughly constant up to this *p*H. At higher *p*H values the potential of the

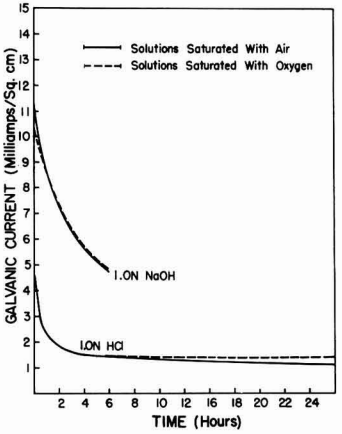

Fig. 7. Relationship between galvanic current-flow and time in normal NaOH and HCl solutions saturated with air and oxygen at 25°C.

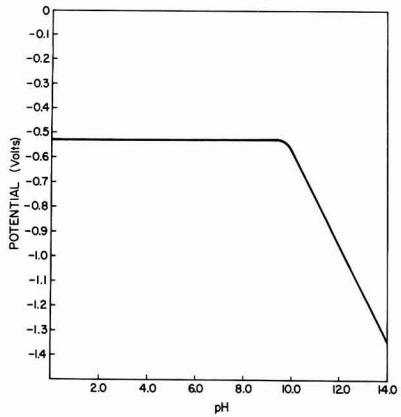

Fig. 8. Effect of pH on closed-circuit potential of the Al-steel couple at 25°C.

couple becomes less noble. Local cathodes on the Al anode should become even more active and so weight loss due to local action increases (Table I). Figure 8 closely parallels the relationship between the corrosion potential of uncoupled Al and pH. Therefore it is apparent that the closed-circuit potential of the galvanic couple is controlled by the corrosion potential of the Al anode. The rate of galvanic corrosion, therefore, is controlled by the current that can be drawn from a steel cathode at the potential of the Al anode.

At pH values up to and including 2.0 and above 12.0, hydrogen is visibly and rapidly evolved from steel cathodes. The presence or absence of dissolved oxygen has no significant effect on the rate of galvanic corrosion. Therefore the steel cathodes within these pH ranges may be considered to be hydrogen electrodes operating at essentially atmospheric pressure of hydrogen. Table IV shows a calculation of the reversible potential for hydrogen evolution as a function of pH within the range where this particular cathodic reaction occurs. Also shown in Table IV is the actual potential at which hydrogen evolution is observed on the steel cathodes (from Fig. 8) and the difference between the two values.

At pH values of 0.2 and 14.0 the difference between the reversible hydrogen potential and the measured potential (Table IV) is much greater than the hydrogen overpotential on steel (0.17 v) (7). Therefore hydrogen evolution from steel cathodes at pH values of 0.2 and 14.0 should be a very easy process. The difference between the reversible hydrogen potential and the measured potential at pH values of 2.0 and 12.0 is less and is more comparable with the hydrogen overpotential on steel; accordingly evolution of hydrogen from steel should be more difficult at these pH values. This general trend is well illustrated in the galvanic results contained in Fig. 4 and 5.

Table IV. Reversible and measured potential of H_2 evolution from steel cathodes

pH	Reversible hydrogen electrode potential,* v	Actual potential of hydrogen evolution, v	Potential difference between two reactions, v
0.2	—0.01	—0.53	0.52
2.0	—0.12	—0.53	0.41
12.0	—0.71	—0.97	0.26
14.0	—0.83	—1.34	0.51

* At 760 mm pressure of hydrogen.

At pH values within the range 4.0 to 10.0 hydrogen evolution is not the primary cathodic reaction on steel cathodes except when the solutions are deaerated. Instead oxygen dissolved in solution will be reduced cathodically according to an equation of the type

$$2H^+ + \tfrac{1}{2}\,O_2 + 2e = H_2O \qquad [1]$$

The E_o value for this reaction is +1.27 v (8). The E_o value corrected for oxygen concentration may also be calculated as a function of pH and compared with the measured potential at which oxygen reduction occurs. Calculation shows that the difference between the two values is also pH dependent and is at a minimum at pH 10.

However, the rate of reduction of dissolved oxygen at a steel cathode will be controlled primarily by the rate at which oxygen diffuses from the bulk of the solution to the cathode surface (1). This rate depends, with the same geometric electrode configuration, on oxygen solubility, temperature, and solution movement. In the galvanic experiments described earlier these variables, with the exception of dissolved oxygen concentration, were held constant. Dissolved oxygen concentration was held constant initially at two levels. Therefore, rate of oxygen depolarization within the pH range of 4-10 should be roughly constant at any one of the two levels of dissolved oxygen concentration. Reference to the galvanic results in Fig. 4 and 5 shows that this is in fact true. Both the weight losses of Al anodes and galvanic current flow are roughly constant when the solutions are initially saturated with dissolved oxygen. Galvanic current flow is somewhat increased at pH 4.0 in solutions initially saturated with air presumably because some hydrogen evolution occurs in these experiments.

During the previous investigation of the Al-steel couple in NaCl solutions it was noticed that the current-time curves were somewhat erratic (1). This same behavior was noticed in this investigation in solutions falling within the pH range of 4.0-10.0. Current-time curves at higher and lower pH values changed in an extremely smooth and highly reproducible manner. In order to understand this behavior it is necessary to consider in more detail the nature of the cathodic reactions occurring on a steel surface at nearly neutral pH values.

When the steel is first immersed in the solutions it is covered with a film of γ-Fe_2O_3 some 50-100 Å thick. This film either may remain stable or may be thinned uniformly and later removed entirely by reductive dissolution to soluble ferrous ions according to the equation (9):

$$Fe_2O_3 + 6H^+ + 2e = 2Fe^{++} + 3H_2O \qquad [2]$$

Table III contains information concerning the stability of somewhat thicker oxide films on steel

specimens coupled to Al anodes at different pH values. It may be seen that, in solutions having pH values of 2.0 and lower and also 12.0 and higher, reductive dissolution of oxide films on steel occurs quite rapidly. Therefore during the galvanic experiments within these two pH ranges evolution of hydrogen is taking place from film-free steel.

It was known previously that iron oxide films were readily reduced to soluble ferrous ions at low pH (5). However rapid reductive dissolution of iron oxide films at pH 14.0 has not been observed previously. Oswin and Cohen (10) reported reductive dissolution of α-Fe_2O_3 films at current densities of 30 $\mu a/cm^2$ in deaerated solutions at pH 11.9. Evidently as the cathodic current density is greatly increased, reductive dissolution of iron oxide films can be achieved at even higher pH values. Normally solutions must be well deaerated to observe reductive dissolution of iron oxide films at high pH since otherwise the reduction of dissolved oxygen is the preferred cathodic process (5). This suggests that, in the present galvanic experiments, a good degree of deaeration is achieved in the vicinity of the steel cathodes within the pH range 12.0-14.0 by the very vigorous evolution of hydrogen.

Table IV shows that the oxide film on a steel cathode remains either unreduced or is only slowly reduced within the pH range 4-10. Therefore, reduction of dissolved oxygen at a steel cathode coupled to an Al anode occurs on the surface of a γ-Fe_2O_3 film rather than on the steel itself. Similar conditions were achieved during the application of constant impressed currents of the order of 20 $\mu a/cm^2$ to oxide covered steel cathodes in nearly neutral chloride solutions (4). Here the current was held constant and the potential of the cathode measured. The potential-time curves were extremely erratic and moved slowly in the noble direction. This suggested a process of film breakdown and repair, with film repair gradually attaining the upper hand. In the present investigation the potential of the cathode remained roughly constant and so the current could vary, provided conditions on the cathode were not constant. The same sequence of local film breakdown (due either to undermining or to highly localized reductive dissolution) and repair due to oxygen in solution should also occur in the present galvanic experiments in the nearly neutral pH range. Since the potential is roughly constant this should result in fluctuation of the galvanic current. This is in fact observed within the pH range 4-10.

At higher and lower pH where the oxide film is rapidly reduced, the steel cathode remains in the bare condition probably throughout the experiment. When the condition of the steel cathode remains constant in this manner the galvanic currents do not fluctuate in an erratic manner with time.

This implies that the mechanism of cathodic protection of a steel cathode by an Al anode is pH dependent. At high and low pH where any pre-existing oxide film on the steel is dissolved reductively, protection must be the result of depression of its potential to a value where it is difficult, on thermodynamic consideration, for iron ions to leave the metallic lattice.

In the intermediate pH range, protection of the steel cathode results largely from the thickening of the original air-formed oxide film (4) despite the fact that local breakdown of the film occurs periodically. In this connection it is significant that the potential of a steel cathode measured immediately after its contact with an Al anode had been broken is found to be ennobled by as much as 300-400 mv from its uncoupled value in the same solution (1). This noble value of potential slowly decays if the Fe remains uncoupled in the NaCl. This kinetic mechanism of cathodic protection of steel in the nearly neutral pH range (4), thus has many features common to the mechanism by which anodic inhibitors prevent the corrosion of steel (11). The action of the cathodic current is similar to that of the anodic inhibitor in that it reduces the rate at which iron ions leave the metallic lattice. This reduced rate of egress of iron ions permits the more effective adsorption of oxygen from solution onto the iron surface so that thicker and more protective films of γ-Fe_2O_3 may be gradually built up.

It is interesting to compare the relative behavior of high-purity Al and Zn as sacrificial anodes for steel in the nearly neutral pH range. Aluminum sacrificially protects steel by the kinetic mechanism outlined above. However, the potential of the Zn-steel couple is some 250 mv less noble than that of the Al-steel couple despite the fact that the galvanic currents are quite similar (1). At these less noble potentials any oxide film on the steel cathode is rapidly reduced (4). Consequently a Zn anode must protect steel cathodically in the neutral pH range by the same mechanism by which Al protects steel at very high and low pH. Current-time curves for the Zn-steel couple in NaCl solution are therefore much less erratic than those for the Al-steel couple (1). It is implicit that any comparison of the relative efficiencies of Al and Zn sacrificial anodes in the nearly neutral pH range should take account of the fact that the mechanism by which the two metals protect steel is different.

Acknowledgment

The authors wish to thank the Kaiser Aluminum & Chemical Corporation for their support of this work and for their permission to publish the results.

Manuscript received Dec. 27, 1957. This paper was prepared for delivery before the Ottawa Meeting, Sept. 28-Oct. 2, 1958.

Any discussion of this paper will appear in a Discussion Section to be published in the June 1959 JOURNAL.

REFERENCES

1. M. J. Pryor and D. S. Keir, *This Journal*, **104**, 269 (1957).
2. H. O. Forrest, B. E. Roetheli, and R. H. Brown, *Ind. Eng. Chem.*, **22**, 1197 (1930).
3. C. Edeleanu and U. R. Evans, *Trans Faraday Soc.*, **47**, 1121 (1951).
4. M. J. Pryor, *Nature*, **178**, 1245 (1956).
5. M. J. Pryor and U. R. Evans, *J. Chem. Soc.*, **1950**, 1259.
6. M. J. Pryor and M. Cohen, *This Journal*, **100**, 203 (1953).

7. J. A. V. Butler, "Electrocapillarity," p. 126, Methuen & Co., London (1940).
8. T. R. Camp, *J. New England Water Works Assn.*, **60**, 188 (1946).
9. M. J. Pryor, *J. Chem. Soc.*, **1950**, 1274.
10. H. G. Oswin and M. Cohen, *This Journal*, **104**, 9 (1957).
11. M. J. Pryor, *ibid.*, **102**, 163 (1955).

Local Cell Action During The Scaling of Metals, II (1)

Christa Ilschner-Gensch[1]

Department of Metallurgy, Massachusetts Institute of Technology, Cambridge, Massachusetts

ABSTRACT

If nickel is covered by a borate melt under an oxygen atmosphere, practically no oxidation takes place. If, however, the nickel sample is in electrical contact with an electronic conductor, e.g., a noble metal gauze, which extends up to the melt-oxygen interface, nickel is attacked rapidly by virtue of local cell action. In this case, electron transfer is accomplished by the metal gauze and ions migrate through the borate melt. Electrochemical measurements show that the reaction is controlled mainly by polarization of the cathode where oxygen molecules are reduced to ions.

The oxidation of nickel to nickel oxide proceeds according to the over-all reaction

$$Ni(s) + \tfrac{1}{2} O_2(g) = NiO(s) \qquad [1]$$

If a dense oxide film is formed, as in this case, the oxidation can advance only by diffusion of the reactants across the oxide film to each other. It has been suggested (2) that the migrating particles are ions and electrons rather than atoms. In the nickel oxide, the electronic conductivity prevails, and therefore the oxidation rate is determined essentially by the ionic conductivity of the oxide. The rate constant for the nickel oxidation at 780°C and 0.1 atm O_2 partial pressure has been determined by different authors (3) to be $k = 10^{-12} - 10^{-11}$ g^2 cm^{-4} sec^{-1} for specimens of different purity.

When Ni is covered by a borate melt, oxidation can take place only inasmuch as oxygen dissolves in the borate melt and diffuses from the outer surface of the melt to the metal-salt interface. The relatively low solubility of oxygen molecules in a borate melt results in a low transport rate and, accordingly, in a low rate of oxidation. If, however, Ni is in electrical contact with an electronic conductor, e. g., Pt extending to the melt-gas interface, the rate of attack will be higher owing to local cell action as shown schematically in Fig. 1 and confirmed by the experiments reported below.

Rate Measurements

In order to investigate the corrosion of Ni under a borate melt, a spiral of Ni wire of 0.068 cm diameter and 20 cm length having a geometrical surface area of 4.3 cm^2 was placed in a porcelain crucible and covered with a dehydrated mixture of 65M % $Na_2B_4O_7$ and 35M % $K_2B_4O_7$, which has a eutectic melting point of 666°C (4). The molten salt had a depth of about 0.3 cm. The crucible, 1.4 cm in diameter at the bottom, was introduced on a support into an electrical furnace preheated to 780°C under N_2 (Fig. 2). After 10-15 min, oxygen was admitted. The amount of attack after periods ranging from 30 to 1560 min was determined by measuring the weight loss of the Ni sample after dissolving the solidified borate melt in water. The observed weight

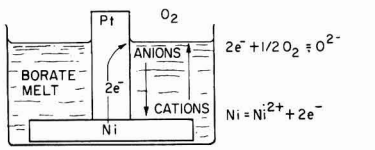

Fig. 1. Local cell action in a cell involving a Ni-Pt couple in a borate melt.

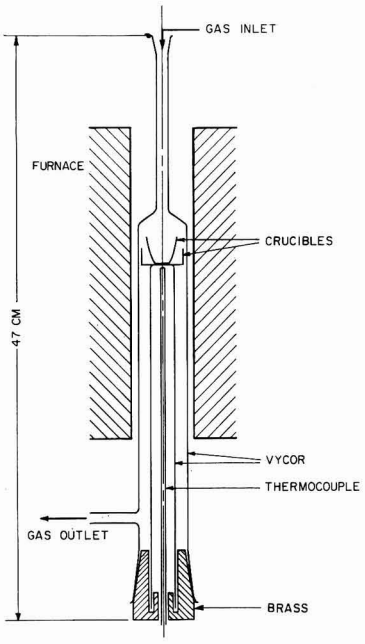

Fig. 2. Set-up for rate measurements

[1] Present address: Zentralforschungsanstalt Fried. Krupp, Essen, West Germany.

Table I. Weight losses of nickel and copper in a borate melt at 1 atm O_2 pressure and 780°C

Sample	Time, min	Weight loss, mg
Ni	60	0.1; 0.2; 0.0
Ni	1560	0.2
Ni-Pt couple	60	9.0; 7.1; 10.9
Ni-Ag couple	60	17.5; 10.0; 13.3
Cu	60	0.0
Cu-Pt couple	60	22.3; 21.8
Cu-Ag couple	60	38.0; 41.5; 35.0
Ni-Pt couple + 1% FeO	60	24.5; 23.1; 26.9

losses shown in Table I did not exceed 0.2 mg which is the limit of error.

Next, the behavior of gauzes of Ag and Pt partially immersed in the borate melt under oxygen was investigated. No appreciable weight changes were found, even after 18 hr.

In order to investigate the behavior of couples consisting of Ni wire and a gauze of Ag or Pt, a piece of noble metal gauze 2.5 cm x 4.5 cm was welded to a nickel spiral and rolled together as shown in Fig. 3. From the dimensions, the metallic surface per square centimeter gauze was estimated to be 2.24 cm^2 for the Ag gauze and 1.29 for the Pt gauze. Composite samples with Ni completely immersed and the noble metal gauze partly in the melt were tested as described above. After dissolving the major portion of the borate in water, there remained some greenish material which was dissolved by agitating the sample in another crucible filled with borate melt over a Bunsen burner for 2 min. As shown in Table I, the resulting weight losses of the composite samples are considerably greater than those of Ni samples without a gauze of Ag or Pt. Similar results were obtained with Cu couples, see Table I. Additional experiments with Ni-Pt composite samples were carried out, in which the noble metal did not extend through the surface but was also completely immersed. No weight loss was observed. This rules out as an explanation the assumption of a high oxygen overpotential at nickel or nickel oxide surfaces as being rate limiting in the first-mentioned experiments.

Significantly higher oxidation rates were observed on adding $FeSO_4$ corresponding to 1 wt % FeO in the presence and likewise in the absence of an electronic conductor. In this case Fe^{2+} ions may be oxidized to Fe^{3+} ions by molecular oxygen near the gas-electrolyte interface, the trivalent iron ions may diffuse toward the platinum-electrolyte or the nickel-electrolyte interface, respectively, where they are reduced to the divalent state, and Fe^{2+} ions may diffuse backward toward the gas-electrolyte interface.

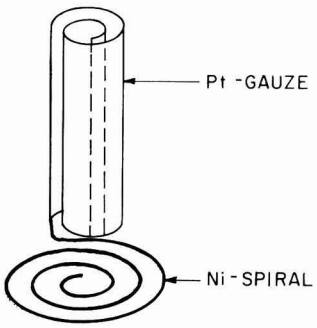

Fig. 3. Pt-Ni couple used for rate measurements

For a comparison, the rate of oxidation of Ni samples as used above under 1 atm oxygen partial pressure was determined. Weight increases from 0.8 to 0.9 mg, corresponding to loss of 3 mg Ni after 1 hr, were observed.

Measurements of Open Circuit Potentials

The open-circuit potentials of Ni-Ag, Ni-Au, and Ni-Pt couples in a borate melt under air were determined by immersing wires of Ni and Ag, Au, or Pt in a borate melt. The potentials were initially low, increased with time, and finally reached steady-state values after about half an hour. Values are shown in Table II. The potentials observed for the Ni-Au and the Ni-Pt couple are close to the equilibrium potential of the galvanic cell

$$\mathrm{Ni(s), NiO(s) \mid borate\ melt \mid oxygen\ electrode} \quad \text{(I)}$$

involving the virtual cell reaction

$$\mathrm{Ni(s) + \tfrac{1}{2}\, O_2\ (g,\ 0.21\ atm) = NiO(s)} \quad [2]$$

on passing two faradays. From data reported by Kiukkola and Wagner (5) the emf of cell (I) at 780°C is calculated to be 0.71 v. Since this value is close to the open-circuit potential of the Ni-Au and the Ni-Pt couple, it may be concluded that in these couples the Ni electrode is essentially a reversible Ni-NiO electrode in spite of the presence of oxygen, and the noble metal electrode essentially a reversible oxygen electrode. The lower open-circuit potential of the Ni-Ag couple of about 0.49 v suggests that the potential of the Ag electrode is a mixed potential resulting from the simultaneous reactions

$$\tfrac{1}{2}\, O_2 + 2e^- = O^{2-} \quad [3]$$

$$2Ag^+ + 2e^- = 2Ag \quad [4]$$

Likewise, the open-circuit potentials of Cu-Pt, Cu-Au, and Cu-Ag couples in a borate melt under air were determined (see Table II). In view of data reported by Kiukkola and Wagner (5), the emf of the cell

$$\mathrm{Cu(s), Cu_2O(s) \mid borate\ melt \mid oxygen\ electrode} \quad \text{(II)}$$

is estimated to be 0.45 v if the difference in the composition of the melt on the left-hand and the right-hand side of the cell is disregarded. This value

Table II. Open-circuit potentials E of Ni-Pt, Ni-Au, Ni-Ag, Cu-Pt, Cu-Au, and Cu-Ag couples in a borate melt under air at 780°C

Couple	E, v
Ni-Pt	0.73
Ni-Au	0.74
Ni-Ag	0.49
Cu-Pt	0.47
Cu-Au	0.40
Cu-Ag	0.28

is not far from the potentials of 0.47 and 0.40 v observed for the Cu-Pt and the Cu-Au couple, respectively, although the melt next to the Cu electrode supposedly was not saturated with Cu_2O. Accordingly, the activity of Cu_2O was less than unity, and elemental oxygen was not excluded. The potential observed for the Cu-Ag couple is considerably lower for reasons mentioned above for the Ni-Ag couple.

Polarization Measurements

The current I in a short-circuited cell involving a Ni and a Pt electrode as used in the rate measurements is related to the emf E as driving force by the equation

$$E = \Delta E_c(I) + \Delta E_a(I) + IR \qquad [5]$$

where ΔE_c and ΔE_a, respectively, are the absolute values of the polarization of the cathode and anode at current I, and R is the resistance of the electrolyte. The conductivity of the K-Na borate melt may be assumed to be equal to that of molten $Na_2B_4O_7$, which is 0.22 ohm^{-1} cm^{-1} (6). The current equivalent to a weight loss of 10 mg Ni/hr is 0.01 amp. Thus the IR drop is estimated to be of the order of 0.01 v, which value is much less than the available driving force E in Eq. [5]. Hence, the current is controlled mainly by polarization.

To determine the value of ΔE_c accounting for polarization of the cathode, a cell involving three Pt electrodes was assembled. The cathode was a Pt gauze of the same dimensions used for the rate measurements. A ring of Pt wire as anode was located at the bottom of the porcelain crucible. In addition, there was a short Pt wire as reference electrode sidewise to the cathode. The crucible was placed in a Vycor tube with closed lower end and flushed with oxygen. The potential was predetermined with the help of a potentiometer, and the resulting current as well as the polarization potential of the cathode vs. the reference electrode was measured by a galvanometer and a tube voltmeter, respectively. The results are shown in Fig. 4. The polarization ΔE_c of the cathode is considerable and amounts to approximately 0.5 v at a current of 0.002 amp. Extrapolation of a logarithmic plot yields $\Delta E_c = 0.7$ v for $I = 0.01$ amp.

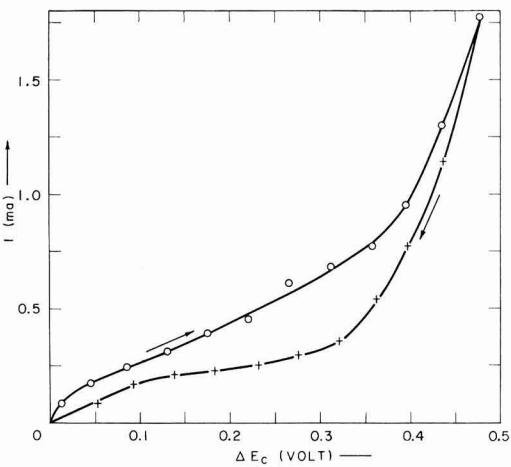

Fig. 4. Current I vs. polarization ΔE_c of a Pt gauze as cathode in a borate melt under oxygen for increasing and decreasing values of the applied potential.

The polarization ΔE_a of a Ni anode of the same size as used in the rate measurements and covered by a borate melt was determined in a similar way. In this case, the polarization ΔE_a was measured for a current $I = 0.01$ amp applied during 1 hr. Values of ΔE_a ranging from 0.005 to 0.02 v were observed. Although results were not well reproducible, these observations indicate that the term ΔE_a in Eq. [5] is only minor.

In view of the foregoing results, it can be concluded that the current in a Ni-Pt couple is controlled mainly by polarization of the cathode at which oxygen molecules are reduced to ions. The essentially exponential shape of the curves especially for higher potentials seems to indicate a large contribution of activation polarization. The same holds supposedly for a Cu-Pt couple.

Observations on the Wettability of Ag, Au, and Pt by a Borate Melt

At present, the individual contributions of activation and concentration polarization of a Pt electrode at which oxygen is reduced cathodically are not known precisely. Possibly concentration polarization also plays some part under the conditions employed in this research because the electrolyte was not stirred. Preliminary calculations suggest that diffusion of oxygen molecules from the gas-electrolyte interface to the portion of the cathode immersed in the melt is not sufficient in order to account for a current of 0.01 amp. Instead, the predominant mechanism of oxygen supply may be diffusion of oxygen molecules across a thin adherent layer of the borate melt wetting the Pt gauze above the general level of the melt. Subsequent migration of oxygen ions parallel to the Pt surface will be limited by resistance of the electrolyte forming the adherent layer. As a result of this, cathodic action at the Pt-electrolyte interface will be restricted to an area the height of which may be smaller than that of the adherent layer. The experimental evidence, in accordance with theoretical estimates, indicates that this is nevertheless sufficient to account for the currents observed.

The occurrence of an adherent layer of the melt on the electrodes is suggested by available observations (7), especially by recent observations by von Wartenberg (8) and Fulrath, Mitoff, and Pask (9). To obtain pertinent information for the borate melt used in the above experiments, small chunks of the solidified melt were placed on sheets of Ag, Pt, and Au in air in a tubular furnace heated to 780°C. With the help of a telescope, it was found that the borate melt spread readily on Ag and Pt, whereas in the case of Au a finite although small contact angle was observed. Thus the occurrence of an adherent layer of borate melt on Ag and Pt has been ascertained, and migration of oxygen molecules across such a layer is suggested tentatively as a mechanism accounting for relatively rapid transfer of oxygen

from the gas phase to the electrode made a cathode. Further experimental work beyond the scope of the present investigation is required in order to test this hypothesis.

Concluding Remarks

The above results are of interest in conjunction with the catastrophic oxidation (10-12) of alloys under conditions where the scale consists of one or several solid oxides and a liquid phase. In this case, ionic conduction may take place in the liquid phase and electronic conduction in the solid oxides. The rate may be controlled by the cathodic reduction of molecular oxygen as in the experiments reported above. Possibly, the rate of oxidation may be even greater than in the foregoing experiments because the solid oxides may form a sponge involving numerous pores filled with liquid phases whereby a large cathodic area is provided. Local cell action may account for relatively high oxidation rates even without the occurrence of different valence states of elements such as iron or vanadium, but presence of such elements may lead to an even higher rate.

Acknowledgment

The author would like to thank Professor Carl Wagner for his continuous advice and interest during this investigation. The work was sponsored by the U. S. Atomic Energy Commission under Contract AT(30-1)-1903.

Manuscript received Jan. 20, 1958.

Any discussion of this paper will appear in a Discussion Section to be published in the June 1959 JOURNAL.

REFERENCES

1. C. Ilschner-Gensch and C. Wagner, *This Journal*, **105**, 198 (1958).
2. C. Wagner, *Z. phys. Chem.*, **B21**, 25 (1933).
3. K. Hauffe, "Oxydation von Metallen und Metallegierungen," pp. 151-155, Springer-Verlag (1956).
4. A. G. Bergmann and I. N. Nikonowa, *J. allgem. Chem. USSR*, **12**, 449 (1942).
5. K. Kiukkola and C. Wagner, *This Journal*, **104**, 379 (1957).
6. B. Stalhane, *Z. Elektrochem.*, **36**, 404 (1930).
7. J. J. Bikerman, *J. Colloid Sci.*, **11**, 299 (1956).
8. H. von Wartenberg, *Angew. Chem.*, **69**, 258 (1957).
9. R. M. Fulrath, S. P. Mitoff, and J. A. Pask, *J. Am. Ceram. Soc.*, **40**, 269 (1957).
10. A. de S. Brasunas and N. J. Grant, *Trans. A.S.M.*, **44**, 1117 (1952).
11. A. de S. Brasunas, *Corrosion*, **11**, 1 (1955).
12. K. Hauffe, "Oxydation von Metallen und Metallegierungen," pp. 211-214, Springer-Verlag (1956).

The Mechanism of Passivating-Type Inhibitors

Milton Stern

Metals Research Laboratory, Electro Metallurgical Company, Division of Union Carbide Corporation, Niagara Falls, New York

ABSTRACT

All passivating-type inhibitors are oxidizing agents. However, not all oxidizing agents are inhibitors. A passivating-type inhibitor functions by producing local-action current which anodically polarizes a metal into the passive potential region and thereby provides the means for obtaining a noble mixed potential. This mechanism is independent of whether passivity is caused primarily by oxide or adsorbed films. The major factors which determine whether a particular system will exhibit passivity are: (*a*) reversible potential of the redox system created by the oxidizing inhibitor; (*b*) electrochemical parameters for reduction of the inhibitor on the metal surface (exchange current, Tafel slope, and limiting diffusion current), and (*c*) critical anodic current and Flade potential of the metal. If oxygen is present in the system, some chemicals may function by changing its reduction kinetics. It is further shown that the amount of inhibitor found associated with the surface is not necessarily related to adsorption. Data are presented for passivation of stainless steel and titanium. The mechanism is discussed in terms of various oxidizing agents including oxygen, chromate, molybdate, and pertechnetate.

In recent years, the most active research in the field of passivity has been concerned with the nature of surface layers believed to be primarily responsible for this phenomenon. In general, the approach has been to obtain some experimental data and interpret these in terms of that type of surface film which is most consistent with the observation. It is possible, however, to explain many observations qualitatively without the necessity of postulating any specific type of surface layer. This can be done with what is now known about the electrochemistry of passive systems. The purpose of this work is to describe the behavior of systems containing passivating-type inhibitors in terms of electrochemical parameters. It is recognized that a film of some type is primarily responsible for passivity, and this description permits one to determine whether a specific type of observation is pertinent

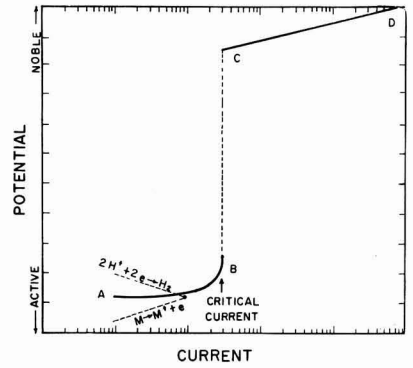

Fig. 1. Typical anodic polarization curve for metals which exhibit passivity, obtained by fixing the anodic current and measuring the potential.

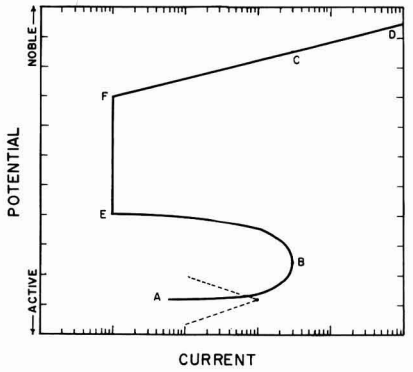

Fig. 2. Typical anodic polarization curve for metals which exhibit passivity, obtained by fixing the potential and measuring the current.

to differentiation between adsorption and oxide films.

General Electrochemical Concepts

For metals which exhibit passive behavior, it is well known that a material in the active state can be passivated by applying sufficient anodic current. Such observations have led to the concept of a "critical anodic current" for passivity. The measurement of this characteristic has proved very useful in explaining the effect of chromium on passivity of iron-chromium alloys (1). One method of obtaining this property, used by Uhlig and Woodside (1), involves applying increasing anodic currents to the metal in the active state and observing that current which creates a marked shift of potential in the noble direction. A schematic representation of the kind of polarization curve obtained is shown in Fig. 1. On the section of the curve labeled AB, the primary anodic (oxidation) reaction is solution of metal to form metal ions in a lower valent state. In the region labeled CD, the primary anodic reaction depends upon the environment but most often involves oxygen evolution. Polarization measurements of this type, which are obtained by adjusting anodic current and measuring potential, are not completely satisfactory. First, measurements along AB are very time-dependent, particularly in the region close to the critical anodic current. Thus, the critical current one measures is dependent on the time at a given current and the current increments one uses. In addition, no information on electrode behavior can be obtained in the potential region between B and C. It is important to understand what processes occur in this region since it may extend over a range of more than 1 v and plays an important role in passivity phenomena.

To overcome some of these difficulties, a different approach has been used to obtain anodic polarization measurements. This method involves fixing the potential of the sample and measuring the current. The type of polarization curve obtained is represented schematically in Fig. 2. As the potential is changed from the active corrosion potential to B, the measured current increases. As the potential is made more noble, the current drops markedly via the route BEF and then finally increases again along FCD.

Several investigators have shown anodic polarization curves of this type for Fe-Cr alloys (2-4) and austenitic stainless steels (5-7) in H_2SO_4 solutions. Such behavior is not limited to alloys; for example, similar observations have been made with Ni (8), Cr (9, 10), and Fe (11, 12). There is little doubt that other metals exhibit similar characteristics under appropriate conditions. Thus, Fig. 2 may be considered as a schematic representation of the anodic polarization behavior of a metal, originally in the active state, which is passivated by anodic current. While the features of this figure may not show all the characteristics of some real systems, it is sufficiently accurate to describe most observations and is general in nature. For the purposes of this discussion, the potential region between B and E, which is usually relatively small, will be called the Flade region. There is some question at present as to whether the line between these points exhibits a finite slope or whether B and E are actually the same potential. Most experimental observations indicate that there is a real difference. The potential at point E will be called the Flade potential or the critical anodic potential, and it is considered that this potential divides the electrochemical behavior of the metal into active and passive states.

If one determines the various electrode processes which occur in the different sections of the polarization curve of Fig. 2, the following observations are made. In the potential range from A to B, the primary oxidation reaction is solution of metal to form ions in a lower valent state. The rate of this process increases from A to B. In the range from B to E, the rate of metal solution decreases markedly and finally reaches a low constant value from E to F. In this region, analysis of the solution reveals that the corrosion products are in a higher valent oxidation state. For example, if the metal contains Fe and Cr, both ferric and dichromate ions are produced in the passive region, whereas ferrous and chromic ions are corrosion products in the active region AB. The processes which occur along the polarization curve FCD depend upon both the metal and the environment. For example, in H_2SO_4 at a

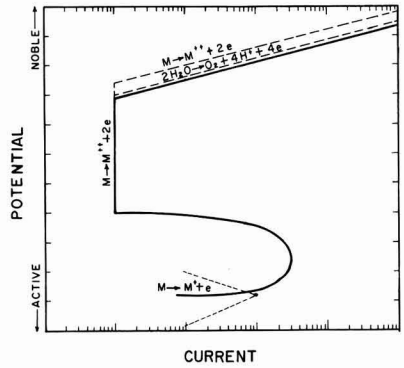

Fig. 3. Anodic polarization curve showing major oxidation reactions which occur in various potential regions.

potential more noble than the equilibrium oxygen electrode potential, oxygen evolution will be one of the primary oxidation reactions. However, metal solution still occurs and generally proceeds at a rate higher than that which exists along EF. Thus, the polarization region FCD represents the summation of more than one electrode process. At any potential along this curve, the current measured is equal to the sum of the current equivalent to oxygen evolution and the current equivalent to metal oxidation. Therefore, Fig. 2 can be changed to include the individual polarization curves of the various electrode processes which occur. This is done in Fig. 3. The two dashed lines show the current equivalent to the individual rates of metal dissolution and oxygen evolution, and the solid line represents the sum of these two processes.

Passivating Inhibitors

Mechanism of Passivating Inhibitors

Since Fig. 3 shows the rate of metal solution as a function of potential, any phenomenon which will produce a metal potential more noble than the Flade potential will create passivity. This can be accomplished by external anodic polarization as already described. There are other possibilities, however, and the question arises as to the mechanism of passivation of various inhibitors. Uhlig and Cobb (13) have shown that ferric and cupric ions inhibit Ti in H_2SO_4 and HCl and proposed that these ions function by adsorption on the metal surface with accompanying satisfaction of surface valences. To support this proposal, Uhlig and Geary (14) measured the potential of Ti and stainless steel in $0.2N$ H_2SO_4 as a function of ferric and cupric ion concentration. They assumed that the change in potential produced by inhibitor addition was the result of dipoles created at the surface by adsorbed ions and showed that their data appeared to follow a Langmuir isotherm. They also reported similar data for Fe in distilled water passivated with chromate ions. Okamoto, Nagayama, and Mitani (15), stimulated by this concept, repeated the work with Fe in chromate solutions and came to a different conclusion. They found that a critical chromate concentration exists where the potential shifts markedly in the noble direction, accompanied by a sudden drop in corrosion rate. They further showed that the passive potentials were mixed potentials, the values of which were determined by local polarization phenomena. It is quite reasonable to consider passive potentials in the light of the mixed potential theory originally treated by Wagner and Traud (16) and described in some detail by Stern (17). This concept can be used to explain many observations of the behavior of passivating inhibitors.

Consider, for example, stainless steel in an environment such as air-free dilute H_2SO_4 where the sample corrodes and is active. Further, consider that the anodic polarization characteristics are as illustrated in Fig. 3. If an oxidizing agent is added to the solution, an oxidation-reduction system now exists with a noble reversible potential. The oxidized species of this redox system can now be reduced on the metal surface with accompanying polarization. Since the mixed potential of the metal occurs at that potential at which the sum of the rates of all the reduction reactions equals the sum of the rates of all the oxidation reactions, a new mixed potential results from the addition of the oxidizing agent. The reversible potential and typical polarization characteristics of the redox system are illustrated in Fig. 4 along with the anodic polarization behavior of the metal. The new mixed potential is also shown. Note that now the potential is in the passive region and that the rate of solution of metal is considerably lower than that which exists at the active potential. Reduction of the oxidizing agent now constitutes the major cathodic reaction. Thus, an oxidizing agent creates passivity by producing local-action current which anodically polarizes the metal into the passive region. There are several features of this concept which warrant detailed discussion in order to show how this mechanism predicts certain characteristics of passive systems and to provide supporting evidence.

Nature of Passivating Inhibitors

The picture presented above indicates that any oxidizing agent which creates a sufficiently noble redox potential should create passivity if the metal exhibits the anodic polarization behavior illustrated

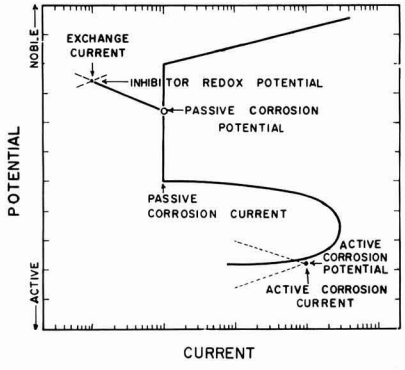

Fig. 4. Polarization diagram for a metal passivated by an oxidizing inhibitor.

in Fig. 3. To check this, seventeen readily available oxidizing agents were evaluated in regard to their ability to passivate Type 304 stainless steel in boiling 1 wt % H_2SO_4.[1] The results are shown in Table I, where it is evident that all were effective in producing a very marked decrease in corrosion rate when present in sufficient quantities. In this test, additions which contained chloride ions were carefully avoided because of the known effect of chloride in destroying passivity of stainless steels.[2] However, passivity of Ti is not particularly affected by chloride, and oxidizing agents can even passivate Ti in HCl. Therefore, tests similar to those described above were conducted with commercially pure Ti in boiling 1% H_2SO_4 and boiling 3% HCl. The results are presented in Table II. Here again, it is evident that all additions were effective in creating passivity when present in sufficient concentration. Thus, it has been demonstrated that twenty different oxidizing agents, including one organic addition, are inhibitors.[3] There appears to be little doubt that other oxidizing agents would behave in a similar manner under appropriate conditions. This is consistent with the description of the electrochemistry of passivity described above where an oxidizing addition is defined as one which produces a noble redox potential in the solution.

Figure 4 also indicates that the corrosion rate which exists when the metal is passivated with an oxidizing agent should be the same as that which occurs when the metal is passivated by anodic polarization to the same potential. Franck and Weil (18) have provided the evidence for this in studies of the passivity of Fe in H_2SO_4. The passive corrosion rate produced by either ceric ion or quinone has been shown to be essentially the same as that produced by anodic polarization.

[1] Tests were conducted in 1-l wide mouth Erlenmeyer flasks using finger-tip type condensers. Oxygen is probably not completely eliminated from the solution, although its concentration should be extremely low.

[2] Probably, chloride ion destroy passivity of stainless steels by markedly increasing the critical anodic current. As will be shown below, the critical anodic current is an important factor in determining whether stable passivity is possible.

[3] Potential measurements on similar systems showed that, in those cases where inhibition was obtained, passive potentials were also achieved.

Table I. Effect of various oxidizing agents on the corrosion of stainless steel in boiling 1% H_2SO_4

Oxidizing agent	Concentration, molar	Weight loss,* mdd
None	—	1150
$Fe_2(SO_4)_3$	0.01	2
$CuSO_4$	0.01	2
Ag_2SO_4	0.01	0
$HgSO_4$	0.01	0
$Ce(SO_4)_2$†	0.01	30
$KAu(CN)_2$	0.01	0
HNO_3	0.01	6110
HNO_3	0.1	1
$NaNO_3$	0.01	6030
$NaNO_3$	0.1	3
$NaNO_2$	0.01	1
$KMnO_4$	0.01	1
$Na_2Cr_2O_7$	0.01	2
Na_2MoO_4	0.01	0
Na_2WO_4	0.01	0
$NaIO_3$	0.01	1
$NaBrO_3$	0.01	15
$NaClO_3$	0.01	11
H_2O_2	0.1‡	0
Quinone	0.01	0

* 24-hr test using 500 ml of solution and approximately 20 cm^2 samples. A corrosion rate of 2 mdd is within the possible weighing error of these tests.
† Addition not completely soluble.
‡ 0.01*M* H_2O_2 decomposed too rapidly to maintain passivity.

Table II. Effect of various oxidizing agents on the corrosion of titanium in boiling 1% H_2SO_4 and boiling 3% HCl

Oxidizing agent	Concentration, molar	Weight loss in* 1% H_2SO_4, mdd	Weight loss in* 3% HCl, mdd
None	—	1130	670
$Fe_2(SO_4)_3$	0.01	0	—
$CuSO_4$	0.01	2	—
Ag_2SO_4	0.01	0	—
$HgSO_4$	0.01	0	—
$Ce(SO_4)_2$†	0.01	0	6
$NaNO_3$	0.01	1	2
$NaNO_2$	0.01	3	16
$KMnO_4$	0.01	0	1
$Na_2Cr_2O_7$	0.01	1	0
Na_2MoO_4	0.01	0	0
Na_2WO_4	0.01	0	0
Na_2IO_3	0.01	0	1
$NaBrO_3$	0.01	1	4
H_2O_2	0.1‡	0	12
Quinone	0.01	0	0
$HAuCl_4$	0.01	0	0
$PtCl_4 \cdot 2HCl$	0.01	1	3
$SnCl_4$	0.01	—	0
$HgCl_2$	0.01	—	1
$CuCl_2$	0.01	—	1
$FeCl_3$	0.01	—	1

* 24-hr test using 500 ml of solution and approximately 20 cm^2 samples. A corrosion rate of 2 mdd is within the possible weighing error of these tests.
† Addition not completely soluble.
‡ 0.01*M* H_2O_2 decomposed too rapidly to maintain passivity.

Effect of Concentration of Passivating Inhibitors

Two other frequently observed phenomena in passivity are consistent with the concept that passivating inhibitors function by producing local-action current which anodically polarizes the metal into the passive region. One is concerned with the fact that an inhibitor concentration higher than some critical value is necessary to produce stable passivity. Below this critical value, the oxidizing agent may actually accelerate corrosion. The other observation is concerned with the unstable nature of passivity when the inhibitor concentration is close to this critical value. In this instance, repeated tests under apparently the same circumstances sometimes lead to passivity and sometimes to an active state. The potentials and corrosion rates are quite different for the two conditions.

When the concentration of an oxidizing agent is changed, the reversible potential of the redox system created by the inhibitor in the solution is changed. Also, the exchange current of the redox system may change, depending on the kinetics of the process. Consider first the case where a change in concentration of oxidizing agent has no effect on exchange current and only changes the reversible potential. The polarization diagram showing how such a change affects the potential and corrosion rate is illustrated in Fig. 5. As the concentration

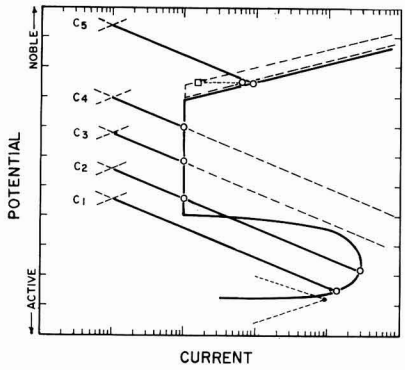

Fig. 5. Polarization diagram illustrating how a change in oxidizing agent redox potential affects corrosion current and corrosion potential.

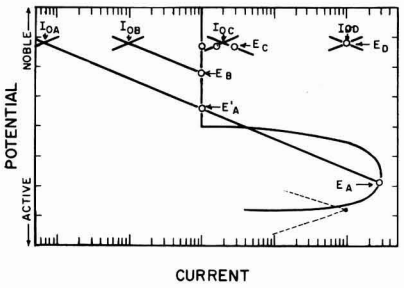

Fig. 6. Polarization diagram illustrating how a change in oxidizing agent exchange current affects corrosion current and corrosion potential.

of the oxidizing agent is increased from C_1 to C_5, the reversible potential becomes more noble in accordance with the Nernst equation. For the concentration C_1, the mixed potential is in the active region and the corrosion rate is increased. An example of this situation is shown in Table I where 0.01*M* nitrate additions to H_2SO_4 accelerated corrosion of stainless steel, whereas a 0.1*M* addition passivates. Concentration C_2 produces an interesting situation since there are two possible mixed potentials, that is, there are two potentials at which the sum of all the rates of oxidation equals the sum of all the rates of reduction. Which potential the metal assumes is dependent upon many intangible factors. However, the passive state is probably not very stable under these conditions. It is quite evident that appropriate conditions could exist where the metal will oscillate between the passive and active potential. It is possible that under these conditions introduction of active metal will produce an active potential, whereas if the metal is already passive, the noble potential will be evident. Concentrations C_3 and C_4 produce stable passivity, and the passive corrosion rate is independent of inhibitor concentration in this region.[4] Concentration C_5 also produces stable passivity although the corrosion rate is increased, as indicated by the square point on Fig. 5.[5] Note that in this case, the sum of the currents equivalent to the rate of metal dissolution and oxygen evolution equals the current equivalent to the rate of inhibitor reduction.

The exchange current of the redox system produced by the oxidizing addition also has a significant influence on behavior. For example, consider four different oxidizing agents added to an actively corroding system in appropriate concentrations necessary to produce the same redox potential. Further, consider that the oxidation-reduction kinetics for the redox systems are such that they exhibit markedly different exchange currents. This situation is shown in Fig. 6.

The system with a very low exchange current, labeled I_{OA}, produces unstable passivity with two possible mixed potentials as described above.

The system with the higher exchange current, I_{OB}, produces stable passivity. It is worth mentioning here that the conditions illustrated by this particular system are necessary in order to use an electrochemical method for measuring passive corrosion rates reported by Vetter (19). He found that the corrosion rate of passive Fe in concentrated HNO_3 can be determined electrochemically by polarizing the surface anodically to the potential of Pt in the same solution. The current required to polarize to the Pt potential is equivalent to the corrosion current. This can only be true if Pt exhibits the reversible redox potential of the environment and if the local anodic polarization curve for the metal is practically vertical. Also, since the applied anodic current required to polarize the passive metal to the reversible potential of the redox system is equal to the difference between the corrosion current and I_{OB}, the exchange current of the redox system on the passive surface should be much smaller than the passive corrosion current. If the passive corrosion potential is more than about 150 mv active to the reversible redox potential of the solution, the error in neglecting the exchange current will probably not be significant. This actually depends on the Tafel slope for reduction of the oxidizing agent on the passive surface. Thus, it is evident that this method of determining the passive corrosion rate can be applied only in special cases. For example, the system shown in Fig. 6, where the redox exchange current, I_{OC}, is somewhat greater than the passive corrosion rate, produces a metal potential only slightly more active than the reversible redox potential.[6] In this case, the anodic current required to polarize to the Pt potential will not be related to the corrosion rate. However, a method previously described (20) is useful here. If the oxidation-reduction kinetics of the redox system can be measured on the passive surface, then the local anodic polar-

[4] The corrosion rate of those metals which do not exhibit a Flade region will of course, increase continuously as the concentration of oxidizing agent is increased.

[5] Behavior in this region, where the metal solution rate again increases with potential, has been termed transpassivity and is an important part of the over-all passivity picture. However, this phenomenon is not pertinent to the present development and is not discussed in detail.

[6] For this condition, the rate of oxidation of the reduced species of the inhibitor becomes an important factor in determining the mixed potential. The three points in a horizontal row in Fig. 6 illustrate the fact that the mixed potential is that value at which the currents equivalent to oxidation of metal and oxidation of the reduced species of inhibitor equals the current equivalent to reduction of inhibitor.

ization curve of the metal can be determined in the region close to the passive potential. For example, it was shown that the local anodic polarization curve for Hastelloy alloy F in a ferric-ferrous chloride system was essentially vertical with a corrosion rate equivalent to only $0.02\mu a/cm^2$. This system is an ideal example of the case shown in Fig. 6 where the oxidizing agent exhibits an exchange current of I_{OC}.

In the case where the redox exchange current, I_{OD}, is much greater than the passive corrosion current, the metal exhibits the reversible redox potential. This has been observed experimentally for stainless steel in ferric-ferrous sulfate solutions (21) and in two other cases which will be described below. In this instance, one cannot determine the passive corrosion rate by electrochemical means. However, if the metal exhibits the same potential as the equilibrium redox potential, the corrosion current must be at least one order of magnitude less than the redox exchange current.[7]

Effect of Critical Anodic Current

There are several other tests which establish the validity of the concept that passivating inhibitors function primarily by creating local-action current which anodically polarizes the metal into the passive region. For example, this concept predicts that a metal with a high critical anodic current for passivity requires a greater critical concentration of oxidizing agent to produce stable passivity than a metal which exhibits a low critical anodic current. This is consistent with the data of Olivier (22) who measured the critical anodic current of Fe and Fe-Cr alloys in 10% H_2SO_4 at room temperature. In this environment, Fe exhibits a critical current of 1 amp/cm², whereas Type 304 stainless steel requires only 2.2 ma/cm² for passivity. It is well known that small additions of ferric ion or other oxidizing agents will passivate stainless steel in this environment, whereas similar additions (or much higher concentrations) accelerate the corrosion rate of iron. This principle is illustrated in Fig. 7.[8]

To obtain more quantitative data concerning the predicted effect of critical anodic current on the concentration of oxidizing agent required to passivate, measurements were conducted with commercially pure Ti in various concentrations of boiling H_2SO_4 containing 5% Na_2SO_4. Critical anodic current measurements were obtained by a method described by previous investigators (22, 23). This method involves polarizing the active metal with a fixed anodic current which is higher than the critical value. The potential of the sample is measured as a function of time as it passes from the active state to the passive state, and a critical time for passivity is selected. This is repeated for a number of anodic currents, and a plot is made of anodic current density as a function of the reciprocal of the time for passivity (t_p). The data fall on a reasonably straight line which is extrapolated to a value of $1/t_p$ equal to zero ($t_p = \infty$). This is considered the critical anodic current density which will produce passivity if one waits for an infinite time and, therefore, provides a convenient method for comparing different alloys or conditions. Measurements reported here were obtained with a Cary Model 31 Vibrating Reed Electrometer which drives a L&N adjustable span, adjustable zero recorder with a chart speed of 30 in./min and a full-scale pen speed of 1 sec. Current was supplied from a stable high-voltage power supply fed through high resistances to minimize current change when the sample becomes passive. The critical time for passivity was selected as the interval between the initial application of anodic current and time at the maximum slope of the potential-time curve. Potential-time curves were similar in shape to those shown by Olivier (22) except that the final passive potential assumed by Ti is considerably higher. Figure 8 shows plots of anodic current density as a function of $1/t_p$. It is evident that an increase in H_2SO_4 concentration increases the critical current for passivity.

To determine the effect of critical anodic current on the amount of oxidizing agent required to passivate Ti, known increments of $Fe_2(SO_4)_3$ were added to a cell in which Ti was active. The Ti potential was measured as a function of ferric ion concentration, the results of which are shown in Fig. 9. It is evident that the concentration of ferric ion required to produce a noble potential increases with increasing acid concentration in a manner similar to the increase in critical anodic current.

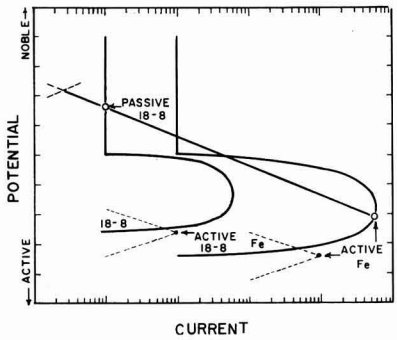

Fig. 7. Effect of critical anodic current on the behavior of passivating inhibitors.

[7] This is an important basic principle which applies not only to mixed potentials where corrosion may be involved, but also to inert electrodes which may exhibit a mixed potential in environments where more than one redox reaction can occur. Thus, Pt is a good indicating electrode for measuring the equilibrium potential of simple redox systems because exchange currents on Pt are usually very high. Side electrochemical processes which result from minor amounts of impurities occur at rates much lower than the exchange rate of the major redox process. Thus, the Pt potential is not significantly affected. However, Pt will exhibit a mixed potential if two or more major redox processes occur on the surface at rates of the same order of magnitude. For example, Pt in hydrogen-saturated 20% H_2SO_4 exhibits the reversible hydrogen electrode potential of -0.20 vs. saturated calomel. If the system is made $0.5M$ in ferric ion and $0.1M$ in ferrous ion, the Pt potential is $+0.50$. Finally, if the hydrogen gas is substituted by nitrogen, the Pt potential is unaffected. In this case, the exchange current for the ferrous-ferric redox system is considerably greater than the exchange current for the hydrogen electrode system so that Pt exhibits the reversible ferrous-ferric redox potential in the hydrogen-saturated solution. However, if the ferrous-ferric exchange current is reduced considerably by decreasing the ferrous ion concentration, then Pt exhibits a mixed potential. Thus, in the same acid with $0.5M$ ferric ion and no intentional addition of ferrous ions, the Pt is $+0.62$ v vs. saturated calomel with nitrogen passed through the solution but only $+0.58$ when the system is hydrogen saturated. These two potentials are reproducible upon alternately passing nitrogen and hydrogen through the acid.

It is probable that Pt does not function as an effective oxygen electrode because the exchange current for this redox system on Pt is relatively low.

[8] This schematic figure does not consider the fact that stainless steel in many environments becomes passive at considerably more active potentials than Fe. This is also consistent with passivation of stainless steel with considerably lower concentrations of oxidizing agent than are required for Fe.

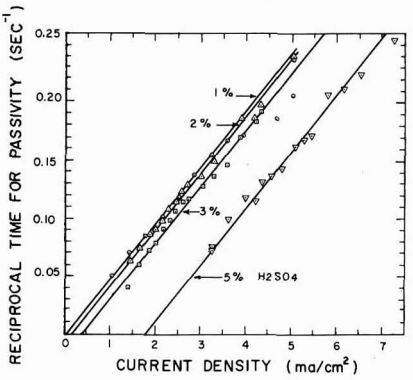

Fig. 8. Reciprocal of time for passivity as a function of applied anodic current for Ti in various concentrations of boiling H_2SO_4 containing 5% Na_2SO_4.

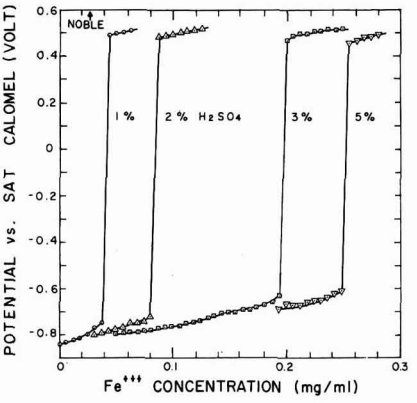

Fig. 9. The potential of Ti as a function of ferric ion concentration in boiling H_2SO_4 solutions containing 5% Na_2SO_4.

The potentials reported here are not final steady-state values, since this is an impossible condition to obtain in such a system. In the active region, the oxidizing agent is consumed in the corrosion process and thus the concentration changes with time. In the passive region, the potentials were stable and close to, but less noble than, Pt in the same solution. For ferric ion concentrations close to the critical value for stable passivity, potentials would oscillate considerably and the reported values are averages.

Corrosion tests showed that when a stable passive potential was achieved, the corrosion rate was negligible, whereas with insufficient inhibitor present, the rate was about equal to the rate with no ferric ion added. It was also found that the marked change in corrosion rate occurred at the critical inhibitor concentration shown in Fig. 9. In order to establish this last observation, it was necessary to add ferric ion to a system in which the Ti was initially active. That is, Ti was placed in the boiling solution until it was active, and then a known increment of ferric ion was added. Blank tests were conducted to determine the weight change during this initial activating period. If Ti was added to a solution in which ferric ion was initially present, then a much smaller concentration of ferric ion would maintain the original passivity created by air exposure of the sample.

Table III. Comparison of corrosion rate, critical anodic current, and critical ferric ion concentration for passivity of Ti in boiling H_2SO_4

H_2SO_4 + 5% Na_2SO_4, %	Corrosion rate, mdd	Critical anodic current, ma/cm²	Critical Fe^{+++} concentration, mg/ml
1	280	0.05	0.040
2	580	0.2	0.085
3	1820	0.4	0.195
5	2880	1.8	0.250

Table III summarizes the effect of H_2SO_4 concentration on the corrosion rate, critical anodic current, and ferric concentration required for passivity. An increase in critical inhibitor concentration with an increase in critical anodic current is consistent with the mechanism of passivating inhibitors described above.

The data of Fig. 8 provide some additional information which, though not pertinent to the mechanism of passivating inhibitors, pertains to the primary cause of passivity. It can be shown that the slope of each line on this figure is inversely proportional to the number of coulombs associated with the passivation process. Since the scatter in the data is too great to determine whether the number of coulombs necessary for passivity is a function of H_2SO_4 concentration, the lines were intentionally drawn parallel. The data show that anodic passivation of Ti requires 0.021 coulomb/cm² where the area measurement is apparent area. Since the Ti surface is activated in the corroding environment, and it is etched, it appears reasonable to assume that the true surface area is from three to five times as large as the measured value. If one prefers to consider that the coulombs required to passivate are used in oxidizing Ti in accordance with the over-all reaction $Ti + 2H_2O \rightarrow TiO_2 + 4H^+ + 4e$, then the calculated oxide film thickness is 25Å using a surface roughness factor of 4. It should be mentioned that this kind of information has also been used to support adsorbed layers of oxygen.

Quantity of Passivator Associated with the Surface

It is important to note that many investigators have used radioisotopes or other sensitive analytical techniques to determine the amount of inhibitor on a passivated metal surface. This kind of information has been used to support either oxide films or adsorption as the basic cause of passivity. Data of this type have not proved particularly conclusive because the amount of material found varies considerably from system to system. For example, Cohen and Beck (25) report the passive film on Fe in chromate solutions may contain as much as 25% Cr_2O_3 with the remainder iron oxide. Hackerman and Powers (26), on the other hand, report that adsorbed chromate at the oxide-solution interface can be responsible for passivity even though the amount of chromate found is equivalent to about three monolayers. In addition, Cartledge (24) has shown that pertechnetate is a remarkably effective passivator for Fe even though the amount of radioactive technetium on the surface corresponds to a very small fraction of a monolayer.

When one considers that the prime function of an oxidizing inhibitor is to produce passivity by providing a redox system capable of anodically polarizing the metal to a noble mixed potential, it becomes obvious that the amount of inhibitor found on the surface is not necessarily related to the nature of the film causing passivity. The rate of reduction of the oxidizing agent is dependent upon the final mixed potential, the exchange current, and the Tafel slopes of the redox process. For example, Cartledge (24) has shown that iron passivated by either pertechnetate or osmic acid exhibits the reversible potential of the redox system in solution. Thus, under these conditions the redox system is essentially at equilibrium on the passive surface, and there is no net reduction of inhibitor. Such a system has been illustrated in Fig. 6 where the exchange current, I_{OD}, is considerably greater than the passive corrosion current. In most cases of passivity, where sufficient data have been reported, the passive potential is active to Pt in the same solution. This means that the passivator is being reduced at some finite rate which is equal to the rate of corrosion of metal in accordance with the theory of mixed potentials. Since the passive corrosion rate may be extremely small, the reduction rate may be quite difficult to detect. It should be mentioned, of course, that the rate of reduction of inhibitor may not be related to the amount observed on the surface, since the reduced species may not remain associated with the surface.

Thus, the mixed potential concept provides a means for explaining large variations in quantity of inhibitor found on passive surfaces without the necessity of postulating adsorption or oxide films.

Discussion

It has been shown that many experimentally observed phenomena may be explained by considering that the prime function of passivating inhibitors is to create a stable mixed potential more noble than the Flade region. This concept was suggested by Kolotyrkin (5, 10), who wrote, "The action of passivators need not involve their direct participation in forming the passivity film. Apparently, their action may be confined to increasing the overall rate of the cathodic reaction and thereby causing a shift of the steady-state potential in the positive direction, conducive to increased passivity." Pourbaix and Van Rysselberghe (27) have suggested a similar mechanism, but the details of their proposal, which is associated with potential-pH diagrams, are quite different from those given here. The concept is also implicit in the work of many others who have treated passive potentials as mixed potentials (18-19, 28, 29). In addition, Uhlig (1) has indicated that any local-action current greater than the critical anodic value is expected to create passivity. This is consistent with the mechanism supported here.

It is of value to discuss the interesting experiments by Cartledge (24) on passivation of Fe by pertechnetate. The rather unusual ability of this ion to passivate may be attributed to a high exchange current on the metal surface in accordance with the mechanism illustrated in Fig. 5 and 6. This is consistent with several experimental observations when one considers, as Cartledge has, that passive potentials are mixed potentials. First, the quantity of inhibitor required, and the loss due to reduction, were found to be highly dependent upon the composition and surface activity of the Fe. This is consistent with the recognized fact that activation overvoltage parameters are sensitive to surface conditions. Also, as described above, the fact that the passive potential is equal to the redox potential, along with the observation that the pertechnetate observed on the surface is constant and extremely small, shows that the exchange current is considerably higher than the passive corrosion current. In addition, the exchange current for pertechnetate must be considerably higher than that for chromate because of the following reported observations: Pertechnetate is an effective inhibitor at lower concentrations than chromate in spite of the fact that chromate is a stronger oxidizing agent. The passive potential of Fe is more noble in pertechnetate solutions than in chromate solutions of equal concentration, although the redox potential of the chromate solution is more noble. These observations can only be explained by considering that pertechnetate exhibits an unusually high exchange current.

In accordance with what has already been described above, the particular behavior of a given passivating inhibitor is determined by the redox potential and oxidation-reduction parameters (particularly the exchange current) on the metal surface. Some other characteristics may be equally important. For example, a given inhibitor species may also affect the critical anodic current by some unspecified mechanism, although as yet there appears to be no direct evidence for this. Should such a situation actually exist, then that inhibitor which reduces the critical anodic current will produce stable passivity at a lower concentration, provided all other factors are the same. Cartledge has shown that the Flade potential of Fe is apparently not affected by various inhibitors, so this factor, which would also influence the amount of inhibitor required for passivity, will not be considered.

Inhibitors may also function by influencing the reduction kinetics of another oxidizing agent in solution, thus enabling the mixed potential to occur in the passive region. For example, while molybdate and tungstate are sufficiently oxidizing in nature to passivate stainless steel and Ti under essentially oxygen-free conditions (Tables I and II), oxygen is required before they will passivate Fe under the conditions described by Pryor and Cohen (30) and Cartledge (24). Thus, while it is possible that the sum of the reduction rates of these weak oxidizing agents and that of oxygen may be sufficient to polarize Fe above the Flade potential (whereas the reduction rate of oxygen alone is insufficient), it is also possible that these inhibitors raise the exchange current or decrease the Tafel slope for oxygen reduction producing a noble mixed potential. There are not sufficient data available to determine which of these possibilities is most likely.

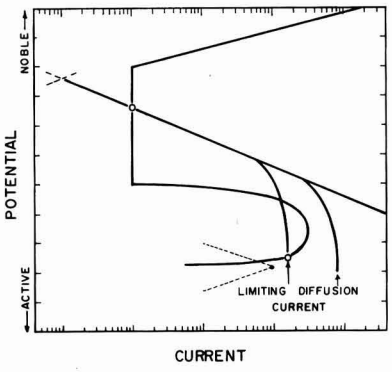

Fig. 10. The effect of concentration polarization on the behavior of passivating inhibitors.

It is possible that either or both of these may play important roles in some systems.[9]

It should be noted that oxygen has been treated in the same manner as any other oxidizing agent. In accordance with the mechanism proposed, there is no apparent need to consider that it functions in a manner different from that of other passivators. This is consistent with the observation of Uhlig and Geary (14) that the passive potential of stainless steel becomes more noble as the partial pressure of oxygen is increased, and becomes less noble as the solution is made more alkaline. Such behavior is expected, since the reversible oxygen electrode potential (determined by the reaction $O_2 + 4H^+ + 4e \rightarrow 2H_2O$) becomes more noble as the oxygen partial pressure and hydrogen ion concentration are increased. As mentioned previously, other species in solution may affect the reduction kinetics of oxygen and thus produce passivity.

The reduction kinetics of the oxidizing agent have been treated only in terms of activation polarization. However, concentration polarization undoubtedly plays an important role under some circumstances as is evidenced by the behavior of oxygen passivation of Fe in pure water (where the critical anodic current is relatively low). Under high solution velocity conditions, passivity may be achieved, whereas stagnant conditions produce an active potential and a relatively high corrosion rate (31). The effect of concentration polarization is illustrated in Fig. 10, where it is evident that when concentration polarization due to local-action currents exists, the mixed potential is active; whereas factors which raise the limiting diffusion current above the critical anodic current create only one possible mixed potential which is in the passive region.

There appears to be little doubt that passivity results from the formation of either an oxide or adsorbed film. The mechanism described here for the creation of passivity by oxidizing agents is independent of whether the unusual anodic behavior of passive metals results from an oxide or adsorbed film. However, it should be pointed out that if the principles described here are accepted, then some of the argument that adsorption is the prime cause of passivity must be re-evaluated, since a good deal of the evidence used to support this mechanism involves the behavior of passivating agents. The ability of CO to inhibit stainless steel in HCl has also been used as strong supporting evidence for adsorption as the principal cause of passivity (32). There is little doubt that CO adsorbs on stainless steel and Fe, as indicated by King and Rau (33). However, this adsorption does not lead to passivity in the electrochemical sense of the term, and it is believed that CO inhibits by the same mechanism as acid pickling inhibitors, which apparently do function by adsorption (34). For example, the potential of CO inhibited stainless steel in 2.45*N* HCl (35) is about 0.35 v more active than the saturated calomel electrode and is only about 0.1 v more noble than the same system without inhibitor. The evidence that CO should be considered in the same category as acid pickling inhibitors, and not included as a passivating inhibitor, is as follows: the inhibited potential is active; the change in potential resulting from inhibition is only about 0.1 v in the noble direction; commercial pickling inhibitors or additions like quinoline ethiodide and carbon disulfide produce similar effects, and finally oxygen passivation produces a much more noble potential.

It is believed that the final answer to passivity will come from an acceptable explanation of metal dissolution kinetics. In particular, one must explain the reason for the existence of the Flade region and also the unusual electrode kinetics which result in a metal dissolution rate which is independent of potential.

Conclusions

1. Inhibitors which create passivity function primarily by producing a mixed potential which is more noble than the Flade region. In order to achieve this, the solution must contain a redox system with a noble reversible potential (an oxidizing agent).

2. The major factors which determine whether a particular system will exhibit passivity are the reversible potential of the redox system created by the oxidizing inhibitor; the oxidation-reduction parameters for reduction of the inhibitor on the metal surface (exchange current, Tafel slope, limiting diffusion current); and the value of critical anodic current and Flade potential of the metal. If oxygen is present in the environment, other species in solution may affect its reduction kinetics and thus produce conditions favorable to passivity.

3. Passivity is favored by high values of redox potential, exchange current, and limiting diffusion current, and by low values for the Tafel slope. A low critical anodic current for the metal and a relatively active Flade region also favor passivation.

4. While there is little doubt that passivity primarily results from either an oxide film or adsorption, the mixed potential concept proposed here is independent of which mechanism predominates. Thus, some of the argument that adsorption is the prime cause of passivity should be re-evaluated, since much of the evidence used to support this

[9] For example, Cartledge (24) has shown that in systems containing both oxygen and pertechnetate, the reversible potential of the pertechnetate system is more active than the Flade potential of Fe. Thus in this case, oxygen is the passivating inhibitor and pertechnetate probably affects the reduction kinetics of oxygen.

mechanism involves the behavior of passivating agents.

5. It is believed that a final answer to passivity will come from an acceptable explanation of metal dissolution kinetics which involves both the Flade region and the potential region where metal dissolution is independent of potential.

Acknowledgment

The author acknowledges the skillful assistance of E J. Bartolomei and N. Darroch who conducted most of the measurements reported here.

Manuscript received Feb. 28, 1958. This paper was prepared for delivery before the Ottawa Meeting, Sept. 28-Oct. 2, 1958.

Any discussion of this paper will appear in a Discussion Section to be published in the June 1959 JOURNAL.

REFERENCES

1. H. H. Uhlig and G. E. Woodside, *J. Phys. Chem.*, **57**, 280 (1953).
2. H. J. Rocha and G. Lennartz, *Arch. Eisenhüttenw.*, **26**, 117 (1955).
3. R. Olivier, "Passivat von Eisen u. Eisen-Chrom-Legierungen," Dissertation, Leiden (1955). For summary, see T. Heumann, "Passivierende Filme und Deckschichten," p. 276, H. Fischer, K. Hauffe, and W. Wiederholt, Editors, Springer-Verlag, Berlin (1956).
4. M. Prazak, "Uber den Aufbau der Passivschicht auf Chromstählen," presented at the International Colloquium on Passivity of Metals, Heiligenberg, 1957. To be published *Z. Elektrochem.*
5. N. Y. Bune and Y. M. Kolotyrkin, *Doklady Akad. Nauk. S.S.S.R.*, **111**, 1050 (1956).
6. C. Edeleanu, *Metallurgia*, **50**, 113 (1954); *Nature*, **173**, 739 (1954).
7. C. Carius, *Arch. Eisenhüttenw.*, **27**, 401 (1956).
8. G. Okamoto, H. Kobayashi, M. Nagayama, and N. Sato, "Effect of Temperature on the Passivity of Nickel," presented at the International Colloquium on Passivity of Metals, Heiligenberg, 1957. To be published *Z. Elektrochem.*
9. T. Heumann, "Uber die Passivierung des Chroms," *ibid.*
10. Y. M. Kolotyrkin, "Electrochemical Behavior and Anodic Passivity Mechanism of Certain Metals in Electrolyte Solutions," *ibid.*
11. J. H. Bartlett and L. Stephenson, *This Journal*, **99**, 504 (1952).
12. U. F. Frank, *Z. physik Chem. (Frankfurt)*, **3**, 183 (1955).
13. H. H. Uhlig and J. Cobb, *This Journal*, **99**, 13 (1952).
14. H. H. Uhlig and A. L. Geary, *ibid.*, **101**, 215 (1954).
15. G. Okamoto, M. Nagayama and Y. Mitani, *J. Electrochem. Soc., Japan*, **24**, 69 (1956).
16. C. Wagner and W. Traud, *Z. Elektrochem.*, **44**, 391 (1938).
17. M. Stern, *This Journal*, **104**, 56 (1957); **104**, 645 (1957).
18. V. F. Franck and K. Weil, *Z. Elektrochem.*, **56**, 814 (1952).
19. K. J. Vetter, *ibid.*, **55**, 274 (1951).
20. M. Stern, *This Journal*, **104**, 600 (1957).
21. M. Stern, *ibid.*, **104**, 559 (1957).
22. R. Olivier, "Proceedings of the Sixth Meeting of the International Committee of Electrochemical Thermodynamics and Kinetics," p. 314, Butterworth's Scientific Publ., London (1955).
23. V. F. Franck, *Z. Naturforsch.*, **4A**, 378 (1949).
24. G. H. Cartledge, *Corrosion*, **11**, 335 (1955); *J. Phys. & Colloid Chem.*, **59**, 979 (1955); **60**, 28, 32, 1037, 1571 (1956); **61**, 973 (1957).
25. M. Cohen and A. F. Beck, "The Passivity of Iron in Chromate Solutions," presented at the International Colloquium on Passivity of Metals, Heiligenberg, 1957. To be published *Z. Elektrochem.*
26. N. Hackerman and R. A. Powers, *This Journal*, **100**, 314 (1953).
27. M. Pourbaix and P. Van Rysselberghe, *Corrosion*, **9**, 313 (1950).
28. K. J. Vetter, "Passivierende Film und Deckschichten," p. 72, H. Fischer, K. Hauffe, and W. Widerholt, Editors, Springer-Verlag, Berlin (1956).
29. H. Beinert and K. F. Bonhoeffer, *Z. Elektrochem.*, **47**, 536 (1941).
30. M. J. Pryor and M. Cohen, *This Journal*, **100**, 203 (1953).
31. T. P. Hoar and U. R. Evans, *ibid.*, **99**, 212 (1952).
32. H. H. Uhlig, "The Adsorption Theory of Passivity and the Flade Potential," presented at the International Colloquium on Passivity of Metals, Heiligenberg, 1957. To be published *Z. Elektrochem*; also, "Advances in Catalysis," Vol. IX, p. 379, Academic Press, New York (1957).
33. C. V. King and E. Rau, *This Journal*, **103**, 331 (1956).
34. A. C. Makrides and N. Hackerman, *J. Phys. & Colloid Chem.*, **59**, 707 (1955).
35. H. H. Uhlig, *Ind. Eng. Chem.*, **32**, 1490 (1940).

A Study of Corrosion Films on Zirconium and Its Alloys by Impedance Measurements

J. N. Wanklyn and D. R. Silvester

Atomic Energy Research Establishment, Harwell, Berkshire, England

ABSTRACT

The oxide films formed on zirconium and some of its alloys during corrosion in steam and water at 325°C have been studied by impedance measurements made by immersion in an electrolyte. A fall in the protective character of the film is accompanied by an increase of capacity, and measurements of the latter provide a useful method of comparing films. The behavior of the resistive part of the impedance and the influence of frequency and electrolyte conductivity are complex, and only a partial interpretation can be given.

The initial reaction of zirconium and its alloys with water and steam at temperatures around 300°C is characterized by a rate of attack which falls with time. After a time which, depending on the alloy and conditions, varies from a few hours to many thousand hours, the rate increases and re-

mains constant until flaking of the oxide film prevents further accurate measurements. The phenomenon causing this change is called "breakaway" or "transition." Although Thomas and Kass (1) recently suggested that transition and breakaway are fundamentally different, the former implying only a change of kinetics, while the latter also involves loss of oxide by spalling, both conditions are explicable by cracking of the film under the compressive stresses due to the expansion (about 50% by volume) accompanying the conversion of metal to oxide. Such stresses have been directly demonstrated by Wheeler (2), and Evans (3) has discussed theoretically the types of cracking to be expected under various conditions.

It seems likely that the corrosion rate is controlled at all times by the diffusion of some species (almost certainly oxygen ions) through the oxide film, and that the change in kinetics occurs because the latter's protective character is reduced by the cracks. If cracking keeps pace with film growth, the effective rate-controlling thickness remains constant and corrosion is linear with time.

Numerous workers (4-6) have measured the capacity of oxide films on metals, generally with the aim of determining their thickness. Young (5) studied the dependence of film capacity and resistance on frequency, reaching conclusions about the structure of the films, particularly the variation of nonstoichiometry through their thickness. All this work referred to nominally crack-free films, generally produced by anodizing. Young, however, reported unduly high capacities for anodic films formed under breakdown conditions, and Misch (7), comparing anodic films formed on various metals in nitric acid found, that porous, nonprotective films had high capacities.

These high values could be due to electrolyte entering cracks, so reducing the effective thickness of dielectric and increasing the observed capacity. Cracks formed in films during corrosion and oxidation should behave similarly. The experiments described below and briefly reported elsewhere (8) were therefore carried out to study such films. This application of capacity measurements is similar to the work of Wormwell (9, 10) and co-workers, who detected the failure of paint films on metal specimens immersed in electrolyte by observing a rise of capacitance.

Experimental

The circuit is shown in Fig. 1. The bridge elements Rx, Ro, and Rs were Muirhead noninductive decade units and C_o a Dawe three-dial decade capacitor giving 0.001 to 1.11 μF. Rx and Ro were generally kept at 10,000 ohms each and the bridge was balanced with C_o and Rs which was variable in steps of 0.1 ohm up to 11,111 ohms. The oscillator (Dawe 400A) was connected to the bridge through a transformer since its output, which was earthed on one side, would be incompatible with the Wagner earthing circuit (see Fig. 1). The a-c voltage imposed on the cell during measurements was only a few tens of millivolts root mean square. Only one capacity was provided in the Wagner earth, and this was switched into whichever limb required it for balance. The 10,000 ohms series resistance provided a fine variation of the capacity adjustment. The detector was a Cossor Type 1049 oscilloscope preceded by Type TAA-16EA amplifier (MIT Radiation Laboratory) which could be turned over the range 500-5000 cps. The oscilloscope was most conveniently used with a simple time-base sweep, the amplified output being applied to the y plates. With this arrangement it was possible to distinguish visually the desired signal from background interference. Tests with standard components showed the bridge to be accurate to about 2-3%.

In the first experiments the d-c potential of the specimen was controlled by the d-c supply. The choke, L, prevented this circuit from short circuiting the a-c detector, while the condenser, C, blocked the latter's low resistance d-c path. The d-c source was adjusted by measuring the potential of the specimen against a saturated calomel electrode with a *p*H meter. When it was found that small variations of d-c potential did not influence the capacities significantly, the d-c source was disconnected and the specimen allowed to assume its natural potential.

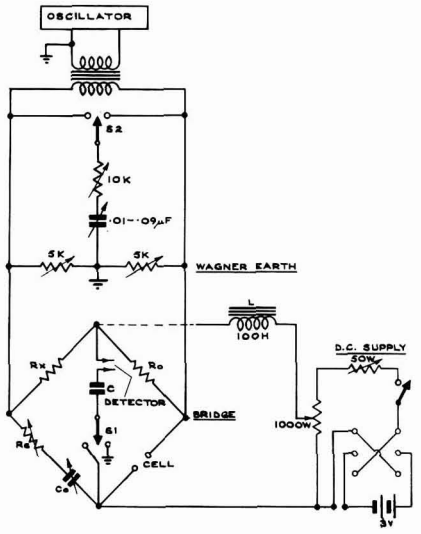

Fig. 1. Bridge circuit

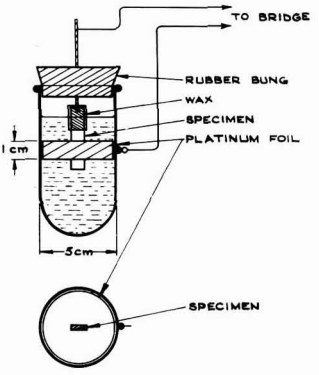

Fig. 2. Measuring cell

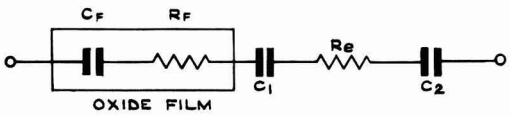

Fig. 3. Equivalent circuit of cell

The cell was as shown in Fig. 2. Specimens were attached to the supporting wire by a small nut and bolt or with a clip and were waxed so as to leave an exposed area of about 1-1½ cm². Edges cut after the corrosion experiment were always waxed, and care was taken not to scratch the surface to be measured. When d-c potentials were to be measured, the cell had a side arm leading to a saturated calomel electrode and filled with cell electrolyte, generally 1*N* H_2SO_4. With this solution the resistance of the cell, measured with a platinized platinum electrode of the same dimensions replacing the specimen, was about 2 ohms.

The oxide film impedance was always expressed as capacity and resistance in series. It is in series with C_1 and C_2, double layer capacities at the specimen and Pt, respectively, and with Re, the electrolyte resistance (Fig. 3). The values of Rs and C_o (Fig. 1) gave the cell impedance as resistance and capacity in series and, since the capacities were always much less than typical double layer values, C_o gave C_f directly. The measured resistance was often much greater than Re, but when it was comparable to Re, the latter was subtracted to give R_f.

The materials studied were Kroll zirconium and binary and ternary alloys based on it. Analyses are given in Table I.

The preparation of the alloys and their fabrication into sheet has been described elsewhere (11). As before, all specimens were pickled in nitric/hydrofluoric acid[1] before the corrosion experiments, which were conducted either in water at 325°C, as described earlier (11), or in steam at 325°C and 1 atm. For the latter the specimens were suspended in a glass reaction chamber in a vertical tube furnace. Steam, raised in a small boiler from which all air was first expelled, was passed through the reaction chamber at about 100 cm³/min. Appropriate weighings gave the weight gain per unit area. Most of the films were adherent (experiments being stopped before the onset of flaking) so that this weight was a good measure of the extent of corrosion and of the film thickness.

Table I. Analyses of materials

Unalloyed Kroll Zr	Sample No. 24, ppm	Sample No. 050, ppm
N_2	50	225
C	280	550
Fe	300	435
Ni	—	32
Cr	100	155
Mg	50	20
Cl	50	20
Cu	—	100
O_2	—	1100
H_2	—	37
Al	100	—

Binary alloys: 1% wt Cr, 2.5% wt Ta, 0.25% wt Al. All nominal compositions, based on Sample No. 24.
Zircaloy 2 (Nominal): 1.5% wt Sn, 0.12% wt Fe, 0.10% wt Cr, 0.05% wt Ni, balance Zr.

Results

At first an area of exactly 1 cm² of specimen was waxed off, but, as this proved difficult to achieve, in subsequent experiments approximately 1 cm² was masked off and carefully measured. Capacity results were converted then to values for 1 cm² by dividing by the actual area, while the resistance values were multiplied by the area.

Capacity values for various alloys are given in Table II which also shows, for comparison, corrosion rates in water at 325°C. Results for specimens of unalloyed Zr after various periods of exposure to steam at 325°C and 1 atm are shown in Tables III to VI. Both these sets of measurements were made in 1*N* H_2SO_4 at a frequency of 1000 cps and are final steady values after at least 24 hr in electrolyte.

The effect of frequency on the impedance of several specimens in 1*N* H_2SO_4 is shown in Fig. 4 and 5. The results are plotted as resistance vs. 1/frequency and 1/capacity vs. log frequency. Young (5) has shown this to give straight lines for crack-free films. According to his theory, the ratio of the slope

[1] HNO_3 (conc), 45 cm³; HF (48% soln), 5 cm³; and water, 50 cm³.

Table II. Capacity values for various alloys after corrosion in water at 325°C (1000 cps)

Alloy	Time of corrosion, hr	Weight gain *W*, mg/cm²	*C*, μF/cm²	1/*CW*	Average linear corrosion rate mg/cm²/mo	Corrosion resistance
Zircaloy 2	72	~0.1	0.039	260	Rate falling with time	Good
	144	0.3	0.029	120		
	228	0.3	0.029	120		
	520	0.3	0.025	130		
Unalloyed	72	0.5	0.143	14		
Zirconium	144	1.3	0.135	5.7	4.4	
(No. 24)	228	2.1	0.140	3.4		Intermediate
	520	3.7	0.179	1.5		
Zirconium	72	1.0	0.093	11		
+ 1% wt Cr	144	2.8	0.257	1.4	14	
	228	4.7	0.129	1.7		
	520	11	0.392	0.24		
Zirconium	72	1.3	0.404	1.9	~10-20 [from	Bad
+ 2.5% wt Ta	520	? Flaking	0.526	—	other expts (11)]	
Zirconium	72	~7	0.726	~0.2	~70	
+ 0.25% wt Al		Flaking				

Table III. Capacity measurements on unalloyed zirconium (No. 050) after exposure to steam at 325°C, 1 atm for various times (1000 cps)

Specimen No.	Time, hr	W, mg/cm²	C, μF/cm²	1/CW	Color of oxide film
1	1	0.058	0.629	27.4	Blue-black
2		0.054	0.688	26.9	
3	2	0.051	0.566	34.6	Blue-black
4		0.047	0.553	38.5	
5	2.5	0.142	0.960	7.35	Dark gray
6		0.128	0.898	8.70	
7	3	0.295	0.744	4.55	Medium gray
8		0.283	0.839	4.22	
9	4	0.351	0.890	3.20	Light gray
10		0.319	0.856	3.66	
11	5	0.475	0.890	2.37	Light gray
12		0.485	0.962	2.15	
13	6	0.497	0.946	2.12	Light gray,
14		0.515	1.135	1.72	White spots
15	10	0.644	0.937	1.66	Light gray,
16		0.662	0.892	1.69	White spots

of the "capacity" plot to that of the "resistance" plot should always be 9.2 (=4 x log e 10). (In this relation C is expressed in Farads per cm².) Figure 5 gives the observed values of the ratio.

Figure 6 shows the change of capacity with time of immersion in electrolyte for cracked and uncracked films.

Table IV shows the effect of varying the electrolyte resistance from 1N H_2SO_4 ($\rho = 5$ ohm-cm) to $N/10$ sodium sulfate ($\rho = 130$ ohm-cm), and Fig. 7 shows the frequency dependence of the resistance of typical specimens of unalloyed Zr in the two electrolytes.

Discussion

Table II shows that, as anticipated, films of lower protective value have higher capacities. Since the capacity of a condenser is inversely proportional to the thickness of dielectric, it is convenient to take 1/capacity as a measure of the "effective thickness" of the protective part of the film. The protective character of different films may be compared by obtaining the ratio of 1/capacity to the total thickness of the film. For adherent films on Zr (which forms only one oxide) the weight gain per unit area during corrosion (W) is a good measure of film thickness. Protective character is thus measured by the quantity $1/CW$. Values of $1/CW$ are given in Table II and comparison with the corrosion rates shows that good alloys are sharply discriminated from bad. In Table III the fall of $1/CW$ with film growth reveals the progressive loss of protective character. This was accompanied by a change of film color usual with corroding Zr alloys, from black through shades of gray to white.

It is not possible to decide certainly whether the best material, Zircaloy 2, forms films which are entirely crack-free, but there are two reasons for supposing that it does. First, if the films are crack-free, their capacities may be calculated approximately as simple parallel plate condensers. Taking the dielectric constant (4) and density of zirconium dioxide as 27 and 5.7 g/cm³, respectively, $C = (3.5 \times 10^{-3} \sigma^2)/W$ μF/cm² where W is the weight gain in mg/cm² and σ is the ratio true surface area/apparent surface area. If calculated and observed capacities for Zircaloy 2 are equated, σ is found to be about 1.5. Adams, *et al.* (12) found $\sigma \sim 2$ for abraded Zr and, by comparison with this, a value of 1.5 for a bright pickled surface seems reasonable. Second, films, such as those on Zircaloy 2, which have "good" values of $1/CW$ (150 or more) behave differently with time from less protective films. The final capacity of the former is established almost

Table IV. Effect of electrolyte resistivity on film impedance (1000 cps)

Specimen No.	W, mg/cm²	1N H_2SO_4 ($\rho = 5$ ohm-cm) C_f, μF	1N H_2SO_4 ($\rho = 5$ ohm-cm) R_f, ohm	$N/10$ Na_2SO_4 ($\rho = 130$ ohm-cm) C_f, μF	$N/10$ Na_2SO_4 ($\rho = 130$ ohm-cm) R_f, ohm	R_f in $N/10$ Na_2SO_4 / R_f in 1N H_2SO_4
1	0.058	0.629	30.7	0.099	239	7.8
2	0.054	0.688	21.0	0.162	158	7.5
3	0.051	0.566	38.4	0.072	410	11
4	0.047	0.553	42.6	0.073	280	6.6
5	0.142	0.960	14.2	0.257	340	24
6	0.128	0.898	16.0	0.067	775	48
7	0.295	0.744	20.3	0.038	1630	80
8	0.283	0.839	20.6	0.027	1690	82
9	0.351	0.890	19.4	0.050	1230	63
10	0.319	0.856	16.0	0.233	357	22
11	0.475	0.890	22.3	0.389	260	12
12	0.485	0.962	20.4	0.235	595	29
13	0.497	0.946	19.7	0.362	350	18
14	0.515	1.135	18.8	0.316	472	25
15	0.644	0.937	17.5	0.775	59	3.4
16	0.662	0.892	17.4	0.735	90	5.2

Table V. Values of R_f at $1/f = 0$

Specimen No.	1/CW	R_f at $1/f = 0$ in 1N H_2SO_4 (ohm)	R_f at $1/f = 0$ in $N/10$ Na_2SO_4 (ohm)
1	27.4	~1	~0*
2	26.9	~2	~0*
3	34.6	~5	~0
4	38.5	~8	~0*
5	7.35	—	~50
6	8.70	~0	—
7	4.55	~1	200-300
8	4.22	~0	~50
9	3.20	0	~100
10	3.66	—	~80
11	2.37	~1	~100
12	2.15	<1	~100
13	2.12	—	~100
14	1.72	<1	~80
15	1.66	~0	~220
16	1.69	<1	~30

* Negative intercept.

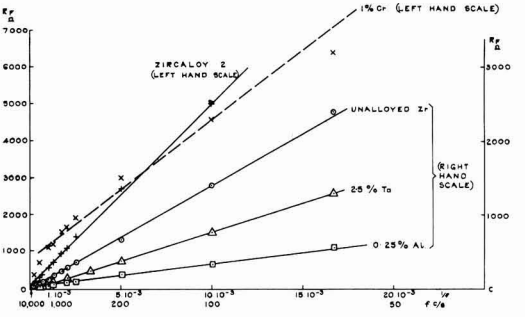

Fig. 4. Variation of R_f with $1/f$ for various alloys

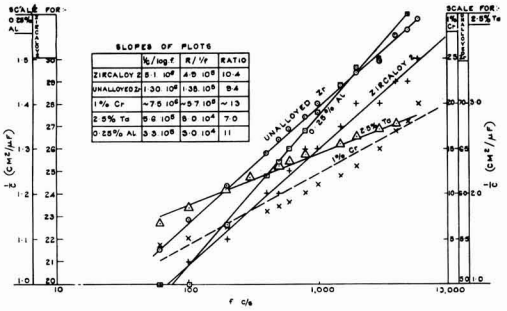

Fig. 5. Variation of 1/C with log f for various alloys

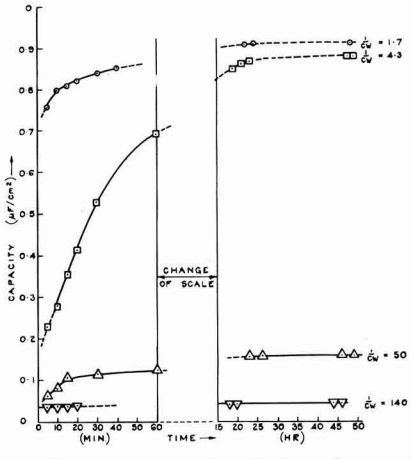

Fig. 6. Variation of capacity with time of immersion in various electrolytes. Values of 1/CW are based on final capacities.

at once, but inferior films show a marked drift with time, presumably due to the slow penetration of electrolyte into cracks. Some typical cases are given in Fig. 6, which also shows that, with a very bad film ($1/CW = 1.7$) the drift diminishes again, doubtless because the cracks are large and numerous.

It was thought that extrapolation to zero time of the plots for cracked films might yield values appropriate to uncracked films of the same thickness. With extensively cracked specimens no consistent results could be obtained, the capacity changing too rapidly for accurate measurement at short times. For a few specimens, with $1/CW$ in the range 30-100, the extrapolated values approximated to the theoretical crack-free value, based on $1/CW \sim 200$.

As discussed more fully later, the film impedance obeyed approximately the relations derived by Young for crack-free films. According to the latter the film resistance is inversely proportional to the frequency and so should fall to zero at $1/f = 0$. With much-cracked films, the capacity is much larger than the uncracked value and therefore must be predominantly composed of impedance elements each connected to the bulk electrolyte by cracks filled with liquid. When, at $1/f = 0$ the resistance of the elements themselves falls to zero, there should remain a resistance characteristic of the electrolyte in the cracks. This might be expected to change by the appropriate ratio when the resistivity of the electrolyte is changed. Values of R_f at $1/f = 0$ in two electrolytes are given in Table V for a number of the specimens exposed in steam at 325°C. The behavior of two specimens is illustrated in Fig. 7.

In H_2SO_4 the resistances are small and the accuracy low, so that one can only say that they are of the order of a few ohms. The sodium sulfate values are also rather imprecise, but those for specimens exposed for intermediate times (No. 5 onward) are definitely larger than in H_2SO_4.

Earlier specimens gave very low values, and sometimes even negative intercepts, which are recorded as "~ zero." This trend may be explained as follows: the first specimens, corroded for short periods only, have films which are only slightly cracked, so that "crack elements" contribute little to their impedance, and their series resistance is little affected by that of the electrolyte in the pores. As exposure increases, the extent of cracking increases and at about specimen No. 7 the resistance of the liquid in the cracks exerts its greatest effect. With still further exposure, however, the cross-sectional area of cracks is so much increased that their contribution to resistance again falls. Thus the increase in R_F on changing to an electrolyte of higher resistivity should be least for uncracked and much-cracked films and should reach a maximum for intermediate specimens. The increase of cracking as corrosion proceeds is illustrated by the successive values of $1/CW$.

This explanation is certainly an oversimplification. For example, with the intermediate specimens

Table VI. Mean protective thickness d and total thickness t, of films formed on unalloyed zirconium in steam at 325°C 1 atm (Sample No. 050)

Specimen No.	W, mg/cm²	1/CW	d, Å	t, Å
1	0.058	27.4	630	4000
3	0.051	34.6	730	3500
6	0.128	8.70	410	8800
7	0.295	4.55	490	20000
9	0.351	3.20	410	24000
11	0.475	2.37	410	33000
13	0.497	2.12	380	34000
15	0.644	1.66	390	44000

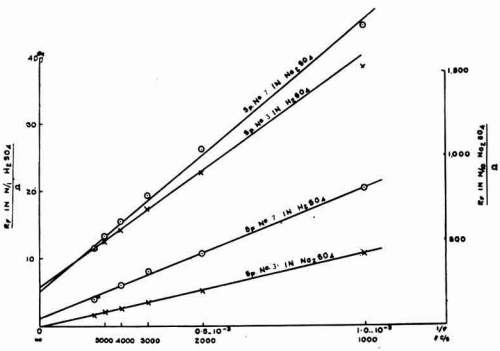

Fig. 7. Determination of R_f at $1/f = 0$, for unalloyed Zr exposed to steam at 325°C, 1 atm.

of Table V, the ratio $[R_f(1/f = 0)$ in $Na_2SO_4]/[R_f(1/f = 0)$ in $H_2SO_4]$ is considerably more than the ratio of the resistivities of the electrolytes themselves, viz., 26. Table IV shows the same to be true of resistances at 1000 cps. Again, when the impedance is predominantly made up of crack elements (i.e., the capacity is much greater than the uncracked value for the thickness in question) the simple picture would suggest that the capacity should not be affected by the change of electrolyte. Table IV shows that this is by no means so, capacity values being much reduced in sodium sulfate. As with the resistances there is a tendency for the intermediate specimens to show the greatest effect.

It is thus not yet possible to explain in detail the impedance of a cracked film, and one cannot use the values to study the cracks, as fully as originally hoped. In particular, it is not possible to calculate separately their area and mean distance of approach to the metal/oxide interface. A crude estimate of the latter may however be made for much-cracked films in the following way.

A crack, although drawn in two dimensions as a line, is in fact a complicated warped surface. A simplified crack may be considered to be a plane fissure of uniform width and thickness. The latter may have any value down to that at which the proximity of the walls begins to affect the entry and properties of the electrolyte. Somewhat arbitrarily the thinnest crack may be taken as 100Å, so that the resistance of a 1 cm length of such a crack, 1 cm wide, filled with 1*N* H_2SO_4 is about 10^6 ohms. Now the capacity of 1 cm^2 of ZrO_2 between electrodes 1 cm apart is about 4×10^{-6} μF so that its impedance ($= 1/C\omega$) at 1000 cps is about 10^5 ohms. Thus such an element of capacity intersected by a crack perpendicular to the faces of the dielectric will have its capacitance impedance completely short-circuited by the crack. This will also be true of thinner capacity elements intersected by oblique cracks, down to elements whose thickness is about 1/100 cm. All cracks, therefore, except those almost parallel to the metal surface, short-circuit the contribution to capacity of the oxide through which they pass. Thus a cracked film constitutes a condenser, one plate of which is the metal and the other a mass of cracks filled with electrolyte, each crack short-circuiting the material above it, so that the effective area of the condenser "plate" will be that of the cracks, projected perpendicularly to the metal surface. If the film is extensively cracked, the whole area of specimen will be covered by cracking so that the projected area will be equal to the (true) area of the specimen. Knowing the area one may calculate the mean thickness of dielectric, i.e., the mean separation of the irregular surface of cracks from the metal/oxide interface. This gives the mean thickness of the protective part of the film. (Since capacity is inversely proportional to thickness, this value is the reciprocal of the mean value of 1/thickness which, compared with the arithmetic mean, gives greater weight to the lower thicknesses.) Some values of the mean thickness d based on a dielectric constant of 27 and a surface roughness of 1.5 are given in Table VI.

The capacity values used are the increases over that for an uncracked film of the same total weight, i.e., they are the contributions due to cracks. For extensively cracked specimens ($1/CW <$ about 10) this is the predominant part of the capacity. The table also gives the total thickness of the film t, obtained from the weight gain, assuming a density of ZrO_2 of 5.7 ($t = 6.9 \cdot 10^4$ WÅ). The figures show that d falls to a fairly constant value of about 400Å. Considering the uncertainty of the roughness factors and dielectric constant one may conclude that the protective part of the film is of the order of 500Å thick.

The lower capacities of the earlier specimens are due either to the cracking not being so deep or to its area being less than that of the whole specimen. Some short experiments in dry oxygen (not quoted here) gave films for which, assuming unit area, $d > t$, which is impossible. On these specimens the area of cracking must have been less than the whole area of the specimen, so that d could be less than t. It is impossible to decide whether or not the first cracks go as close to the metal as the final protective thickness. It is tempting to consider that, while the "resistance ratio" (in two electrolytes, see above) is increasing during the early part of the test, the cracks are becoming deeper and that, when the resistance ratio begins to fall again, they have reached their greatest depth and thereafter are increasing in extent. There is, however, no proof of this. Determination of the limiting protective thickness for different alloys and conditions of corrosion might be illuminating, and it is hoped to do this.

That the values of d are reasonable may be seen by noting that, if diffusion through the protective part of the film controls the corrosion rate, the latter should, like the capacity, be inversely proportional to d. It should also, again like the capacity, be proportional to the projected area of the cracks, for it is by the latter that the corroding medium approaches the metal/oxide interface. As discussed for the capacity, the projected area approaches unity as corrosion proceeds so that the final rate should be equal to that found in the early part of the experiment when the film is still uncracked and is of thickness equal to the final protective thickness. Thus a line of slope equal to the final corrosion rate should touch the initial part of the curve at a point equivalent to the protective thickness (Fig. 8). In-

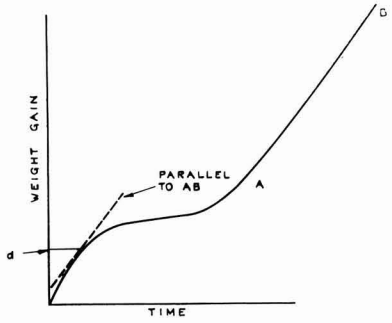

Fig. 8. Mean protective film thickness (diagrammatic)

sufficient data are available to check this point thoroughly, but a few results in oxygen at 325°C support it approximately.

It has already been said that the capacity and resistance of corrosion films follow approximately the frequency dependance derived (5) for crack-free films by considering the properties of the oxide itself. Figures 4 and 5 show that fair straight lines are obtained, and the ratio values given in Fig. 5 agree approximately with the theoretical value of 9.2, although the individual slopes vary tenfold between specimens.[2] This suggests some similarity in the "equivalent circuit" of sound and cracked oxide films, although the impedance of the latter owes much to the liquid in the cracks (cf. Table IV).

The problem may be approached by considering a cracked film not, as heretofore, as a combination of individual resistance/capacity elements, but as a block of material of constant dielectric constant whose resistivity varies through the thickness. This is how Young treats crack-free films; and in the present case conductivity due to cracks filled with electrolyte must be substituted for conductivity due to nonstoichiometry. Resistivity variation due to varying nonstoichiometry is replaced by variation due to the change of area of cracks through the thickness of the film. Formal comparison with Young's treatment shows that his relations will be obeyed if the total cross-sectional area of cracks at any plane in the film parallel to the outer surface is an exponential function of the distance from that surface.[3] Thus, if α_x is the fraction of the area of a plane at distance x from the surface which is composed of cracks, and α_o is the value at the outer surface.

$$\frac{\alpha_x}{\alpha_o} = e^{-x/k}$$

k being a constant. There are at present no independent grounds for expecting an exponential variation of cracking with thickness. Possibly one might be reached by considering the mechanical properties of the film substance in which case a comparison of k and α as between different alloys might be illuminating.

Although the results give fair straight lines when plotted according to Young's relations, further use of the latter does not yield sensible values for the resistivities of the cracked films. For example, with a dielectric constant of ~27, the above relations lead to:

$$\log \rho_d = \frac{1}{C_{1000} \times S} + 7.8$$

and

$$\log \rho_o = \log \rho_d - (2.9 \times 10^8 W)/S$$

where ρ_o, ρ_d are the resistivities at the outside and inside of the film respectively, W is the weight gain in mg/cm², S is the slope of $1/C$ vs. log f, and C_{1000} is the value at 1000 cps, in farads/cm². Conductivity being due to electrolyte in the cracks, the degree of cracking should be given by the ratio of electrolyte resistivity to film resistivity, and at the outer surface α_o should be equal to $\frac{\rho \text{ electrolyte}}{\rho_o}$, but most of the well cracked films ($1/CW \sim 30$ or less) gave impossibly low values of ρ_o, though some specimens with little cracking ($1/CW \sim 100$) gave figures which were at least plausible. This suggests that a cracked film is not well represented by a capacity shunted by a varying resistance, principally because a large part of the latter is so low as to short-circuit completely the capacity with which it is in parallel. This conclusion was also reached earlier by considering the resistance of individual cracks.

Further complications are suggested by some recent experiments in sodium nitrate solution which, though almost equal to $1N$ H_2SO_4 in resistivity, gave very different results. The capacities were much less, and the resistances greater, the values departing more from those in H_2SO_4 than do those in $N/10$ sodium sulfate, whose resistivity is 26 times greater. This suggests that electrolytes behave specifically, more properties than their resistivity being important.

Conclusions

The impedance of Zr specimens carrying oxide films formed by corrosion and immersed in electrolyte show higher capacities with the less protective films. This is due to penetration of electrolyte into cracks in the latter. The degree of cracking may be assessed by evaluating the quantity $1/CW$, where C is the capacity and W the weight gain due to corrosion. The impedance measurements also yield a resistive component which is less easy to interpret, although approximate correlation to the progress of cracking may be made. The impedances are influenced by the resistivity of the electrolyte, and other properties of the solution may be important. The frequency behavior of capacity and resistance follow approximately the relations applicable to crack-free films.

It has not been possible to use observations to determine the extent and depth of cracking in any detail, but the mean thickness of the uncracked part of the film at late stage in corrosion can be crudely estimated. The present usefulness of impedance measurements is confined to the comparison, by values of $1/CW$, of films formed on different alloys under different conditions of corrosion. Here they can be of value.

Acknowledgments

The authors wish to thank Mr. C. N. Davey for assistance with the apparatus. They are also indebted to Dr. H. M. Finniston and Mr. R. A. U. Huddle for encouragement and criticism, and to Dr. L. Young, Dr. P. Jacobs, and Dr. A. R. Bray for helpful discussions.

[2] In this connection it is important to consider an adequate range of frequency, viz., about 50-5000 cps. Over 1000-5000 cps one can obtain fair straight lines and a slope ratio of about 10 from a simple circuit of fixed resistance and capacity in parallel, the values being chosen to give an impedance typical of films. Over the full frequency range, however, the simple model departs from these relations far more than do the film impedances.

[3] The reasonable assumption is here made that $\alpha << 1$ so that the dielectric properties of the film are independent of x, as Young assumes. This is not contrary to the earlier assumption that the effective area of condenser plate formed by the cracks is unity; for that area was the projected area of an irregular surface of cracks, while we are here considering the traces of individual cracks cutting an infinitely thin plane.

Manuscript received Jan. 7, 1958. This paper was prepared for delivery before the Ottawa Meeting, Sept. 28-Oct. 2, 1958.

Any discussion of this paper will appear in a Discussion Section to be published in the June 1959 JOURNAL.

REFERENCES

1. D. Thomas and S. Kass, *This Journal*, **104**, 261 (1957).
2. R. Wheeler, *U.S.A.E.C., K.A.P.L.* 39190 (Appendix) (1955).
3. U. R. Evans, *This Journal*, **91**, 547 (1947).
4. A. Charlesby, *U.K.A.E.A., A.E.R.E.*, M/R. 1176 (1953).
5. L. Young, *Trans. Faraday Soc.*, **51**, 1250 (1955).
6. Guntershulze and Betz, "Elektrolytkondensatoren," Krayn, Berlin (1937).
7. R. D. Misch and W. E. Ruther, *This Journal*, **100**, 531 (1953).
8. J. N. Wanklyn, *Nature*, **177**, 849 (1956).
9. F. Wormwell and D. Brasher, *J. Iron Steel Inst.*, **164**, 141 (1950).
10. F. Wormwell and D. Brasher, *J. Iron Steel Inst.*, **169**, 228 (1951).
11. J. N. Wanklyn and C. F. Britton, *U.K.A.E.A., A.E.R.E.*, M/R. 1924 (1956).
12. G. B. Adams, M. Maraghini, and P. Van Ryssel-berghe, *U.S.A.E.C., A.E.C.U.*, 2918 (1954).

The Reaction of Germanium with Aqueous Solutions

I. Dissolution Kinetics in Water Containing Dissolved Oxygen

Walter W. Harvey and Harry C. Gatos

Lincoln Laboratory, Massachusetts Institute of Technology, Lexington, Massachusetts

ABSTRACT

The dissolution of germanium in water was studied as a function of oxygen partial pressure, temperature, crystallographic orientation, and mobile-carrier density. It was found that, although thermodynamically feasible, germanium does not react with water, freed of oxygen, in the temperature range studied (up to 100°C). In the presence of oxygen the dissolution rate in pure water is a function of oxygen partial pressure, reaching a limiting value of the order of 1 μg/cm^2/hr at 35°C under oxygen partial pressures greater than approximately 0.5 atm. For a given oxygen pressure the dissolution rate is approximately trebled for a ten-degree temperature rise, the measured activation energy for the dissolution reaction being 19 $\pm$ 2 kcal/mole. The order of dissolution rates for the three principal crystallographic faces was found to be {100}> {110}> {111}. No effect on the dissolution rate was found to result from changes in mobile-carrier concentrations brought about by doping or illumination. From dissolution rates and potentials it is concluded that the dissolution process is under cathodic control and that the rate-determining step is the reduction of oxygen by germanium.

With the recent advances in semiconductor theory and technology, a great deal of interest has centered about the reactions of germanium surfaces with various ambients and the resulting changes in electronic properties. Chemical etching and polishing in solutions containing strong oxidizing agents have been studied extensively on a more or less empirical basis in order to meet the needs for reproducibly smooth and undistorted surfaces. However, systematic studies of the reaction of Ge with aqueous solutions containing no oxidizing agents other than dissolved oxygen have not hitherto been reported. Also lacking is an understanding of the electrochemistry of dissolution without externally applied emf.

It is known that direct interaction of Ge with water is thermodynamically possible (1)

$$Ge + 2H_2O = GeO_2 + 4H^+ + 4e^-; \quad E^\circ = -0.15 \quad [1]$$

It was found in this laboratory, however, that at ordinary temperatures (up to 100°C) this reaction does not proceed at a significant rate. In the presence of oxygen, the dissolution rate of Ge in water can be measured conveniently by analysis of the solution for Ge.

The present study was undertaken in an attempt to elucidate the role of oxygen in the dissolution of Ge in water and in aqueous solutions of nonoxidizing electrolytes. Emphasis has been placed on the kinetics and electrochemistry of the dissolution process, taking into account the semiconductor properties of Ge. This paper deals primarily with the kinetics of the dissolution of Ge in water containing dissolved oxygen.

Experimental

Materials

Germanium.—Thin rectangular slabs were cut from single crystals grown in this laboratory from high purity, zone-refined Ge. The dimensions of the slabs were 15 x 20 x 1 mm. A 1-mm diameter hole was drilled ultrasonically into each slab for convenience in handling. The crystals (diamond structure) were oriented by x-ray techniques before cutting, so that the two large faces of the slabs corresponded to {100}, {110}, or {111} surfaces.

Water.—High resistivity water was prepared in two stages of distillation using tin-lined stills in tandem. Dissolved CO_2 was removed by bubbling CO_2-free gas (O_2, N_2, or a mixture of the two gases)

through a presaturator for several hours before forcing the presaturated water (neutral to within 0.2 pH unit) into the reaction cells.

Gases.—Cylinder gas was passed through a U-tube containing Ascarite for removal of CO_2 and then dispersed in distilled water contained in a gas-scrubbing tube before being admitted into the reaction cells. Commercial prepurified nitrogen was used.

CP-4 etchant.—The chemical polishing agent commonly known as "CP-4" was prepared from chemical reagent grade conc. HNO_3 (5 parts by volume), glacial CH_3COOH (3 parts), 48% HF (3 parts), and Br_2 (0.06 part).

Surface treatment.—Gross irregularities on the surfaces of the Ge slabs were removed by lapping on a flat glass plate using a slurry of water and 1600-mesh garnet powder. The freshly abraded slabs were then treated with CP-4 for a time (usually 30 sec to 1 min) sufficient to remove all traces of the pits formed by grinding. The resulting surfaces were microscopically smooth and highly polished. The roughness factor of CP-4 treated Ge surfaces has been reported to be 1.3 (2).

Before immersion, the Ge slabs were given a brief cleansing etch in freshly prepared CP-4 and rinsed thoroughly with doubly distilled water. No Ge could be detected analytically in the last portion of rinse water. After rinsing, the slabs were transferred immediately to the reaction cells.

Analytical.—Samples of solution were taken during the course of an experiment (see below) and analyzed colorimetrically for Ge employing the oxidized-hematoxylin method (3). The stability of the reagents was checked by analyzing standard Ge solutions along with each set of samples. Ageing of the hematoxylin reagent for several weeks or longer before use led to enhanced color stability. Using a Beckman Model *DU* spectrophotometer the useful range of Ge concentration was 0-2 μg/ml with a sensitivity of 0.005 μg/ml or better and an accuracy of about 1%.

Standard solutions for analysis were prepared by bubbling oxygen gas over Ge slabs immersed in boiling water under reflux and determining the weight loss with a microbalance. The color intensities of solutions so prepared fell along the same calibration curve as for standards prepared from high purity GeO_2 powder, but the former values were somewhat more consistent and reproducible, possibly because of the tendency of GeO_2 to form colloidal solutions on dissolving in water.

Apparatus and Procedure

Three to eight Ge slabs were mounted on a holder made of glass rod and separated by spacers cut from 3-mm glass tubing. The holder was suspended in a reaction cell as illustrated in Fig. 1. Three such cells were employed simultaneously. Beginning with the gas-scrubbing tubes, the apparatus was constructed entirely of glass. The stream of water-saturated gas bubbles entering the reaction cell through the capillary orifice did not come into direct contact with the Ge specimens. Continuous bubbling of gas during the runs at a rate of 80 or 100 ml/min

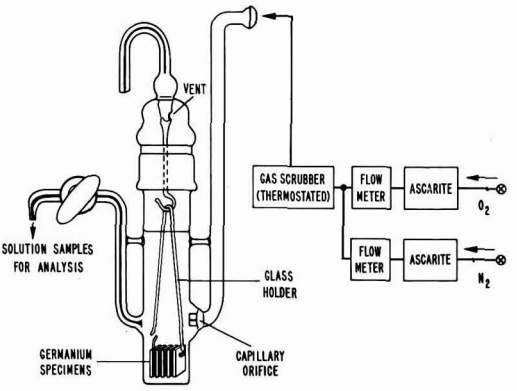

Fig. 1. Apparatus for dissolution experiments

provided vigorous agitation and maintained saturation of the solution with oxygen at the desired partial pressure. For varying the partial pressure of oxygen and, thus, the concentration of dissolved oxygen, streams of O_2 and N_2 at predetermined flow rates were mixed in the gas-scrubbing tubes and passed into the reaction cells.

The initial volume of solution in each cell was approximately 40 ml. During the course of the reaction, samples of the solution were withdrawn through the capillary sidearm by closing off the exit tube in the cap (Fig. 1). Depending on the effect being studied, 5-10 samples (generally 1.5 or 2.5 ml) from each cell were discharged into weighed vials for subsequent analysis. The amount of solution remaining in the cell at the end of the experiment was determined by pipetting into a weighed flask. A correction was made for solution retained by the specimens upon removal. Sample and residual solutions weights were determined to 0.01 g.

In studies of the effect of light on the dissolution process, illumination was provided by 40-watt incandescent lamps of tubular shape immersed in the water bath on either side of the cell. Temperature rise in the cell during illumination was prevented by adjustment of the operating temperature of the water bath. Without compensation the solution temperature increased 0.15°C as a result of thermal radiation. In all experiments reported herein the temperature was controlled to ±0.01°C.

Dissolution rates were obtained from plots of amount of Ge dissolved as a function of time. Results are reported in terms of micrograms of Ge dissolved per square centimeter of geometrical surface per hour ($\mu g/cm^2/hr$). Since the observed dissolution rates are very small, they are likely to be affected even by slight differences in surface treatment. For this reason direct comparisons of rates for different specimens were usually made by employing three sets of Ge slabs which were etched and rinsed simultaneously, and hence received nearly identical surface treatment before they were placed in individual reaction cells. The dependence of rate on temperature, oxygen partial pressure, or illumination was evaluated by changing the experimental conditions midway in a given run.

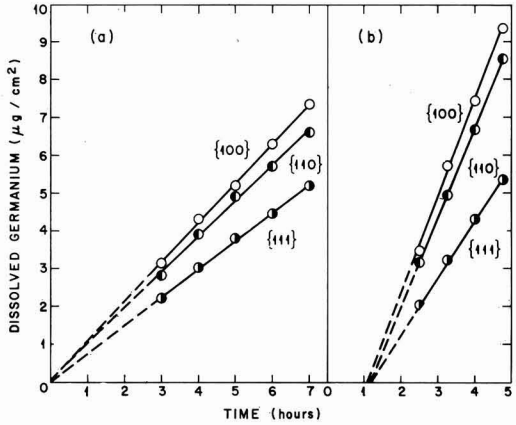

Fig. 2. Typical data showing amount of Ge dissolved in oxygen-saturated water at 35°C with and without an induction period: comparison of {100}, {110}, and {111} surfaces.

Preliminary Experiments

Initial measurements carried out in nitrogen-, air-, and oxygen-saturated water established that reaction [1] does not take place or proceeds at exceedingly slow rates between 30° and 40°C. In air-saturated water the average dissolution rate was 0.57 $\mu g/cm^2/hr$ at 30°C, and in oxygen-saturated water it was 0.72 $\mu g/cm^2/hr$ ({100} surfaces). One $\mu g/cm^2$ corresponds approximately to 10 atom layers of Ge. The observed dissolution rate in nitrogen-saturated water (0.024 $\mu g/cm^2/hr$) is likely the result of trace amounts of oxygen introduced with the prepurified nitrogen or not removed by nitrogen bubbling. Indeed, Ge was found to be completely inert to boiling water refluxing under a nitrogen atmosphere; even after prolonged immersion (40 hr) no detectable amounts of Ge were found in solution. It is therefore evident that dissolved oxygen is essential for the dissolution of Ge in water.

Dissolution as Function of Time. Induction Period

Typical data relating the amount of Ge dissolved to time of immersion in oxygen-saturated water are plotted in Fig. 2. It is seen that the rate of dissolution (slope) remains constant for rather long periods of time. This behavior was observed for the various temperatures, surface orientations, and oxygen partial pressures.

The period of induction for the reaction as determined by graphical extrapolation (Fig. 2b) varied unpredictably from experiment to experiment and is believed to be a manifestation of commonly encountered differences in surface treatment. Although apparent induction periods as long as 1.7 hr were occasionally observed, an average value of 0.5 hr was found for a number of independent runs at 35°C. Regardless of the length of the induction period, however, relative dissolution rates were satisfactorily reproducible. In general, absolute dissolution rates were higher and also less reproducible when the apparent induction period was relatively long (say more than 30 min). Thus, in 12 runs with nearly zero induction period the average dissolution rate was 1.03 ± 0.09 $\mu g/cm^2/hr$ at 35°C for {110} surfaces. On the other hand, in 28 runs with an average induction period of 0.5 hr, the average dissolution rate was 2.2 ± 1.1 $\mu g/cm^2/hr$. Samples with {100} and {111} surface orientations gave similar statistical results.

The existence of an induction period preceding Ge dissolution is believed to be associated with surface changes brought about by treatment with CP-4. With this reagent an invisible GeO_2 film is formed on the Ge surface; this film is believed to be several atom layers thick (4) and usually has the properties of the soluble hexagonal modification. The formation of insoluble, tetragonal GeO_2 is also possible, and its presence on the surface together with the soluble modification would lead to an apparent induction period preceding Ge dissolution. This difficultly soluble film is most likely formed by reaction with CP-4 vapor during transfer of the specimens to the rinsing bath. Accordingly, it was found that, by displacing the CP-4 with a large volume of dilute HF before removal of the specimens, the induction period could usually be eliminated. Treatment with HF following removal of the specimens from the CP-4 did not have this effect. The higher rates measured when Ge dissolution was preceded by an induction period are probably associated with an increase in submicroscopic surface roughness resulting from undermining of the insoluble oxide residue or may be the result of galvanic action. No attempt was made to clarify this point experimentally.

Dependence of Dissolution Rate on Crystallographic Orientation

For the three principal crystallographic faces the order of the observed dissolution rates was {100}>{110}>{111} (Fig. 2). Absolute and relative dissolution rates at 30° and 35°C are listed in Table I. The ratio of absolute rates corresponding to short or zero induction periods is computed from the table to be {100}/{110}/{111} = 1.00/0.91/0.70 at 35°C, in fair agreement with relative rates obtained in a large number of experiments and averaged without regard to apparent time of induction (or absolute value of rate). It is significant that electron microscopic examination of CP-4 treated Ge specimens revealed no characteristic differences in microstructure among the various surface orientations.

Comparable differences in dissolution rate were found by Camp (5) in a study of the etching of

Table I.

	Absolute* dissolution rates ($\mu g/cm^2/hr$)		
	{100}	{110}	{111}
35°C	1.13 ± 0.08	1.03 ± 0.09	0.79 ± 0.08
30°C	(0.68)	(0.60)	(0.41)
	Relative† dissolution rates		
	{110}/{100}	{111}/{100}	{111}/{110}‡
30°C	0.89 ± 0.03	0.63 ± 0.04	0.73 ± 0.04
35°C	0.90 ± 0.03	0.62 ± 0.06	0.72 ± 0.04

* Averages of runs exhibiting very short induction periods. At 30°C the values listed represent the average of only two runs.
† Average ratios for all runs involving comparison of different orientations regardless of induction period.
‡ Values in this column are experimental ratios; they may be compared with values calculated from the first and middle columns.

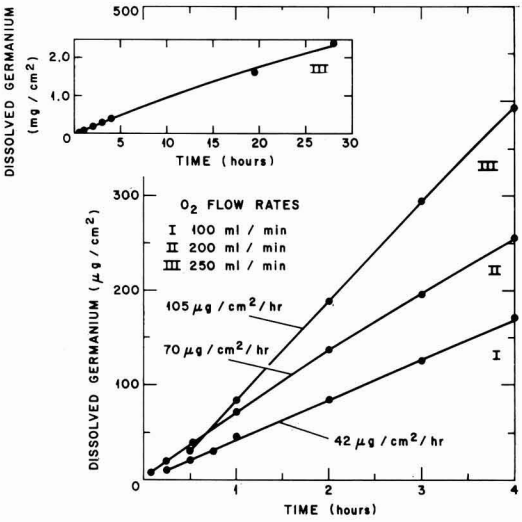

Fig. 3. Dissolution of Ge in water, 100°C, refluxing under oxygen at various flow rates.

oriented Ge surfaces in H_2O_2-HF-H_2O solutions. The observed order for this system above 25°C was {110}>{100}>{111}; below 25°C the order of {100} and {111} was reversed. By comparison, Rösner (6) concluded from a study of the action of a number of etching media on Ge that the effect of surface orientation was not pronounced, but that {100} surfaces may be somewhat more strongly attacked.

Temperature Dependence

The activation energy of the dissolution process was evaluated in individual experiments by allowing the reaction to proceed for a time at a given temperature and then bringing the bath to a higher (by 5° or 10°) or lower temperature. The temperatures employed were 30°, 35°, and 40°C. In general, rates were increased threefold for a 10°C rise in temperature. No consistent variation of the calculated activation energy with surface orientation was found; the average value of ΔE^* for 15 determinations employing {100}, {110}, and {111} surfaces was found to be 19.3 ± 1.9 kcal. Moreover, since the average relative rates (Table I) do not vary appreciably in the temperature range considered, it follows that inherent differences in activation energy among the various orientations must be small, probably less than 2 kcal.

The validity of comparing the dissolution rates obtained at different temperatures might appear questionable owing to the temperature variation of oxygen solubility. However, the solubility of oxygen in water at a total pressure of 760 mm varies only from 1.112 x 10^{-3} to 0.964 x $10^{-3}M$ between 30° and 40° (7). Furthermore, the observed dissolution rates do not change appreciably with oxygen partial pressure in the vicinity of 1 atm (see below).

Taking the activation energy as 20 kcal and the dissolution rate at 35°C as 1.0 μg/cm²/hr, the rate at 100°C and at the same concentration of dissolved oxygen (1.0 x $10^{-3}M$), is calculated to be about 300 μg/cm²/hr. Experimental results on the dissolution of Ge at 100°C for several oxygen flow rates are shown in Fig. 3. The partial pressure of oxygen in the system can be only approximated (from the flow rate of the gas and the rate of reflux of the water); at 100 ml O_2/min, p_{O_2} was about 0.03 atm. The observed dissolution rates (e.g., 40 μg/cm²/hr at 100 ml O_2/min) seem quite reasonable in terms of the rates pertaining to lower temperatures (cf. below). A dissolution rate of 22 μg/cm²/hr was reported by Rösner (6) for Ge immersed in boiling water. Considering that in the latter case the supply of oxygen was not controlled, the agreement between the two results is satisfactory.

After dissolution at 100°C the Ge specimens became visibly etched, in contrast to the experiments near room temperature where the specimens retained their high luster. Microscopic examination under polarized light revealed that the surfaces were pitted but free of bulk oxide. Etching takes place soon after immersion, which may account for the fact that the observed dissolution rates at 100°C did not vary appreciably with time (see inset in Fig. 3).

Variation with Oxygen Partial Pressure

Dissolution rates of {110} surfaces were determined at 40°C for various oxygen partial pressures by bubbling N_2-O_2 mixtures of known composition through the reaction cells. The data obtained are summarized in Fig. 4. In the inset of the figure, steady-state dissolution rates are plotted as a function of oxygen partial pressure. The experimental results can be expressed by the following general equation

$$r = k_1 p^n / (1 + k_2 p^n) \qquad [2]$$

where r is the dissolution rate, p is the oxygen partial pressure, k_1 and k_2 are constants, and n is an exponent not greater than unity. Numerical values of

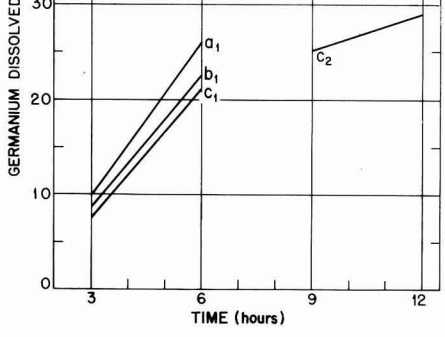

Fig. 4. Dissolution of Ge in water, 40°C, saturated with oxygen at various partial pressures. For clarity, runs d, e, and f have been omitted from the lower part of the figure. In each case, steady-state dissolution rates were measured at an initial oxygen partial pressure (subscript 1) and again, in the same run, at a lower oxygen pressure (subscript 2).

k_1 and k_2 were calculated using the method of least squares for the case $n = ½$ and $n = 1$. A better fit was obtained using $n = 1$, the correlation coefficient being 0.948 as compared to 0.899 for an assumed value of $n = ½$. Furthermore, on setting n equal to unity, the calculated limiting rate ($k_2 p^n >> 1$) is 5.0 $\mu g/cm^2/hr$, in good agreement with observation, whereas for $n = ½$ the corresponding limiting rate is 10.4. A first-order dependence on p_{O_2} is, thus, more compatible with the experimental data.

It is, of course, possible that a still better correlation could be found using some fractional power of p_{O_2}, between 0.5 and 1.0; the scatter of the data, however, discouraged a more detailed statistical analysis.

Effect of Mobile Carriers

In the experiments described thus far, nearly intrinsic, n-type single crystals were employed; however, dissolution rates were also determined for both n- and p-type Ge of various resistivities from 3 to 40 ohm-cm. No significant variation in dissolution rate was observed with changes in sign or bulk concentration of the majority carrier.

It is well known that the densities of carriers of both types can be augmented considerably by illumination. Moreover, since the relative increase in the density of the minority carrier is comparatively large, the effect of illumination can be used to determine the role of holes or electrons in reactions involving semiconductor surfaces. Brattain and Garrett (8) have investigated the effect of light on Ge electrodes and have shown that rate of the anodic reaction is controlled by the supply of holes at the Ge/electrolyte interface. Accordingly, during anodic current flow the photoeffect was very much greater on n-type Ge than on p-type. The detailed mechanism of anodic dissolution proposed by Turner (9), viz.

$$Ge + 2e^+ + 2\,OH^- = Ge(OH)_2^{++} + 2e^- \qquad [3]$$

$$Ge(OH)_2^{++} + 2\,OH^- = H_2GeO_3 + H_2O \qquad [4]$$

or a somewhat modified form thereof, may apply to the anodic component of the over-all dissolution reaction.

In order to elucidate the role of mobile carriers in the dissolution of Ge in oxygenated water, a series of experiments was carried out in which the reaction was allowed to proceed for a time in nearly total darkness and then under strong illumination. No significant photoeffect was found in the dissolution rate for either n- or p-type material, although under the same experimental conditions the dissolution potential of n-type (but not that of p-type) Ge shifted toward a more anodic value by approximately 100 mv. This shift in potential as a result of illumination decreased with decreasing oxygen partial pressure and was essentially zero in the absence of oxygen.

Discussion

The foregoing experimental results show that the rate of dissolution of Ge in water is determined primarily by the concentration of dissolved oxygen, temperature, and surface treatment; to a lesser extent the rate depends on the crystallographic orientation, but is not significantly affected by changes in free carrier densities, as brought about by doping or illumination.

Direct interaction of Ge with water according to Eq. [1] does not take place, or proceeds at a negligible rate in the temperature range studied (up to 100°C). In the presence of dissolved oxygen, however, Ge reacts at a measurable rate via reduction of oxygen. By employing large Ge surfaces (powdered samples) Schwab (10) was able to measure oxygen consumption in this reaction. It is generally recognized that the stable Ge species in neutral or acidic solutions and in the absence of complexing agents is metagermanic acid, H_2GeO_3 (11). Accordingly, the over-all dissolution reaction of Ge in water containing dissolved oxygen may be represented as follows:

$$Ge + O_{2(aq)} + H_2O(l) = H_2GeO_{3(aq)} \qquad [5]$$

The driving force for this reaction corresponds to a large free energy decrease, calculated from the data given by Jolly and Latimer (12) to be 113 kcal/g-atom. On the basis of the known dissociation constants of H_2GeO_3 (13) and the amount of Ge dissolved, pH changes were calculated for reaction [5] which were consistent with those measured in our sample solutions.

The dissolution of Ge under the present experimental conditions is activation, rather than diffusion controlled, as evidenced by the following: (*a*) for diffusion control the temperature coefficient is in general less than 1.5 per 10°C and for activation control greater than 2.0 per 10°C (14) (in the present case a temperature coefficient of approximately 3.0 per 10°C was observed); (*b*) for a given oxygen partial pressure, changes in the rate of stirring had no effect on the dissolution rate except at much lower stirring rates than those normally employed; (*c*) the observed variation of the dissolution rate with crystallographic orientation is not compatible with diffusion control.

The plot of dissolution rate as a function of oxygen partial pressure (Fig. 4) has the form of a Langmuir adsorption isotherm. The fact that Eq. [2] better describes the data for $n = 1$, rather than $n = ½$, suggests that oxygen is molecularly adsorbed. The differential heat of adsorption of water on Ge has been reported to be 16 kcal/mole at monolayer coverage (15). Thus, dissolved oxygen chemisorbs by displacing chemisorbed water. Owing to the high heat of adsorption of oxygen [found in this laboratory to be approximately 80 kcal/mole at a coverage corresponding to one monolayer (16)], displacement of water by oxygen is energetically feasible, although the present system is not directly comparable to those for which the heats of adsorption were determined.

The steady-state dissolution potential of Ge in water becomes more cathodic as the oxygen partial pressure, and therefore the dissolution rate increases (Fig. 5). Moreover, the potential is far removed from the oxygen reversible potential. This behavior indicates that the dissolution process is primarily under cathodic control. Undoubtedly the over-all dissolution process is modified by the high ohmic re-

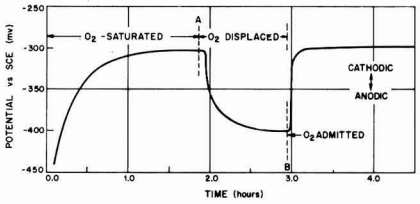

Fig. 5. Effect of oxygen on the dissolution potential of Ge

sistance of the water (combined cathodic and ohmic control). Thus, small amounts of electrolyte enhance the dissolution rate at a given oxygen partial pressure, while the process remains under cathodic control. Specific effects of added electrolytes will be discussed in a future communication.

On the basis of our findings we conclude that the Ge is in adsorptive equilibrium with dissolved oxygen and that the rate-determining step in the dissolution process lies in the reduction of oxygen. Although a detailed mechanism for the reduction of oxygen by Ge cannot be formulated at present, a mechanism which is reasonable from the point of view of solution thermodynamics involves the formation of peroxide ion, accompanied by proton exchange with water:

$$O_2 + H_2O + 2e^- = HO_2^- + OH^- \qquad [6]$$

Yeager and co-workers (17) have found a similar mechanism for the reduction of oxygen at a graphite electrode, and Handler (18) has considered formation of a peroxide structure as a possible mode of chemisorption of oxygen onto bare germanium. Rösner (6) has proposed that the etching of Ge in oxidizing liquid media proceeds by the intermediate formation of H_2O_2, which subsequently reacts as follows:

$$Ge + H_2O_2 \rightarrow GeO + H_2O \qquad [7]$$

$$GeO + H_2O_2 \rightarrow GeO_2 + H_2O \qquad [8]$$

Attempts were made in the present study to detect H_2O_2 among the soluble reaction products of the dissolution of crushed Ge samples presenting a very large surface area, but no H_2O_2 was detected. This result does not, of course, exclude the formation of a peroxide intermediate at the surface.

The observed variation of dissolution rate with crystallographic orientation of the Ge surface for the three principle low-index planes may be attributable to differences in the number of sites available for chemisorption. A correlation is shown in Table II between relative dissolution rates in oxygen-saturated water and densities of unfilled orbitals at the various surfaces. A significant point to be made is that the observed differences in dissolution rate are considerably smaller than one would expect on the basis of entirely different modes of oxygen chemisorption [cf. Handler (18)].

Table II. Correlation between density of free surface bonds and dissolution rates in O_2-saturated H_2O

Orientation	Free bonds/cm²	Relative free bond density	Relative dissolution rates
{100}	1.25×10^{15}	1.00	1.00
{110}	8.83×10^{14}	0.71	0.89
{111}	7.22×10^{14}	0.58	0.62

The absence of a photoeffect in our dissolution rates is in contrast to the results reported by Schwab (10) who found that the rate of uptake of oxygen by n-type Ge shaken with oxygen under water was accelerated by light, whereas the reaction of p-type was retarded. Schwab also noted that in the dark the rate of oxidation was somewhat lower for p-type Ge and concluded that the rate is determined by the free-electron concentration. However, his explanation in terms of separation of carriers from immobile impurity atoms by absorption of light is not consistent with the fact that donor and acceptor impurities in Ge are virtually completely ionized at room temperature (19). The shift of the dissolution potential toward more anodic values, which was observed on illumination of n-type Ge electrodes, could result from depolarization of the anodic reaction. On this basis and since the dissolution process is under cathodic control, only a very small photoeffect is to be expected in the dissolution rates. It is, thus, possible that in pure water the photoeffect lies within the limits of experimental error.

The role of electrolytes in the dissolution process and the electrode behavior of Ge under no externally applied emf will be discussed in future communications.

Acknowledgment

The authors wish to express their sincere appreciation to A. A. Menna for his skillful assistance with the experiments.

The research reported in this paper was supported jointly by the Army, Navy, and Air Force under contract with Massachusetts Institute of Technology.

Manuscript received Jan. 27, 1958. This paper was prepared for delivery before the Buffalo Meeting, Oct. 6-10, 1957.

Any discussion of this paper will appear in a Discussion Section to be published in the June 1959 JOURNAL.

REFERENCES

1. W. M. Latimer, "The Oxidation States of the Elements and Their Potentials in Aqueous Solutions," 2nd ed., p. 146, Prentice-Hall, Englewood Cliffs, N. J. (1952).
2. J. T. Law, *J. Phys. Chem.*, **59**, 543 (1955).
3. H. Newcombe, W. A. E. McBryde, J. Bartlett, and F. E. Beamish, *Anal. Chem.*, **23**, 1023 (1951).
4. R. H. Kingston, *J. Appl. Phys.*, **27**, 101 (1956).
5. P. R. Camp, *This Journal*, **102**, 586 (1955).
6. O. Rösner, *Z. Metallk.*, **46**, 225 (1955).
7. N. A. Lange, "Handbook of Chemistry," 5th ed., Handbook Publishers, Inc., Sandusky, Ohio (1944).
8. W. H. Brattain and C. G. B. Garrett, *Bell System Tech. J.*, **34**, 129 (1955).
9. D. R. Turner, *This Journal*, **103**, 252 (1956).
10. G.-M. Schwab, "Semiconductor Surface Physics," p. 283, R. H. Kingston, Editor, University of Pennsylvania Press, Philadelphia (1957).
11. E. Gastinger, *Fortschr. chem. Forsch.*, **3**, 603 (1955).
12. W. L. Jolly and W. M. Latimer, *J. Am. Chem. Soc.*, **74**, 5757 (1952).
13. W. Pugh, *J. Chem. Soc.*, **1929**, 1994.
14. M. B. Abramson and C. V. King, *J. Am. Chem. Soc.*, **61**, 2290 (1939).
15. J. T. Law, *J. Phys. Chem.*, **59**, 67 (1955).

16. M. Green, J. A. Kafalas, and P. H. Robinson, "Semiconductor Surface Physics," p. 349, R. H. Kingston, Editor, University of Pennsylvania Press, Philadelphia (1957).
17. M. O. Davies, M. Clark, E. Yeager, and F. Hovorka, Technical Report to ONR, No. 6 (1956).
18. P. Handler, "Semiconductor Surface Physics," p. 23, R. H. Kingston, Editor, University of Pennsylvania Press, Philadelphia (1957).
19. W. Shockley, "Electrons and Holes in Semiconductors," p. 24, D. Van Nostrand Co., New York (1950).

Anodic Oxide Film Formation on Zirconium Kinetics with and without Concurrent Oxygen Evolution

George B. Adams, Jr., Tien-Shuey Lee,[1] Samuel M. Draganov,[2] and Pierre Van Rysselberghe[3]

Department of Chemistry, University of Oregon, Eugene, Oregon

ABSTRACT

Comparative studies were made with zirconium to determine whether differential formation fields measured below oxygen evolution potentials agreed with those measured at high voltages. It was found that the low-voltage field is some fifteen to thirty per cent higher than the corresponding field obtained at high voltages. However, the field lowering of the activation energy for the anodic oxidation is the same whether derived from high or low-voltage measurements. This is also true of the activation energy.

These results confirm the view that the metal is anodically oxidized to the corresponding oxide at unit current efficiency below the reversible oxygen evolution potential. Ionic current efficiencies are reported for zirconium at several current densities in the high-voltage range and for the low-voltage localized oxygen evolution process.

In previous work (1, 2) it was found that the equation

$$I = Ae^{BF} \qquad [1]$$

held for the variation of ionic current density with formation field, F, in the growth of anodic zirconium dioxide films. In Ref. (2) values were reported for the differential formation fields required to oxidize Zr anodically to the amorphous oxide in aqueous solution. These values were obtained by polarization with constant currents at potentials below that required for the reversible evolution of oxygen. Agreement was obtained with formation field values reported for the same process occurring at higher voltages with concurrent evolution of oxygen (1). A more recent determination of the high-voltage differential field for this process (3) casts some doubt on the agreement in the low- and high-potential field results obtained previously.

The present investigation is an attempt to clear up this point. That is, to determine whether the polarization process which occurs with Zr and Nb on low-potential anodization is actually the formation of the oxide at unit current efficiency.

Since it is known that oxide films of these metals are formed on anodic oxidation at high voltages (1), a comparison of the values of the formation fields required for the growth of the high-voltage oxide films with those derived from polarization measurements at low potentials was indicated. Quantitative agreement would be good evidence for formation of the oxide at unit current efficiency in the potential range below oxygen evolution.

The work consists of several individual investigations; each is a comparison of equivalent measurements for the low and high-potential ranges: first, Zr fields are compared at one temperature and at a single current density; then, fields, field lowerings of activation energies, and activation energies are compared.

I—Comparison of Formation Fields (Zirconium)

Experimental Approach and Results

The high-potential differential field[4] was derived from polarization measurements at constant total current over a potential range where the current efficiency remained essentially constant. The average current efficiency for each polarization run was measured polarographically from the increase in oxygen concentration which occurred over the polarization interval. From a number of these runs taken at the same total current density, an average value of the differential field was obtained for the resulting average ionic current density. Low-potential polarization measurements were then carried out with the same electrode at a current density equal to the average ionic current density which was measured for the corresponding series of high-potential runs. Differential fields obtained from the two series of runs were then compared (see Table I).

Both the Kroll process and the iodide process zirconium were used. Electrode surfaces were pre-

[1] Present address: Research Laboratories, Westinghouse Electric Corporation, Pittsburgh, Pennsylvania.

[2] Present address: United States Borax and Chemical Corporation, Los Angeles, California.

[3] Present address: Department of Chemistry, Stanford University, Stanford, California.

[4] Fields reported are apparent fields, F/σ, where σ is the roughness factor of the electrode surface. (Values for parameters b and B, referred to later, are also apparent, i.e., σb and σB.)

Table I. Formation of anodic oxide films on zirconium. Direct comparison of differential fields measured with and without oxygen evolution (1.0N Na_2SO_4, 26°C)

	Electrode	Surface	Current density, $\mu a/cm^2$	Mean ionic current efficiency, %	Mean low-potential field,* v/cm x 10^{-6}	Mean high-potential field, v/cm x 10^{-6}	Per cent difference
1	E-1 (Kroll)	Abraded	750	6.3 ± 4.8	3.49 ± 0.07 [14]	3.56 ± 0.23 [6]	2
2	E-2 (Iodide)	Abraded (Emery)	750	81.2 ± 0.5	3.46 ± 0.08 [10]	4.17 ± 0.09 [6]	17
3	E-3 (Iodide)	Abraded (SiC)	750	73.6 ± 8.3	3.65 ± 0.19 [9]	4.20 ± 0.31 [10]	13
4	E-3 (Iodide)	Abraded (SiC)	100	47.6 ± 6.5	3.30 ± 0.11 [25]	3.60 ± 0.29 [8]	8
5	E-3 (Iodide)	Chemically polished	100	66.0 ± 6.6	4.67 ± 0.17 [33]	4.17 ± 0.16 [8]	12

* Number of determinations in brackets.

pared by both abrasion and by chemical polishing. All of the results are for a single temperature, and each comparison was made at a single current density.

Typical chronopotentiograms are shown in Fig. 1-5 for both the low-and high-potential polarizations and for several electrode surface states. The break in slope observed at about 40 v for the high voltage regression lines is quite apparent and appears to be characteristic of the metal, rather than of the surface preparation.[5] Most of the curves for Kroll process metal did not show this break. Much of the data was taken above the 40-v break. A value of 5.7 was taken for the density of the oxide, following Charlesby.

Table II lists ionic current efficiencies as measured polarographically for abraded surfaces along the low-potential "flat" in the chronopotentiogram (Fig. 1). At this potential the electrode is depolarized by the passage of electronic current through low resistance paths (pores) in the oxide film. After these pores become sealed the electrode may be polarized to high voltages.

[5] Schmidt and Mickel (5) have reported chronopotentiograms for the anodic oxidation of P-type silicon which show breaks in slope at potentials between 100-250 v. They ascribe these breaks to sparking effects.
With the zirconium electrodes used in this work, visible sparking usually occurred around 150 v. This sparking so greatly affected subsequent polarographic measurements as to render them completely invalid. Since normal polarograms were obtained at the slope-break points in the chronopotentiograms and over the potential range above these break points, it does not seem likely that sparking, visible or invisible, causes the break in this case.

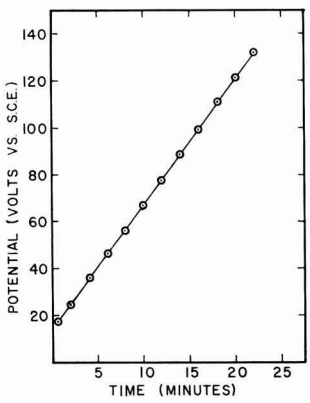

Fig. 1. Chronopotentiogram at 750 $\mu a/cm^2$. Kroll process Zr, 1.0N Na_2SO_4 at 26°C.

Discussion

From Table I it is seen that there is agreement between low- and high-potential values of the field for abraded Kroll process zirconium at 750 $\mu a/cm^2$. The agreement is rather poor, however, for abraded iodide process metal at 750 $\mu a/cm^2$, but considerably better at 100 $\mu a/cm^2$.

For abraded surfaces, the apparent formation fields determined from low-potential measurements are generally lower than those obtained at high potentials. This may be the result of a lower roughness factor for the relatively thick oxide films found at high potentials.

The ratio of the low-potential field values at 100 $\mu a/cm^2$ for chemically polished to abraded surfaces is 1.41. This ratio for the high-potential fields is 1.14. The roughness factor for the chemically polished surfaces is 1.2. This would make the roughness factors for abraded surfaces 1.7 at low potentials and 1.4 at high potentials.

The elimination of much of this uncertainty in surface roughness was the principal reason for

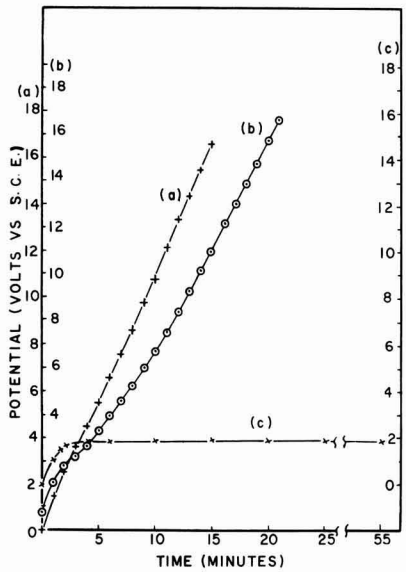

Fig. 2. Chronopotentiogram at 100 $\mu a/cm^2$. Iodide process Zr, 1.0N Na_2SO_4 at 26°C. (a) chemically polished; (b) abraded (#280C silicon carbide paper); (c) abraded (3/0 emery cloth).

Table II. Ionic current efficiencies along the flat of the potential-time curve (1.0N Na_2SO_4, 26°C)

Current density, $\mu a/cm^2$	Current efficiency, %
100	3.0
300	6.0
300	6.3
500	3.3
500	6.0

working with chemically polished surfaces. However, the low-potential results here turn out to be anomalously high; the discrepancy is definitely greater than the experimental uncertainties in the measurements.

Further work along these lines has confirmed this anomaly but has also provided additional information for interpretation. This work constitutes another study and is described below.

II—Comparison of Formation Fields, Field Lowerings of the Activation Energies, and Activation Energies

Experimental Approach

The primary purpose of this work was to determine the temperature dependence of the Tafel slope for the low-potential anodization process. Another aim was to provide equivalent low-potential data for comparison with a high-potential kinetic study which was also in progress. Unfortunately, the precision of the data obtained from the low-potential work was too low to provide a valid test of Tafel slope temperature dependence. But it served as another comparative test of low and high-potential fields.

Low-potential differential formation fields were obtained from constant current chronopotentiograms taken at five current densities for each of four temperatures. Five runs were taken at each current density. Chemically polished surfaces were used exclusively in this work and in the high-potential study described below.

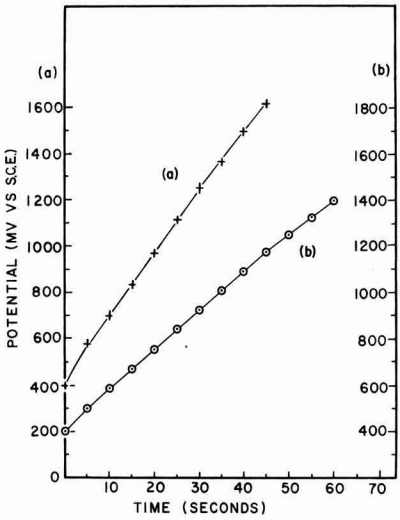

Fig. 4. Low-potential chronopotentiogram at 100 $\mu a/cm^2$, iodide process Zr, 1.0N Na_2SO_4 at 26°C. (a) chemically polished; (b) abraded (#280C silicon carbide paper).

The high-potential work itself constitutes an investigation which will be reported in detail later (4). Some results which are applicable to the present comparative study are included here.

The work at constant voltage proved to be the most reproducible and is used in the present equivalent high-potential comparison. In this work formation fields were measured as a function of ionic current density and temperature at constant voltage. The methods used were similar to those reported by Vermilyea (5). A standard color gauge was prepared and calibrated by means of microbalance measurements of weight increases, using ca-

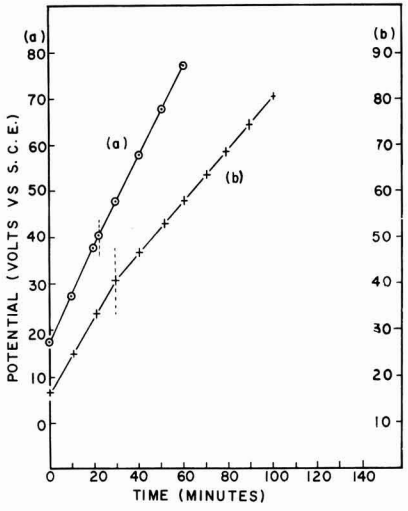

Fig. 3. Chronopotentiogram at 750 $\mu a/cm^2$. Iodide process Zr, 1.0N Na_2SO_4 at 26°C. (a) abraded (3/0 emery cloth); (b) abraded (#280C silicon carbide paper).

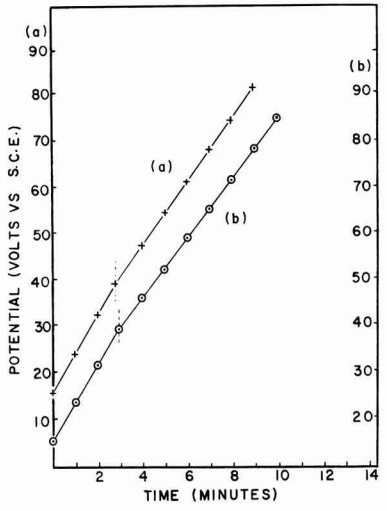

Fig. 5. Chronopotentiogram at 100 $\mu a/cm^2$, iodide process Zr, 1.0N Na_2SO_4 at 26°C. (a) chemically polished; (b) abraded (#280C silicon carbide paper).

Table III. Parameters in the formation of anodic oxide films on zirconium at low potentials (constant current)

	6.5°C	35°C	50°C	65°C
$F_{10} \times 10^{-6}$ (volt cm^{-1})	5.17	4.82	4.24	4.17
$F_{100} \times 10^{-6}$ (volt cm^{-1})	5.63	5.29	4.72	4.56
$F_{1000} \times 10^{-6}$ (volt cm^{-1})	6.08	5.75	5.18	4.95
$B \times 10^{6}$ (cm volt^{-1})	5.07	5.00	4.90	5.91
BF_{100}	28.5	26.5	23.1	27.0
b(Å)	3.0	3.7	3.4	2.8

pacitance measurements as a secondary standard for determination of oxide film thicknesses. Film thicknesses were then measured as a function of time at constant potential. All measurements were made above 40 v.

Results

Tables III and IV[6] summarize the results of this comparison. The ratio of the low- to high-potential fields ranges from 1.17 to 1.30. But the dimensionless product BF which is a measure of the lowering of the activation energy for the oxidation process by the applied field, is the same for both low- and high-potential results. This would indicate that the activation energy itself was probably the same for the oxidation, whether it occurs with or without simultaneous evolution of oxygen. This proved to be correct, as shown below.

Activation energies for both the low- and high-potential processes were obtained by plotting fields vs. absolute temperature and extrapolation to the absolute zero using the form of Eq. (1) given by the Mott and Cabrera theory (6)

$$W = bqF - k/bq \ln (I/A_o)T \qquad [2]$$

where $A = A_o e^{-W/kT}$, $B = bq/kT$, A_o is a constant, W is the height of the metal-oxide interfacial barrier, q is the charge on metal ions crossing the barrier, and b is the barrier half-width. These results are compared in Table V. A logarithmic current density dependence is apparent.[7] These values

[6] The figures in Tables III and IV are smoothed values obtained from the best straight lines through the Tafel plots. The data at 65°C, for the low-potential runs, especially, scattered rather badly. Less weight should be given to the last three figures in column four of Table III.

[7] Equation [2] requires that the regression lines for the F vs. T plot should extrapolate to a common intercept at the absolute zero. For both the low- and high-potential data however, the slopes for the lines at increasing constant currents remain essentially constant. The line for unit current density, however, should pass through the correct intercept since the current-dependent term drops out. The extrapolation to unit current density indicated in Table V gives the equivalent result.

Table IV. Parameters in the formation of anodic oxide films on zirconium at high potentials (constant voltage)

	6.5°C	35°C	50°C	65°C
$F_{10} \times 10^{-6}$ (volt cm^{-1})	4.40	3.71	3.41	3.14
$F_{100} \times 10^{-6}$ (volt cm^{-1})	4.81	4.08	3.78	3.50
$F_{1000} \times 10^{-6}$ (volt cm^{-1})	5.22	4.44	4.16	3.90
$B \times 10^{6}$ (cm volt^{-1})	5.62	6.31	6.14	6.06
BF_{100}	27.1	25.7	23.2	21.2
b(Å)	3.4	4.2	4.3	4.4

Table V. Comparison of activation energies for anodic oxide film formation on zirconium at low and high potentials

I (μa/cm^2)	Low potentials	High potentials
1000	1.17	1.19
100	1.12	1.13
10	1.08	1.08
1	1.05 (extr.)	1.04 (extr.)

are obtained for an assumed barrier half-width, b, of 2.5Å. This value of 1.04 ev for the activation energy is in agreement with a value of 1 ev reported by Charlesby The jump distances derived from the low-potential data are less than those obtaining at high potentials, but still rather high.

The average temperature coefficient of the field is -1.96 and -2.33×10^{4} volt cm^{-1} deg^{-1} for the low- and high-potential results, respectively.

Conclusions

The agreement in both the activation energies and the field lowering of the activation energies is good evidence for the view that the metal is oxidized to the oxide at unit current efficiency below the reversible potential for oxygen evolution.

That fact that a larger field is required to pass a given current when all of that current is ionic rather than being partially electronic might be ascribed to an intrinsic difference in the jump distances for a barrier located at the metal-oxide interface and for an internal barrier located within the oxide. With both barriers the same height a shorter barrier half-width distance at the metal-oxide interface would then require a larger field to provide a field lowering of the activation energy equal to that given by the larger jump distance for the internal barrier. This interpretation is rather unattractive for several reasons.

The jump distances obtained experimentally from the kinetics for high voltage anodic oxide films are always anomalously larger than seem reasonable for the lattice parameters involved (4, 5).

It would also seem that, if there were to be a shift in rate control from an interfacial barrier to an internal barrier, the transition should be a rather gradual one. But for zirconium the observed decrease in field appears to set in abruptly as soon as an electronic component of the current through the oxide film sets in.

It would seem that a more reasonable view would be that the low-potential field is intrinsically larger than that obtained from high-potential measurements. The jump distances obtained from the low-potential kinetics agree somewhat better with what one would anticipate from the lattice parameters involved. The lowering of the field observed when concurrent oxygen evolution sets in is then to be

ascribed to the action of this electronic component of the anodic current traversing the oxide film. This leakage current probably flows through low-resistance paths in the oxide film (9). This would effectively decrease the average field across the metal-oxide interfacial barrier. An anomalously large jump distance (larger fraction of this decreased field) would then be required to provide the necessary lowering of the activation energy for the metal oxidation to proceed at a given rate.

Experimental Details

Description of the experimental methods used in this work may be found elsewhere (4, 7, 8). Some of the more salient points are sketched here.

Metal Samples

Zirconium analyses appear in Table VI. Kroll process sheet and iodide process crystal bar rod were used in the first part of this paper and 70 mil sheet, rolled from iodide process rod was used in the second part. All zirconium samples were vacuum annealed at 750°C.

Electrodes

Detailed descriptions of the electrodes used in the sections on Comparison of Formation Fields and in Comparison of Formation Fields, Field Lowering, and Activation Energy appear elsewhere (4, 7). A brief description appears in Table VII.

Electrode Surface Preparation

Abrasives used were 3/0 emery cloth (Behr-Manning) and #280-C silicon carbide paper (TRI-M-ITE). In the first part of this paper chemically polished surfaces were prepared by swabbing with a solution of 50% concentrated HNO_3, 45% water, and 5% of 48% HF (all by volume). In the second part of this paper electrodes were chemically polished by swirling in this solution until maximum brightness was obtained.

Table VI. Zirconium analyses

Impurity	Kroll sheet ppm	Iodide rod ppm	Iodide sheet ppm
Al	50	80	30-60
C	140	—	100
Ca	—	—	< 50
Cr	50	10	10-20
Cu	100	10	5
Fe	800	300	400-600
Hf	<500 (est.)	<300 (est.)	100-150
N	80	50	10-25
Ni	< 5	< 5	25-60
O	1450	—	200
Pb	50	300	< 10
Si	20	20	20-80
Sn	50	10	< 10
Ti	< 50	< 50	20-40
W	—	—	<100
	99.6%	99.8%	99.8+%

Table VII. Construction of electrodes

Reference	Electrode	Approximate area (cm^2)	Masking	Description
	Zr-E-1	5.3	Baked enamel	Two coupled square electrodes 1.6 x 1.6 cm—from 70 mil sheet
Part I	Zr-E-2	12.0	Baked enamel	Three coupled circular-faced electrodes—from segments of half inch rod—six faces
	Zr-E-3	13.5	Baked enamel	Single electrode—one face—rectangular with semicircular ends 2 x 7 cm
Part II	Zr	5.5	None	Single electrode 1.6 x 1.6 cm. Both sides and edges exposed—from 70 mil sheet

The roughness factor for a zirconium surface prepared by dry abrasion on 3/0 emery cloth as determined by Krypton adsorption was reported previously as 2.1 ± 0.2 (1) and is 1.2 ± 0.1 as determined by the same method for chemically polished surfaces prepared as in Part II.

Solutions

The anolytes were 1.0*N* Na_2SO_4 in Part I, and 0.5*N* Na_2SO_4 in Part II, all made up from the AR salt and distilled water.

Acknowledgments

This work was carried out under a contract between the University of Oregon and the U. S. Atomic Energy Commission, whose support is gratefully acknowledged.

Zirconium samples and analyses were obtained from the U. S. Bureau of Mines, Albany, Oregon, through the cooperation of Dr. E. F. Hayes and from the U. S. Atomic Energy Commission, Pittsburgh Area Office, through the courtesy of Dr. E. Epremian.

The roughness factor determination for chemically polished zirconium was carried out by Mr. E. S. Snavely, Jr., at the University of Texas, through the courtesy of Professor Norman Hackerman.

Manuscript received May 7, 1957. This paper was prepared for delivery before the Buffalo Meeting, Oct. 6-10, 1957.

Any discussion of this paper will appear in a Discussion Section to be published in the June 1959 JOURNAL.

REFERENCES

1. A. Charlesby, *Acta Met.*, **1**, 340 (1953).
2. G. B. Adams, Jr., M. Maraghini, and P. Van Ryssel-berghe, *This Journal*, **102**, 502 (1955).
3. J. J. Polling and A. Charlesby, *Proc. Phys. Soc.*, **B67**, 201 (1954).

4. G. C. Willis, "Kinetic Studies on the Electrolytic Formation of Insulating Oxide Films on Zirconium," Doctoral Thesis, University of Oregon, June, 1958.
5. D. A. Vermilyea, *Acta Met.*, **1**, 282 (1953).
6. N. Cabrera and N. F. Mott, *Repts. Prog. Phys.*, **12**, 163 (1948-49).
7. T. S. Lee, "Formation Fields and Current Efficiencies in the Anodic Oxidation of Zirconium," Master's Thesis, University of Oregon, 1956.
8. G. B. Adams, Jr., T. S. Lee, and P. Van Rysselberghe Technical Report to the U. S. Atomic Energy Commission AECU-3500, 1957.
9. D. A. Vermilyea, *J. Appl. Phys.*, **27**, 963 (1956).

Electrochemical Calorimetry

J. M. Sherfey and Abner Brenner

National Bureau of Standards, Washington, D. C.

ABSTRACT

The heat effects of electrochemical processes have been measured calorimetrically to find those areas where such measurements might prove useful. The determination of reaction heat (ΔH) is one such area. The ΔH of the reaction $W + 2H_2O + 2NaOH\ (aq) = Na_2WO_4\ (aq) + 3H_2$ was measured. The results indicate that the heat of formation of Na_2WO_4 (aq) given in the literature is in error by at least 12 kcal. The heat of the reaction $Cu^\circ + nCN^- + H_2O = Cu(CN)_n^{(n-1)-} + OH^- + \frac{1}{2} H_2$ was determined as a function of the cyanide to copper ratio of the electrolyte. These data confirm the existence of the $Cu(CN)_4^{=}$ ion.

Another application for such measurements is in studies of electrode polarization. Equations are derived which show the relation between polarization and the other heat-producing phenomena in electrolytic cells. This treatment is extended to include simultaneous reactions, such as alloy deposition, and to compare the calorimetric measurement of polarization with the more conventional methods.

Researches on the thermodynamics of electrochemical processes are most often based on voltage measurements or on calculations which employ independently derived thermodynamic data. It is rather surprising that there have been few calorimetric measurements of the energy relations of electrochemical processes.

Most studies of this type have been concerned with the so-called electrolytic Peltier effect. These have been reviewed in a comprehensive treatment of this subject by Lange [1] who has himself contributed significantly to the field. Jahn (2-4) attempted to evaluate these energy relations by immersing in a calorimeter the battery used to drive the cell under study. Richards (5) electrolyzed a dilute solution of H_2SO_4 in a cell contained within a calorimeter and was able to demonstrate that the energy associated with overvoltage appears as heat in the cell.

This paper describes the initial results of a continuing research program concerned with the calorimetric measurement of the heat effects which attend electrochemical processes. The primary objective is to identify those areas in which such measurements might prove to be a useful tool. There has been no attempt to accumulate a large mass of data or to refine the measurements too highly.

The work reported here entailed the simultaneous measurement of at least three quantities; (*a*) the heat evolved by an electrochemical process; (*b*) the electrical energy necessary to effect this process; and (*c*) the extent of this process as indicated by the number of faradays passed. The necessary apparatus can be described very briefly on this basis as consisting of two parts: a calorimeter in which the reaction takes place and an electrical circuit which supplies electrical energy to the reaction and permits the measurement of both current and voltage as a function of time.

Since this apparatus is different from that of conventional calorimetry, a detailed description is given in the appendix. The two calorimetric techniques employed, the "rate method" and the "total heat method," are also given in the appendix.

Determination of Reaction Enthalpy

The simplest application of electrochemical calorimetry is the measurement of the enthalpy change (ΔH) which accompanies electrochemical reactions.

This is accomplished by measuring the electrical energy supplied to the cell and the heat energy released as a result of the electrolysis. The difference between these two quantities represents the enthalpy change of the process.

If there is no gas evolution or other pressure-volume work, this conclusion is a direct consequence of the first law of thermodynamics, $\Delta H = \Delta E = Q - W$, where ΔH is the enthalpy change, ΔE the change in internal energy, Q the heat absorbed by the system, and W the work done by the system. Neglecting sign, Q is determined by the temperature rise of the calorimeter in which the reaction takes place, and W is the electrical energy necessary to effect the reaction.

This reasoning is equally valid if the reaction produces a gas. This can be shown by dividing W into two parts, W_e, the electrical work performed, and W_{pv}, the work resulting from gas evolution. Then,

$$\Delta E = Q - (W_{pv} + W_e)$$
$$\Delta H = \Delta E + W_{pv}$$

and adding

$$\Delta H = Q - W_e$$

Experimental

Heat of the reaction $H_2O = H_2 + \frac{1}{2} O_2$.—The method and apparatus were evaluated by studying a reaction having an accurately known reaction heat. The heat of decomposition of water was chosen for several reasons. First, this reaction fulfills the above condition and, second, it presents a rather severe test in that it involves gas evolution, a complicating experimental factor. Because of the large polarization voltages at both electrodes, it involves a relatively large amount of irreversible heat, also a complicating factor.

Bright platinum was used for both electrodes and the electrolyte was 0.5*N* NaOH.

Initially the ΔH values obtained were several kilocalories low and seemed to be somewhat dependent on current density. It was believed that this difficulty was caused by recombination of dissolved hydrogen and oxygen on the platinum electrodes to give water (6). Consequently, the number of faradays passed was not an accurate measure of the over-all extent of the reaction.

This reverse reaction can be eliminated by either of two expedients: changing the electrode materials or enclosing one of the electrodes in a diaphragm in such a way as to prevent mixing of the dissolved hydrogen and oxygen by convection. The latter course was chosen because a need for such a diaphragm in future work was anticipated, and it seemed best to solve any problems involved while the apparatus was being tested.

Several diaphragm materials were tested for this application, including porous alumina and sintered glass. A synthetic membrane,[1] selectively permeable to cations, was finally chosen, not because of this selectivity, but because this type of membrane offers a relatively small resistance to the passage of ions yet is nearly impermeable to the flow of water and, presumably, dissolved gases.

[1] "Amberplex C-1", Rohm and Haas Company.

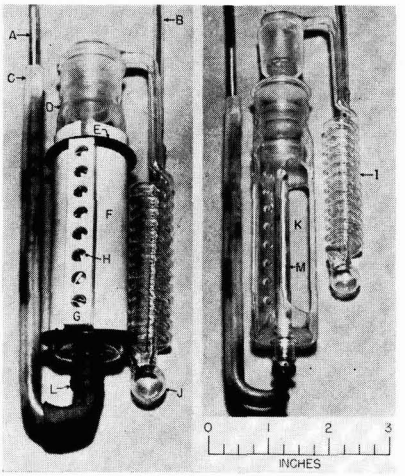

Fig. 1. Cathode compartment shown (left) assembled and (right) disassembled. A, current lead to cathode; B, hydrogen exhaust tube leading to chimney; C, plastic cover for current lead to cathode; D, electrolyte level; E, rubber compression rings (stretched "O" rings); F, membrane; G, plastic clamping block (opposing block on inside of frame not visible); H, stainless steel screws; I, spiral glass tube; J, spray trap; K, opening in glass frame; L, rubber tubing; M, cathode.

The membrane, in the form of a sheet 4 in. x 4 in. x 1/32 in., was stretched around a cylindrical glass frame to form a cathode compartment, illustrated in Fig. 1. The hydrogen generated in this compartment was carried off by a spiral glass tube which passed through the anolyte and out of the calorimeter through a chimney. This spiral brought the evolved hydrogen into thermal equilibrium with the anolyte and also acted as a spray trap. An enlargement of the tubing at the bottom of the spiral served as a reservoir for the trapped spray. Both of these functions were considered important because the catholyte was at a significantly higher temperature during the electrolysis than was the anolyte. The bright platinum anode used in previous experiments was retained, and no provision was made for trapping the spray caused by oxygen evolution.

There runs were made with this improved apparatus, all based on the total energy method. One was discarded because of experimental difficulties. The other two gave values of 68.1 and 67.8 kcal/mole. These must be corrected for the heat required to vaporize the water carried off by the evolved gases, about 0.5 kcal/mole of water decomposed. This decreases the above values to 67.6 and 67.3 kcal/mole. The accepted value is 68.317 kcal/mole (7). Recalculating to standard conditions produces a negligible change as does correcting for the heat of dilution of the 0.5*N* NaOH.

The precision of the heat capacity measurements indicates that random calorimetric errors were less than 0.1 kcal/mole. However, a significant error could have been introduced by heat lag. The cathode compartment, which had about one-tenth the volume of the calorimeter, was more or less thermally isolated from the bulk of the electrolyte. This introduced a lag which was in one direction during

Table I. Heat capacity determination

1. Approx. heater current (amp)	0.60	0.53
2. Approx. heater voltage (v)	11.5	10.2
3. Heating period (min)	19.00	20.00
4. Integrated current-voltage-time product (watt min.)	130.16	108.72
5. Observed temperature rise (ohm)	0.3071	0.2648
6. Calorimeter constant (min^{-1})	0.00495	0.00493
7. Corrected temperature rise (ohm)	0.2866	0.2396
8. Heat capacity (watt min ohm^{-1})	454.1	453.8

an electrolysis run and in the opposite direction during a heater run.

Our results show that recombination of the gases was much reduced by the presence of the membrane, but the fact that the values obtained were low indicates that this effect was not completely eliminated.

The above values for the heat of decomposition of water are looked upon as being sufficiently accurate to justify confidence in both theory and method. This is especially true when considered in the light of the above difficulties. This accuracy could be greatly improved by suitable modification of the calorimeter and electrodes.

Heat of the reaction $W + 2NaOH(aq) + 2H_2O = Na_2WO_4(aq) + 3H_2$.—*The main advantage of electrochemical calorimetry* over conventional calorimetry is that it affords a direct one-step determination of certain heats of reaction instead of the devious multi-step determinations that would be otherwise necessary. For example, tungsten does not react spontaneously with aqueous sodium hydroxide, but it does dissolve readily when made the anode of an electrolytic cell. This reaction was chosen because it exemplifies this advantage of the electrochemical method and because the literature value for the heat of formation of aqueous Na_2WO_4 seemed to be of doubtful accuracy.

The anode current efficiency of the reaction was studied by electrolyzing a 1*N* NaOH solution between a tungsten anode and a bright platinum cathode. Both electrodes were in the form of rectangular sheets about 5 cm x 10 cm. Based on the weight loss of the anode, a value of 100.15% was obtained at an anode current density of 6 amp/dm^2. At 4 amp/dm^2 the current efficiency dropped to 99.05%. Analysis of the anode gave a tungsten content of 99.9 ±0.1%.

Calorimetric runs were made, two at the higher current density and one at the lower using the total energy method. The values obtained for the reaction as written above were −8.37, −8.04, and −5.65 kcal/mole. The data and calculations are given in abbreviated form in Tables I and II.

The agreement between the first two values for the heat of reaction is within the estimated experimental error. The difference between either of the first two and the third is about equal to the error that would be introduced if 1% of the current had been diverted to a side reaction, such as the evolution of oxygen at the anode. The current efficiency values indicate that this is very possible. In short, those results are mutually consistent and, in view of the work on decomposition of water, we have a considerable amount of confidence in a value of −7 ±1.5 kcal/mole.

The heat of formation of Na_2WO_4 (aq) was calculated using this reaction heat and the heats of formation of NaOH (aq) and H_2O (7). A value of −368 kcal/mole was obtained. Graham and Hepler report the heat of solution of Na_2WO_4 to be −1.59 kcal/mole (8). This heat of solution, together with the heat of formation of Na_2WO_4 (c) (−395 kcal/mole) (7), gives −396.5 kcal/mole for the heat of formation of Na_2WO_4 (aq). This value is in serious disagreement with the literature value for Na_2WO_4 (aq) (−380.9 kcal/mole) and both are considerably larger than the value of −368 kcal/mole reported here.

The value −380.9 kcal/mole depends on the work of Huttig and Kurre (9) who calculated the heat of formation of H_2WO_4 from data on the vapor pressure-temperature relations of the system H_2WO_4-WO_3-H_2O. These results are uncertain because of the irreversibility of this system. Only two points of the *dp/dt* curve were related to the reaction $WO_3 + H_2O = H_2WO_4$ and one of the two temperatures used was given as "red heat."

The heat of formation of Na_2WO_4 (c) was obtained from Mixter's (10) measurement of the heat of reaction of tungsten powder with excess Na_2O_2. Mixter assumed the reaction to be $W + 3Na_2O_2 = Na_2WO_4 + 2Na_2O$ but did not demonstrate that the indicated products were obtained. It is possible that complex tungstates or peroxytungstates form in this reaction. Several experiments were performed

Table II. Determination of ΔH of the reaction $W + 2NaOH\ (aq) + 2H_2O = Na_2WO_4\ (aq) + 3H_2$

1. Approx. current density (amp/dm^2)	6	6	4
2. Approx. current (amp)	2.8	2.8	1.8
3. Electrolysis period (min)	22.00	21.00	22.00
4. Integrated current-time product (amp min)	62.29	59.31	39.55
5. Integrated current-time product (faraday)	0.03874	0.03688	0.02459
6. Approx. cell voltage (v)	2.0	2.0	1.7
7. Integrated current-time-voltage product (watt min)	124.49	118.63	68.09
8. Observed temperature rise (ohm)	0.3072	0.2945	0.1931
9. Calorimeter constant (min^{-1})	0.0491	0.0491	0.0492
10. Corrected temperature rise (ohm)	0.2825	0.2689	0.1535
11. Heat capacity of calorimeter from Table I (watt min/ohm)	454.0	454.0	454.0
12. Energy equivalent of temperature rise (watt min)	128.26	122.08	69.69
13. Item 7 less item 12 (watt min)	−3.77	−10.40	−1.60
14. Item 13 divided by item 5 (watt min/faraday)	−97.3	−93.5	−64.9
15. Item 13 divided by item 5 (kcal/mole)	−8.37	−8.04	−5.65

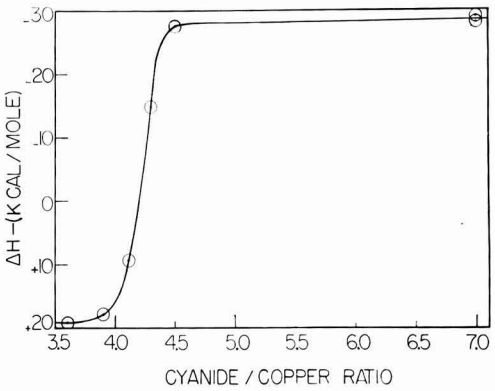

Fig. 2. Enthalpy change per equivalent of the reaction $Cu^{\circ} + nCN^{-} + H_2O = Cu(CN)_n^{(n-1)-} + OH^{-} + \frac{1}{2} H_2$ as a function of the ratio of total dissolved cyanide to total dissolved copper.

in this laboratory in order to confirm or disprove this supposition, but all were inconclusive. It must be concluded that the heats of formation of Na_2WO_4 and H_2WO_4 are not known with any degree of certainty and should be the subject of a careful redetermination. The reaction WCl_6 or WF_6 with aqueous NaOH might be suitable for this determination.

Study of Complex Equilibria in Solution

There are several papers in the literature that deal with the calorimetric determination of the formulas and the equilibria of complex ions in solution (11-13). Such studies can be made by means of electrochemical as well as conventional calorimetry.

For example, we have studied the system CuCN-NaCN-H_2O. This was done by dissolving copper anodically into solutions containing various ratios of cyanide to copper and determining the enthalpy change per faraday as a function of the composition of the solution. The results of these experiments are shown graphically in Fig. 2. The pronounced change in the heat of the reaction at cyanide to copper ratios in the range 3.5 to 4.5 confirms the existence of the $Cu(CN)_4^{\equiv}$ ion.

Electrochemical calorimetry is not readily applicable to solutions containing low ratios of cyanide to copper because of poor anode corrosion. Therefore, these experiments were continued by means of conventional calorimetry. From this the formulas of the various complexes present, their heats of formation, and one of the equilibrium constants involved were determined.

A detailed discussion on this will be reported separately.

Polarization

The voltage, E, of a cell operating at a finite rate differs in general from E^e, the voltage of the same cell operating under strictly reversible (equilibrium) conditions. The dynamic voltage, E_D, may be defined as E less the ohmic voltage drop across the electrolyte,

$$E_D = E - IR$$

Then the polarization of the cell may be defined as

$$P = E_D - E^e \qquad [1]$$

This definition is equally applicable to a cell or an electrode.

Polarization, or overvoltage, is present when the system is operated under irreversible conditions. It represents the effect of all irreversible elements, other than Joule Heat, in the total system. Because of this its value depends on the current density. Here the system is considered under steady-state conditions only, i.e., constant current density and no concentration or thermal gradients. In practice, these gradients exist but can be minimized experimentally and their effects are undoubtedly small. The major irreversibility occurs in the region of the electrode-electrolyte interface.

A detailed theory of electrode polarization must relate the overvoltage to the various rate processes occurring at the electrode interface. However, we are concerned here primarily with the problem of measurement of polarization. In some cases E_D and E^e can be directly measured as voltages by means of a reference electrode and the familiar Luggin capillary.

Polarization may also be evaluated from measurements of the total heat evolved during the operation of the cell. As this method has not been used previously, it is treated here in some detail as applied to the steady-state system.

Since polarization is a voltage, the energy associated with it equals PIt joules or 0.2390 PIt cal, where P is the polarization in volts, I is the current in amperes, and t the time in seconds. The relation between the heat developed in a cell and the polarization is derived as follows. If a finite number of coulombs could be passed through an electrolytic cell reversibly, the heat effect per mole of reaction would be equal to the $T\Delta S$ of the cell process. To eliminate the heat due to the resistance of the electrolyte in this hypothetical process, either the electrodes would have to be placed an infinitesimal distance apart or an infinitesimal current would have to be passed through the cell. In a real cell there are heat effects from two sources other than the entropy change, that due to the resistance of the electrolyte and that due to polarization at the two electrodes. The relation between the measured heat effect in calories and the other quantities is:

$$q = T\Delta SIt/96{,}500\,n + 0.2390\,[I^2Rt + (P_c + P_A)It] \qquad [2]$$

$$Q = T\Delta S/n + 23{,}060\ (IR + P_c + P_A) \qquad [3]$$

where q is calories evolved in a given reaction; Q, calories per equivalent of reaction; T, absolute temperature; ΔS, molar entropy change of the reaction; I, current, amp; R, resistance of the solution between electrodes, ohms; t, period of electrolysis, sec; n, number of faradays per mole of reaction; P_A, anode polarization, volts; and P_c, cathode polarization, volts.

The measurement of polarization based on Eq. [1] will be referred to as the voltage method and the indirect measurement made through its heat effect, and based on Eqs. [2] or [3], will be referred to as the heat method. The results of polarization studies are usually presented in the form of a curve

which is obtained by plotting the current density as ordinate against a voltage as abscissa. When the voltage used in plotting is the polarization, P, of the cell or electrode, the curve will be referred to as the polarization curve. When the voltage is the dynamic potential, E_D, of the cell or electrode, the curve will be referred to as the cd-ptl curve. These two curves are identical in shape but differ in their positions on the voltage axis by the value of E^e.

Comparison of the Measurement of Polarization by the Voltage and by the Heat Method

Measurement of electrode polarization by the voltage method requires that the reversible potential of the electrode be known. However, reversible electrodes are the exception rather than the rule, and most of the combinations of metals and solutions that are of interest in electrodeposition and corrosion do not form reversible systems. Since the equilibrium potentials are seldom available, the polarization ordinarily cannot be calculated, and other methods of reporting the data must be used. One such method consists of plotting the i vs. E curve with no attempt to estimate true polarization values, thus sidestepping the issue. The other method involves using the static potential as a basis of reference in place of the true E^e of Eq. [1]. The values of polarization obtained by the latter procedure, when applied to an irreversible electrode process, have no thermodynamic significance and cannot be used to establish an energy balance for the cell.

The measurement of polarization by the heat method (see Eq. [3]) requires a knowledge of the entropy change of the reaction and the resistance of the electrolyte. The latter can be measured by conventional procedures which are described later. The former, however, often presents a difficulty. The entropies of the metals and the standard state values of many of the common ions have been determined and are tabulated in the literature (7, 14, 15). When only these known quantities are involved, the entropy change can be calculated without introducing significant error.

However, the entropies of many of the less common metallic ions, particularly the oxy- and complex ions, are not available. When this is the case, the situation is similar to that encountered when an attempt is made to use the voltage method without a knowledge of E^e. The curve representing current density as a function of potential can be obtained, but the position of this curve along the voltage axis cannot be established. In the one case, the unknown additive constant is the $T\Delta S$ of the cell process; in the other it is the equilibrium voltage.

In the absence of a reliable value for the equilibrium voltage of a cell and for the entropy change of the cell reaction, the heat method has an apparent advantage over the voltage method. Calculation of E^e involves not only the entropy change but also the change in enthalpy. Since the latter is ordinarily about four times as large as the former, this introduces a new and probably greater uncertainty in the calculation.

Polarization at an Electrode at Which Two or More Reactions Occur Simultaneously

The discussion above is restricted in its application to electrodes at which only one reaction is taking place (hereinafter referred to as an OR electrode). The polarization at an alloy cathode or any electrode at which two or more simultaneous reactions are occurring (hereinafter referred to as an SR electrode) is not subject to this relatively simple theoretical treatment. This does not seem to have been recognized previously. The accepted practice when studying the polarization at an SR electrode is to use as E^e the static potential of that reaction which occurs at the lowest current density, i.e., in the case of a cathode process, at the most noble potential. This method of measuring polarization is not consistent with the definition of polarization given above.

To determine the polarization of an SR electrode, the departure of each reaction from equilibrium must be measured, that is, there must be an equation similar to Eq. [1] for each reaction. Furthermore, since these reactions are occurring at different rates, the current must be prorated among the various reactions. These relations are expressed in the following equation which represents the polarization of the electrode as the sum of the partial polarizations due to each reaction.

$$\text{Polarization} = f_a(E_D - E^e_a) + f_b(E_D - E^e_b) + f_c(E_D - E^e_c) + \ldots \quad [4]$$

In this equation, f represents the fraction of the current used for an electrode reaction ($\Sigma f = 1$); E_D is the dynamic potential of the electrode, and E^e is the static equilibrium potential of a reaction. The value of f must be determined by some suitable analytical scheme.

The corresponding equation for the heat method is similar to Eq. [3], except that it contains the sum of the entropies of the various reactions prorated according to the fraction of the current used for each.

$$Q = T\left(\frac{f_a\Delta S_a}{n_a} + \frac{f_b\Delta S_b}{n_b} + \frac{f_c\Delta S_c}{n_c} + \ldots\right) + 23{,}060\ (IR + P_c + P_A) \quad [5]$$

Equations [4] and [5] are both restricted in their application to electrode processes involving no secondary reactions such as the formation of an intermetallic compound at an alloy cathode.

If Eq. [4] is applied to an SR cathode and E^e_a is the equilibrium potential of the reaction which takes place at the most noble potential, then it can be seen that the conventional method for obtaining the polarization amounts to a disregard for all the terms on the right side of Eq. [4] except the first, and f_a becomes unity. It can also be seen that this approach produces polarization values which are larger than the true polarization as defined by Eqs. [4] and [5]. The latter conclusion follows from the fact that the difference between the dynamic potential and the most noble equilibrum potential $(E_D - E^e_a)$ must be the largest of the bracketed quantities in Eq. [4].

In the discussion of the polarization of an OR electrode, it was pointed out that i vs. E curve had the same shape as the true polarization curve, from which it differed only by a constant. This relation does not hold for simultaneous electrode reactions, since under these circumstances both position and shape are different. It follows that in dealing with SR electrodes the more rigorous definition of polarization assumes a correspondingly increased importance.

The discussion of polarization at an OR electrode also indicates that estimation of entropies ordinarily introduces a smaller error than does the estimation of equilibrium voltages. This advantage of the heat method over the voltage method is equally applicable to the polarization at SR electrodes.

Comparison of the Voltage and Heat Method with Respect to Experimental Difficulty

The voltage method is by far the simpler to apply experimentally. The simplest technique in using this method involves the use of a Luggin capillary. This method has the advantage that it largely circumvents the IR drop through the solution and yields directly the potential of a single electrode. Alternatively, as in the Haring cell, the IR drop in the solution is measured with probes and subtracted from the cell potential.

The heat method is much more difficult because (a) measurement of heat change is inherently more difficult than measurement of a voltage; (b) the IR drop required for Eq. [5] would in some instances be a relatively large quantity and must therefore be determined with a considerable degree of accuracy; and (c) it gives directly the cell polarization but not the polarization at only one of the electrodes.

The last difficulty can usually be overcome by means of a technique which employs as a reference an electrode through which current is flowing. In applying this method the cell consists of the electrode under study and any other counter electrode which has a reversible static potential. This will be referred to as the "dynamic counter electrode." It is necessary that this electrode have a static potential which approximates the equilibrium value because the essence of the procedure consists of measuring its polarization by the voltage method and subtracting this value from the cell polarization. This method yields at the same time the value of the IR drop in the solution.

The details of this technique for measuring the polarization of a single electrode by the heat method are as follows. The working electrodes consist of the one under study and a dynamic counter electrode. The capillary tip of a calomel half-cell or some other conventional reference electrode is pressed against the electrode under study. The potential between calomel cell and the dynamic counter electrode, with no current flowing between the working electrodes, is the equilibrium potential of the dynamic counter electrode vs. the calomel cell. With current flowing between the working electrodes, the potential between the dynamic counter electrode and the calomel half-cell is measured again. The difference between this potential and the one obtained when no current was flowing equals the sum of the IR drop in the solution and the polarization at the dynamic counter electrode. The only other information required for the calculation of the polarization at a single electrode is the heat produced by the process and the entropy change involved.

The experimental work on polarization will be reported separately.

Acknowledgment

The authors gratefully acknowledge the financial support of the Atomic Energy Commission, Research Division, which made this work possible.

Manuscript received May 16, 1958. This paper was prepared for delivery before the Cleveland Meeting, Sept. 30-Oct. 4, 1956.

Any discussion of this paper will appear in a Discussion Section to be published in the June 1959 JOURNAL.

APPENDIX

The Calorimeter

The calorimeter is made from a one-pint, cylindrical Dewar flask. Cemented to its rim is a copper flange. The lid of the calorimeter is a circular plate of copper which can be bolted against this flange to form a fluid-tight seal by means of an "O" ring. Vertical chimneys in the lid permit the introduction of the various calorimeter components: stirrer, heater, cooler, thermometer, electrode leads, and, on occasion, probes of a reference half-cell.

The relatively large currents used during electrolysis require that the electrode leads have very low resistance and No. 6 copper wire (0.41 cm diameter) was used. The low resistance thermal path formed by such heavy leads caused the temperature of the room to be reflected into the calorimeter even though the leads were passed through chimneys. To avoid this, the chimneys were reduced in length to about 2 cm and the leads were brought out through rubber stoppers. With this arrangement the bare leads pass through the constant temperature bath for a distance of at least 7 cm before coming in contact with the air. Oil is therefore required as a thermostat liquid to minimize leakage currents between the leads.

In most cases the electrodes were rectangular sheets of metal, several centimeters wide and about 10 cm long. These were attached to the current leads by a silver solder joint near the bottom of the electrode. Therefore, the lead passed through at least 10 cm of the electrolyte before passing out through the chimney. This design was adopted to prevent loss of heat along the electrode leads due to the fact that the electrodes during electrolysis are at a higher temperature than the solution that surrounds them. The copper leads and the silver solder joint were thoroughly masked to prevent attack.

In this work it is necessary to time a series of temperature readings. An ordinary stopwatch is not suitable because the accurate timing of each temperature would require stopping the watch, thus rendering impossible the timing of subsequent temperature readings. The watch used in this work is not subject to this objection and is ideally suited to this application. It is known as a "Split second timer" and is described in Federal Specification GG-W-111a under the heading "Type C."

The watch was started in synchrony with the 1-sec radio time signal and checked against it on every run. The electrical power going to the calorimeter (heater or electrolytic cell) was turned on and off manually

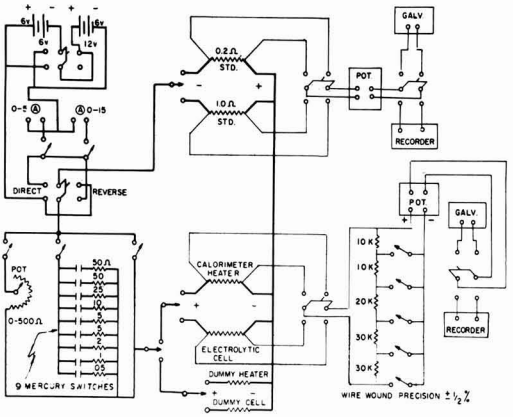

Fig. 3. Circuit diagram

and was also timed by means of the sound of this radio signal. Bath temperature, 29.6°C, was maintained with a constancy of about ±0.001°C by means of a vibrated thermoregulator. The resistance of the thermometer was read with the usual Mueller bridge and a sensitive galvanometer.

Electrical Circuit

The basic circuit consists of a battery connected to the following elements in series: a variable resistor, the electrolytic cell in the calorimeter, and a standard resistor. The variable resistor controls the current. A potentiometer across the cell measures the cell voltage, and a potentiometer across the standard resistor gives, indirectly, the cell current. Numerous additions of this basic circuit are necessary to increase flexibility, accuracy, and convenience. For example, a switching arrangement makes it possible to substitute the calorimeter heater for the electrolytic cell, thus making possible an electrical determination of the heat capacity of the calorimeter. The circuit is shown in Fig. 3. Heavy lines indicate those wires that carry appreciable currents. Light lines indicate the potential measuring circuit. The two batteries in the upper left corner of the diagram are automotive-type lead cells.

The dummy heater is a coil of Manganin wire made in the same way as the heater coil. The resistances of these two elements should be approximately the same. The dummy cell is a slide wire resistor set to have about the same resistance as the electrolytic cell being studied. These dummy units make it possible to bring the batteries to a steady-state condition before activating either the electrolytic cell or the heater. There is nothing critical about the nine resistors in the parallel bank except that they should be able to withstand a 12-v drop.

All switches in that portion of the circuit indicated by heavy lines must be rugged enough so that their resistance does not change appreciably if they are subjected to vibration. Toggle switches rated at 15 amp were unsatisfactory in this application, and either 30-amp mercury switches or 100-amp airplane-type switches were used. The toggle switches were satisfactory in the voltage measuring circuit.

The total resistance of the voltage divider bank must be large enough so that the heater or electrolytic cell is not appreciably short circuited and small enough so that the potentiometers are stable. The values shown totaling 10 kohm are a satisfactory compromise. The various ratios available from this circuit must be determined accurately and must be redetermined periodically to detect any drift. An erratic variation of about 5 parts in 10,000 was noted in these ratios until they were placed in a glass well immersed in the constant temperature bath.

Two potentiometers are necessary, one to measure the drop across the standard resistor (E_I), thus giving indirectly the value of the current, and the other to read the voltage (E_E). During the first few minutes of electrolysis, both of these values change rather rapidly, sometimes as much as 20 or 30 mv, although a change of 5-10 mv is more common. Since it is necessary to know the total electrical energy delivered to the calorimeter, these changes must be known accurately as a function of time. This presents a difficulty in that the changes are too rapid to follow with a manually operated potentiometer. A recording potentiometer can follow the changes but lacks the necessary accuracy by at least an order of magnitude.

This problem was solved by using a potentiometer and a recording potentiometer in combination, one pair for E_I and another for E_E (Fig. 3). The potential to be determined is applied to a potentiometer, the galvanometer terminals of which are connected to either a galvanometer or a recording potentiometer with a 0-10 mv range.

Each potentiometer-recorder combination is operated as follows. The approximate value of the voltage to be measured is determined in preliminary experiments with the potentiometer connected to the galvanometer. The potentiometer is then set to a reading about 5 mv less than this voltage. When the current to the electrolytic cell (or heater) is turned on, the recorder, which has been connected in place of the galvanometer, indicates the difference between the potentiometer setting and the voltage being measured. In other words, the desired potential is the sum of the readings of the two instruments. If the recording pen goes off scale, it is only necessary to reset the potentiometer to bring it back.

The recorders have a 3 second traverse time and sometimes take almost this long to "find" the voltage. This section of the curve must be extrapolated to the instant when the current was started. The accuracy of this extrapolation is unimportant, however, and a minimum accuracy of 1 part in 1,000 (0.1 mv in 0.1 v) is easily obtained with the above arrangement. An accuracy of 1 part in 10,000 (0.1 mv in 1.0 v) is more usual.

A third standard resistor with a value of 0.5 ohm would be a very useful addition to the circuit. An addition to the potential measuring circuit which would permit measurement of the voltage across either dummy unit would also be helpful.

Calorimetric Technique

Before the actual calorimetric measurements are made it is necessary to determine the current efficiency of the process as a function of current density and electrolyte composition. The nature and extent of side reactions, if any, must also be determined. Ideally the electrodes should be shaped so that the current density is constant over the entire surface of the electrodes (e.g., concentric cylinders). This latter refinement has not been observed in the present work.

The application of the two basically different techniques used to the determination of a reaction heat is given below.

The "rate method."—Heat leak and stirring energy both affect the temperature of the calorimeter and it is necessary to evaluate the sum of these two effects as a function of calorimeter temperature. The calorimeter is first cooled to a temperature 3° to 4°C below that of the constant temperature bath by passing ice water through a tube immersed in the electrolyte. When the desired temperature has been reached, the flow is stopped and the water in the tube is blown out with a stream of compressed air. The calorimeter is then left undisturbed except for stirring for a period of about 15 min in order to attain a steady state, after which the temperature is read every minute for a period of about 5 min. The temperature is then raised about 0.5°C by means of the heater and, after waiting

for a steady state, another series of time-temperature readings is taken. This is continued until bath temperature is reached. From the above data a "rating curve" is plotted showing the rate of temperature rise due to heat leak and stirring energy as a function of the calorimeter temperature.

The next step is the determination of the heat capacity of the calorimeter in terms of a rate of temperature rise. The calorimeter is cooled again and, without waiting for equilibrium, the heater is turned on. The current and voltage are followed by means of two recording potentiometers. When these two quantities and the time rate of temperature rise have attained constancy, another series of time-temperature readings is taken. This rate of temperature rise must be corrected by subtracting the contribution attributable to heat leak and stirring energy. This correction is obtained from the rating curve described above by noting the rate which corresponds to the average temperature during the calibration. The heat capacity is then inversely proportional to this corrected rate of temperature rise and is expressed in watt sec ohm^{-1}. (All temperatures are expressed in terms of the resistance of the thermometer.)

In performing the actual determination, the calorimeter is cooled and the procedure immediately above is repeated except that current is directed through the electrolytic cell instead of through the heater. It is usually necessary to start at a lower temperature than when making the determination of the heat capacity, because the cell requires a longer time to reach an approximately steady state with regard to rate of temperature rise, current, and voltage. For best precision, the temperature range over which the time-temperature readings are taken and the rate of temperature rise should be approximately the same as obtained during the heater run.

The time-rate of temperature rise observed during this run is also corrected for heat leak and stirring energy by means of the above rating curve and this corrected value (in ohm sec^{-1}) is multiplied by the heat capacity of the calorimeter (in watt sec ohm^{-1}) to get a value for the rate at which heat was being released (in watts). Subtracting this value from the power delivered to the cell under steady-state conditions and dividing the difference by the current in equivalents per second gives ΔH in joules per equivalent which is converted to kilocalories per mole.

The "total energy" method.—This method is based on measuring the total heat evolved by the cell process and simultaneously the total electrical energy used to effect this process.

Determination of the heat evolved, with regard to both experimental procedure and the method of calculation, has been treated fully elsewhere (16, 17).

The energy supplied to the heater during calibration or to the electrolytic cell during electrolysis is obtained by graphical integration of the charts from two recording potentiometers, one indicating voltage, and the other current (see appendix). This integration is performed in such a way that the number of faradays is obtained in the same calculation. Knowing the heat developed in the cell, the electrical energy supplied to the cell, and the number of faradays passed, the ΔH of the reaction can be calculated.

Sources of Error

Calorimeters made from Dewar flasks are not ordinarily used for work requiring the utmost accuracy because the thermal lags which are characteristic of such devices introduce significant errors in the heat leak correction. This is the reason for the development of the all-metal calorimeter on which most modern precision calorimetry is based. A metal calorimeter was not used in the experiments described in this paper because such a calorimeter would have to be coated with an insulating lacquer to prevent parasitic currents. It can be seen that the demands placed on this coating would be very stringent in that it would have to be completely free of breaks, chemically inert, and, ideally, a good thermal conductor.

It is fortunate that errors due to heat lag present less of a problem in electrochemical calorimetry than in conventional calorimetry. This is a result of the fact that the former method affords complete control over reaction rate and thus makes it possible to approximate closely, during the experimental run, the temperature interval and time rate of temperature rise that obtained during the calibration run. If this approximation is sufficiently close, a correction for heat leak would be unnecessary and error due to thermal lag would be eliminated. This conclusion is equally valid for both the rate method and the total heat method. Errors due to heat lag could also be eliminated by using adiabatic calorimetry. Electrochemical calorimetry is well suited to this technique because of the above mentioned control of reaction rate.

A second source of error is applicable to only the rate method and arises from the fact that completely steady values of voltage and current are never attained, if for no other reason, because the rise in the calorimeter temperature during the experiment causes a change in the resistance of the cell. Even though these changes are slow, they result in an appreciable error and, what is more serious, there is no obvious way of correcting for such changes. There is some evidence that because of heat lag the instantaneous rate of temperature rise is a consequence of the rate of heat release about one minute prior to that instant, but this has never been demonstrated conclusively. A correction based on this supposition can only be approximate since it fails to take into account the variation of current (and reaction rate) with time.

In short, it seems that the rate method cannot be used for highly accurate work without some modification. However, the calculations involved in this method are simpler and the equipment needs are less in that the recorders are a convenience rather than a necessity. For these reasons it would be the method of choice in some situations.

So far as is known, the total heat method is free of intrinsic weaknesses and with suitable refinements should yield results as accurate as those obtained by conventional calorimetric techniques.

REFERENCES

1. "Handbuch der Experimentalphysik," Vol. XII, Part 2, No. 7, Akademische Verlagsgesellschaft M.B.H. Leipzig (1933).
2. H. Jahn, *Z. physik, Chem.*, **18**, 399 (1895).
3. H. Jahn, *ibid.*, **26**, 385 (1898).
4. H. Jahn, *ibid.*, **29**, 77 (1899).
5. J. W. Richards, *Trans. Faraday Soc.*, **9**, 140 (1913).
6. M. J. Joncich and N. Hackerman, *J. Phys. Chem.*, **57**, 674 (1953).
7. "Selected Values of Chemical Thermodynamic Properties," Circular of the National Bureau of Standards No. 500, U. S. Government Printing Office, Washington, D. C.
8. To be published in *J. Am. Chem. Soc.*
9. G. F. Huttig and B. Kurre, *Z. anorg. Chem.*, **126**, 167 (1923).
10. W. G. Mixter, *Am. J. Sci.*, **26**, 125 (1908).
11. S. K. Siddhanta, *J. Indian Chem. Soc.*, **25**, 579 (1948).
12. S. K. Siddhanta, *ibid.*, **25**, 584 (1948).
13. S. K. Siddhanta and M. P. Guha, *ibid.*, **32**, 355 (1955).
14. W. M. Latimer, "Oxidation Potentials," 2nd ed., Prentice-Hall, Inc., New York (1952).
15. W. M. Latimer, K. S. Pitzer, and W. V. Smith, *J. Am. Chem. Soc.*, **60**, 1829 (1938).
16. F. D. Rossini, "Experimental Thermochemistry," John J. Wiley & Sons, Inc., New York (1950).
17. W. P. White, "The Modern Calorimeter," Reinhold Publishing Corp., New York (1928).

Ten-Gram Levitation-Melted Ingots

G. Comenetz and J. W. Salatka

Research Laboratories, Westinghouse Electric Corporation, Pittsburgh, Pennsylvania

ABSTRACT

Levitation of melts of about 10 grams in a protective atmosphere is described. There is a list, based on random experience, of materials that have been melted. Change of coil permits some temperature control. Shapes can be cast. There is a comparison with the technique of arc-melting buttons, and a list of applications. An approximate formula for levitating force is given.

A scale on which electromagnetic levitation in an inert atmosphere is possible for a variety of molten metals was first described by Polonis, Butters, and Parr (1). Their method was based on the earlier work of Wroughton, *et al.* (2). The latter aimed at melts of the order of 100 g, employing a frequency of 10 kc, but succeeded only with Al. The former used 400 kc and succeeded with 5-8 g of Al, Ti, Fe, Ni, and Ti-Fe alloys.

The first to propose levitating molten metal was Muck (3). By 1953 Scheibe had levitated 4.5 cm diameter spheres of several metals at 10 kc *in vacuo*, continuing to levitate after melting (4). In 1953 Gilbert levitated 1-10 g of several metals molten in a protective atmosphere at 100 kc (5). With a dished "meander coil" Mager has floated 140 g of molten aluminum *in vacuo* and the same weight of molten magnesium in argon (6). A spoon-shaped coil at the Leningrad Polytechnic Institute is said to have handled up to 100 g of medium-density metals (7).

Apparatus

The chamber, Fig. 1, is like that of Polonis, *et al.* The glass cylinder is 5 in. in ID and 7½ in. high.

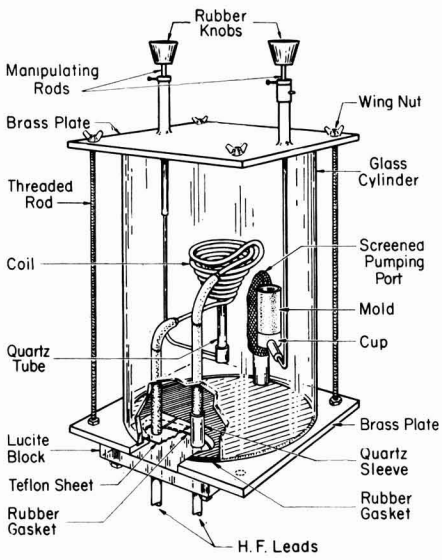

Fig. 1. Levitation chamber

The coil shown is the same as (A) in Fig. 2. It is coated with refractory cement. The left manipulating rod supports a quartz tube which can be inserted into the coil from beneath, as shown, and can be raised up within the coil. The right rod supports a cup into which a mold is set and swings the mold beneath the center of the coil after the quartz tube has been swung aside. The chamber stands on a 450 kc, 10 kw Westinghouse R.F. generator. The coil is water-cooled separately from the generator. Capacitors amounting to 0.067 μf are set on the generator and connected in parallel with the coil. An electrostatic voltmeter is connected across the leads, a little below the chamber.

Coil A, Fig. 2, has seven direct turns and one reverse turn. Coil D has seven direct and two reverse. Coils B and C, not shown, have five direct-one reverse, and five direct-two reverse, respectively.

Procedure

The charge can have any shape that does not depart too far from spherical; a flat charge sets itself on end and falls. Generally the charge is a ½-in. diameter compact of mixed metal powders or chips, from ⅜ to ¾ in. long. Components need not be well mixed, since the melt is stirred electromagnetically. Weights have ranged from 4 to 28 g.

A ferromagnetic compact must be preheated to the Curie temperature or it will not float. Preheating is sometimes used also to set off an exothermic reaction. During preheating the compact is raised on the quartz tube, out of contact with the coil. The chamber usually contains argon or helium at atmospheric pressure, but not a vacuum.

To levitate, voltage is raised rapidly to between 500 and 900 v, depending on the charge and the coil.

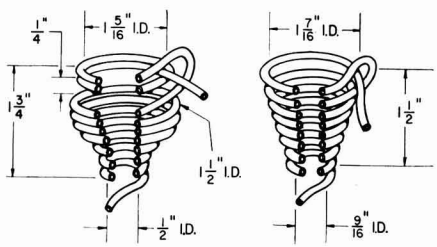

Fig. 2. Levitation coils. At left: coil D. At right: coil A, similar to that of Polonis, et al.

As much as 4 kw appears in the coil water as heat. Temperature of the floating charge is increased by lowering voltage: the charge sinks to where the field is shaped to heat better despite decreased intensity. Melting usually takes less than a minute. In coil A, Ti and lower-melting metals float not only molten, but above 2000°C. Metal vapor rises, amounting to only a small fraction of charge weight in the usual run, but sometimes so rich in a minor constituent as to alter composition.

Coils B and D are "cooler" than A, and C is cooler than B or D; Ti, for example, does not melt in C. If the tilt of A is not adjusted with care, the charge floats to one side; D requires less care.

Floating is often unsteady: the charge bobs about, although generally it does not touch the coil. Arcing sometimes occurs and may cause the charge to fall. Alloys containing Ba and Na have arced especially, perhaps owing to the low ionization potentials of those elements.

Casting is effected either by reducing voltage fairly rapidly or cutting it suddenly. If the former, some field is still present during the pour, constituting an "electromagnetic funnel" warding the melt from the bottom turn of the coil. Often the melt disappears quietly into the mold, but sometimes there is spatter.

Results

Table I is a list of materials that have been levitation-melted in the sense of continued levitation of a complete melt, weighing between 8 and 12 g, in argon, except where otherwise stated. Alloys are in weight per cent except where a/o indicates atomic per cent.

Melts repeated under seemingly identical conditions do not all succeed. Yet the record can be good: 11 out of 14 melts of Nb, 8 out of 9 of La-Zr, 8 out of 8 Mo-Ti. On the other hand, Ba-Zr is more likely to fail than not.

Casting

The levitation coil supplies a suddenly dropped melt which is small, but except for very high-melting metals can be much superheated, so that shapes can be cast.

The simplest casting is a ½-in. diameter button. The mold is a copper cup of ¼-in. wall thickness. Even if the melt is cast only a few seconds after melting becomes complete, there is at most microsegregation, which can generally be eliminated by an overnight anneal.

Flat plates ⅝ x ¾ x 1/16 or ⅛ in. thick have been cast in split Cu molds; and rods 2 in. long, ⅛ to ¼ in. in diameter, in Cu or stainless steel molds suitably vented. The rod molds do not fill quite completely. Sounder rods are cast if the mold cavity is tapered, e.g., from 3/16 in. diameter at the bottom to ⅜ in. at the top.

Tensile specimens, 1½ in. in length and 3/16 in. in gauge diameter, have been cast of Ti in a split Cu mold. A specimen was pulled, and gave reasonable values, namely, 50,000 psi yield strength, 87,000 psi ultimate strength, and 9% elongation, but a small pore could be seen at the fracture surface. Such castings of nickel-base alloys cracked transversely, no doubt owing to contraction of the cooling casting and expansion of the heating mold.

Table I. Materials levitation-melted

Al, 6 g. There was a skin at first, vanishing by degrees as the melt superheated, until no skin remained unless at the bottom which was not visible owing to rising vapor.

Ag, 4½ g. The melt was of carrot rather than the usual pear shape.

Au. A 4½ g mass floated 2 sec, then fell partly melted.

Si, 97% pure. (Pure Si would require preheating by other means.)

Cu, Fe, Ni, Co, Ti, Zr.

Cr, in hydrogen as well as argon, but castings in hydrogen were spongy. This is evidence that hydrogen is more soluble in liquid than in solid Cr.

Mo, Nb, 13½ g each.

C, Zr carbide, Zr nitride: floated without melting. The Zr nitride was sintered for 10 min at 2050°C by optical pyrometer, in an argon-ammonia mixture.

90 Fe-10 Al, 80 Ni-20 Fe, 90 Ni-10 Al, 50 Ni-50 Al, 65 Ni-25 Al-10 Mo, 60 Co-20 Ni-20 Cr, 40 Co-30 Ni-20 Cr, and about 30 other alloys of Al, Co, Cr, Fe, Mo, Ni. Chemical analysis of some Ni-base alloys showed nominal percentages were attained within ½% when pure Ni powder was used. With less pure powder, slag (probably alumina) floated on the melt, and the ingot proved low in Al.

Type 304 stainless steel, 20 g.

20 a/o Sn-Ti, 6 and 8 a/o Mo-Ti, 12 a/o In-Mg.

Zr with less than 5% of La, Ba or Sr. A dense white smoke rises from Ba-Zr; when it stops, the Ba is gone.

90 Cr-10 Mo, 80 Cr-20 Mo, . . . ,10 Cr-90 Mo (9 alloys).

11% Zr-Nb, 11 and 25% Cr-Nb. Loss of weight of 11% Cr-Nb was less than 0.1 g out of 11 g in a 30-sec run.

25 to 45 a/0 Mo-Mn: failed by arcing.

W, 43 g: floated solid, failed by arcing.

Ta, 10 g: would not lift.

For melts that float with high superheat, there is the possibility of welding one casting to another. Thus, 10% Al-Fe was first cast into a 3/16 in. diameter rod. A ½ in. diameter button was then poured around a ¼ in. length at the top of the rod. Welding was effected to the top ⅛ in. of the rod.

If melts were floated simultaneously in a number of coils and cast in succession into a mold which passed rapidly from one coil to another, welding of the hot strata would be more effective; in fact, the mold would receive something approaching a continuous pour from a ladle. Immediate recharging of the coils would open the way to continuous casting. Another approach to multiple casting is to dispose coils vertically, the higher coil dropping its melt into the lower one, which then casts the combined melts; or more than two coils might be used (8).

Comparison with arc-melting.—The technique of preparing "buttons" by arc-melting on a cold hearth is well known. It has the advantages that melts of the order of 100 g can be made, and vacuum can be employed. On the other hand, casting is not done readily, homogeneity is not always satisfactory, and

sometimes there is contamination from electrode or hearth. The power source for levitation costs more, but may be able to serve other equipment in addition to the levitation furnace.

Applications

The following applications have turned up for levitation on the small scale described above.

Casting of buttons for hardness measurement, precipitation hardening tests, corrosion tests, and metallographic and other examination connected with phase diagram studies.

Casting of plates for x-ray diffraction and as stock to be fabricated for service trials.

Casting of rods for magnetic susceptibility measurements.

Multiple castings of Mo-Ti alloys (six ¾-in. diameter buttons cast one upon another to form a partially welded 46-g cylinder 1 5/16 in. high) for specific heat determinations.

Sintering of refractories that conduct electrically when hot.

Charging molten Ti with hydrogen (a 5-min run) for solubility studies.

Preparing castings of a series of stainless steels for which, indeed, crucibles could have been found; but levitation was simpler (given the power supply) than crucible melting and casting.

A Levitation Formula

There has been no adequate theoretical treatment of the levitation of a liquid mass. The problem is not only that of total levitating force, but also of local support, in particular at the bottom tip of the melt, a tip which must exist with coils of nearly cylindrical symmetry. The solution should involve surface tension, and the effect of an oxide or other surface film if there is one.

There is a formula for total levitating force. While it is hedged with several limitations, it does give perspective as to the influence of some parameters. The limitations are that the charge is spherical, homogeneous and nonmagnetic, and small compared to distance over which the magnetic field can be assumed linear in the coordinates x, y, z.

The formula tells the ratio of levitating force F to charge weight W, a ratio which must be unity for stable levitation. The geometrical shape of the coil and the location of the center P of the floating charge relative to the coil are supposed given, but not the actual dimensions.

There are six parameters; two material, determined by the composition of the charge, two electrical, and two geometrical: δ (g/cm^3) charge density; ρ (ohm cm) charge resistivity; ν (cycles/sec) frequency; I (rms amp) current; R_1 (cm) a selected coil dimension; R_2 (cm) charge radius.

The formula is

$$\frac{F}{W} = \lambda \frac{I^2 G(x)}{g \delta R_1^3}$$

$$x = 2\pi R_2 \sqrt{\frac{\nu}{10^9 \rho}}, \quad G(x) = 1 - \frac{3}{4x} - \frac{\sinh 2x - \sin 2x}{\sinh^2 x + \sin^2 x}$$

The dimensionless x is ratio of charge radius to "skin depth" of the current; $G(x)$ is approximately $8 \times 4/315$ for $x < 1$, 0.025 at $x = 1$, 0.25 at $x = 2$, and $1 - 3/2x$ for $x > 2$; g is 980 cm/sec^2; and the dimensionless λ depends on coil shape, the location of P, and the choice of R_1.

For example, let the coil consist of two circular loops, each of the same radius R_1, having a common vertical axis. The distance between the planes of the loops is 0.81 R_1, and current directions are opposed. Along the axis, the largest value of λ is 0.026, at a point P located 0.15 R_1 above the plane of the lower loop. To float a 1-cm diameter ball of hot iron ($\rho = 120 \times 10^{-6}$, $\delta = 7.8$) at 450 kc in such a coil having loop diameter 4 cm would therefore take 1800 amp. The formula is derived by a generalization of an argument given elsewhere, whence also may be deduced the above value, both calculated and measured, of λ (9).

At a given point P in a coil of given shape, λ can be determined by a single experiment in which the other quantities in the formula are measured. This can be done at a low current, F being measured by a balance, or it may be able to be done at a current high enough to levitate, P then being the point of levitation. For example, in coil A, Fig. 2, 410 amp at 450 kc would cause a 1-cm diameter hot iron ball to float at a point P about ½ in. below the top turn. Choosing for R_1 the inside radius of the top turn, 1.9 cm, it follows that λ is 0.42.

Voltage across the coil equals current times coil impedance. The latter is almost wholly inductive, is not decreased much by a floating charge, and depends but slightly on frequency. If scale of size (R_1) is changed, inductance changes proportionately. The inductances of coils A and D, Fig. 2, are 0.57 and 0.65 microhenry, respectively.

Acknowledgment

The writers are grateful to G. M. L. Sommerman and C. S. Williams for much help with electrical problems, and to P. A. Flinn, to whom many findings and points of technique are due.

Manuscript received Aug. 30, 1957. This paper was prepared for delivery before the Washington Meeting, May 12-16, 1957.

Any discussion of this paper will appear in a Discussion Section to be published in the June 1959 JOURNAL.

REFERENCES

1. D. H. Polonis, R. G. Butters, and J. G. Parr, *Research*, **7**, S10, 272 (1954); D. H. Polonis and J. G. Parr, *Trans. AIME*, **200**, 1148 (1954).
2. D. M. Wroughton, E. C. Okress, P. H. Brace, G. Comenetz, and J. C. R. Kelly, Jr., *This Journal*, **99**, 205 (1952). Same authors, *J. Appl. Phys.*, **23**, 545, 1413 (1952). D. M. Wroughton and E. C. Okress (to Westinghouse Electric Corp.), U.S. Pat. 2,686,-864, Aug. 17, 1954. J. C. R. Kelly, Jr. (to Westinghouse Electric Corp.), U.S. Pat. 2,686,865, Aug. 17, 1954. P. H. Brace (to Westinghouse Electric Corp.), U.S. Pat. 2,664,496, Dec. 29, 1953. J. C. R. Kelly, Jr., "High Temperature Symposium," p. 187, Stanford Res. Inst., Menlo Park, Calif. (1956).
3. O. Muck, German Pat. 422004, Oct. 30, 1923.
4. W. Scheibe, *Metall*, **7**, 751 (1953) and private communication.

5. P. T. Gilbert, Jr., Private communication.
6. A. Mager, Patentschrift Nr. 12997, Deutsche Demokratische Republik, 8 April 1957; and private communication.
7. C. G. Goetzel, Private communication.
8. F. C. Hull, Private communication.
9. Pp. 547-549 of *J. Appl. Phys.* ref. in (2). Cf. also R. Becker, "Theorie der Elektrizität," vol. I, 13th ed., p. 88, Teubner, Leipzig (1944), and I. Simon, *J. Appl. Phys.*, **24**, 19 (1953).

High-Purity Crystalline Boron

David R. Stern and Lahmer Lynds

American Potash & Chemical Corporation, Whittier, California

ABSTRACT

Vapor phase reduction of boron trichloride with hydrogen on electrically heated filaments in flow systems was investigated as a potential method for the preparation of high-purity boron. Experiments were conducted on laboratory and bench-scale flow reactors. Conversion efficiency was a function of mole ratio of reactants, residence time, mass of deposit, and deposition temperature.

Massive deposits of crystalline boron analyzing as high as 99.6% by direct chemical analyses were obtained. Purity of boron appeared to be a function of both filament diffusion and boron trichloride purity.

Titanium filaments were found to be most satisfactory, since contamination due to titanium could be removed by chlorination at 300°C. X-ray diffraction studies indicated that titanium probably existed in solid solution with boron rather than as a boride.

Boron was first obtained by Moissan (1) in 1895 by reduction of boric oxide with magnesium in a thermite-type reaction, and appears to be the best preparational method at the present time for large quantities of relatively impure boron. Electrolysis of fused oxides, borates, or fluoborates has also produced elemental boron.

Although these primary methods are adaptable to commercial processes, it has not been demonstrated that boron of 99.0% purity, by direct analyses, could be obtained. Leaching and high-temperature degassing techniques can increase the boron purity from these processes to higher values.

Limitations on product purity focused attention on the vapor phase reduction of boron halides with hydrogen on electrically heated filaments with the objective of preparing boron of 99.0% purity or better. Filament techniques for the preparation of crystalline boron have been reported by a number of investigators (2-10).

This investigation was divided into two phases: the first dealt with relatively small deposits prepared in glass equipment; the second phase involved the formation of massive deposits in a larger stainless steel reactor.

The free-energy change for the reaction

$$BX_3(g) + 3/2H_2(g) \rightleftharpoons B(s) + 3HX(g) \qquad [1]$$

as a function of temperature was calculated for all the boron halides except the triiodide. Calculated results based on the Gibbs-Helmholtz relation and heat capacities as functions of temperature are presented in Fig. 1 (11-13). All components were assumed to behave ideally.

An examination of the mass expression

$$\frac{[HX]^3}{[BX_3]\,[H_2]^{(3/2)}} = K_p \qquad [2]$$

and the free energy equation

$$\Delta F^\circ = -nRT \ln K_p \qquad [3]$$

indicates that the reaction may go favorably in the presence of excess hydrogen even if the free-energy change is positive. Figure 1 shows that the boron trifluoride reaction requires temperatures far beyond any practical limit, while the tribromide requires a theoretically lower temperature.

Distribution of components at equilibrium.—The theoretical conversion and distribution for various mole ratios of hydrogen to boron trichloride were calculated and the results are presented in Table I.

Considering these equilibrium calculations and economic factors as a basis, a comparison of the respective halides can be made: (*a*) the percentage boron in the halides increases with decreasing molecular weight; (*b*) thermodynamic reduction temperature increases with decreasing molecular weight; (*c*) boron tribromide reduction theoretically requires the lowest temperature; (*d*) cost of the ha-

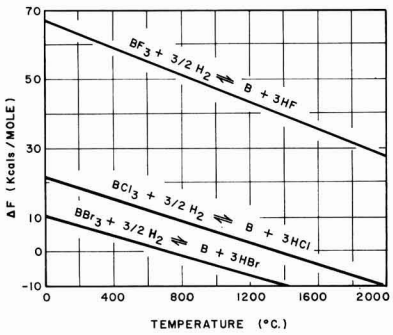

Fig. 1. Free energy of reaction as function of temperature (1 atm).

Table I. Distribution of components at equilibrium* (1100°C, 1 atm)

Mole ratio H_2/BCl_3	Mole fraction at equilibrium BCl_3	HCl	H_2	Wt (%) conv. to boron
20	0.009	0.113	0.878	80.8
16	0.014	0.131	0.856	75.6
12	0.024	0.154	0.823	68.3
8	0.046	0.184	0.770	56.9
3	0.161	0.235	0.604	32.9

* $BCl_3 + 3/2H_2 \rightleftharpoons B + 3HCl$.

lides decreases with decreasing molecular weight; (*e*) from the standpoint of availability, boron trichloride is potentially the cheapest halide in the group.

On this basis, the scope of research was limited to the reduction of boron trichloride with hydrogen. Although theoretical considerations give the general areas of operational conditions, it was necessary to determine the optimum conditions and the effect of metallic filaments in a laboratory flow reactor.

Laboratory Equipment and Procedures

A schematic diagram of the reaction tube used for the laboratory investigation is presented in Fig. 2. It consisted of a Pyrex tube (38 cm in length and 10 cm in diameter) arranged vertically with standard taper joints on each side and a large joint on the bottom. Through a water-jacketed glass cap were placed two 0.25 cm tungsten leads (one 35 cm, the other 2.5 cm in length) to provide for the vertical suspension of filaments. Filaments, which were generally 8-10 cm in length, were placed between two 1.25 cm graphite rod bushings. The bottom bushing extended into a mercury well providing both mechanical freedom and an electrical contact.

Operational procedure.—Boron trichloride and hydrogen were continuously metered into the reactor. By-pass gas sampling networks were placed before and after the reaction tube. Hydrogen was deoxidized by passing through a Deoxo catalytic purifier followed with a dehydration column. Boron trichloride was redistilled prior to use in order to remove the silicon tetrachloride and phosgene. Surface deposition temperatures were observed with an optical pyrometer.

Analytical procedure.—Samples were ground to a −100 mesh, hydrochloric acid leached or treated with chlorine under conditions to be described later under Boron Upgrading. Finely ground boron was rendered water soluble by a sodium carbonate fusion and was then titrated as the mannitol complex (14). The standard deviation for 16 duplicate analyses on different samples was ±0.4%. Many samples were analyzed spectrographically which proved very effective for small quantities of impurities. However, it should be kept in mind that this is an indirect analytical method for boron and does not account for elements such as oxygen, nitrogen, and hydrogen. Comparisons between spectrographic and chemical methods indicated that spectrographic analysis consistently gave slightly higher boron values. Exhaust gases from the reactor were monitored periodically in the gas sampling network and analyzed by infrared spectrophotometry.

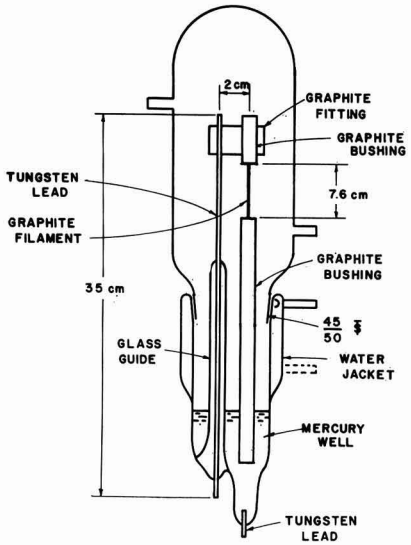

Fig. 2. Schematic diagram of laboratory flow reactor

Laboratory Experimental Results

Mixtures of boron trichloride and hydrogen were allowed to contact an electrically heated filament suspended in the apparatus of Fig. 2. All tests were made in an observed deposition surface temperature range of 1030°-1125°C. It was necessary to increase the filament current periodically to maintain a deposition surface temperature within the prescribed range. Effects of mole ratios of reactants and residence times on conversion percentages were studied. There was no evidence that the reaction variables effected boron purity in any way.

Major contaminants appeared to be the filament material, silicon, from the tetrahalide in the boron trichloride, and iron from the crushing operation.

Deposition on molybdenum, tungsten, and tantalum.—Boron was deposited on molybdenum, tungsten, and tantalum wires (8-10 cm in length, 0.15 cm in diameter). It was found that these filaments were short-lived under experimental conditions. During the first hour of operation, the filament and its deposit became extremely brittle and generally broke. Microscopic examination of the deposit showed that the boron appeared quite metallic and crystalline with a high luster. No distinct interface existed between the metal filament and boron. Analyses of some representative boron deposits on tantalum presented in Table II indicate that diffusion into boron was considerable (96.7% B and 3.2% Ta).

Deposition on graphite.—Boron was deposited on a spectrographic grade graphite filament (8-10 cm in length, 0.25 cm in diameter). During the first hour of operation, the filament generally developed "hot spots" which eventually healed. As deposit mass increased, it tended to crack and flake off. After cooling below 900°C, deposits became essen-

Table II. Filament data and chemical analyses for several typical tests

Filament material	Filament temp (°C)	Reaction duration (hr)	Weight of deposit (g)	Chemical analysis weight per cent					
				B	Fe	Si	Ti	Ta	Diff.
Ta	1200–1250	10.0	6.7	97.5	2.1				0.4
Ta	975–1025	7.0	3.6	96.7				3.2	0.1
Graphite	1000–1200	11.0	5.0	96.1					3.9
Graphite	1100–1200	7.5	5.2	95.9	0.21				3.9
Graphite	1100–1150	8.0	8.5	98.4					1.6
Graphite*	1050–1130	26.5	19.7	99.0	0.04				1.0
Graphite*	1075–1125	22.0	20.5	99.5	nil				0.5
Graphite*	1080–1120	16.5	18.5	99.0	0.45	0.13			0.4
Graphite	1075–1125	18.2	19.2	98.7	0.21	0.33			0.8
Ti	1100	5.5	3.5	95.0	0.03	0.13	2.03		2.8

* Surface sample only.

tially nonconductive and could not be reheated. Boron has a negative temperature coefficient of resistance.

Under microscopic examination the boron appeared quite metallic and crystalline with a high luster in some areas. It was observed that deposition occurred in concentric layers and that a distinct boron-carbon interface did not exist. The latter was probably due to carbon diffusion into boron. A noticeable difference in appearance of the crystalline habit between boron produced on graphite and other filament materials was observed. Data obtained with graphite filaments are also included in Table II. Surface samples analyzed as high as 99.5% boron; however, the analysis of the entire deposit varied from 95-98.7% boron depending on the severity of carbon diffusion into boron and size of deposit.

Deposition on titanium.—The deposit on a titanium filament (5-6 cm in length, 0.15 cm in diameter) appeared, on microscopic examination, quite metallic and crystalline with a high luster. Cooler areas of the deposit were black and probably less crystalline. A distinct interface between the boron and a hard central core was observed. Fortunately, the boron was easily separated from the hard central core which is probably a titanium-boron system. The titanium-boron core rendered the deposit conductive such that low resistance was realized in all temperature ranges and intermittent operation was permissible. Titanium filaments appeared to resist hydriding under the experimental conditions. Chemical analysis (Table II) indicated that diffusion of titanium into the boron lattice was considerable. This product contained 95.0% boron and 2.03% titanium.

Variables effecting deposition.—Effects of mole ratio of reactants and residence time on deposition rate and conversion were studied. All tests were made at observed constant deposition surface temperatures of 1050°-1125°C.

Results obtained in several typical experiments are presented in Fig. 3 and 4. Figure 3 indicates that with a mole ratio $[H_2]/[BCl_3]$ of 12.0, a 38.0% conversion per pass, based on feed rate, was obtained with an average deposition rate of 0.875 g boron/hr; however, these results were obtained under flow rates varying in the range of 350-1450 cm³/min. Figure 4 presents conversion per pass as a function of residence time or total gas flow for a constant mole ratio. A mole ratio $[H_2]/[BCl_3]$ of 12.0 with a residence time of 2.75 min (800 cm³/min) resulted in a deposition rate of 0.64 g boron/hr and 39.5% conversion per pass. All tests were conducted over approximately the same time intervals in order to avoid mass effects. Results indicate that mole ratio has a greater effect than residence time (or total

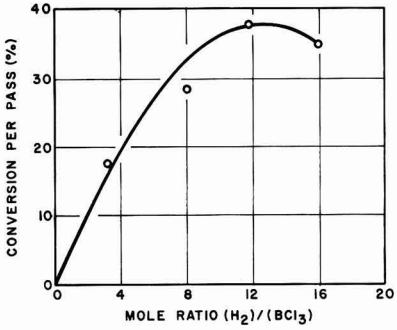

Fig. 3. Conversion per pass as a function of mole ratio. Gas reference conditions: pressure = 1 atm, temperature = 25°C. Volume of reactor = 2350 cm³. Flow rates = 365 to 1445 cm³/min. Graphite filament dimensions = 8 cm length, 0.25 cm diameter. Filament temperature = ≅1100°C.

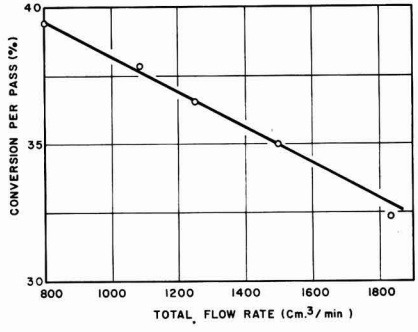

Fig. 4. Conversion per pass as a function of flow rate. Gas reference conditions: pressure = 1 atm, temperature = 25°C. Volume of reactor = 2350 cm³. Mole ratio $[H_2]/[BCl_3]$ = 12. Graphite filament dimensions = 8 cm length, 0.25 cm diameter. Filament temperature = ≅1100°C.

Table III. Deposition rates and energy requirements for graphite filaments
(Mole ratio $[H_2]/[BCl_3]$ of 12.0)

Temp. range (°C)	Reaction time (hr)	Flow rate[a] (cm^3/min) Mixture $H_2 + BCl_3$	Deposition rate (g/hr)	Conversion per pass[b] (%)	Conversion per pass based on equilibrium conditions (%)	Energy (kw-hr/g)
1100–1120	7.0	800	0.64	39.5	57.9	0.72
1030–1120	22.0	1250	0.93	36.7	53.8	0.52
1080–1120	16.5	1500	1.12	36.8	53.9	0.67
1050–1125	19.0	1840	1.19	32.4	47.5	0.64
1075–1125	18.2	1500	1.06	34.7	50.9	0.69
1075–1125	17.0	1500	1.09	35.9	52.6	0.68
1100–1125	19.5	1500	1.07	35.0	51.3	0.67
1075–1125	15.5	1500	1.05	34.5	50.5	0.66

[a] 25°C at 1 atm.

[b] Conversion per pass (based on feed rate) $= \frac{\text{Experimental Yield}}{\text{B in } BCl_3 \text{ Feed}} \times 100.$

flow) on conversion per pass within the specified experimental range.

Table III presents some typical data on deposition rate and energy.

Bench-Scale Reactor

Apparatus

A larger reactor was designed in order to study problems associated with producing massive deposits of crystalline boron and thus reducing the degree of filament contamination.

A schematic diagram of the reactor is presented in Fig. 5. It was fabricated from stainless steel pipe (30.5 cm in diameter, 61.0 cm in length) fitted with flanges at each end. Two sight glasses in the reactor shell made it possible to measure filament temperatures with an optical pyrometer. The filament (46 cm in length) was suspended between two graphite bushings (6.5 cm in diameter). As in the laboratory reactor, the bottom bushing was suspended in a water-cooled mercury well which provided for both an electrical contact and mechanical freedom for expansion. Thus the reactor shell became one electrical contact, and the lead to the top filament bushing was inserted through a gas-tight insulated flange.

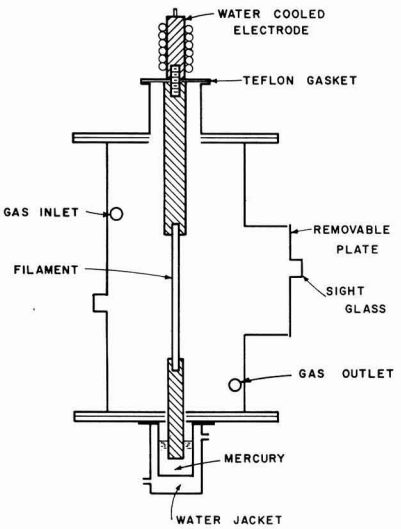

Fig. 5. Schematic diagram of bench-scale reactor

Boron trichloride and hydrogen were metered into this reactor, and the same techniques of gas monitoring and deoxidation of hydrogen were employed as in the small glass reactor. Since large quantities of unreacted boron trichloride were involved, a refrigeration system was necessary for recovery and recycling. The system consisted of a single tube heat exchanger and a condenser maintained at dry ice temperatures (−78°C) with dry ice-Methyl Cellosolve mixtures.

Experimental Results

Most of the experimental work was done with vertically supported titanium filaments varying from 15.25 cm to 30.5 cm in length and having a 0.45 cm diameter. As in the smaller glass system, the deposit developed "hot spots" which eventually healed. It was necessary to increase current periodically to maintain a deposition surface temperature of 1000°-1200°C. Deposits tended to grow in length and, in some cases, up to 50% of their original length. As a result of this growth, the deposits generally became distorted, structurally weak, and eventually broke. Deposits of greater than 450 g were obtained over a 72-hr period with average deposition rates of 6-8 g/hr. Conversion per pass of 8-20% based on feed rate were obtained with overall yields (based on recycled boron trichloride) consistently near or better than 90%. A 454-g boron deposit approximately 5 cm in diameter and 20 cm long required an 8 kw power input in order to maintain a 1000°-1200°C surface temperature.

On microscopic examination, massive deposits appeared metallic and crystalline with a high luster. Cooler areas were black and probably less crystalline. The filament was generally dispersed throughout the deposit and no specific growth formations were observed. Surface samples analyzed as high as 99.7% but always contained 0.1-0.2% titanium indicating diffusion of titanium. Massive deposits, including all of the original filament, were ground to a −100 mesh in large steel mortars. Typical anal-

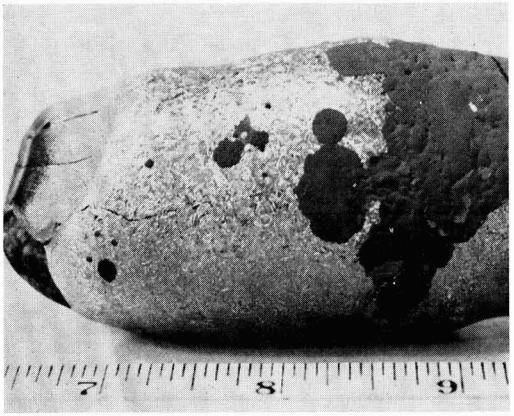

Fig. 6. Typical boron deposit (Scale in inches)

yses are 97.5-98.5% boron, 0.5% titanium, and the remainder was mostly iron. Further details on analyses and upgrading techniques are presented in a later section on Upgradng and in Table VII. An illustration of a typical deposit segment is presented in Fig. 6.

Some representative results obtained are presented in Table IV. These results indicate in a general way that a deposit of considerable size could be obtained with titanium filaments, if runs of sufficient duration could be maintained.

In order to study the relationship between deposit weight, instantaneous deposition rate, and time, tests were operated at constant mole ratio ($[H_2]/[BCl_3] = 8.4$), residence time (2.4 min), and with initial filament dimensions (15.25 cm in length, 0.475 cm in diameter) under as close temperature control as possible. Weight of the deposit as a function of time is presented in Fig. 7. Under the specified experimental conditions, a deposition rate of 14.0 g/hr was realized after 72 hr of operation.

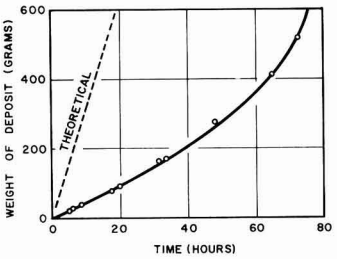

Fig. 7. Deposition weight as a function of time. Gas reference conditions: pressure = 1 atm, temperature = 25°C. Residence time = 2.4 min. Volume of reactor = 44,500 cm³. Mole ratio $[H_2]/[BCl_3] = 8.4$. Titanium filament dimensions = 15.25 cm length, 0.475 cm diameter. Filament temperature = ≅1100°C. Equilibrium conversion = 58%.

If the slopes of the curve presented in Fig. 7 are plotted as a function of total deposition weight, a good linear curve is obtained up to about 72 hr or deposit weight of 500 g. An equation for this linear curve involving deposition rate and weight is:

$$\frac{dw}{d\theta} = 0.02w + 3.8 \qquad [4]$$

The solution of this differential equation results in the relation

$$w = 190\ (e^{\frac{\theta}{50}} - 1) \qquad [5]$$

w = weight (g), θ = time (hr). However, this equation is empirical, and applies only for the stated conditions.

It was observed that the rate of deposition was proportional to the mass (or volume) of the deposit and not to the apparent geometric surface area. Since the rate of deposition is proportional to the mass of the deposit, it is probable that the requirements for optimum conversion are also a function of the deposit mass or time. Therefore, to maintain

Table IV. Boron deposition on titanium filaments[a]
(Mole ratio $[H_2]/[BCl_3] = 8.4$)

Reaction duration (hr)	Ti filament dimensions (dia. × length) (cm)	Deposit temp range (°C)	Weight boron (g)	Conversion[b] per pass (%)	Average rate of deposition (g/hr)	Yield B[c] (%)
126.3	0.475 × 15.25	960–1300	776.9	10.8	6.2	98
75.0	0.475 × 15.25	1080–1100	563.4	14.4	7.5	94
5.3	0.475 × 15.25	1000–1200	19.4	4.2	3.7	69
39.5	0.475 × 15.25	1025–1225	242.2	8.2	6.1	77
50.0	0.475 × 15.25	1075–1200	396.5	9.0	7.9	92
34.5	0.475 × 15.25	1050–1200	214.5	7.1	6.2	85
76.8	0.475 × 15.25	950–1225	568.0	14.5	7.5	—
12.0	0.475 × 30.5	1075–1500	103.7	16.1	8.6	88
7.5	0.475 × 30.5	1060–1100	61.7	15.2	8.2	73
9.8	0.475 × 30.5	1070–1100	79.0	15.5	8.1	85
40.0	0.475 × 30.5	1050–1125	352.5	16.3	8.1	84
10.3	0.475 × 30.5	1065–1085	96.3	17.1	9.4	80
50.0	0.475 × 61.0	1050–1125	546.0	20.9	10.8	96

[a] Residence Time = $\frac{\text{Reactor Volume}}{\text{Flow Rate (cm}^3\text{/min)}}$ = 2.4 min.
Reactor volume = 44,500 cm³; reactor flow = 18,600 cm³/min; reference conditions = 1 atm at 25°C.

[b] Conversion Per Pass = $\frac{\text{Experimental Yield}}{\text{B in } BCl_3 \text{ Feed}} \times 100$.

[c] Based on BCl_3 recovered from refrigeration cycle.

Table V. Principal x-ray diffraction "d" lines, Cu K_α radiation

Reported (7) *		Titanium filament 1075°-1125°C		Titanium filament 1100°-1200°C		Graphite filament 1075°-1125°C	
5.03	VS	5.12	S	7.82	S	5.40	W
		4.74	M	5.03	VS	5.03	W
4.40	VS						
3.92	VS	4.00	W	4.67	VS	3.40	VS
3.56	W	3.25	W	4.44	S	2.88	W
3.33	M	3.21	W	3.70	M	2.70	W
2.70	W	2.87	W	3.54	M	2.55	M
2.53	S			2.86	M		
2.42	VS	2.64	M	2.60	M	2.42	VW
2.34	W			2.47	M		
2.19	W			2.40	M		
		2.13	S				
2.02	S	2.05	VS	2.03	M	2.04	VW
1.74	W	1.77	M	1.76	M	1.76	VW
1.54	W	1.55	W	1.55	W		
		1.52	M			1.52	S
1.43	S	1.43	W	1.43	M	1.43	W
1.37	M	1.38	M	1.38	M		
				1.35	M		
1.30	W	1.31	VW			1.29	VW

* VS—very strong line; S—strong; M—medium; W—weak; VW—very weak.

maximum conversion would necessitate constant readjustment or programming of the reaction conditions. As the reaction proceeds, it is probable that the deposition rate would approach the limit (58% theoretical equilibrium conversion or 30.3 g/hr) established by equilibrium and flow conditions.

Crystallinity.—X-ray diffraction studies indicated that several different samples exhibited a certain degree of crystallinity. Data in Table V compare the observed "d" values of boron deposited on graphite and titanium elements and the reported "d" values of crystalline boron whose structure has been established as a tetragonal unit with fifty atoms arranged to form four nearly regular linked icosahedra (7). In all cases no boride lines were detected, indicating that titanium or carbon and boron form mainly solid solutions rather than crystalline compounds at the deposition temperatures indicated. A wide variation in "d" line spacings was observed; however, a sample from a region in excess of 1200°C showed a resemblance to values reported in the literature. Boron deposited on titanium exhibited a considerably greater degree of crystallinity than boron deposited on graphite filaments. It has been shown previously that the crystal structure of boron is a function of temperature and may explain the differences observed in crystallinity of boron deposited on titanium filaments (15).

Examination of reaction products.—Exhaust gases from the reactor were monitored and analyzed with an infrared spectrophotometer. Small quantities of diborane (B_2H_6) were identified in the exhaust gases as well as hydrogen chloride and excess boron trichloride.

Since diborane was observed in the exhaust gases, the mechanism for the formation of boron may involve a stepwise reduction such as:

$$BCl_3 \rightarrow BH_3 \rightarrow B_2H_6 \rightarrow B$$

Borine (BH_3) has never been observed chemically or spectroscopically, although there is indirect evidence for borine (16-18).

Boron Upgrading

Attempts were made to upgrade boron produced both in the laboratory and bench-scale reactors, since metal contamination appeared to be significant in all deposits. Two techniques were empolyed: density classification and a chlorine treatment.

Density classification.—Several boron samples containing titanium (D = 4.5) were ground to a −100 mesh, leached in 6M HCl to remove iron introduced by grinding, and were then subjected to a density classification in methylene bromide (D = 2.49). This mixture separated into high and low density components. The heavier component consisting of particles richer in titanium readily separated from the lighter boron (D = 2.33-2.39). However, there was a considerable amount of intermediate material (D = 2.39-2.49) which could not be separated by this technique. Analysis showed a slight "upgrading." Results are presented in Table VI.

This technique was also applied to boron containing tantalum (D = 11.2) which was readily separated resulting in marked "upgrading." One sample was upgraded from 81.5% to 99.8% (Table VI). Carbon (D = 2.45) could not be separated from boron by this method due to the proximity of their densities.

Chlorination.—One pound charges or larger of boron containing titanium were ground to a −100 mesh, and were treated with chlorine in a Pyrex tube reactor A reaction was observed between 300° and 350°C resulting in a volatile liquid which was identified as titanium tetrachloride. Small quantities of volatile iron chlorides were also detected. Infrared spectra of the reaction products proved that boron trichloride was not being formed within the prescribed temperature range. A 900-g sample (−100 mesh) analyzing 97.5% boron, 1.1% titanium, and 0.10% iron was upgraded to 99.6% boron, 0.3% titanium, and 0.07% iron by the chlorine treatment. Results obtained in several typical treatments are presented in Table VII.

Conclusions

1. Rate of boron formation in the vapor phase reduction of boron trichloride depends mainly on four variables: mole ratio of hydrogen to boron trichloride, residence time of gas mixture in the reactor, deposition temperature, and mass of deposit. For maximum deposition rates, large hydrogen to boron

Table VI. Density classification of boron containing tantalum and titanium

Filament impurity	Per cent boron	
	Before classification	After classification
Ti	94.5 (5.4% Ti)	97.0 (2.1% Ti)
Ta	90.8	98.4
Ta	92.2	97.7
Ta	86.4	90.1
Ta	90.1	98.7
Ta	81.5	99.8

Table VII. Analyses of boron deposited on titanium before and after chlorination (Bench-scale reactor)

% B	% Ti	% Fe	% Mg	% Si	% Cu	Analysis	Remarks
95.8	4.0	0.098	0.0026	0.050	0.014	Spec.	Before chlorination
99.7	0.18	0.054	0.0024	0.030	0.0034	Spec.	After chlorination
96.9	1.79	0.04		0.05		Chem.	Before chlorination
99.6	0.32	0.026	0.00058	0.028	0.0017	Spec.	After chlorination
94.6	4.3	0.01		0.26		Chem.	Before chlorination
99.6	0.36	0.03	0.0017	0.022	0.0058	Spec.	After chlorination
97.5	1.1	0.10		0.26		Chem.	Before chlorination
99.6	0.28	0.074	0.0011	0.017	0.074	Spec.	After chlorination
98.0	1.7	0.24	0.0024	0.036	0.015	Spec.	Before chlorination
99.0	0.76	0.090	0.0015	0.12	0.016	Spec.	After chlorination
99.4	0.79	0.05		0.06		Chem.	After chlorination
99.4	0.50	0.052	0.00064	0.018	0.0036	Spec.	After chlorination

trichloride mole ratios on the order of 8-12 are desirable. Deposition temperatures in excess of 1000°C and low residence times are also desirable.

2. Since contamination is inevitable during the process of depositing boron on metallic filaments, it is better to use filament materials that are least objectionable from a weight standpoint and ease of removal. Titanium appears to be suitable as a filament metal, since it can be readily removed from boron by treatment with chlorine at temperatures (300°-350°C) well below the reported temperature (550°C) for boron-chlorine combination. Also, titanium forms a good conductive core in the deposit such that low resistance is realized in all temperature ranges. High deposit-to-filament-diameter ratios should be obtained in order to minimize metal contamination and this is possible with titanium as a core.

3. Crystalline boron of 99.0-99.6% purity by direct assay can be produced by vapor phase reduction followed by a chlorination step.

4. Crystallinity appears to be a function of temperature and may be a function of filament material.

5. A relationship between weight of deposit and reaction time was determined, which indicates that the rate of deposition is a function of deposit weight.

Manuscript received Feb. 10, 1958. This paper was prepared for delivery before the New York Meeting, April 27-May 1, 1958.

Any discussion of this paper will appear in a Discussion Section to be published in the June 1959 JOURNAL.

REFERENCES

1. H. Moissan, *Ann. Chim. et phys.*, (7) **6**, 296 (1895).
2. E. Weintraub, *Trans. Am. Electrochem. Soc.*, **16**, 165 (1909).
3. L. Hackspill, A. Stieber, and R. Hocart, *Compt. rend.*, **193**, 776 (1931).
4. D. P. Mellor, S. B. Cohen, and E. B. Underwood, *Australian Chem. Inst. J. & Proc.*, **3**, 329 (1936).
5. A. E. Van Arkel, U. S. Pat. 1,774,410, Aug. 6, 1930.
6. K. Becker, "Hochschmelzende Hartstoffe und ihre Technische Anwendung," Verlag Chemie, Berlin (1937).
7. A. J. Laubengayer, D. T. Hurd, A. E. Newkirk, and J. L. Hoard, *J. Am. Chem. Soc.*, **65**, 124 (1943).
8. M. Formstecher, *Comp. rend.*, **221**, 747 (1945).
9. G. H. Fetterley, U. S. Pat. 2,542,916, Feb. 20, 1951.
10. G. M. Murphy, Separation of Boron Isotopes, U. S. Atomic Energy Commission, Oak Ridge, Tennessee (1952).
11. F. D. Rossini, D. D. Wagmen, W. H. Evans, S. L. Levine, and I. Jaffe, Selected Values of Chemical Thermodynamic Properties, Circular of the National Bureau of Standards 500, (1952).
12. K. K. Kelley, *U. S. Bur. Mines Bull. 371* (1934).
13. H. M. Spencer, *J. Chem. Phys.*, **14**, 729 (1946).
14. J. A. M. Van Liempt, *Z. anorg. u. allgem. Chem.*, **111**, 151 (1920); M. G. Mellon, and V. N. Morris, *Ind. Eng. Chem.*, **16**, 123 (1924).
15. V. P. Jacobsmeyer, L. W. Friedrich, L. J. Badar, Semiconducting Properties of Boron, Armed Services Technical Information Agency No. 52266.
16. A. Stock and E. Kuss, *Ber.*, **56B**, 789 (1923).
17. G. C. Pimentel and K. S. Pitzer, *J. Chem. Phys.*, **17**, 882 (1949).
18. H. I. Schlesinger and A. B. Burg, *Chem. Revs.*, **31**, 1 (1942).

Methods for Preparing Pure Scandium Oxide

F. H. Spedding, J. E. Powell, A. H. Daane, M. A. Hiller, and W. H. Adams

Institute for Atomic Research and Department of Chemistry, Iowa State College, Ames, Iowa

ABSTRACT

A review of the techniques for isolating scandium in a pure state is presented, including the newest cation-exchange methods. These methods include elution with ethylenediaminetetraacetate and N-hydroxyethylethylenediaminetriacetate solutions and the use of copper and lead ions, respectively, as retaining ions which permit passage of scandium but retain rare earth ions. A new approach to opening thortveitite ore by treating with ammonium bifluoride and reducing the mixed metal fluorides to the metallic state with calcium is presented.

In connection with its studies of the rare earth elements, the Ames Laboratory has been interested in the isolation and purification of scandium. Methods used in the past to prepare pure Sc salts include fractional precipitation, sublimation, solvent extraction, and ion exchange.

Scandium may be precipitated as the phosphate, fluoride, oxalate, basic tartrate, basic thiosulfate, basic carbonate, basic acetate, hydroxide, and various double sulfates (1). No attempt is made here to evaluate all of these methods individually. Suffice it to say, no one precipitant isolates Sc quantitatively from all of the elements with which it is contaminated in its natural states. The great utility of precipitational methods lies in their use as concentrating steps in which the Sc is gradually upgraded. Combinations of these methods will, of course, eventually yield pure Sc with losses occurring depending on the precipitants used and proportional to the number of repetitions required to achieve the desired purity.

The sublimation of acetylacetonates (1) and the volatilization of chlorides (2), likewise, do not generally result in complete separation of Sc from all of the contaminating elements.

Solvent extraction procedures have a distinct advantage over precipitational methods in that repetitions of the extractive procedure are easily carried out. Since the materials remain in a liquid phase, no redissolution steps are necessary. Such procedures have been used frequently in the isolation of Sc and include extraction of scandium acetylacetonate by benzene or ethyl acetate (1), the chloride and nitrate by tri-n-butyl orthophosphate (3), the thenoyltrifluoroacetonate with benzene (4, 5), the cupferrate with chloroform (6, 7), and the thiocyanate with diethyl ether (1). The latter procedure will be mentioned again in connection with methods employed at Iowa State College for the purification of Sc.

Several ion-exchange techniques have been applied to the isolation of Sc. For example, an anion-exchange resin in conjunction with chloride mixtures in 12*N* HCl has been used to separate Sc from those elements which are not capable of forming anionic chloride complexes (8), and successful elutions have been made from cation-exchange resins using citric acid (9), nitrilotriacetic acid (10), glycolic acid (11), ethylenediaminetetraacetic acid (10), and hydrazine-N,N′-diacetic acid (12). Some of these methods have been demonstrated only on the tracer scale, while with larger quantities the investigators were sometimes plagued with the formation of precipitates in the resin bed. It is likely that the precipitates which formed were due to an unfortunate choice of the retaining ion, improper *p*H of the eluant, or excessive concentration. Nevertheless, it is apparent that the ion-exchange techniques used to date could be improved upon.

Recently, several hundred grams of thortveitite ore were obtained from the Norsk Feldspat Company of Norway. Marble and Glass (13) have reported that such material contains about 45% SiO_2, 34% Sc_2O_3, 11% rare earth oxides (primarily ytterbium, lutetium, thulium, erbium, dysprosium, yttrium, and gadolinium), 5% Al_2O_3, and 3% Fe_2O_3. As will be seen later, thortveitite also contains traces of many other elements. Marble has described the difficulty encountered in dissolving this ore which is occasioned by its very high silica content. The classical procedure used by Urbain and Urbain (14) involved a series of caustic fusions followed by removal of most of the resultant sodium silicate by water leachings. The residue of Sc and other insoluble metal hydroxides was then treated with dilute mineral acid to obtain the metal values in soluble form. This procedure is not entirely satisfactory owing to the difficulty encountered in filtering the slimy hydroxides from the leachate and in removing the remainder of the silica after the hydroxide residue has been dissolved in dilute acid. Other procedures used in the past for opening thortveitite ore include those of Iya (15), Vickery (16), and Adamoli (17).

Iya heated the pulverized ore with 1.2 parts of carbon for 30 min at 1800°C in order to form a mixture of carbides. The various metal carbides decomposed in dilute HCl giving a solution of chlorides which could be separated from the residue of excess carbon, silica, and silicon carbide.

Vickery obtained crude $ScCl_3$ from the ore by mixing finely ground thortveitite with carbon and heating in a tube furnace at 800°-850°C in a stream of chlorine. Since $ScCl_3$ does not volatilize below about 970°, it was finally leached from the melt with water.

Adamoli extracted Sc from its ores in a novel manner. He developed a process in which the ore was mixed with a sparingly soluble metal fluoride (CaF_2 for example). Next he added a solution of a mineral acid and an alkali metal salt of that acid (HCl and NaCl for example). The resulting paste was heated at a low temperature to form a water-soluble salt of the metal which was originally added in the form of a sparingly soluble fluoride ($CaCl_2$ formed in this particular instance). The liquid and the water-soluble salts were then removed and the residue was briquetted and fired at a high temperature in order to form a water-soluble complex fluoride of Sc. The resulting hexafluoscandate ion was then leached from the reaction mass.

Recent work in this laboratory on the preparation of rare earth fluorides by reaction of the oxides with ammonium bifluoride suggested a similar treatment for thortveitite which would eliminate silicon as the volatile tetrafluoride. The resulting mixture of metal fluorides, containing the Sc, could be reduced to the metallic state with an active metal such as Ca or Mg. The metals would then be easily soluble in dilute acid and the Sc could be purified by solvent extraction and/or ion exchange.

Experimental

Preparation of Crude Scandium Fluoride

The thortveitite was ground to a powder by mortar and pestle and then ball-milled. A portion weighing 307 g was mixed with 950 g of dry ammonium bifluoride (about 25% excess) and heated overnight at 375°-400°C in a platinum boat. A slow stream of air was passed through the apparatus to remove the gaseous products. The reaction may be represented as:

$$R_2O_3 \cdot SiO_2 + 10NH_4HF_2 \rightarrow 2RF_3 + SiF_4 +$$

$$10HF + 10NH_3 + 5H_2O$$

The symbol R represents Sc, Al, Fe, and rare earths. The product of this reaction was light brown in color and weighed 240 g.

Reduction of Crude Scandium Fluoride with Calcium

The fluoride mixture prepared above was divided into two portions of 120 g each. Each batch was combined with 75 g of Ca metal (about 10% excess) in a Ta crucible, and reduced by heating the crucible and its contents to 1400°C under an argon atmosphere. This is the same general procedure used to prepare the rare earth metals. A clean separation was obtained between the metal and slag in each case, but the metal adhered to the Ta crucible. Consequently, the Ta foil, of which the crucibles were constructed, had to be peeled away to obtain the metal buttons. One weighed 50 g and the other 48.2 g.

Purification of the scandium by extraction with ether from a thiocyanate solution.—The metal buttons were dissolved separately in HCl and each solution was treated with ammonium thiocyanate and extracted with diethyl ether according to the procedure of Fischer and Bock (1). After evaporating the ether, the residues were ignited at 800°C and subjected to qualitative spectrographic analyses. The results are shown in Table I.

It is apparent that all of the contaminants, except Be, tend to concentrate in the aqueous phase, but the separation of Sc from rare earths, Fe, and many other elements is not complete after a single extraction of scandium thiocyanate with ether. Although the product undoubtedly could have been improved greatly by further extractions of this sort, it was decided to try an ion-exchange method for the separation of Sc from the remaining impurities.

Purification of scandium by ion-exchange elution with N-hydroxyethylethylenediaminetriacetic acid.—The enriched scandium oxide samples were combined and dissolved in HCl. The Sc was then adsorbed on a resin bed of 40-50 mesh Amberlite IR-120, 2 in. in diameter and about 4 ft long, in the hydrogen ion cycle. After rinsing the bed with distilled water, elution was begun with an eluant containing 5 g of N-hydroxyethylethylenediaminetriacetic (HEDTA) acid per liter, buffered to a pH of 7.4-7.6 with ammonium hydroxide. Two additional beds, 1 in. in diameter by about 4 ft long, in the hydrogen cycle, were used as retaining beds. A flow rate of 2-3 ml/min was maintained while consecutive fractions were being caught.

Since no band fronts were visible, the collection of samples was begun immediately after the start of elution. The first 60 l of eluate yielded almost no

Table I. Qualitative spectrographic analysis of oxide fraction obtained after ether extraction of the thiocyanate

Contaminant	First Batch		Second Batch	
	H_2O phase (wt 19.4 g)	Ether phase (wt 44.2 g)	H_2O phase (wt 18.4 g)	Ether phase (wt 44.9 g)
Al	M	W	M	W
Be	W	M	W	M
Ca	M	VW	M	VW
Co	T	—	T	—
Cr	W	T	W	—
Cu	W	FT	W	T
Dy	W	—	W	—
Er	W	—	W	—
Fe	S	M	S	M
Gd	W	—	W	—
Lu	M	W	M	W
Mg	W	VW	W	VW
Mn	M	W	M	W
Ni	VW	—	VW	—
Sc	M	VS	M	VS
Sn	VW	—	VW	VW
Th	T	—	T	—
Ti	W	T	W	T
Tm	M	—	M	—
Y	S	W	S	W
Yb	M	VW	M	VW

VS, very strong; VW, very weak; S, strong; M, moderate; W, weak; T, trace; —, not detected.

Table II. Fractions obtained by elution of crude scandium with N-hydroxyethylethylenediaminetriacetic acid

Sample No.	Vol	Solution color	Oxide color	Wt of oxide	Composition
1 – 3	60	Colorless	Brown	0.17	Chiefly Fe,Ca
4	4	Yellow	Tan	0.07	Chiefly Fe,Ca
5	12	Yellow	Brown	1.83	Sc with Fe
6	6	Yellow	Tan	4.10	Sc with Fe
7	10	Lt. yellow	Cream	7.20	Sc; tr. Fe; ~0.01%Y
8	7.5	Pale yellow	Yellowish	5.13	Sc; tr. Fe; ~0.03%Y
9	10	Colorless	Yellowish	7.02	Sc; tr. Fe; ~0.01%Y, Lu, Yb
10	10	Colorless	White	8.13	Sc; ~0.01%Y, Lu, Yb
11	10	Colorless	White	8.36	Sc; ~0.01%Y, Lu, Yb
12	10	Colorless	White	9.41	Sc; ~0.01%Y, Lu, Yb
13	10	Colorless	White	8.43	Sc; ~0.01%Y, Lu, Yb
14	10	Colorless	White	5.11	Sc; ~0.01%Y, Lu, Yb
15	20	Colorless	White	6.35	Sc; ~0.01%Y, Lu, Yb
16	10	Colorless	White	2.94	Sc; ~0.01%Y, Lu, Yb
17	10	Colorless	White	6.26	Sc; ~0.02%Y; ~0.01%Lu; ~0.02%Yb
18	15	Colorless	Dirty white	2.64	Sc; ~0.03%Y; ~0.9%Lu; ~0.1%Yb
19	13	Colorless	Tan	3.00	Sc&Y; rare earths; tr.Mn
20	12	Pink	Brown	1.35	Sc,Y&Mn; rare earths
21	15	Colorless	Tan	0.12	
			Total weight recovered	84.00 g	

residue upon evaporation and ignition.[1] At this point, the eluate turned slightly yellow and the next 22 l, spread over several individual samples, gave oxide residues varying in color from a light tan to dark brown and back to a light tan. The weights of recovered oxide over this same region increased from nothing to about 6.8 g/10-l fraction. The next three consecutive samples gave a pale cream-colored oxide weighing a little more than 7 g/10-l fraction. The next four samples, totaling 40 l, contained more than 8 g of white oxide per 10-l fraction. The weights then began tapering off and only 20.8 g of white oxide were realized from the next 50 l of eluate. The oxide recovered from the last 55 l of eluate diminished gradually in weight and also underwent a change in color ranging from cream to brownish-tan to brown with a tinge of blue and then back to light tan. Analyses of the fractions are given in Table II.

Only 84 g of residues were obtained from an original 89 g of crude oxide. Since a great deal of care was taken in evaporating down and recovering all the residues from the final purification, it is thought that the 5-g loss was due to undecomposed scandium sulfate in the crude oxide sample taken for this experiment. It is possible that some sulfate could have formed during the ignition of the scandium thiocyanate to what was thought to be scandium oxide. Sulfate would be eliminated as the scandium was loaded on the ion-exchange columns. In any event, a yield of 48.73 g of very pure Sc_2O_3 was obtained by this elution with HEDTA and another 19.35-g portion was obtained which showed only a trace of iron. This latter material could be freed from iron with little difficulty. Since most of the other fractions contain larger amounts of impurities, they will be resubmitted to the thiocyanate extraction process before being processed further by ion-exchange.

Other methods for purifying scandium by ion-exchange elution.—Two other methods have been used in preparing pure scandium oxide at the Ames Laboratory. One takes advantage of the fact that cupric ion will retain all the rare earths and many common impurities such as Ni, Pb, Zn, Co, Cd, Mn, Ca, Mg, Be, Sr, and Ba when ethylenediaminetetraacetic acid (EDTA) is used as the eluant, but will not retain Sc. By eluting a crude mixture containing Sc down a cupric-state resin bed with 0.0153*M* EDTA solution at a *p*H of 8.4, a very good yield of pure Sc has been obtained. The chief difficulty with this method is that the Sc is first obtained as a mixture with cupric ion and must be purified further either by electroplating out the Cu or by preciptating the Cu as copper sulfide. Also, cupric ion retains ferrous, but not ferric ion.

The other method is very similar, except that Pb is used as the retaining ion and N-hydroxyethylethylenediaminetriacetic acid is used as the eluant. Again, most cations, including the rare earths, are retained while Sc is not. A good yield of pure Sc has been obtained by eluting a mixture containing Sc down a lead-state resin bed with 0.018*M* HEDTA at a *p*H of 7.6 and removing lead from the Sc fractions by precipitation with H_2S. Copper and nickel are not retained by Pb and, therefore, must also be considered if they are present. Copper, of course, is removed along with the lead during treatment with H_2S so that its presence creates no real problem. Scandium and nickel can be separated readily by the thiocyanate extraction process mentioned earlier.

Summary

Although there are a number of alternative approaches by which Sc might be purified, the methods

[1] Recovery of all samples was accomplished by boiling the eluate to dryness and destroying the organic matter with nitric acid. From previous experience, it was found that during treatment with HNO_3, the residue frequently burst into flame, expelling some of the ash from the beaker. For this reason, large beakers were used and they were kept covered, since it appeared that the gaseous products evolved in the reaction were capable of controlling the burning rate if they were confined over the burning ash. Attempts to ignite material taken to dryness before destroying the organic matter resulted in the material swelling several times its size and toppling out of the crucible like "Pharaoh's Serpents" during the charring process.

described herein are quite straightforward. First of all, the removal of silicon by treatment with ammonium bifluoride is elegant in its operational simplicity. Next, the mixture is converted to soluble form by reduction to the metallic state and subsequent dissolution in HCl. Anyone who has attempted to filter silicate solutions or who has attempted to redissolve insoluble fluorides in quantity will appreciate the advantages of these procedures. The thiocyanate procedure is simple to perform and removes a major amount of the impurities but would have to be repeated a number of times in order to achieve the separation from rare earths that can be obtained by ion-exchange. Consequently, we have chosen to perform only one thiocyanate extraction before resorting to ion-exchange.

Manuscript received May 8, 1958. This paper was presented at the New York Meeting, April 27-May 1, 1958. It is Contribution No. 634; work was performed in the Ames Laboratory of the Atomic Energy Commission.

Any discussion of this paper will appear in a Discussion Section to be published in the June 1959 JOURNAL.

REFERENCES

1. W. Fischer and R. Bock, *Z. anorg. Chem.*, **249**, 146 (1942).
2. R. J. Meyer and H. Winter, *ibid.*, **67**, 398 (1910).
3. D. F. Peppard, J. P. Faris, P. R. Gray, and G. W. Mason, *J. Phys. Chem.*, **57**, 294 (1953).
4. A. Broido, A.E.C. Document No. AEC-2616, July 29, 1947.
5. H. J. Bronaugh and J. F. Suttle, A.E.C. Report No. LA-1561, June, 1953.
6. G. E. F. Lundell and J. I. Hoffman, "Outlines of Methods of Chemical Analysis," John Wiley & Sons, New York (1948).
7. C. C. Miller, *J. Chem. Soc. (London)*, **1947**, 1347.
8. K. A. Kraus, F. Nelson, and G. W. Smith, *J. Phys. Chem.*, **58**, 11 (1954).
9. P. Radhakrishna, *Anal. Chim. Acta*, **8**, 140 (1953).
10. V. K. Iya and J. Loriers, *Compt. rend.*, **237**, 1413 (1953).
11. D. C. Stewart, Proc. Intern. Conf. Peaceful Uses of Atomic Energy, Geneva, 1955, **7**, 321 (1956).
12. R. C. Vickery, *J. Chem. Soc. (London)*, **1955**, 245.
13. J. P. Marble and J. J. Glass, *Am. Mineralogist*, **27**, 696 (1942).
14. P. Urbain and G. Urbain, *Compt. rend.*, **174**, 1310 (1922).
15. V. K. Iya, *ibid.*, **236**, 608 (1953).
16. R. C. Vickery, *J. Chem. Soc. (London)*, **1956**, 3113.
17. C. Adamoli, U. S. Pat. 2,250,851, July 29, 1941.

Cathode Potentials during the Electrodeposition of Molybdenum Alloys from Aqueous Solutions

D. W. Ernst[1] and M. L. Holt

Chemistry Department, University of Wisconsin, Madison, Wisconsin

ABSTRACT

Cathode potential measurements are used to explain the cathode reactions that result in the electrodeposition of molybdenum alloys. Potentials were measured by the direct method during the electrolysis of aqueous ammoniacal citrate solutions containing sodium molybdate and the sulfate of a codepositing metal, iron, nickel, or cobalt. The results indicate that the reduction of molybdate ion in this type of bath is probably not accomplished in one step with six electrons, but with one, two, or three electrons depending on the codepositing metal and its oxidation state in the bath. The results also indicate that hydrogen is involved in the molybdate reduction process. A two-step mechanism for the reduction of molybdate ion in the presence of a codepositing metal is proposed and an explanation of why this metal must be iron, cobalt, or nickel rather than such metals as chromium, manganese, copper, or zinc is presented.

Molybdenum readily codeposits with Fe, Co, or Ni from aqueous solutions; however, in contrast to this, the electrodeposition of appreciable amounts of pure Mo from aqueous solution has not been accomplished. The purpose of this work was to obtain experimental data that would help to explain this cathodic behavior of Mo. Cathode potential measurements made during electrolysis seemed to be a logical approach to the problem since previous studies of the effect of the various bath constituents, pH, current density, and temperature on cathode current efficiency and alloy composition did not yield sufficient information (1). Frantsevich-Zabludovskaya (2) utilized polarization curves in the recently reported results of his investigation of the deposition of Ni-Mo, Fe-Mo, and Fe-Ni alloys.

[1] Present address: National Bureau of Standards, Washington, D. C.

Experimental Details

The cathode potentials reported here were measured by the direct method. The cell design permitted the cathode to be removed for weighing and also allowed the tip of the capillary bridge to be placed in the same position for each run. The capillary tip connecting the cathode with the reference electrode was placed near the face of the cathode, but it could have been located in other positions on or near the cathode (3-6). The cell,

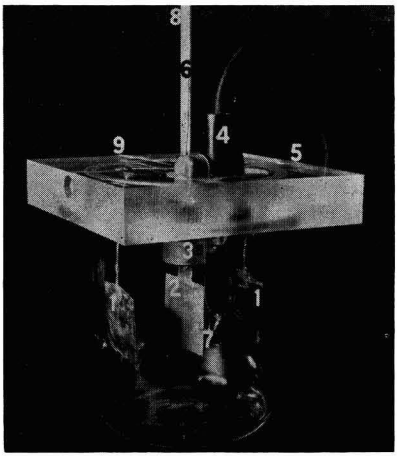

Fig. 1. Cathode potential cell showing: 1, anodes; 2, cathode; 3, Lucite nut on cathode holder; 4, calomel reference electrode; 5, anode connection; 6, Pt wire for cathode connection; 7, tip of glass bridge; 8, thermometer; 9, screw for holding cathode assembly.

Fig. 1, was made from a cut-down 500 ml tall-form Pyrex beaker fitted with a Lucite cover 10.2 cm x 10.2 cm x 1.9 cm. There were openings in the cover for two anodes, 3 cm x 3 cm x 0.03 cm, a cathode of the same size, a thermometer, and a glass bridge for the reference electrode. Each Pt anode was held in position approximately 3 cm from the centrally placed cathode held in a special holder. The removable cathode holder consisted of a fiber rod (3.8 cm x 0.64 cm) machined with a tapered thread and slot on one end; the slot was closed by tightening a Lucite nut. The Pt cathode had a tab, 0.8 cm x 0.7 cm, which fitted into the slot on the fiber rod. A Pt wire having a similar Pt tab on one end was inserted in the fiber rod to serve as the cathode connection. When the two tabs were placed in the slot and the nut tightened a good electrical connection was made. The cathode assembly was placed in the Lucite cover and held in place by a screw.

The bridge for the reference electrode was made from 12 mm Pyrex tubing with one end drawn out to a tip 1 mm in diameter and 4 cm long. Two 90° bends perpendicular to each other were made in the tip. The glass-sleeved calomel reference electrode fitted into the other end of this glass bridge. The position of the completed bridge was adjustable because it was seated into the Lucite cover with a rubber washer. It was found possible to consistently place the capillary tip to within 0.1 to 0.2 mm of the cathode surface.

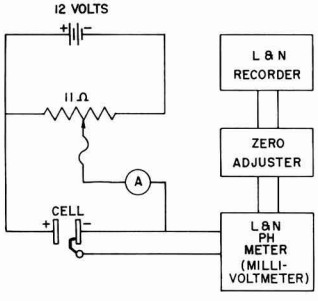

Fig. 2. Electrical circuit used for measuring cathode potentials.

This cell, Fig. 1, has the error due to *IR* drop, inherent in any direct method for measuring cathode potentials, and it does not provide a uniform current density on the cathode. A simple calculation gives the approximate magnitude of the *IR* error. The potential across the anode and cathode at the maximum current density used was approximately 5 v, and the distance over which this *IR* drop occurred was approximately 30 mm; this gives an *IR* drop of about 0.16 v/mm. Since the tip of the pickup bridge was about 0.15 mm from the cathode surface, the maximum error due to *IR* drop is approximately 20 mv. A uniform current density is obtained only with a concentric cylindrical electrode system (7), and with the parallel electrode system of this cell the current density is highest at the edges. These factors and others make cathode potential measurements somewhat uncertain so the potentials reported here are considered reproducible to ±30 mv.

The cell was used in the circuit shown in Fig. 2. The source of current was a storage battery since the rectifiers available had enough ripple to be picked up by the line-operated *p*H (millivolt) meter. The recorder was one designed for use with a chromel-alumel thermocouple, and a zero adjuster was used to set the zero point of the millivoltmeter wherever desired on the chart paper of the recorder.

The baths contained 0.3 mole per liter (m/l) of metal(II) sulfate (Fe, Co, or Ni), 0.3 m/l of sodium citrate in the Co and Ni baths and 0.45 m/l of sodium citrate in the Fe baths, and either 0.00, 0.02, or 0.75 m/l of sodium molybdate. Nickel baths containing 0.15 m/l of sodium molybdate were also studied. Each bath was adjusted to *p*H 10.5 with ammonium hydroxide. The baths were maintained at 25° ± 1°C during and after electrolysis. The Fe-Mo bath was used immediately after preparation because some iron(III) hydroxide precipitated on standing and during an electrolysis run. Two liters of each bath were made up and divided into eight 250-ml aliquots for electrolysis at currents of 0.18, 0.36, 0.54, 0.72, 0.90, 1.15, 1.45, and 1.80 amp to give cathode current densities of 1.0, 2.0, 3.0, 4.0, 5.0, 6.4, 8.0, and 10.0 amp/dm^2, respectively. Each 250-ml aliquot was used for two runs at each of the eight current densities. In the first run the potential was recorded up to a minute before the end of the run and when the time of electrolysis was over the cathode was removed immediately, washed, dipped in alcohol, dried, and readied for analysis. In the second run the cathode was allowed to remain in the bath after the current was shut off and the recording of the potential continued in order to obtain the formal potential, E_f. The same total current was used in each run at the various current densities; 1080 coulombs for the Ni-Mo and Co-Mo baths and,

because of its lower cathode current efficiency, 2160 coulombs were used with the Fe-Mo bath. No salts were added between runs, and the runs were made in no specific order. The *p*H of the baths after electrolysis was usually 0.1 to 0.2 *p*H unit lower than the initial *p*H.

Experimental Data

The cathode potentials obtained in the two runs at the same current density were averaged and used in making plots on semi-log paper of current (i) vs. potential (E). The results for the three types of plating solutions studied are given in Fig. 3, 4, 5 and it can be seen that the addition of sodium molybdate lowers the cathode potential in the single metal baths. Although no potential-current plots were obtained for a molybdate solution (0.2 m/l Na_2MoO_4, 0.3 m/l citrate, and no codepositing metal ion) due to the fact that the cathode becomes highly polarized, it can be stated that the addition of Fe, Co, or Ni sulfate lowers the cathode potential in the molybdate solution. It should be noted that in these potential-current plots (Fig. 3-5) the lines are drawn to indicate the region of deposition and the start of the line indicates the current density where deposition was observed to begin in the plating solution being used.

The experimentally determined potentials, in addition to E_c the cathode potential, were E_d the discharge potential and E_f the formal potential. The potentials calculated from these experimental values were E_o overpotential, E_a activation overpotential, and E_p polarization. These various potentials are defined below and are shown pictorially in Fig. 6.

E_c, *cathode potential,* the potential of the cathode measured with the millivoltmeter while current is actually flowing.

E_d, *discharge potential of the metal ions,* the potential at which metal deposition takes place at an appreciable rate. This potential is hard to determine and is not known to have any theoretical significance.

E_f, *formal potential,* the equilibrium potential of the metal in the plating solution, measured while no current was flowing. It can be considered as the $E°$ of the metal corrected to the metal ion activity in the plating solution. It is the potential at which plating should begin in the absence of cathode polarization.

E_o, $(E_c - E_f)$ or $(E_a + E_p)$, *overpotential* or *overvoltage,* the potential in excess of the formal potential which must be impressed across the cell to cause the cell reaction to proceed at an appreciable rate.

E_a, $(E_d - E_f)$, *activation overpotential,* the extra potential above E_f necessary to cause metal deposition at an appreciable rate. This is the metal overvoltage.

E_p, $(E_c - E_d)$, *electrochemical overpotential* or *polarization,* the departure of E_c from E_d due to the passage of current.

The formal potential, E_f, was difficult to measure as an equilibrium value since the deposits were continually dissolving in the plating solutions. The Co alloys dissolved completely in 1 hr and gave the most steady potential, while the Fe and Ni alloys dissolved slowly over a period of several hours. The value of E_f was arbitrarily chosen as the potential ½ hr after the current had been turned off. E_p values were calculated using the values of E_c at 11.1

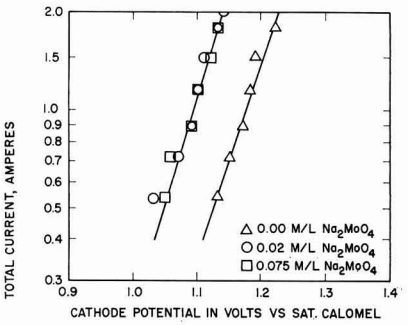

Fig. 4. Potential-current curves for the Co bath (no Na_2MoO_4) and for Co-Mo baths containing 0.02 and 0.075 m/l of Na_2MoO_4.

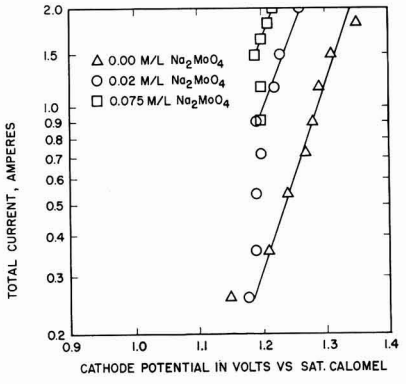

Fig. 3. Potential-current curves for the Fe bath (no Na_2MoO_4) and for Fe-Mo baths containing 0.02 and 0.075 m/l of Na_2MoO_4. (Note: In Fig. 3, 4, and 5 lines are drawn to indicate the region of deposition and the start of a line indicates the current density where deposition was observed to begin in that plating solution).

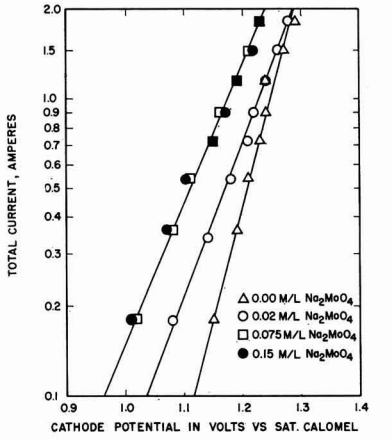

Fig. 5. Potential-current curves for the Ni bath (no Na_2MoO_4) and for Ni-Mo baths containing 0.02, 0.075, and 0.15 m/l of Na_2MoO_4.

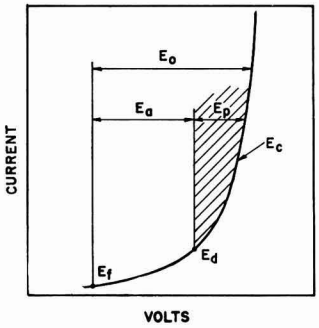

Fig. 6. Schematic diagram showing the relationship between the experimentally determined potentials, E_c cathode potential, E_d discharge potential, and E_f formal potential, and the calculated potentials, E_o overvoltage, E_a activation overpotential, and E_p polarization.

amp/dm^2 (taken directly from the graphs where $i = 2.0$ amp) and because of this the values of E_p reported are maximum ones; E_p ranges from zero to this maximum over the range of current densities studied. Values of E_o, the sum of E_a and E_p, range from E_a to $E_a + E_p$ over the same current densities. The discharge potential, E_d, was arbitrarily taken since it is hard to determine when plating actually begins; therefore, values of E_a are less than or equal to the values reported, and values of E_p are greater than or equal to those reported since, at the value of E_a chosen, plating was occurring. It should be noted that no attempt was made to exclude air while these measurements were being made. Table I gives the experimental and calculated E values for all baths studied.

Since Fe, Co, and their alloys with Mo do not deposit at the lower current densities, it is possible to set limits for $E_a + E_p$ in the opposite direction. For these metals it is found that at a potential 0.02 v lower than E_d deposition of the metal is not occurring; however, in most cases there is deposition of a molybdenum oxide or hydroxide. Thus it is possible that the E_a values may be 0.02 v lower than those reported; in terms of free energy the 0.02 v is equal to approximately 1 kcal for a two-electron reaction.

The following observations are made from the data in Table I. The formal potential of the three metals, Fe, Co, and Ni is increased by the formation of a Mo alloy indicating that Mo may be less noble than the other metals. The metal overvoltage is highest for Fe and lowest for Ni in both the single metal and alloy baths, indicating that the deposition of Ni is easier than the deposition of Fe. The metal overvoltage is lower for the alloy baths than for the single metal baths, including the sodium citrate-molybdate bath, indicating that deposition of the alloys is easier than deposition of the single metals. The cathode in the molybdate solution is highly polarized (high E_p) and this polarization is reduced by the addition of the sulfates of Fe, Co, and Ni. Whereas polarization in the Fe and Co baths is reduced by the addition of sodium molybdate it is increased in the Ni bath.

Table I. Experimentally determined values of E_c, E_d, and E_f and calculated values of E_a and E_p for the plating baths studied

Plating bath	Na_2MoO_4 m/l	E_c* v	E_d v	E_f v	E_a, (E_d-E_f) † v	E_p, (E_c-E_d) † v
Fe	0.00	1.34	1.20	0.58	0.62	0.14
Fe-Mo	0.02	1.26	1.20	0.61	0.59	0.06
Co	0.00	1.23	1.11	0.59	0.52	0.12
Co-Mo	0.02	1.14	1.03	0.67	0.36	0.11
Co-Mo	0.075	1.14	1.03	0.63	0.40	0.11
Ni	0.00	1.29	1.12	0.63	0.49	0.17
Ni-Mo	0.02	1.29	1.03	0.84	0.19	0.26
Ni-Mo	0.075	1.24	0.96	0.83	0.13	0.28
Ni-Mo	0.15	1.24	0.96	0.84	0.12	0.28

* At 11.1 amp/dm^2.
† Potentials are given vs. the saturated calomel electrode.

The cathode deposits obtained in the various cathode potential runs were analyzed by the usual means and the results used to make calculations of current efficiency and current for each deposition reaction. From the percentages of Mo and codepositing metal in each deposit and the total current used it was possible to calculate the cathode current efficiency for each deposition reaction. The current used for each reaction (i_{Mo}, the current used for deposition of molybdenum and $i_{C.M.}$, the current used for deposition of the codepositing metal) was then calculated by multiplying the total current, i_t, by the calculated current efficiency of the reaction. Plots were then made on semi-log paper of i_t, i_{Mo} and $i_{C.M.}$ vs. E_c for each alloy bath as shown in Fig. 7, 8, and 9.

The number of electrons, n, involved in the reduction can be calculated from the slope $\left(\frac{n\alpha}{0.06}\right)$ of the lines in Fig. 7, 8, and 9. Alpha is the transfer coefficient and may range from 0.0 to 1.0; in many electrochemical processes it is 0.5. If a value of 0.5 is used, the expected electron changes of two for Ni and six for Mo are not obtained. If it is assumed

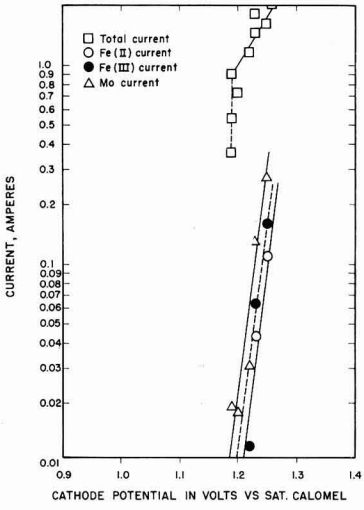

Fig. 7. Potential-current curves for the Fe-Mo bath containing 0.02 m/l of Na_2MoO_4. Lines show the total current (observed) as well as the current (calculated) used for depositing Mo and Fe.

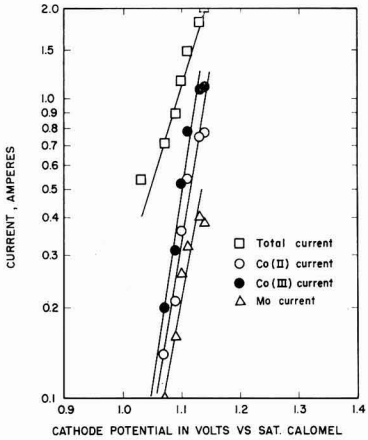

Fig. 8. Potential-current curves for the Co-Mo bath containing 0.02 m/l of Na_2MoO_4. Lines show the total current (observed) as well as the current (calculated) used for depositing Mo and Co.

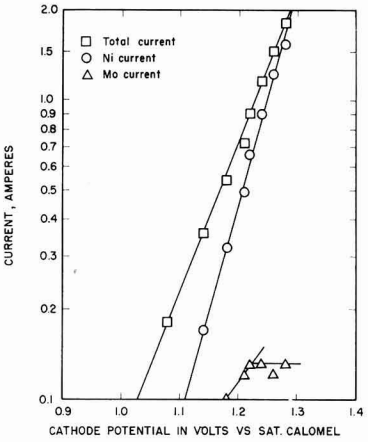

Fig. 9. Potential-current curve for the Ni-Mo bath containing 0.02 m/l of Na_2MoO_4. Lines show the total current (observed) as well as the current (calculated) used for depositing Mo and Ni.

that Mo and Ni are deposited from the same activated complex, then α can be the same for both deposition reactions. Alpha was then calculated from the slope of the $i_{C.M.}$ vs. E_c plots and known values of n for Fe, Co, and Ni. The α thus calculated was then used to calculate n for the molybdate reduction using the slope of the i_{Mo} vs. E_c plot. Table II gives the calculated values of α for the three metals, Fe, Co, and Ni and n for the molybdate ion.

The number of electrons involved in the Mo reaction depends on the codepositing metal and its oxidation state in the bath. The slope of the Mo reaction is nearly equal to the slope for the Co or Fe reduction so that whatever oxidation state, II or III, is used to calculate α, that value is the number of electrons involved in the molybdate reduction. Due to the ease of oxidation of Co(II) to Co(III) in ammonical solutions, it is very likely that the Mo reaction involves three electrons when Co is the codepositing metal and this may also be true with Fe. It appears that n for the molybdate reduction in a Ni bath is one.

Table II. Transfer coefficients, α, for the Fe, Co, and Ni deposition reactions and the number of electrons, n, calculated for the reduction of molybdate ion

Plating bath	Na_2MoO_4 m/l	Fe, Co or Ni*		Mo	
		m†	α	m†	n
Fe	0.0	0.23	0.13	—	—
Fe-Mo	0.02	0.04	0.75	0.04	2.0
Fe-Mo	0.075	0.10	0.30	0.11	1.8
Co	0.00	0.22	0.14	—	—
Co-Mo	0.02	0.00	0.35	0.09	1.9
Co-Mo	0.075	0.14	0.22	0.13	2.1
Ni	0.00	0.13	0.23	—	—
Ni-Mo	0.02	0.14	0.21	0.37	0.8
Ni-Mo	0.075	0.17	0.18	0.31	1.1
Ni-Mo	0.15	0.15	0.20	0.23	1.3

* Oxidation state is II.
† m = slope.

It was also observed that the Fe, Co, and Ni single metal baths operate at different cathode current efficiencies. The efficiency of the Fe bath is between 14% and 18%; the Co bath has a peak efficiency of 65%; and the Ni bath has the highest current efficiency, 90-97%. The alloy baths operate with cathode current efficiencies which are slightly (about 10%) lower than those of the single metal baths. With an alloy bath the relative amount of Mo in the deposit decreases and the total cathode efficiency of the bath increases as the current density is increased; however, if the individual reactions are considered, the cathode current efficiency of the Mo reaction remains nearly constant throughout the full range of current densities whereas the efficiency of deposition of the alloying metal increases.

The appearance of the cathode deposits depends somewhat on the current density used. All the Ni-Mo alloys were completely metallic. All the Co-Mo alloys were metallic, except that those obtained at the lower current densities were black and nonmetallic in the center of the cathode. None of the Fe-Mo alloys were completely metallic but had a black nonmetallic center with a metallic edge. The black compound on the cathode is believed to be an oxide or hydroxide of Mo, probably $Mo(OH)_3$, since it is black and would involve a three-electron change. Observations made while washing the plated cathodes indicate that the Fe and Co deposits contain more absorbed hydrogen than the Ni deposits; this is supported by the high cathode current efficiency of the Ni baths. These observations are also in accord with data on the hydrogen content of electrodeposited metals (8).

Discussion

On the basis of the data presented the following two step reduction of molybdate ion is proposed:

$$MoO_4^{=} + 4H_2O + ne^- \rightarrow Mo(OH)_{(6-n)} + (2+n)OH^- \quad [1]$$

$$Mo(OH)_{(6-n)} + (6-n)H + M \rightarrow M \cdot Mo + (6-n)H_2O \quad [2]$$

In these equations n is one, two, or three and M is Fe, Co, or Ni. The supposition is that the metal M and the molybdate ion are deposited from the same activated complex and that hydrogen deposits simultaneously with them. The high overvoltage of the sodium citrate-molybdate bath and the fact that appreciable amounts of Mo are not deposited from it can be explained by using Eq. [1]. If the molybdate reduction is accomplished in steps by electrons according to Eq. [1], the formation of a molybdenum oxide or hydroxide such as $Mo(OH)_3$, $Mo(OH)_5$, or $MoO(OH)_3$ is possible. If this is the case, deposition is no longer occurring on the original cathode material but on the oxide, and thus the various overvoltages involved will be changed. For further reduction to occur it is necessary to overcome the Mo overvoltage which is the molybdate ion's ability to find a position in a lattice on the cathode and be discharged (9); the oxide may not supply the right lattice for deposition to continue easily causing a high overvoltage. In addition, the hydrogen overvoltage (10) could be increased since metal-hydrogen bonds[2] would not be readily established on the oxide surface. However, the reaction which occurs is the one that has the lowest potential and if the overvoltage for the deposition of Mo on its oxide is higher than the overvoltage for hydrogen deposition on the oxide, hydrogen would be liberated in preference to further deposition of Mo or an oxide. This is perhaps the situation since only a thin film of oxide is formed and large quantities of hydrogen are liberated.

It is possible, by carrying the ideas a step further, to give an explanation for the necessity of the codepositing metals Fe, Co, and Ni. The number of electrons involved in the reduction of molybdate ion has been calculated to be less than six. It is now assumed that in addition to electrons another reducing agent is needed; the agent chosen is hydrogen as given in Eq. [2]. The fact that in the deposition of Ni-Mo alloys the current for the hydrogen reaction is always larger than or equal to the Mo reduction current would seem to indicate a connection between the two. If there was no connection between Mo and hydrogen, it should be possible to deposit an alloy from the Ni-Mo bath with 100% current efficiency; this was not observed. The reason why alloy deposition is possible and the overvoltage, E_o, of the sodium citrate-molybdate bath is reduced may be that hydrogen reduces the molybdenum oxide or hydroxide which was formed according to the reaction given in Eq. [1]. Hydrogen is capable of doing this and is held in place for this reaction by the metal-hydrogen bond formed with the codepositing metal that has also deposited. The reduction of this oxide changes the overvoltage factors involved. Hydrogen and molybdenum are no longer depositing on the oxide but on the Mo alloy. The Mo overvoltage would be reduced since the ability of the molybdate ion to find a lattice position in an alloying metal lattice already established should be easier. The hydrogen overvoltage for Mo alloys would then be the same or nearly the same as for the codepositing metals since the hydrogen overvoltages on all metals concerned here are close together (11). A separate study of hydrogen liberation should be made and other possible side reactions checked to determine whether or not hydrogen is the reducing agent. Actually the complete reduction of molybdate ion requires six electrons regardless of the mechanism considered. It would be difficult to determine whether the reduction is accomplished by one electron followed by a five hydrogen atom reduction (which requires five electrons) or by six electrons in one step. It may be possible that hydrogen is involved only in breaking down the molybdenum hydroxide or oxide.

Molybdenum codeposits with Fe, Co, and Ni but does not codeposit in appreciable amounts with Cr, Mn, Cu, or Zn from the ammoniacal citrate type of bath. The hydrogen overvoltage factor may be one explanation for this since the overvoltage of hydrogen on Fe, Co, and Ni is lower than it is on other metals. However, due to the many factors which affect overvoltage this cannot be the complete answer. Another explanation involving the electronic configuration of the atoms of these metals can be presented. Slater, using Krutter's calculations of the zones in elemental Cu, proposed a theory for the occurrence of ferromagnetism in this group of metals (12). According to Krutter's calculations the 3d and 4s levels of the atoms are filled as given in Table III. From this table it can be seen that the

Table III. Distribution of the outer electrons in the first row of transition elements

Element and At. No.	Outer electrons: Total	4s	+3d*	−3d*	Unpaired 3d*
$_{24}$Cr	6	0.6	2.7	2.7	0
$_{25}$Mn	7	0.6	3.2	3.2	0
$_{26}$Fe	8	0.6	4.8	2.6	2.2
$_{27}$Co	9	0.7	5.0	3.3	1.7
$_{28}$Ni	10	0.6	5.0	4.4	0.6
$_{29}$Cu	11	1.0	5.0	5	0

* The 3d level can accommodate 10 electrons per atom, 5 with a plus (+) spin and 5 with a minus (−) spin. Electrons generally fill up the +3d levels first and then go into the −3d levels. The unpaired electrons which produce the ferromagnetism result because the −3d electrons cancel an equal number of +3d electrons (12).

Table IV. Maximum atomic percentage of molybdenum in the alloys

Alloy	Atomic % Mo: Theoretical	Experimental
Fe-Mo	42.5	47
Co-Mo	36.5	36.8
Ni-Mo	16.7	16.8
Ni-Mo	10.7*	—

* Based on 5 hydrogen atoms to reduce $Mo(OH)_5$.

[2] According to Glasstone, Eyring, and Laidler (10) one possibility for hydrogen overvoltage is the ease or difficulty of the transfer of a proton from the solution to the surface of the electrode. If the cathode material forms a strong metal-hydrogen bond, the oxygen atom of the water molecule attached to the electrode surface will have an increased tendency to attract a hydrogen atom from another water molecule in the solution because one of its original hydrogen atoms is strongly attached to the metal; thus the transfer of a proton is made easier and the overvoltage is low. On the other hand if the electrode surface does not establish a strong metal-hydrogen bond, the hydrogen atom that should be attached to the metal surface will remain attached to the oxygen atom and the proton transfer is made more difficult and results in a high overvoltage.

elements with which Mo readily codeposits are the ferromagnetic elements which have unpaired 3d electrons. It was postulated previously that metal-hydrogen bond formation was necessary and that the hydrogen reduced the molybdenum oxide. The formation of this metal-hydrogen bond could be connected with the unpaired 3d electrons of Fe, Co and Ni (Table III); hydrogen having one unpaired electron in its outer shell could form a covalent bond with the unpaired 3d electrons. Thus an atom of iron with its 2.2 unpaired 3d electrons could hold an average of 2.2 hydrogen atoms, the cobalt atom with 1.7 unpaired 3d electrons could hold 1.7 hydrogen atoms and each nickel atom with 0.6 unpaired 3d electron could be expected to hold only 0.6 of a hydrogen atom. It is then possible, if these assumptions are considered to be correct, to calculate the theoretical maximum atomic percentage of Mo in each of the alloys. The results of the calculations[a] are given in Table IV. No extensive studies were made to determine the experimental maximum atomic per cent of Mo in the alloys, but the values given in Table IV are those that were obtained in this work. In the case of Fe the experimental percentage is larger than the theoretical percentage because the deposit is not completely metallic but was covered in the center with molybdenum oxide.

[a] One M atom can hold y hydrogen atoms and it requires 3 hydrogen atoms to reduce one $Mo(OH)_3$ to Mo; therefore the number of atoms of M required to give one atom of Mo is $3/y$. The atomic per cent of Mo is then

$$\frac{1Mo}{1Mo + \frac{3M}{y}} \text{ or } \frac{1}{1 + \frac{3}{y}} \text{ or } \frac{y}{y + 3}.$$

In summary, it is postulated that the reduction of molybdate ion in these alloy baths proceeds according to the reactions expressed by Eqs. [1] and [2] given above. In these equations the best value for n seems to be three and M must be a metal which has some unpaired electrons such as Fe, Co, or Ni.

Manuscript received Feb. 10, 1958. This paper was prepared for delivery before the Washington Meeting, May 12-16, 1957, and was abstracted from the thesis of D. W. Ernst submitted in partial fulfillment of the requirements for the Ph.D. degree at the University of Wisconsin.

Any discussion of this paper will appear in a Discussion Section to be published in the June 1959 JOURNAL.

REFERENCES

1. D. W. Ernst, R. F. Amlie, and M. L. Holt, *This Journal*, **102**, 461 (1955).
2. T. F. Frantsevich-Zabludovskaya, *Zhur. Priklad. Khim.*, **28**, 700 (1955); *C. A.*, **50**, 1497 (1956).
3. R. Piontelli, Trans. Inst. Met. Finishing Advance Copy No. 5, **1954**, 31.
4. S. Barnartt, *This Journal*, **99**, 549 (1952).
5. M. Eisenberg, C. W. Tobias, and C. R. Wilke, *ibid.*, **102**, 415 (1955).
6. P. Delahay, "New Instrumental Methods in Electrochemistry," Chap. 16, Interscience Publishers, Inc., New York (1954).
7. J. Kronsbein, *Plating*, **39**, 165 (1952).
8. D. P. Smith, "Hydrogen in Metals," p. 38, Univ. of Chicago Press, Chicago (1948).
9. S. Glasstone, "Introduction to Electrochemistry," pp. 462-463, D. Van Nostrand, New York (1942).
10. S. Glasstone, H. Eyring, and K. Laidler, "Theory of Rate Processes," p. 589, McGraw Hill Book Co., New York (1941).
11. J. O'M. Bockris, *Trans. Faraday Soc.*, **43**, 417 (1947).
12. C. Barrett, "Structure of Metals," p. 309, McGraw Hill Book Co., New York (1952).

Brief Communication

Thermally Regenerative Ionic Hydride Galvanic Cell

R. E. Shearer and R. C. Werner

MSA Research Corporation, Callery, Pennsylvania

Studies have been made of the electrochemical formation of ionic hydrides in fused salt media and of the thermal regeneration of the reactants. Typical reactions are:

$$H_2 + Ca \rightleftarrows Ca^{++} + 2H^-$$

and

$$\tfrac{1}{2}H_2 + Li \rightleftarrows Li^+ + H^-$$

In a calcium hydride cell with a solid calcium electrode, an open-circuit voltage of 0.56 v was obtained in the eutectic of the fluoride and the chloride of calcium at 644°C. Regeneration of the calcium and hydrogen was obtained by raising the temperature to about 1000°C. In one measurement, 89% of the hydrogen consumed reacted electrochemically with the calcium.

Widely differing open-circuit voltages were obtained with lithium hydride cells, depending on the composition of the electrolyte. With the eutectic of the bromide and the fluoride of lithium, 0.3 v was obtained. With a chloride-fluoride eutectic, 0.6 v was obtained at about the same temperature, approximately 550°C. In both cases, operating temperatures were above the melting point of lithium so that design of a simple closed cycle continuous system can readily be envisioned.

In an unoptimized cell, a current density of about 150A/ft^2 of lithium electrode area was obtained under maximum power output conditions. Engineering estimates indicate that a specific power output of 90 w/ft^3 should be readily attainable; this might be increased greatly with new development work. A similar estimate for a 2-w cell indicates a weight of 1 lb/w output. These values do not make allowances for the heat source or heat sink. Carnot cycle efficiencies of 35% are indicated for a lithium hydride cell based on cell operation at the eutectic temperature of the bromide and the fluoride of lithium (450°C) and on a regenerative temperature at which the decomposition pressure of the pure hydride is 1 atm (850°C).

Acknowledgment

Thanks are due to J. W. Mausteller for advice and discussions and to J. C. King for his work on assembly of cells and on measurements. The authors are also indebted to C. B. Jackson, Vice-President and Director of Research of MSA Research Corporation, for his support.

Manuscript received July 21, 1958.

Any discussion of this article will appear in a Discussion Section to be published in the June 1959 JOURNAL.

June 1959 Discussion Section

A Discussion Section, covering papers published in the July–December 1958 JOURNALS, is scheduled for publication in the June 1959 issue. Any discussion which did not reach the Editor in time for inclusion in the December 1958 Discussion Section will be included in the June 1959 issue.

Those who plan to contribute remarks for this Discussion Section should submit their comments or questions in triplicate to the Managing Editor of the JOURNAL, 1860 Broadway, New York 23, N. Y., *not later than March 2, 1959*. All discussion will be forwarded to the author, or authors, for reply before being printed in the JOURNAL.

New amplifier battles "noise"

Four-stage junction diode amplifier was developed at Bell Telephone Laboratories by Rudolf Engelbrecht for military applications. Operates on the "varactor" principle, utilizing the variable capacitance of diodes. With 400-mc. signal, the gain is 10 db. over the 100-mc. band.

The tremendous possibilities of semiconductor science are again illustrated by a recent development from Bell Telephone Laboratories. The development began with research which Bell Laboratories scientists were conducting for the U. S. Army Signal Corps. The objective was to reduce the "noise" in UHF and microwave receivers and thus increase their ability to pick up weak signals.

The scientists attacked the problem by conducting a thorough study of the capabilities of semiconductor junction diodes. These studies led to the conclusion that junction diodes could be made to amplify efficiently at UHF and microwave frequencies. This was something that had never been done before. The theory indicated that such an amplifier would be exceptionally free of noise.

At Bell Laboratories, development engineers proved the point by developing a new kind of amplifier in which the active elements are junction diodes. As predicted, it is extremely low in noise and efficiently amplifies over a wide band of frequencies.

The new amplifier is now being developed for U. S. Army Ordnance radar equipment. But it has numerous other possibilities. In radio astronomy, for example, it could be used to detect weaker signals from outer space. In telephony, it offers a way to increase the distance between relay stations in line-of-sight or over-the-horizon communications.

BELL TELEPHONE LABORATORIES

WORLD CENTER OF COMMUNICATIONS RESEARCH AND DEVELOPMENT

FUTURE MEETINGS OF
The Electrochemical Society

Philadelphia, Pa., May 3, 4, 5, 6, and 7, 1959

Headquarters at the Sheraton Hotel

Sessions probably will be scheduled on

Electric Insulation, Electronics (including Luminescence and Semiconductors), Electrothermics and Metallurgy (including a Projected Symposium on "Mechanical Properties of Intermetallic Compounds"), Industrial Electrolytics, and Theoretical Electrochemistry

★ ★ ★

Columbus, Ohio, October 18, 19, 20, 21, and 22, 1959

Headquarters at the Deshler-Hilton Hotel

★ ★ ★

Chicago, Ill., May 1, 2, 3, 4, and 5, 1960

Headquarters at the Lasalle Hotel

★ ★ ★

Houston, Texas, October 9, 10, 11, 12, and 13, 1960

Headquarters at the Shamrock Hotel

★ ★ ★

Papers are now being solicited for the meeting to be held in Philadelphia, Pa., May 3-7, 1959. Triplicate copies of each abstract (*not exceeding 75 words in length*) are due at Society Headquarters, 1860 Broadway, New York 23, N. Y., *not later than January 2, 1959* in order to be included in the program. *Please indicate on abstract for which Division's symposium the paper is to be scheduled, and underline the name of the author who will present the paper.* Complete manuscripts should be sent in triplicate to the Managing Editor of the JOURNAL at 1860 Broadway, New York 23, N. Y.

A Visit to Moscow

Abner Brenner

Chemistry Division, National Bureau of Standards, Washington, D. C.

As a representative of The Electrochemical Society, I attended the All Union Scientific-Technical Conference on Corrosion and Protection of Metals, which was held in Moscow from the 19th to the 24th of May 1958, under the auspices of the USSR Council of Scientific and Engineering Societies. I was accompanied by my wife, and we spent eight days in Moscow. The trip has been of more than ordinary interest because visits to Russia are still rather infrequent despite the opening up of several Russian cities to regular tourist travel.

My trip materialized rather suddenly. The invitation was received about the last week of April. Since the Conference was to begin on Monday, May 19, not much time was allowed for obtaining the Russian visas. As a matter of fact, when the visas were not forthcoming by the Wednesday preceding the Conference, I was forced to cancel all of the travel arrangements. However, the visas finally arrived at the last possible moment—shortly before noon on Friday, May 16. As it was necessary to leave by plane the following morning, my wife and I had a rather phrenetic time: arranging for care of the children, buying luggage, obtaining transportation, making arrangements with the Intourist Agency, and, finally, packing—all on less than one day's notice.

The flight, including the stopovers which were of short duration, took about 30 hours. The first stop was Hamburg, then Copenhagen, and Stockholm. Here we changed to a Russian, two-motored plane of the Aeroflot system. The plane stopped at Riga where passport and custom matters were cleared, and we then proceeded to Moscow where we arrived late Sunday night. We were pleasantly surprised and pleased to be met at the air terminal by Dr. Ya. M. Kolotyrkin and Dr. V. V. Losev of the Karpov Institute, and Mr. V. Panov, the Secretary of the Conference. They accompanied us to our hotel and arranged to send an interpreter around the next morning to guide me to the meeting place which was several blocks away.

The Conference was attended by 15 foreigners. Of these, only three were from the Western countries. Besides myself, there was Edmund C. Potter, who is head of the Boiler Corrosion Research Lab. of the Central Electricity Generating Board of England, and Joseph B. Cotton, who is head of the Corrosion Lab. of the Research Dept. of the Imperial Chemical Industries, Ltd. Other scientists had been invited from the Western countries but had not made the trip. The other foreign guests were from Hungary, Czechoslovakia, Poland, East Germany, and Yugoslavia.

The Conference began with a large meeting held in the Polytechnic Institute, which is a museum something like the Museum of Science and Industry in Chicago, although on a smaller scale. The opening talk was given by A. N. Frumkin to an audience of from 500 to 1000 people. The auditorium was crowded, both the main floor and balcony, and people were standing in the aisles. The first day of the Conference was devoted to general subjects. On the following days, the Conference broke up into six groups. I was pleased to find that one of these groups dealt with electrodeposition and that an electroplating exhibition was held in conjunction with the meeting. The meetings ran from 9:00 A.M. to 1:30 P.M. with only a 15-minute break at 11:00 A.M. The meetings were resumed at 3:00 P.M. and ran to 6:00 P.M. The last day of the Conference was also a general or plenary session.

All of the papers were presented to the Conference in Russian, and interpreters were supplied to the foreign visitors. I had my personal interpreter, a young lady who had a college degree in the art of languages and interpreting. She accompanied me not only to the Conference meetings but also on the sight-seeing tours and at the social functions. This was not an unpleasant experience!

Two hundred papers were presented at the Conference. Of these, 40 dealt with electrodeposition and allied subjects. The synopses were printed in seven booklets—one for each of the six sessions and one for the general session—comprising a total of about 400 pages.

The following are the names and some of the main topics of the sessions:

1. General Corrosion; dealt with the effects of stress, atmospheric exposure, sea water, gases, and molten electrolytes.
2. Underground Corrosion; dealt with protective coatings, electrochemical protection, and protection from stray currents.
3. Corrosion Inhibitors and Protective Greases.
4. Metal Coatings and Chemical Treatment of Metals; including cleaning of metals, phosphate coatings, various types of plating processes, anodizing, and automatic equipment.
5. Lacquer Coatings; their application for solving special corrosion problems.
6. Nonmetallic Chemically Stable Materials; including synthetic rubber, plastics, graphitic materials, acid resistant ceramics, and enamels.
7. Plenary Meeting; dealt with general and theoretical topics.

I have had the titles of all of these papers translated, but of the synopses, only those dealing with electrodeposition.

I presented two talks at the Conference. The main one was entitled "Protection of Metals from Oxidation at Elevated Temperatures by Means of Electrodeposited

Coatings" and was in part based on our paper[1] which appeared in the August issue of this JOURNAL. I had not brought along a manuscript as I had expected to deliver the talk in English and to have an interpreter translate it as I spoke. However, it was necessary to write out the talk in longhand. It was translated and delivered by one member of the Conference. The same was done for the papers of the two English visitors. The Conference was very accommodating to do the lengthy translations on a few days' notice. My other talk had not been originally scheduled and consisted of a summary of our paper on electroless plating that had appeared in the December 1957 issue of *Plating* magazine.

One of the most interesting phases of the trip was the visits to scientific laboratories which the Conference arranged for its foreign guests. The scientists whom we met were quite frank and open about their researches. Some of the scientists spoke English well and were able to explain their work without interpreters.

The first laboratory visited was the Institute of Physical Chemistry, which has a personnel of 800 divided into 20 sections. Dr. A. N. Frumkin, who is head of the Electrochemistry Division, personally conducted us through his laboratories and spent a considerable amount of time describing his researches. He spoke English very well and a few other languages in addition.

In Frumkin's laboratory, we saw an apparatus for studying the passivity of metals. The metal was outgassed and cleaned in a vacuum and then brought into contact with a degassed electrolyte. Polarization measurements were made with controlled amounts of oxygen admitted to the system. Another apparatus consisted of a cell divided by an iron membrane. Hydrogen which was evolved on one side of the membrane diffused through to the other side. The effect of the diffused hydrogen in lowering the hydrogen overvoltage of the steel was being studied. Other studies dealt with the double layer and with the measurement of the Volta potential. The latter was measured at temperatures of −80°C. On warming the metal up to room temperature, the sign of the potential changed. Another piece of apparatus had an electrode sealed into a system by means of a corrugated glass mounting so that the electrode could be vibrated and the effect of the vibration on potentials could be determined. Frumkin also spoke of working with a vacuum of the order of 10^{-10} mm which was produced with the aid of getters.

Work done in some of the other laboratories of the Institute dealt with the following subjects: the use of radioactive tracers for investigating electrode kinetics and for studying the structure of the double layer; the effect of adsorbents on the lowering of the exchange current; relation between the adsorption of ions and the potential of a platinum electrode; and the intergranular penetration of radioactive iodine into platinum. Measurements of the differential electrode capacity, which are usually made with mercury electrodes, were applied to solid metal electrodes, particularly to silver. The differential capacitance is independent of the frequency with mercury electrodes but not with solid metals.

One of the most valuable results of this visit was meeting Dr. A. T. Vagramyan, who is head of the Electrodeposition Section of the Institute, and some of his associates whose papers I had read. This section was carrying on a large program of basic investigations of electrodeposition.

We next visited the Karpov Institute, which is the main theoretical institute under the Ministry of Chemistry. It was organized in 1918. It is directed by Dr. Ya. M. Kolotyrkin, who is a well-known electrochemist with his chief interests in the field of corrosion. The institute dealt with physical chemistry, with the properties of materials and with polymerization using radiation. V. I. Vysilovski was head of the laboratory of electrochemistry. Kolotyrkin, himself, was actively working on electrode kinetics.

The following is a partial listing of some of the studies to which we were introduced: the effect of adsorption of radioactive iodine by a silver electrode on hydrogen overvoltage; the passivation of metals by oxidizing agents, as determined by the relation between current density and electrode potential; electrochemical determination of adsorption on electrodes by using alternating current and measuring a capacitative effect; properties of semiconductors, particularly the effect of ultraviolet light on semiconducting films of oxide. Vysilovski was studying the effect of gamma radiation on electrochemical processes and corrosion. He used a cobalt 60 source which had an intensity of 120 curies. Irradiated metal electrodes which adsorbed hydrogen or oxygen gave electrode potentials characteristic of hydrogen or oxygen, respectively. In some cases, iron and nickel became more chemically active; in others, they became passive, as noted by their potentials. A second effect of radiation dealt with its effect on semiconducting oxides such as zinc oxide. It changed the properties of the semiconductor just as ultraviolet light did. Studies were also in progress on the effect of radiation on other oxides, for example aluminum oxide.

The third research laboratory visited was the Central Scientific Research Institute for Technology and Machine Construction. The laboratory employs 2000 people and carries on applied research and testing for about 500 or more Russian plants. It also gives technical training and grants a type of degree. We visited only the part of the institute that dealt with metallurgical research on metals that could be used for turbine blades operating at 600°C. The laboratory was well equipped for metallurgical investigations. There was equipment for creep testing, an oscillating machine for studying fretting corrosion, and apparatus for studying stress corrosion and gas corrosion or erosion at elevated temperatures. In the routine testing laboratory, we saw spectrochemical equipment. There was no automatic spectrochemical equipment.

We visited one manufacturing plant, the First Ball Bearing plant, which employs 12,000 people. It was built in 1932, and many of the workers in it had been with the plant during the 26 years of its existence. The director of the plant received us in his office and took time to brief us on the general background of the history and importance of the plant. The plant had two sections, one for ordinary methods of production, the other for fully automatic production. Even the assembly of the balls in the races and the testing of the bearings was done automatically. We were free to observe whatever we wanted and all our questions were cheerfully answered. I noted that all of the automatic lathes and other machinery had Russian name plates on them and apparently were manufactured in Russia. In the Russian Pavilion at the World's Fair, I subsequently saw two bearings which had been produced in the plant; one was a large roller-bearing assembly one or two feet in diameter, and the other a small ball-bearing assembly a fraction of an inch in diameter.

My general impressions regarding the trips to the scientific and technical institutions were that the laboratories were well supplied with equipment, most of it of Russian manufacture; they were well staffed; and were doing high-level fundamental investigations in

[1] D. E. Couch, H. Shapiro, J. K. Taylor, and A. Brenner, *This Journal*, **105**, 450 (1958).

electrochemistry. A large proportion, perhaps half, of the scientific personnel were women.

The Conference entertained its foreign visitors on a more lavish scale than we are accustomed to treat foreign visitors to scientific conferences. In addition to several sight-seeing trips, we were taken to the opera where we saw the performance of Eugene Onegin, and to a ballet to see Swan Lake. The latter performance was particularly outstanding. Our visits to scientific institutes also were not without social festivities. At the conclusion of each of our visits to the Institute of Physical Chemistry and to the Karpov Institute, we were treated to a cocktail party. Also, on the Saturday evening following the close of the Conference, a reception was held. At these affairs, we were served everything from caviar to cognac.

Among the other courtesies extended to the foreign visitors was the processing of baggage through customs without it's being opened, either on arrival or on departure. Also, on a day's notice, the Intourist Bureau arranged for my wife to spend a day at an elementary school and a teacher's college. My wife, who is employed in a county educational system, was quite appreciative of this courtesy and of the time given to her by the staff of the institutions.

During our stay in Moscow, my wife and I were treated with cordiality. At no time did any member of the Conference discuss political matters or make critical comments about the United States. We were willing to let well enough alone and did not attempt to ask questions of a political nature. On our return, we have been asked frequently whether we were subjected to any restrictions. We were not subjected to any kind of surveillance and were free to come and go as we liked. Furthermore, there were no restrictions on taking photographs at any of the places we visited, except on the interior of certain museums.

We found Moscow a very interesting city. Because of its large squares and wide streets, it seemed quite open. Also, it was kept clean. There were some tall and ornate buildings but no appreciable number of skyscrapers. The sidewalks were crowded, but the automobile and street traffic were light and crossing the streets was not difficult. Space does not permit a recounting of the places of interest which were seen or visited. These can only be mentioned: the Kremlin with its numerous cathedrals and museums; the great Agricultural and Industrial Exposition which is on the scale of a World Fair; new housing projects; Moscow University; and the architecturally beautiful and scrupulously clean subways.

Because of the short duration of our visit, I am not able to comment on life in the City, but a few observations might be of interest. Visitors were given a rate of exchange of 10 rubles to the dollar and were not allowed to take rubles out of the country. At this rate of exchange, housing, transportation, and use of the telephone was low priced. The price of meat was high, but I made no observations on other food items. Prices for clothing were particularly high, which explains why the people on the streets were dressed less stylishly than in some of the other European cities that we visited subsequently.

Our visit to Moscow was of interest for several reasons. I hope that reciprocity will now be in order so that the further interchange of scientific data—and scientific personalities—between the two countries can be considerably augmented.

All Union Scientific-Technical Conference on Corrosion and Protection of Metals, 1958

(Collection No. 1)
Section on General Corrosion

I. General Problems of the Corrosion of Metals

A. I. Krasilshtsikov, T. N. Sharanova. Concerning the Mechanism of Corrosion of Metals with Oxygen Depolarization.

N. P. Shuk. Some Problems on the Corrosion of Metals with Oxygen Depolarization.

L. K. Lepin, A. Ya. Vayvadye, Z. F. Oshis. Concerning the Mechanism of Retardation and Acceleration of Corrosion of Iron with Aqueous Solutions of Mixtures of Salts.

V. V. Skorchellyetti, I. A. Stepanov. Electrochemical Investigation Conducted in the Molten System Copper-Zinc in the Range α and β Solid Solution.

V. S. Komissarova, A. I. Golubev. Self-Solubility and Anodic Behavior of Magnesium.

Ya. M. Kolotirkin, N. Ya. Bunee, V. M. Knyasheva, G. M. Florianovich. Mechanism of Anodic Inhibition of Metals and Alloys in Solutions of Electrolytes.

A. V. Byalobsheskii. Influence of Ionization Emissions on the Corrosion of Metals.

E. N. Mirolyubov, M. M. Kurtepov, N. D. Tomashov. Corrosion and Electrochemical Behavior of Rustless Steel in Active State in Solutions of Nitric Acid.

N. D. Tomashov, M. A. Vedenyeyeva. Influence of Chemical Composition and Thermal Treatment of Steel, and also the Composition of the Corrosive Medium on Intercrystalline Corrosion of Steel Type CH18N9.

V. N. Iordanskii. Corrosion Resistance of Aluminum Alloys of the System Al-Mg.

S. E. Pavlov, S. M. Ambartsumyan, K. A. Shigalova. Corrosion and Protection of High-Stability Aluminum Alloys.

V. S. Nabokov, N. D. Tomashov, E. N. Paleolog. Investigation of the Structure of Protective Films on Metals by the Absorption Method.

A. S. Afanasev, E. N. Chankova, V. V. Shevchenko. Oxygen Electrode on Iron.

II. Corrosion of Metals under Tension

A. V. Ryabchenkov, V. P. Sidorov. Corrosion Cracking of Austenitic Steel in Alkaline Media at Increased Temperature.

L. A. Glickman. Constructive Factors Influencing Corrosion-Fatigue Endurance.

V. S. Sinyavskii, S. G. Vedenkin. Corrosion-Fatigue Endurance of Aluminum Alloys.

E. P. Fedorova, V. N. Novikov. Increasing the Corrosion Resistance of Piston Rods Using Surface Hardening, etc.

I. L. Faerman. Corrosion Endurance of Steel in Sub-petroleum Water in Petroleum Deposits.

O. N. Muravkin, A. V. Ryabchenkov. Investigation in the Area of Fretting-Corrosion of Metals.

V. A. Veller. Influence of Fretting-Corrosion on the Fatigue Resistance of Shafts.

M. G. Timberbulatov, G. I. Babushkina. Cavitation and Corrosion Resistance of Different Types of Steel and Alloys on Copper Bases.

N. A. Bushye. Cavitation Decomposition of Bearings, of Cast Babbit.

V. V. Romanov, V. V. Dobrolyobov. Influence of Cathodic and Anodic Polarization on the Rate of Corrosion Cracking of Steel 1Ch18N9.

III. Atmospheric Corrosion of Metals

G. B. Klark, M. I. Michailovskaya, N. D. Tomashov. Electrochemical Investigation of Corrosion of Metals in Humid Atmospheres with Various Contents of Sulfur Dioxide.

V. G. Chernashkin, A. E. Babaeva. Corrosion of Structural Steel under Natural Conditions.

A. A. Babakov, D. G. Tufanov. Corrosion of Steel in Atmospheric Conditions.

IV. Corrosion of Metals in Sea Water and Other Neutral Solutions

I. L. Rozenfeld, K. A. Shigalova. On the Mechanism of Corrosion of Metals with Periodic Wetting by Electrolytes.

B. V. Strokan. Models for Corrosion Experiments with Moving Sea Water.

V. F. Negreev, A. M. Kazimov, D. M. Abramov, S. A. Mechmandarov, A. A. Farchadov, B. A. Zamanov, M. R. Nuriev. Sea Corrosion of Steel and Methods of Protecting Sea Construction, Ships, and Pipelines

G. G. Koshelev. Investigation of Corrosion Stability of Carbon and Light Alloyed Steel in the Barents Sea.

A. I. Zub. Effectiveness of Zinc Protection in a Moving Medium.

S. A. Ivanov. On the Possibility of Hydrogenation of Metal during Cathodic Protection of Steel Construction in Sea Water.

A. F. Shurachovskii, I. N. Frantsyevich. Protectors on Zinc and Aluminum Bases, Containing Calcium.

A. E. Gopius, V. P. Molchanova. Investigating Stream Corrosion of a German Silver Condenser Tube.

E. M. Zimneva. Study of the Corrosion Stability of Different Types of Light Alloys in Sea Water and Sea Mist.

F. B. Slomyanskaya, A. I. Lipovyetskaya. The Protection of Aluminum Tubes of Automobile Radiators from Corrosion.

F. N. Tavadze, S. N. Mandshgaladze. Study of the Corrosion of Metals in Mineral Water.

V. Gaseous Corrosion of Metals and Corrosion of Metals in Molten Salts

N. I. Tugarinov, A. A. Eremen. The Nature of the Heat Resistance of Nickel-Chrome Alloys.

A. V. Ryabchenkov, A. I. Maximov, E. A. Davidovskaya, E. L. Kaziminovskaya, P. V. Sorokin, Investigation in the Field of Gaseous Corrosion and Its Influence on the Heat Resistance Properties of Steel.

M. M. Krystal, N. V. Chochlova. Corrosion of Steel in Molten Mixtures of Sulfate Salts.

N. V. Bogoyavlenskaya, Ya. N. Lipkin. Etching Tubes of High Alloy Type Steel.

K. G. Potaskayev, Z. P. Menshikova, M. E. Prostakov, A. L. Tarasova. Removing Scale by Means of Its Reduction with Sodium Hydride.

VI. Corrosion of Titanium and Its Alloys

V. V. Andryeyeva, V. I. Kazarin. Corrosion Resistance and Electrochemical Properties of Titanium and Its Alloys.

R. M. Altovskii, N. D. Tomashov. Influence of Halide Ions on Corrosion and Electrochemical Behavior of Titanium in Acid Media.

L. Chirkova. The Influence of Contact with Different Metals on the Corrosion Resistance of Titanium Alloys.

VII. Corrosion of Metals in the Chemical and Other Industries

M. L. Rutkovskii, R. V. Tsvetkova. Corrosion of Metals in Aqueous Solutions of Calcium and Ammonium Nitrate, Saturated with Ammonia.

E. V. Zotova. Corrosion of Iron Alloys in Solutions of Sulfuric Acid.

G. L. Schwartz, Yo. S. Kusnetsova. Alloys for Equipment Used with Sulfuric Acid.

Z. A. Tkacheck. Study of Corrosion of Parts of an Electrolyzer for Electrolyzing Water.

F. A. Orlova. Corrosion of Steel in Hot Solutions of Caustic Alkali under Conditions of Evaporating the Liquid.

A. E. Romanushkina, K. K. Polyakova. Corrosion of Metals with Chloride-Chlorate Solutions and Corrosion of Apparatus for the Production of Chlorine Dioxide and Sodium Chlorite.

F. B. Slomyanskaya, A. N. Krutikov. Corrosion of Welded Parts of Aluminum Apparatus for Boiling Concentrated Nitric Acid.

A. I. Brodovich, E. I. Gromov. Corrosion of Benzol Columns in the Coke-Chemical Industry and in Apparatus for Rectifying Raw Phenol.

V. F. Negreev, M. A. Dalin, A. B. Neiman, L. N. Petuchova. Corrosion of Apparatus for the Process of Direct Hydration of Ethylene.

V. N. Poddubnii, A. I. Polyakov, B. I. Golub. Corrosion of Chromium in Special Liquids.

Stalinogorski Chemical Group. Protection of Apparatus under High Pressure in the Production of Synthetic Methanol, in GSChK.

Stalinogorski Chemical Group. Corrosion and Protection of Apparatus in Factories Producing Urea in GSChK.

F. N. Tabadze, T. A. Lashchi. Investigation of Corrosion Resistance of Various Metals in Grape Wine.

M. V. Konradi. Corrosion Resistance of Rustless Steel under Conditions of Working-Up Peat under Tar Water.

(Collection No. 2)

Section of Underground Corrosion

I. General Problems of Underground Corrosion

(Investigation of the Electrochemical Processes of Soil Corrosion of Metals. Methods of Determining the Corrosion Danger of Soils and the Corrosion State of Underground Construction. Experiments to Prevent Corrosion of Underground Construction in Densely Populated Cities.)

N. D. Tomashov, Yo. N. Michailovskii. Investigation of the Electrochemical Process of the Soil Corrosion of Metals.

N. I. Ryabtsev. Construction of a Gas Line Grid in the Sixth Five-Year Period and Protection of Them from Corrosion.

A. A. Spirin, M. M. Salam-Zade, K. N. Afonskii. On the Method of Determining the Corrosion Danger of Soil and the Corrosion State of Underground Construction in Field Conditions.

L. I. Akinfiev. Investigation of Corrosion in the Territory of Moscow.

N. A. Tsekin. Experimental Complexity of Protecting Underground Construction in Densely Populated Cities.

K. A. Aliev. Protection of Underground Gas Pipes in Cities from Corrosion.

II. Anti-Corrosion Coatings for Underground Construction

L. Ya. Tsikerman. Theory and Calculation of Protective Coatings for Underground Metallic Supply Pipes.

V. S. Artamonov. Protection from Underground Corrosion of Reinforced Concrete Construction for Transportation.

S. R. Rafikov, V. G. Benkofskii, V. G. Gutsalyok, M. N. Michailov. Experimental Use of Polychlorvinyl Plastic for Protecting Underground Pipes.

E. A. Andryeyeva. Stability of Bitumin Isolation Coatings in Conditions of Cathodic Protection.

M. A. Aliev. Enamel Coatings for Protecting Underground Pipes.

III. Electrochemical Protection of Underground Construction

A. F. Marchenko. On the Possibility of Intensive Corrosion of Lead Wrapped Cables for Cathodic Polarization at Constant Current and Protective Potentials.

M. S. Trifle. On the Influence of Certain Factors on the Distribution of Potentials along Pipelines for Electrochemical Protection.

V. G. Kotik. Cathodic Protection of the Main Line Pipes and Experiments with Its Use.

V. V. Krasnoyarskii. Distribution of Current and Potential along an Expanse of Construction and Its Cathodic Protection.

I. N. Frantsyevich, I. S. Gerenrot, B. D. Kyzmenko. Effectiveness of the Action of the Surrounding Complex Electroprotection of Gas Pipes in Dashava-Kiev.

IV. Protecting Underground Construction from Corrosion, Caused by Stray Currents

I. N. Frantsyevich, V. A. Grimailovskii, F. A. Rogoza. Experimental Use of Electrical Drainage Protection of Underground Gas Pipes in Industrial Regions of the U.S.S.R.

D. K. Tomlyanovich. Systems of Electrical Supply to the Electro-Transportation in Towns and Their Influence on the Problem of Protecting Construction from Corrosion by Stray Currents.

I. M. Ershov. Methods of Estimating the Effectiveness of Actions for Lowering Leakage of Traction Current from Rails of Electrified Railroads.

P. G. Doroshenko, V. I. Glazkov. Electro-Protection of Main Line Pipes from Corrosion Caused by Stray Currents and Choice of Protective Media.

E. V. Chebotarev. Regulation of the Potential at Drainage Points of Rails of a Streetcar Network Using Special Rectifier Setups.

I. A. Kornfeld, V. A. Pritula. Electro-Corrosion of Reinforced Concrete.

K. K. Nikolskii. Influence of Current from Electro-Transmission Lines with a Constant Current System "Conductors—Earth" on the Corrosion State of Underground Metallic Construction.

L. D. Razumov. Calculating the Danger from Corrosion of Cable Wrapping Couplings, Found in Fields of Stray Current Electrical Traction.

(Collection No. 3)

Section on Corrosion Inhibitors and Protective Greases

I. Volatile Inhibitors

V. P. Persiyantseva, I. L. Rosenfeld, M. A. Novitskaya, T. I. Akimova, A. L. Labutin. On the Mechanism of the Protection of Metals from Corrosion by Volatile Inhibitors.

R. M. Golubeva, S. D. Byeskov. Study of the Phosphate of Monoethenolamine as an Inhibitor to Atmospheric Corrosion.

O. I. Golyanitskii. Theoretical Basis and Practical Results of Conservation of Parts of Machines Using Some Volatile Inhibitors.

Lekareva. Experimental Protection by Volatile Inhibitors for Parts for Long-Time Storage.

II. Retarding Corrosion in Neutral, Acid, and Alkaline Media

Z. A. Iofa. On the Joint Action of Sulfur-Containing Inorganic Anions and Organic Inhibitors to Acid Corrosion and Embrittlement of Iron.

G. V. Kleshtseva, S. A. Balezin. The Influence of Ammonia and Some of Its Salts toward Corrosion of Carbon Steel.

I. P. Anoshtsenko. The Joint Influence of Urotropine, Atebrin, and Potassium Iodide on the Corrosion of Iron in Hydrochloric and Sulfuric Acids.

N. M. Malin. Investigation of the Products of Corrosion of Low-Carbon Steel in Neutral and Weakly Acid Media with Added Stimulators and Inhibitors.

S. A. Balezin, S. D. Beskov, L. P. Zaitsev. Jet Etching and Inhibition of Some Metallic Objects.

T. Ch. Monachova, V. F. Negryeyev, D. M. Rudkovskii, P. Yo. Alekperova. Organic Retarders of Corrosion of Steel in Water Containing Hydrogen Sulfide.

V. B. Ratinov, O. I. Dobshik. Corrosion of Steel in Cementing Materials and Retarders of Corrosion.

A. V. Shreider, M. M. Lifshutz. Choice of Retardants for Protection of Metals from Corrosion Submitted to the Action of Protective Mixtures in Coal Mines.

V. P. Grigorev, L. I. Antropov. Combination Protection of Iron from Corrosion in Neutral and Weakly Alkaline Media.

A. S. Afanasev, G. V. Shuk. Investigation of the Protective Action of Mixtures of Some Corrosion Retardants in Neutral Media.

V. V. Romanov, S. A. Balezin, Fello N. I. Podobaev. The Influence of Corrosion Inhibitor PB-5 on Corrosion Cracking of Steel 18/9 in a 42% Solution of $MgCl_2$.

V. N. Poddubnii, A. I. Polyakov, E. I. Osipov. Corrosion of Copper Alloys in Hydraulic Fluids.

I. F. Gridnev, I. L. Rozenfeld. Inhibiting Parts of Cast Iron and Steel by Placing into Solutions of Sodium Nitrate for the Purpose of Long-Time Storage.

V. A. Chitrov, N. A. Dugin, V. F. Chmelkov. The Influence of Temperature on Corrosion Resistance and Electrochemical Behavior of Low-Carbon Steel in Acid Inhibitor Media and the Use of Sodium Arsenate for Retarding Corrosion of Steel in Aqueous Solutions of Sulfuric and Hydrochloric Acid.

A. I. Filko, S. A. Balezin. The Problem of the Mechanism of the Protective Action of Thiourea toward the Solubility of Steel in Acids.

A. R. Myagkov, I. N. Putilova. Inhibitors of Corrosion of Lead in Water.

III. Inhibitors of Corrosion in Hydrocarbons and Protective Greases

B. V. Lockov. Anticorrosion Additives to Motor Oils, Their Nature and Mechanism of Action.

D. S. Velikovskii, I. I. Kashdan. Multifunctional Additive to Oils and Greases, to Increase Their Anticorrosion Properties.

K. S. Ramaiya, V. S. Zavelskii, R. Ch. Sils. Investigation of Additives to Oil for the Purpose of Inhibiting Corrosion of Parts of Automobile Motors.

I. N. Putilova, A. R. Myagkova. The Products of Corrosion of Lead in Hydrocarbon Solutions.

V. G. Kuznetsov, E. F. Reshetikova. Improving, with the Help of Inhibitors, the Protective Properties of Greases for the Roller Bearings of Railroads.

(Collection No. 5)

Section on Lacquer Coatings

I. New Anticorrosion Lacquer Materials

P. M. Bogatirev. Basic Directions in the Development of Production of Synthetic Resins for Lacquer Coatings.
K. P. Belyaeva, A. M. Grozovskaya, A. K. Myromtsev. Phosphate Primers.
N. G. Konstantinova, M. A. Kyotner. Thermally Stable Lacquer Coatings.
P. K. Kozlova. Industrial Utilization of Reaction Primer.
B. Ya. Gorovoy. Bacteriocide Lacquer Materials.

II. Use of Lacquer Coatings for Protection from Atmospheric and Chemical Corrosion

V. V. Chebotarevskii, P. I. Wasserman. The Mechanism of Protective Action of Lacquer Coatings on Wetting.
L. V. Nitsberg, S. V. Yakubovich. Electrochemical Investigations of the Anticorrosion Properties of Lacquer Materials and Coatings.
A. I. Reibman. Corrosion-Resistant Lacquer Coatings and Protection of Equipment and Metal Construction from Chemical Corrosion.
E. I. Megalinskii. Improving the Quality of Lacquer Coatings.
B. L. Chomitskii. The Relative Estimate of Different Anticorrosion Coatings on Magnesium Alloys.

III. Protective Lacquer and Bitumen Coatings in Sea Conditions

E. S. Gyrevich, I. N. Nikiforov. Newest Achievements in the Field of Ship Painting.
N. P. Myagkov, L. K. Lepin. On the Question of Joint Lacquering and Protection.
V. G. Chernashkin, A. E. Babaeva. Protecting Structural Steel in an Atmosphere of Sea Air.
E. I. Grishin. 1. Protection of Under-Water Parts of Ship Shells and Surfaces which are under Conditions of Increased Humidity, Oil-Free Anticorrosion Coatings.
2. Water-Resistant Noncombustible Oil-Free Coatings Based on Perchlorvinyl Lacs and Enamels.
I. Ya. Bogorad, E. V. Iskra. Corrosion of the Exterior Face of Under-Water Parts of Ship Shells and the Use of Characteristic Protective Coatings.
E. V. Iskra. Ethinol Paints and Their Use in Ship Construction.
R. G. Gadshieva, L. N. Zemskova, Ya. G. Gacanov, A. G. Chanlarova, Ch. M. Mirbagirova, M. I. Mamedov. Protective Lacquers and Bitumen Coatings in Sea Conditions.
A. Sakalo. The Stability of Protective Coatings on Objects Transported by Sea Vessels.
Y. I. Arie. New Lacquer Coatings for Regions Having Tropical Climates.

IV. Methods of Investigating Protective Properties of Lacquer Materials. Preventive Compositions

S. N. Kazarnovskii, G. M. Skalina. Experiments with Lacquer Materials under Different Climatical Conditions.
S. V. Yakubovich, M. I. Karyakina. Methods of Investigating Lacquer Coatings Intended for the Tropics.
M. M. Goldberg, S. N. Kazarnovskii. New forms of Preventatives and Washing Compositions for Lacquer Coatings.

(Collection No. 6)

Section of Nonmetallic Chemically Stable Materials

I. Organic Chemically Stable Materials

A—Synthetic Rubber and Polyisobutylene

A. L. Labutin. Use of Synthetic Rubber in Anticorrosion Techniques.
I. V. Biryokov. Experimental Rubberizing of Chemical Apparatus with Chloroprene Resin.
D. A. Gofen. Practical Use of Polyisobutylene for Protection from Corrosion of Apparatus and Construction Materials.

B—Use of Organic Chemically Stable Materials

V. E. Volodin. Experimental Protection of Chemical Apparatus and Building Construction from Corrosion.
A. M. Zak. Chemically Stable Armatures Based on Organic Chemically Stable Materials.
L. F. Emets and P. A. Afanasev. Sealing Materials for Chemical Apparatus Construction.

C—Plastic Compositions

T. N. Nikolaeva. Anticorrosion Coatings of Floroplastic-3.
T. L. Fabrikant. Experiments of the Last Year on Using the Lacquer "Ethinol" and a Means of Improving Asbestovinyl Compositions.
G. V. Shemchyshin. Faolite and Its Use in the Chemical Industry.
M. Greenberg. Combined Faolite-Wood Slabs and Frames for Filtering Acid Suspensions.

D—Graphitic Materials

V. K. Smiriov. Experiments Using Graphite Materials for Protection from Corrosion.
P. A. Afanacev. Methods of Determining Some Constants of Graphite Materials.
P. P. Neurodov. Cold Casting of Objects on a Graphite Base.

II. Inorganic Chemically Stable Materials

A—Concrete and Cement Acid-Resistant Ceramics

V. M. Moskvin. Corrosion of Concrete and Reinforced Concrete Construction.
Yo. V. Dereshkevich. Basic Principles of Construction of Apparatus and the Protective Linings of Nonmetallic Materials.

B—Use of Inorganic Chemically Stable Materials. Glass Pipelines. Enameled Chemical Apparatus

I. M. Doronenkov. Investigation of Corrosion of Structural Materials and Protection of Building Construction from Corrosion.
I. E. Shapiro. The Status and Perspective of the Production of Glass Tubing in the U.S.S.R.
Z. I. Simchovich. The Status and Perspective of the Production of Enameled Chemical Apparatus in the Soviet Union.

III. Organization and Experimental Work on Anticorrosion in Shops in the Chemical Business

A. S. Gorina. Anticorrosion Shops in the Chemical Business.
G. Z. Vashin. Organic Anticorrosion Agents Used in the Chemical Business.
Vorobeva. Protection from Corrosion in the Hydrolysis, Sulfite-Alcohol and Glucose Industries.

(Collection No. 7)

Plenary Meetings

1. A. N. Frumkin. Electrochemical Kinetics and the Theory of Corrosion.
2. N. D. Tomashov. Development of the Electrochemical Theory of Corrosion of Metals.
3. S. G. Vedenkin. Concerning the Destruction of Metals by the Joint Action of Corrosion and Mechanical Factors.
4. I. L. Rozenfeld. Theory of Atmospheric Corrosion.
5. V. P. Batrakov. On the Theory of Corrosion and Protection of Metals in Oxidizing Media.
6. S. A. Balezin. Inhibitors of Corrosion of Metals.
7. I. Ya. Klinov. The Basic Direction in the Fight against Corrosion by *Means of Using Nonmetallic Chemically Stable Materials.*
8. N. T. Kudryabtsev and A. T. Vagramyan. Improvements in the Field of Electroplating.

New Members

In August 1958, the following were approved for membership in The Electrochemical Society by the Admissions Committee:

Active Members

Fred Barson, International Business Machines Corp.; Mail add: International Business Machines Corp., Poughkeepsie, N. Y. (Electronics)

Shannon W. Brown, Columbia Southern Chemical Corp.; Mail add: 208 Wheeling Ave., Glen Dale, W. Va. (Industrial Electrolytic)

Jan Boeke, Research Consultant; Mail add: 70 Monument St., Concord, Mass. (Battery, Theoretical Electrochemistry)

Hugh K. Cameron, Research Labs., General Electric Co., Ltd., Wembley, Middlesex, England (Corrosion, Electric Insulation, Electrodeposition, Electronics, Electro-Organic, Electrothermics and Metallurgy, Industrial Electrolytic, Theoretical Electrochemistry)

Sahag Dakesian, Raytheon Mfg. Co.; Mail add: 91 Irving St., Somerville 44, Mass. (Electrodeposition)

William P. Devan, McGean Chemical Co., 5621 Commonwealth, Detroit 8, Mich. (Electrodeposition)

Philip Diamond, Perkins Engineering Corp., 345 Kansas St., El Segundo, Calif. (Corrosion, Electrodeposition, Electrothermics and Metallurgy, Industrial Electrolytic, Theoretical Electrochemistry)

George A. Di Pietro, Vacuum Specialties Co.; Mail add: 6 Campbell Rd., Arlington 74, Mass. (Electrothermics and Metallurgy)

Vance H. Dodson, Jr., Electric Auto-Lite Co.; Mail add: 825 Brighton Ave., Toledo 9, Ohio (Battery, Corrosion, Electrodeposition)

Harry A. Durney, Jr., Kennecott Titanium Development Corp.; Mail add: 440 Krick Rd., Box 169, Bedford, Ohio (Electrothermics and Metallurgy)

Sydney Forbes, Columbia-Southern

ECS Membership Statistics

The following three tables give breakdown of membership as of Oct. 1, 1958. The Secretary's Office feels that a regular accounting of membership will be very stimulating to membership committee activities. In Table I it should be noted that the totals appearing in the right-hand column are *not* the sums of the figures in that line since members belong to more than one Division and, also, because Sustaining Members are not assigned to Divisions. But the totals listed are the total membership in each Section. In Table I, Sustaining Members have been credited to the various Sections.

Table I. *ECS Membership by Sections and Divisions*

Section	Division: Battery	Corrosion	Electric Insulation	Electro-deposition	Electronics	Electro-Organic	Electrothermics & Met.	Industrial Electrolytic	Theoretical Electrochem.	No Division	Total as of 1/1/58	Total as of 10/1/58	Net Change
Boston	14	26	7	38	60	7	25	13	25	7	131	145	+14
Chicago	15	34	4	45	25	11	14	12	22	14	111	128	+17
Cleveland	59	37	2	53	40	10	31	34	40	14	203	210	+ 7
Columbus, Ohio	3	12	0	15	5	2	25	4	9	4	45	49	+ 4
Detroit	9	20	5	50	8	7	8	6	21	20	84	90	+ 6
India	7	6	3	18	8	6	9	13	14	3	36	35	— 1
Indianapolis	11	7	3	11	10	4	6	2	6	2	40	41	+ 1
Midland	9	15	0	5	2	2	7	16	11	2	45	43	— 2
Mohawk-Hudson	5	14	13	8	14	1	8	3	12	4	51	54	+ 3
New York	86	106	26	141	141	33	76	70	99	44	482	520	+38
Niagara Falls	16	25	1	21	9	5	80	66	31	21	175	184	+ 9
Ontario-Quebec	12	25	1	17	6	3	36	27	9	14	75	82	+ 7
Pacific Northwest	5	10	0	8	3	1	9	10	10	10	47	43	— 4
Philadelphia	24	32	4	37	64	12	23	19	50	30	174	183	+ 9
Pittsburgh	4	48	3	26	30	5	38	18	37	9	130	134	+ 4
San Francisco	6	15	2	21	17	4	16	22	21	4	64	70	+ 6
S. Calif.-Nevada	16	21	2	28	32	4	16	16	25	10	95	106	+11
Washington Baltimore	34	37	7	39	24	3	13	9	31	6	128	130	+ 2
U. S. Non-Section	56	92	14	87	80	44	69	77	118	34	395	417	+22
Foreign Non-Section	42	60	6	62	32	30	39	61	75	89	224	261	+37
Total as of Jan. 1, 1958	409	638	100	705	518	193	479	485	620	313	2735		
Total as of Oct. 1, 1958	433	642	103	730	610	194	548	498	666	341		2925	
Net Change	+24	+4	+3	+25	+92	+1	+69	+13	+46	+28			

Table II. *ECS Membership by Grade*

	Total as of 1/1/58	Total as of 10/1/58	Net Change
Active	2448	2563	+115
Faraday (Active)	—	30	+ 30
Deutsche Bunsen Gesellschaft (Active)	—	14	+ 14
Delinquent	61	70	+ 9
Active Representative Patron Members	8	10	+ 2
Active Representative Sustaining Members	70	91	+ 21
Total Active Members	2587	2778	
Life	16	17	+ 1
Emeritus	54	50	— 4
Associate	31	31	0
Student	42	45	+ 3
Honorary	5	4	— 1
Total	2735	2925	+190

The figures pertaining to Patron and Sustaining Member Representatives, and Faraday and Deutsche Bunsen Gesellschaft members subscribing to the JOURNAL, have been added to reflect reclassifications and changes in membership status.

Table III. *ECS Patron and Sustaining Membership*

	Total as of 1/1/58	Total as of 10/1/58	Net Change
Patron Member Companies	4	5	+ 1
Sustaining Member Companies	127	140	+ 13

Chemical Corp.; Mail add: 985 Lindendale Dr., Pittsburgh 16, Pa. (Industrial Electrolytic)

James W. Franklin, Engineering & Mining Journal; Mail add: Box 73, Buttzville, N. J. (Electrothermics and Metallurgy, Industrial Electrolytic)

Ralph O. Grubel, General Electric Co.; Mail add: 226 Cleveland Blvd., Fayetteville, N. Y. (Electronics)

Ralph J. Hach, Texas Instruments Inc., 6000 Lemmon Ave., Dallas 9, Texas (Electronics-Semiconductors)

Robert W. Haisty, Texas Instruments Inc., Materials Research, 600 Lemmon Ave., Dallas 9, Texas (Electronics)

Elton H. Hall, Battelle Memorial Institute, 505 King Ave., Columbus 1, Ohio (Electrothermics and Metallurgy)

David M. Heinz, General Electric Co., 40 Federal St., West Lynn, Mass. (Electronics)

John A. Hooton, American Lava Corp., Chattanooga 5, Tenn. (Corrosion, Electric Insulation, Electrothermics and Metallurgy, Theoretical Electrochemistry)

Carl Horowitz, Ions Exchange & Chemical Co.; Mail add: 5607 Fillmore Ave., Brooklyn 34, N. Y. (Battery)

Philip M. Jaffe, Westinghouse Electric Corp.; Mail add: 54 Hastings Ave., Nutley 10, N. J. (Electronics)

Daniel F. Kane, Jr., Gahagan Inc., Waterman Ave., Esmond, R. I. (Electronics)

Philip Kuznetzoff, RCA Semiconductor and Materials Div.; Mail add: 70 Phillips Rd., F. T., New Brunswick, N. J. (Electronics)

Tien Shuey Lee, Westinghouse Research Labs., Pittsburgh 35, Pa. (Corrosion, Theoretical Electrochemistry)

Samuel L., Marshall, Cowan Publishing Corp.; Mail add: 262 Sullivan Pl., Brooklyn 25, N. Y. (Electronics)

Ichiro Muraki, Fuji Electrochemical Co., Ltd.; Mail add: 614, Kosaicho-Washizu, Hamanagun, Shizuoka-Ken, Japan (Battery, Electrodeposition, Theoretical Electrochemistry)

James A. O'Connell, International Business Machines Corp.; Mail add: 29 Wenliss Terrace, Wappingers Falls, N. Y. (Corrosion, Electric Insulation, Electronics, Electro-Organic)

Joseph R. O'Connor, Air Force Cambridge Research Center; Mail add: 8 Forest St., Saugus, Mass. (Electronics)

Elinor H. Ostrander, National Bureau of Standards; Mail add: 10913 Clermont Ave., Garret Park, Md. (P. O. Box 527) (Battery)

Richard E. Panzer, U. S. Naval Ordnance Lab., Corona, Calif. (Battery, Electrodeposition, Theoretical Electrochemistry)

Marvin R. Paullus, Monsanto Chemical Co., Box 526, St. Louis 3, Mo. (Industrial Electrolytic)

William B. Pearson, Div. of Pure Physics, National Research Council, Ottawa, Ont., Canada (Electronics)

Harlan T. Pierpont, Jr., Norton Co.; Mail add: 84 William St., Worcester, Mass. (Electrothermics and Metallurgy)

John L. Porter, Sylvania Electric Products Inc.; Mail add: 261 Proctor Ave., Revere 51, Mass. (Electrodeposition, Electronics, Electrothermics and Metallurgy)

Eugene N. Schroeder, International Business Machines Corp., Dept. 509, Owego, N. Y. (Electronics)

Ramniklal A. Shah, M/S. Ronuk Industries Ltd.; Mail add: 11A, Worli Sea Face, Bombay 18, India (Electrodeposition)

Yasuichi Shibasaki, (Until Jan. 31, 1959) Dept. of Chemistry, Ohio State University, Columbus 10, Ohio; (after Jan. 31, 1959) 30 Daimachi, Kanagawa-ku, Yokohama, Japan (Battery, Electrodeposition, Industrial Electrolytic)

Richard C. Sirrine, General Electric Co.; Mail add: 201 Buckingham Ave., Syracuse 10, N. Y. (Electronics)

Joseph P. Stanavage, Radio Corp. of America; Mail add: 914 Landis Ave., Lancaster, Pa. (Electronics)

Alden Stevenson, Pacific Semiconductors Inc., 10451 W. Jefferson Blvd., Culver City, Calif. (Electronics)

Robert F. Sullivan, Electrolyser Corp., Ltd.; Mail add: 15 Botany Hill Rd., Scarborough, Ont., Canada (Industrial Electrolytic, Theoretical Electrochemistry)

Philip G. Thornhill, Falconbridge Nickel Mines Ltd., Falconbridge, Ont., Canada (Corrosion)

Stephen M. Toy, Westinghouse Atomic Power Div.; Mail add: 4750 Centre Ave., Pittsburgh 13, Pa. (Corrosion, Theoretical Electrochemistry)

J. Dale Turner, Hughes Products; Mail add: 1429 Midvale Ave., Los Angeles 24, Calif. (Electronics)

Joseph E. Varga, Texas Instruments Inc.; Mail add: 3738 Park Lane, Dallas 20, Texas (Electronics, Electrothermics and Metallurgy)

Marcel J. Vogel, I.B.M. Research Lab.; Mail add: 51 King St., Redwood City, Calif. (Electronics)

James H. Whitley, AMP Inc., Harrisburg, Pa. (Electric Insulation)

Robert P. Williams, Texas Instruments Inc.; Mail add: 9107 Lynbrook Dr., Dallas 18, Texas (Electronics)

Keith H. Wycoff, Plectron Corp.; Mail add: Rt. #1, Overton, Neb. (Battery, Electronics, Electro-Organic, Theoretical Electrochemistry)

Student Associate Members

Marvin L. Kronenberg, Western Reserve University; Mail add: 1576 Coventry, Cleveland 18, Ohio (Electrodeposition, Theoretical Electrochemistry)

Ramakrishnaiyer Raman, Dielectrics Lab., General Chemistry Dept., Indian Institute of Science, Bangalore 3, India (Theoretical Electrochemistry)

Transfer from Associate to Active Membership

Alkis C. Makrides, Metals Research Labs., Electro Metallurgical Co., P. O. Box 580, Niagara Falls, N. Y. (Corrosion, Theoretical Electrochemistry)

Deceased Members

D. J. Demorest, Columbus, Ohio

Louis J. Donroe, Newark, N. J.

R. W. Sanderson, Wembley, England

John A. Upper, Niagara Falls, Ont., Canada

By action of the Board of Directors of the Society, all prospective members must include first year's dues with their applications for membership.

Also, please note that, if sponsors sign the application form itself, processing can be expedited considerably.

Section News

Boston Section

At a meeting of the Executive Committee of the Boston Section on August 27, 1958, Richard A. Peak, Raytheon Manufacturing Co., 55 Chapel St., Newton 58, Mass., was appointed Secretary-Treasurer for the 1958-1959 year, replacing G. W. Waring.

R. A. Peak, *Secretary-Treasurer*

Cleveland Section

The officers of the Cleveland Section for 1958-1959 are:

Chairman—D. E. Kinney, General Electric Co., 1099 Ivanhoe Rd., Cleveland 12, Ohio

Vice-Chairman—M. E. Sibert, Horizons, Inc., 2891 E. 79th St., Cleveland 4, Ohio

Treasurer—F. A. Shirland, Harshaw Chemical Co., 1945 E. 97th St., Cleveland 6, Ohio

Secretary—R. A. Powers, National Carbon Research Labs., P. O. Box 6116, Cleveland 1, Ohio.

R. A. Powers, *Secretary*

Detroit Section

The following are the new officers of the Detroit Section for the 1958-1959 term:

Chairman—Sam Piken, 2632 Lari Court, Route 1, Orchard Lake, Mich.

1st Vice-Chairman—A. E. Remick, 14425 Archdale, Detroit, Mich.

2nd Vice-Chairman—Manuel Shaw, 19411 Winthrop, Detroit, Mich.

Secretary-Treasurer—S. E. Beacom, 38621 Jonathan Drive, Mt. Clemens, Mich.

Local Section Councilors—L. O. Case and Frank Passal.

Manuel Ben, *Past Chairman*

Personals

Paul S. Brallier, technical assistant to the president of Stauffer Chemical Co., retired on September 1 after almost 42 years of service with Stauffer and with Niagara Smelting Co., which became part of Stauffer Chemical in 1930. Mr. Brallier joined Niagara Smelting in 1916 after graduation from Pennsylvania State College with a B.S. degree in chemistry. He rose successively through positions as chemist, chief chemist, technical director, and plant manager at Niagara Falls. In 1950 he was transferred to New York City to be in charge of market development. He assumed his present position in 1955. Mr. Brallier resides at 90 W. Garden Rd., Larchmont, N. Y.

Samuel Korman, formerly of Phelps Dodge Corp., has been named consultant to the Vitro Labs. Div.

Notice to Members

By now you have received your official voting ballot from Society Headquarters. If you have not already done so, please return the ballot *by December 15* so that your vote can be included in the final election count.

and to U. S. Manganese Corp. Dr. Korman's assignments deal with metallurgical and other process developments in areas related to high-temperature processes. He has pioneered, with Dr. Charles Sheer, several high-intensity electric arc processes. Dr. Korman is also a consultant to Ford, Bacon & Davis, Inc. In this capacity he visited several mining and mill installations in Bolivia between 1956 and 1958. He has been consultant to the Davison Chemical Corp. and the U. S. Atomic Energy Commission, and is adjunct professor of metallurgical engineering at the Polytechnic Institute of Brooklyn.

George B. Adams, Jr., who had been with the Dept. of Chemistry, University of Oregon, has joined the Lockheed Aircraft Corp., Solid State Electronics Dept., Missile Systems Div., Sunnyvale, Calif.

Morris Feinleib is now associated with the Electrochemistry and Solid State Chemistry Section of Lockheed Missile Systems Div., Sunnyvale, Calif., as a research scientist. He had been with the Kaiser Aluminum & Chemical Corp. in Permanente, Calif.

Morris V. Boley has been transferred from the U. S. Mint in San Francisco to the office of the Director of the Mint in Washington, D. C.

John H. Zauner, of the Lane-Wells Co., a Div. of Dresser Industries, Inc., has transferred from Los Angeles to Houston, Texas. He is vice-president and technical director.

John Kronsbein, previously with Evansville College, Evansville, Ind., is now at the University of Florida, Dept. of Mechanical Engineering, Gainesville.

C. G. Grimes, who had been with the Electric Storage Battery Co. in Philadelphia, has transferred to the company's Research Center in Yardley, Pa.

News Items

1958 Tone Medal Awarded to Joseph H. Brennan

Joseph H. Brennan, chief metallurgist of the Electro Metallurgical Co., Div. of Union Carbide Corp., Niagara Falls, N. Y., has been named as recipient of the Frank J. Tone Medal Award. The Medal is awarded annually by the Niagara Frontier Section of the American Institute of Mining, Metallurgical, and Petroleum Engineers. The announcement was made by Loren W. Smith, Chairman of the Jury of Medal Award.

The Medal was established in 1956 by F. Jerome Tone and Franchot Tone to honor the memory of their father, Dr. Frank J. Tone, pioneer industrialist of the Niagara Frontier, and a Past President of The Electrochemical Society. It is awarded to a person who has made outstanding and important contributions to the science and practice of metallurgy. The recipient must be a resident of the Niagara Frontier community.

After two years with the U. S. Bureau of Mines, Mr. Brennan joined the Electro Metallurgical Co. in 1920. He has been connected with the ferroalloy industry during his entire career. He holds more than a dozen U. S. patents on the purification and production of metals and alloys and several times that number of foreign patents. One of his major contributions was the development of a process for the production of ferrochrome of very low carbon content. Other specific contributions have been the development of processes for the production of low-carbon ferromanganese and manganese metal, and for the elimination of phosphorus and arsenic in the smelting of manganese ores; procedures for the selective refining of silicon and ferrosilicon alloys with respect to calcium and aluminum; and an improved method for the silicothermic smelting of tungsten ores. Mr. Brennan is the co-inventor of a process for treating low-grade tungsten ores which was used for

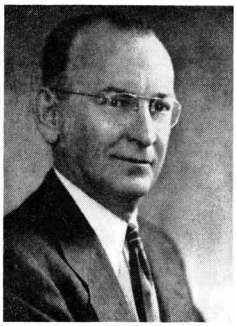

J. H. Brennan

the larger part of America's production during World War II. He collaborated on the design, construction, and operation of the cobalt refinery which supplied most of the United States cobalt requirements during the war years.

Mr. Brennan has served as a consultant to the National Research Council, the Manhattan Project, and the Atomic Energy Commission.

He is a Fellow of the Institute of Chemistry, past chairman of the Niagara Falls Section of The Electrochemical Society, and in 1950 was the recipient of the Schoellkopf Medal, awarded annually by the Western New York Section of the American Chemical Society. Mr. Brennan is also a member of the American Society for Metals, the American Association for the Advancement of Science, the Prospectors and Developers Association (Ontario), and the Society of the Chemical Industry (Britain).

The Tone Medal will be presented to Mr. Brennan at the annual award meeting which will be held in Niagara Falls on November 19. The presentation will be made by Loren W. Smith, chairman of the Niagara Frontier section of the sponsoring society.

"Technology of Columbium (Niobium)" Now Available

The Electrochemical Society is pleased to announce the availability of the latest volume in the ECS Series, sponsored by the Society, and published by John Wiley & Sons, Inc.

"Technology of Columbium (Niobium)," published August 1958, is a compilation which includes most of the papers presented at the Symposium on Columbium (Niobium) of the Electrothermics and Metallurgy Division of The Electrochemical Society in Washington, D. C., May 15 and 16, 1958. It provides vital information on niobium, discussed by 25 authorities active in the field of high-temperature technology.

The 120-page book, listed at $7.00, is available to ECS members at the 33 1/3% member discount. To obtain the discount, orders must be sent to Society Headquarters, 1860 Broadway, New York 23, N. Y. The Society will forward orders to Wiley who will ship the volume with the invoice. Nonmembers, including subscribers, should send their orders directly to John Wiley & Sons, Inc., 440 Fourth Ave., New York 16, N. Y.

New Sustaining Member

Grace Electronic Chemicals, Inc., Baltimore, Md., recently became a Sustaining Member of The Electrochemical Society.

Commerce Dept. Announces Services of New Foreign Technical Information Center

A Foreign Technical Information Center is now operating in the U. S. Dept. of Commerce to provide American science and industry with access to translations of a large amount of Soviet technical information. The Center is a part of the Office of Technical Services, Business and Defense Services Administration, with John C. Green as Director of OTS.

The services of the Foreign Technical Information Center include publication of abstracts of all articles appearing in 141 Soviet technical journals, translations of important sections of *Referativnvy Zhurnal* (the Russians' own abstract journal), and a semimonthly review of various areas of Soviet science compiled by the Central Intelligence Agency. Abstracts of each issue of the 141 journals may be purchased from OTS on a subscription or single issue basis, as may CIA's *Scientific Information Report*. The various sections of *Referativnvy Zhurnal* will be sold initially by single issues, but subscription sales may be offered later.

OTS will soon begin distributing complete translations of articles and books, Director Green said. Translations will be listed in an abstract journal, publication to have begun about September.

Much of the material collected by OTS will be from Government sources, principally the intelligence agencies. This volume is estimated to run at 50,000 abstracts and 10,000 complete translations a year. Eventually, material from other sources is expected to be added to the collection. This will provide a central point to which science and industry may look for comprehensive information on Soviet bloc developments.

Congress appropriated $510,000 for the operation of the foreign technical information program in fiscal 1959. Functions of the program are

1959 Bound Volume

Members and subscribers who wish to receive bound copies of Vol. 106 (for 1959) can receive the volume for the low, prepublication price of $6.00 if their orders are received at Society Headquarters, 1860 Broadway, New York 23, N. Y., *by December 1, 1958*. After that date, members will be charged $12.00, and nonmembers, including subscribers, $18.00.

Bound volumes are *not* offered independently of JOURNAL subscription.

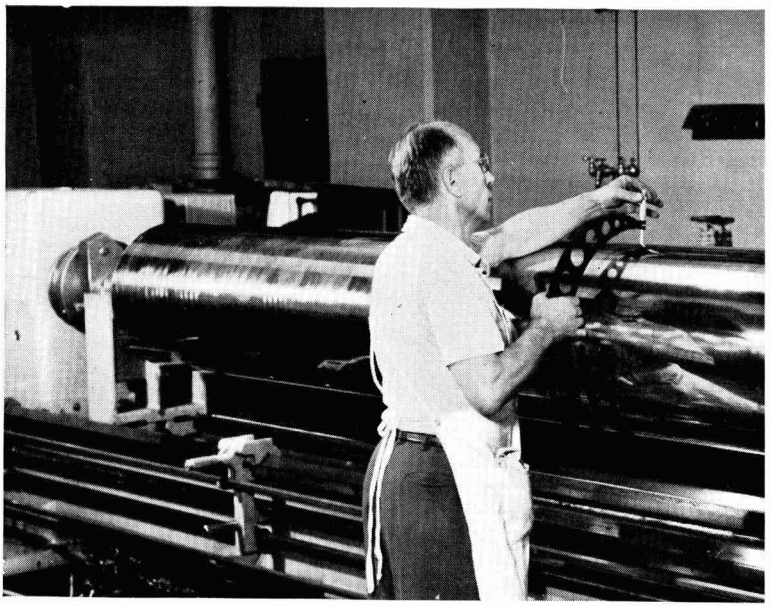

The 152-in.-long, 3-ton rotogravure cylinder above will be used to print patterns on vinyl-plastic floor coverings. National Gravure

New rotogravure plant plates rolls up to 152" long — keeps quality high, costs low with "Plus-4" Copper Anodes

The big new plant of National Gravure Cylinders, Inc., in Long Island City, N.Y., was designed to embody the most modern equipment, new and improved methods for the economic production of quality gravure cylinders.

In king-size acid-copper electroplating tanks, 152-in., 3-ton, rolls shown above get a dense, uniform shell of copper .030" thick. Other tanks produce cylinders in sizes more commonly used. All tanks have used "Plus-4" Phospho-

to collect, catalog, print, and sell abstracts and complete translations of foreign technical documents.

Publications of the Foreign Technical Information Center

General

PB 131891T, *Scientific Information Report.* Issued semimonthly, $28.00 a year, $2.75 single issue. A general review of current Soviet scientific developments compiled by the Central Intelligence Agency.

Abstract Journals

Referativnvy Zhurnal (Russian abstract journal). Translated sections of the biology, chemistry, and physics series are available. Write to OTS for monthly price list.

Abstracts of Soviet Technical Periodicals

All articles in each issue of 141 publications are abstracted in English on abstract cards. Abstract cards may be purchased on a subscription basis at the prices indicated. Abstracts of a single issue of any publication are 50 cents per set.

"Analytical Abstracts"

Analytical Abstracts, a monthly publication of The Society for Analytical Chemistry which was first published in January 1954 on the cessation of publication of *British Abstracts C, Analysis and Apparatus,* covers the analytical literature of the world.

It contains upwards of 4000 abstracts per year prepared by abstractors who are experts in particular fields of analytical chemistry. Many abstracts are prepared by chemists in the countries of publication of the original papers. Analysts will appreciate the advantage of having all abstracts dealing with their subject in a single publication.

Analytical Abstracts can be obtained from January 1, 1959 for $14.00 per year, postage-free, including index. Some earlier volumes are still available. The subscription rate including *The Analyst* is $23.52 per year, postage-free, including both indexes.

Analytical Abstracts is also available printed on one side of the paper, so that abstracts can easily be incorporated into existing reference systems. Price per year without index, $15.05; with index, $18.48.

Subscriptions should be sent directly to the Secretary, The Society for Analytical Chemistry, 14 Belgrave Square, London, S.W.1., England.

Stokes Offers Laboratory Facilities for Vacuum Metallurgy Research Projects

Companies who want to carry out limited-scale research projects in vacuum metallurgy which require the melting of small quantities of material for experimental evaluation of new products or developing new processing and fabricating techniques—but whose own facilities may be temporarily overloaded or who do not wish to make the capital outlay for the necessary equipment —will welcome the announcement by F. J. Stokes Corp., 5500 Tabor Rd., Philadelphia, that the facilities of its vacuum metallurgy laboratory are now available for use by outside firms at nominal cost.

A. D. Garwood, manager of Stokes' vacuum furnace department, is in charge of the laboratory facilities and all inquiries about the new custom-research service should be addressed to him.

International Corporation to Develop Bauxite Deposits and Produce Alumina

A new international corporation to develop vast bauxite deposits in French Guinea (French West Africa) and to produce alumina there was announced recently in the United States by Olin Mathieson Chemical Corp.

Known as FRIA Compagnie Internationale pour la Production de l'Alumine, the new corporation involves: 1. An estimated total cost of $135,000,000; 2. Participation by five corporations from four nations of the free world; 3. Plans to build the world's largest alumina plant in

(Continued on page 239C)

Russian Scientific Journals Available in English

Approximately 60,000 pages a year of key Soviet scientific and technical journals are now available in English translation to United States scientists and engineers, the National Science Foundation announced recently. In releasing a compilation of translated Russian journals, the Foundation indicated that there are now in print 53 English editions of Russian journals, 4 extensive series of translated Russian abstracts of scientific papers, and 4 series of partial translations of important Russian journals.

Support of these translations is provided by Government agencies—the National Science Foundation, the National Institutes of Health, the Office of Naval Research, and the Atomic Energy Commission (the latter two working through the National Science Foundation)—and by six commercial translating and publishing firms working without Government funds.

The National Science Foundation has maintained a foreign science information program since early 1952; its first Russian-to-English translation program was initiated in June of that year. The number of translated journals supported by the Foundation has now reached 31, with most of the major fields of science being served.

Foundation-supported translation projects, continually increasing in number, are conducted by U. S. professional scientific societies and university groups which have chosen the Russian material to be translated and which have requested the financial support of the Foundation. These organizations administer their own projects and provide expert consultation to translators to help insure accuracy. The translations are sold on a subscription basis with the resulting income used to defray part of the costs of the projects, thus reducing the need for Government support.

The following compilation by the Office of Scientific Information, National Science Foundation, includes a list of those translated journals of especial interest to electrochemists, information on the source of financial support, if any, and the names and addresses of publishers as well as annual subscription prices.

National Science Foundation Projects

Title	Institution receiving grant or contract[a]	Subscription price per year
The Physics of Metals and Metallography (Fizika Metallov i Metallovedenie), bimonthly	Acta Metallurgica, Dr. J. H. Hollomon, Sec.-Treas., P. O. Box 1088, Schenectady, N. Y. (Order from Mr. D. J. Raymond, Pergamon Institute, 122 E. 55th St., New York 22, N. Y.)	$30.00
The Journal of Abstracts—Metallurgy (Referativnyi Zhurnal—Metallurgiia), monthly	"	$20.00
Journal of Technical Physics (Zhurnal Teknicheskoi Fiziki), monthly	American Institute of Physics, 335 E. 45th St., New York 17, N. Y.	$75.00 $35.00[b]
Proceedings of the USSR Academy of Sciences (Doklady Akademii Nauk SSSR), bimonthly physics sections	"	$35.00 $15.00[b]
Journal of Experimental and Theoretical Physics (Zhurnal Eksperimentalnoi i Teoreticheskoi), monthly	"	$60.00[c] $75.00[d]
[Translation journal known as *Soviet Physics—JETP*]		$35.00[b]
Crystallography (Kristallografiia), bimonthly	"	$25.00 $10.00[b]
Journal of General Chemistry of the USSR (Zhurnal Obshchei Khimii), monthly	Consultants Bureau, Inc., 227 W. 17th St., New York 11, N. Y.	$90.00 $30.00[b]
Journal of Applied Chemistry (Zhurnal Prikladnoi Khimii), monthly	"	$60.00 $20.00[b]
Bulletin of the Academy of Sciences of the USSR, Division of Chemical Science (Izvestiia Akademii Nauk SSSR—Otdelenie Khimicheskikh Nauk), monthly	"	$45.00 $15.00[b]
Instruments and Experimental Techniques (Pribory i Teknika Eksperimenta), bimonthly	Instrument Society of America, 313 Sixth Ave., Pittsburgh 22, Pa.	$25.00 $12.50[b]
Measurement Techniques (Ismeritel'naya Tekhnika), bimonthly	"	$25.00 $12.50[b]
Automation and Remote Control (Avtomatika i Telemekanika) monthly	Mass. Institute of Technology, Professor W. N. Locke, Director of Libraries, Cambridge 30, Mass. (Order from Instrument Society of America, 313 Sixth Ave., Pittsburgh 22, Pa.)	$30.00 $15.00[b]

Commercial Translation Agencies

Title	Where to order	Subscription price per year
Metal Science and Treatment (Metallovedenie i Obrabotka Metallov), monthly	Henry Brutcher, Technical Translations, P. O. Box 157, Altadena, Calif.	—
Bulletin of the Academy of Sciences, USSR: Physics Series (Izvestiia Akademii Nauk SSSR: Seriia Fiziki), monthly	Columbia Technical Translations, 5 Vermont Ave., White Plains, N. Y.	$215.00

Commercial Translation Agencies (Cont'd)

Title	Where to order	Subscription price per year
Atomic Energy (Atomnaia Energiia), monthly	Consultants Bureau, Inc., 227 W. 17th St., New York 11, N. Y.	$75.00
Journal of General Chemistry of the USSR[g] (Zhurnal Obshchei Khimii), monthly	"	$90.00 $30.00[b]
Journal of Analytical Chemistry (Zhurnal Analiticheskoi Khimii), bimonthly	"	$80.00
Bulletin of the Academy of Sciences of the USSR, Division of Chemical Science[g] (Izvestiia Akademii Nauk SSSR—Otdelenie Khimicheskikh Nauk), monthly	"	$45.00 $15.00[b]
Journal of Applied Chemistry[g] (Zhurnal Prikladnoi Khimii), monthly	"	$60.00 $20.00[b]
Proceedings of the Academy of Sciences of the USSR (Doklady Akademii Nauk SSSR)		
Chemistry Section (Otdel Khimii), bimonthly	"	$95.00[h]
Chemical Technology Section (Otdel Khimicheskaia Tekhnologiia), bimonthly	"	$15.00[h]
Physical Chemistry Section (Otdel Fizicheskoi Khimii), bimonthly	"	$160.00
Applied Physics Section (Otdel Prikladnoi Fiziki), bimonthly	"	$200.00
Metallurgist (Metallurg), monthly	"	$95.00
Atomic Energy (Selected Papers) (Atomnaia Energiia), incorporated in *British Journal of Nuclear Energy*, 3 vol./yr	Pergamon Press, Ltd., 122 E. 55th St., New York 22 N. Y., or Pergamon Press, Ltd., 4 & 5 Fitzroy Square, London, W. 1, England	$9.80/vol. $20.00/vol.

[a] Publications are generally available from the institution receiving the grant or contract. However, distribution is sometimes made by a company which is listed in parentheses following this institution.
[b] Price per year to libraries of educational institutions.
[c] Renewal price.
[d] New subscription price.
[e] Price per year to libraries.
[f] Price to be announced in late 1958.
[g] Sponsored by National Science Foundation.
[h] These four sections of the Proceedings are available as a unit for $125.00 per year.

News Items

(Continued from page 237C)

French Guinea; 4. Development of one of the world's largest known bauxite deposits.

Representing one of the largest international efforts for the development of a metals raw material in an underdeveloped industrial area, the FRIA group consists of Olin Mathieson Chemical Corp.; two French companies, Pechiney Compagnie de Produits Chimiques et Electrometallurgiques and Societe d'Electrochimie, d'Electrometallurgie et des Acieries Electriques d'Ugine; Aluminum Industrie Aktiengesellschaft of Zurich, Switzerland; and The British Aluminium Company Ltd.

Television Color Standards

Brightness standards for color television tubes have been made available by the National Bureau of Standards in cooperation with the Joint Electron Tube Engineering Council of the Radio-Electronics-Television Manufacturers Association. Each set consists of three standards—red, green, and blue—closely matching in spectral energy the three phosphors which in the tube act together to produce various colors in the image. The standards are used to calibrate instruments for measuring the color and brightness of the phosphors. They thus provide a simple, accurate means for achieving uniform color reproduction in television tubes.

Sets of the standards are available from the Photometry and Colorimetry Section, National Bureau of Standards, Washington 25, D. C., at $250.00 a set. To facilitate the use of these standards, a detailed report of their design and calibration is included with each set.

Announcements from Publishers

"Spectrochemical Analysis for Trace Elements—STP 221." Published by American Society for Testing Materials, 1916 Race St., Philadelphia 3, Pa., 1958. Price $2.75.

This volume contains extensive references and late discussions of papers presented at a symposium held at the Annual Meeting of the ASTM in 1957.

"The Properties of Gases and Liquids," Their Estimation and Correlation, by Robert C. Reid and Thomas K. Sherwood. Published by McGraw-Hill Book Co., New York, 1958. 386 pages; $10.00.

This new addition to the McGraw-Hill Series in Chemical Engineering completely covers the literature to 1956 and includes many new articles published in 1956 and 1957.

"The Historical Background of Chemistry," by Henry M. Leicester. Published by John Wiley & Sons, Inc., New York, 1956. 260 pages; $6.00.

This book traces the development of chemistry and the effects and interrelationships of chemical concepts —the thoughts and ideas of chemists—from their first appearance in the ancient world to the present day. The author has also indicated some of the areas in which chemistry has had an influence on world history,

and other areas in which the conditions of the world have influenced the chemist himself. All phases of the subject—electrochemistry, organic and inorganic chemistry, and biochemistry—are treated as they appear on the historical scene.

"Manual of Analytical Methods: Volume II, Part I—Analysis of Refined Materials and By-Products." AEC report A-2912,* Jan. 1946. 154 pages; 85 cents.

"Phosphating Treatments — Patent Literature Survey," E. C. Tinsley, Rock Island Arsenal Lab., U. S. Army Ordnance Corps, April 1957. Report PB 131356,* 148 pages; $3.75.

"Development of Electroplating Processes to Eliminate Hydrogen Embrittlement in High-Strength Steel," J. E. Chilton, Stanford Research Institute, for Wright Air Development Center, U. S. Air Force, Jan. 1958. Report PB 131721,* 84 pages; $2.25.

This report describes the properties of the electrodeposition of cadmium on a high-strength, aircraft quality steel. Properties data were drawn from an attempt to plate cadmium on steel without hydrogen embrittlement. The static sustained load beam test was used for evaluation of the effects of hydrogen embrittlement caused by plating cadmium on SAE 4340 steel from different baths and by different techniques.

"Solubility of Water in Molten Alkali Chlorides," July 1957. AEC Report ISC-929,* 45 pages; $1.50.

"Corrosion Preventive Additives," Armour Research Foundation, for Wright Air Development Center, U. S. Air Force, March 1952. Report PB 131459,* 120 pages; $3.00.

This is a final report of a year (1951-1952) of Air Force-sponsored research aimed at development of new corrosion inhibitors to supplement or replace petroleum sulfonates as lubricant additives. At the outset of the project, a study was made of petroleum sulfonates to determine the nature of the compounds showing corrosion inhibition. Separation of a commercial sodium petroleum sulfonate and fractionation of the

* Order from Office of Technical Services, U. S. Dept. of Commerce, Washington 25, D. C.

sulfonates showed the sulfonates to be alkyl benzene derivatives with the alkyl group in the para position to the sulfonic acid group. A large number of commercially available organic compounds were evaluated by the Static Water Drop Test and a galvanic couple system. Several good inhibitors were found, and general information was obtained concerning the type of organic compounds which will inhibit galvanic corrosion. The research produced many synthetic organic compounds showing corrosion inhibiting properties. Among these were glyoxalidines, alkyl aryl sodium sulfonates, amine salts of 2-ethylhexoic, oleic, nicotinic, pelargonic, linoleic, and dodecylbenzenesulfonic acids.

Employment Situations

Positions Available

Engineers (Aeronautical, Electrical, Electronic, Industrial, General, Mechanical, and Power Plant), **Electronic Scientists, Metallurgists, Physicists, Technologists**—Vacancies exist for professional personnel in the above positions. Starting salaries range from $4490 to $10,130 per annum. The Naval Air Material Center is currently engaged in an extensive program of aeronautical research, development, experimentation, and test operations for the advancement of Naval aviation. Experimental work is also being conducted in the guided missile field. Personnel are needed for work on projects involving modification, overhauling, and testing of aeronautical equipment, materials, accessories, power plants, launching and arresting devices, and for modification and structural testing of aircraft. Also, for work involving the basic design of catapults, launchers, arresting gear and their component parts; test and development work at shore stations and on board U. S. Navy ships; evaluation of new equipment and establishment of performance parameters, and applied research on the many problems relevant to this field.

Interested persons should file an Application for Federal Employment, Standard Form 57, with the Industrial Relations Dept., Naval Air Material Center, Naval Base, Philadelphia 12, Pa. Applications may be obtained from the above address or information as to where they are available may be obtained from any first or second class post office.

Advertiser's Index

Position Wanted

Please address replies to box shown, c/o The Electrochemical Society, Inc., 1860 Broadway, New York 23, N. Y.

Physical Chemist, Ph.D. 1958, desires research position in electrochemistry and/or solid state. Strong instrumentation background; research experience; publications; honor societies. Will consider position in New York City or Metropolitan New Jersey area only. *Reply to Box 365.*

The Electrochemical Society

INSTRUCTIONS TO AUTHORS OF PAPERS

Address all correspondence to the Editor, JOURNAL OF THE ELECTROCHEMICAL SOCIETY, 1860 BROADWAY, NEW YORK 23, N. Y.

FORM

Manuscripts submitted for publication should be in triplicate to expedite review. They should be typewritten, double-spaced, with 2½-4 cm (1-1½ in.) margins.

Title should be brief, followed by the author's name and his business or university connection.

Abstract of about 100 words should state the scope of the paper and give a brief summary of results.

ILLUSTRATIONS

Drawings will be reduced to column width, 8.3 cm (3¼ in.), after reduction should have lettering at least 0.15 cm (1/16 in.) high. Original drawings in India ink on tracing cloth or white paper are preferred. Curves may be drawn on coordinate paper only if the paper is ruled in blue. All lettering must be of lettering-guide quality. See sample drawing on reverse page.

Photographs must be glossy prints and mounted flat.

Captions for all figures must be included on a separate sheet. Captions and figure numbers should not appear in the body of the figure.

General—Figures should be used only when necessary. Omit drawings or photographs of familiar equipment. Figures from other publications are to be used only when the publication is not readily available, and should always be accompanied with written permission for reprinting.

SYMBOLS

If more than a few symbols are used, these should be defined in a list at the end of the paper, for example:

$a, b \ldots$ = empirical constants of Brown equation
f_i° = fugacity of pure ith component, atm
D_v = bulk diffusion coefficient, cm²/sec

REFERENCES

Literature and patent references should be listed at the end of the paper on a separate sheet, in the order in which they are cited. They should be given in the style adopted by *Chemical Abstracts*. For example:

R. Freas, *Trans. Electrochem. Soc.*, **40**, 109 (1921).

H. T. S. Britton, "Hydrogen Ions," Vol **1**, p. 309, D. Van Nostrand Co., New York (1943).

H. F. Weiss (To Wood Conversion Co.), U. S. Pat. 1,695,445, Dec. 18, 1928.

UNITS OF MEASUREMENT

Metric units should be used throughout but, where desirable, English units may be given in parentheses.

Corrosion rates in the metric system should preferably be expressed as milligrams per square decimeter per day (mdd), and in the English system as inches penetration per year (ipy).

In reporting electrode potentials, the sign of the standard Zn/Zn^{++} electrode potential should be taken as negative; Cu/Cu^{++} as positive.

ABBREVIATIONS

Abbreviations should conform with the American Standards Association's list of "Abbreviations for Scientific and Engineering Terms."

GENERAL

Authors should be as brief as is consistent with clarity, and must omit all material which can be regarded as familiar to specialists in the particular field.

The use of proprietary names, trade-marks, and trade names should be avoided if possible. If used, these should be capitalized so that the owner's legal rights are not jeopardized.

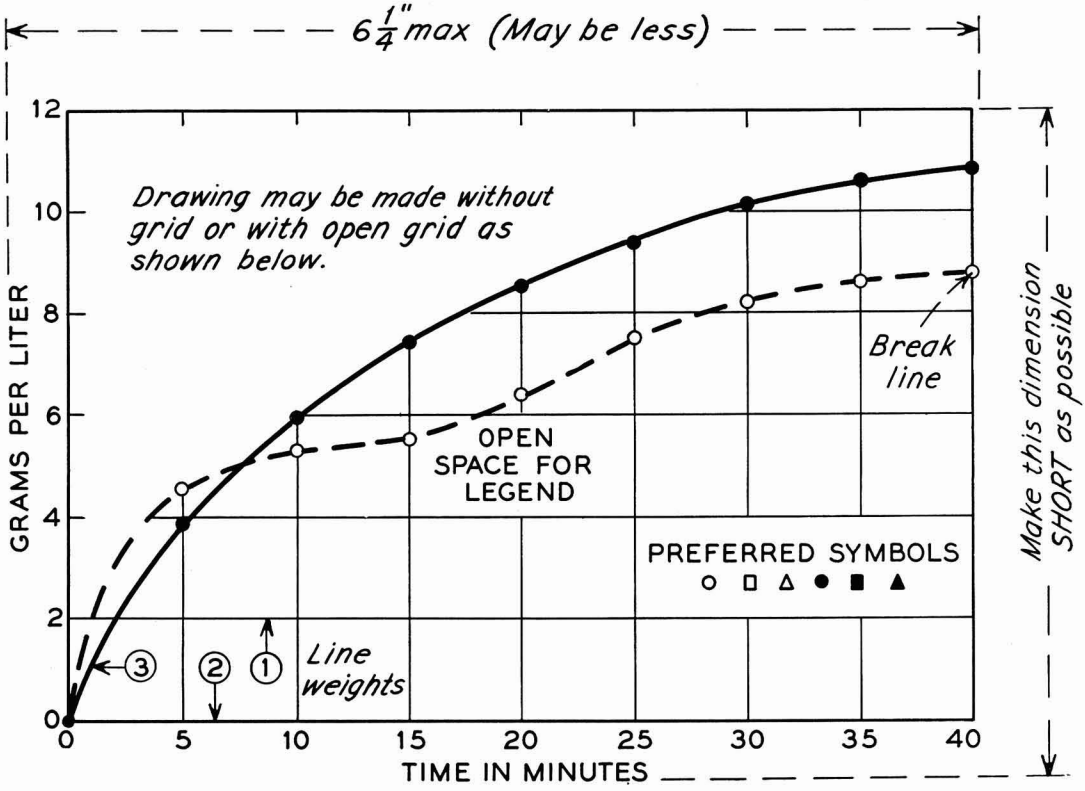

Remarks: Line weight 2 is used for borders and zero lines. When several curves are shown, each may be numbered and described in the caption. Lettering shown is approximately ⅛ in. In plotting current or potential as ordinate, increasing negative values should go down.

SAMPLE CURVE DRAWING FOR REDUCTION TO $\frac{1}{2}$ SIZE

The Electrochemical Society

Patron Members

Aluminum Company of Canada, Ltd., Montreal, Que., Canada
International Nickel Company, Inc., New York, N. Y.
Olin Mathieson Chemical Corporation, Niagara Falls, N. Y.
Industrial Chemicals Division, Research and Development Department
Union Carbide Corporation
Divisions:
Electro Metallurgical Company, New York, N. Y.
National Carbon Company, New York, N. Y.
Westinghouse Electric Corporation, Pittsburgh, Pa.

Sustaining Members

Air Reduction Company, Inc., New York, N. Y.
Ajax Electro Metallurgical Corporation, Philadelphia, Pa.
Allied Chemical & Dye Corporation
General Chemical Division, Morristown, N. J.
Solvay Process Division, Syracuse, N. Y. (3 memberships)
Alloy Steel Products Company, Inc., Linden, N. J.
Aluminum Company of America, New Kensington, Pa.
American Machine & Foundry Company, Raleigh, N. C.
American Metal Company, Ltd., New York, N. Y.
American Platinum Works, Newark, N. J. (2 memberships)
American Potash & Chemical Corporation, Los Angeles, Calif. (2 memberships)
American Zinc Company of Illinois, East St. Louis, Ill.
American Zinc, Lead & Smelting Company, St. Louis, Mo.
American Zinc Oxide Company, Columbus, Ohio
M. Ames Chemical Works, Inc., Glens Falls, N. Y.
Auto City Plating Company Foundation, Detroit, Mich.
Bart Manufacturing Company, Bellville, N. J.
Bell Telephone Laboratories, Inc., New York, N. Y. (2 memberships)
Bethlehem Steel Company, Bethlehem, Pa. (2 memberships)
Boeing Airplane Company, Seattle, Wash.
Burgess Battery Company, Freeport, Ill. (4 memberships)
C & D Batteries, Inc., Conshohocken, Pa.
Canadian Industries Ltd., Montreal, Que., Canada
Carborundum Company, Niagara Falls, N. Y.
Catalyst Research Corporation, Baltimore, Md.
Chrysler Corporation, Detroit, Mich.
Ciba Pharmaceutical Products, Inc., Summit, N. J.
Columbian Carbon Company, New York, N. Y.
Columbia-Southern Chemical Corporation, Pittsburgh, Pa.
Consolidated Mining & Smelting Company of Canada, Ltd., Trail, B. C., Canada (2 memberships)
Continental Can Company, Inc., Chicago, Ill.
Cooper Metallurgical Associates, Cleveland, Ohio
Corning Glass Works, Corning, N. Y.
Crane Company, Chicago, Ill.
Diamond Alkali Company, Painesville, Ohio (2 memberships)
Dow Chemical Company, Midland, Mich.
Wilbur B. Driver Company, Newark, N. J. (2 memberships)
E. I. du Pont de Nemours & Company, Inc., Wilmington, Del.
Eagle-Picher Company, Chemical Division, Joplin, Mo.
Eastman Kodak Company, Rochester, N. Y.
Electric Auto-Lite Company, Toledo, Ohio
Electric Storage Battery Company, Philadelphia, Pa.
The Eppley Laboratory, Inc., Newport, R. I. (2 memberships)
Federal Telecommunication Laboratories, Nutley, N. J.
Food Machinery & Chemical Corporation
Becco Chemical Division, Buffalo, N. Y.
Westvaco Chlor-Alkali Division, South Charleston, W. Va.
Ford Motor Company, Dearborn, Mich.
General Electric Company, Schenectady, N. Y.
Chemistry & Chemical Engineering Component, General Engineering Laboratory
Chemistry Research Department

(Sustaining Members cont'd)

General Electric Company (cont'd)
Metallurgy & Ceramics Research Department
General Motors Corporation
Brown-Lipe-Chapin Division, Syracuse, N. Y. (2 memberships)
Guide Lamp Division, Anderson, Ind.
Research Laboratories Division, Detroit, Mich.
Gillette Safety Razor Company, Boston, Mass.
Gould-National Batteries, Inc., Depew, N. Y.
Grace Electronic Chemicals, Inc., Baltimore, Md.
Great Lakes Carbon Corporation, New York, N. Y.
Hanson-Van Winkle-Munning Company, Matawan, N. J. (3 memberships)
Harshaw Chemical Company, Cleveland, Ohio (2 memberships)
Hercules Powder Company, Wilmington, Del.
Hooker Electrochemical Company, Niagara Falls, N. Y. (3 memberships)
Houdaille-Hershey Corporation, Detroit, Mich.
Hughes Aircraft Company, Culver City, Calif.
International Business Machines Corporation, Poughkeepsie, N. Y.
International Minerals & Chemical Corporation, Chicago, Ill.
Jones & Laughlin Steel Corporation, Pittsburgh, Pa.
K. W. Battery Company, Skokie, Ill.
Kaiser Aluminum & Chemical Corporation
Chemical Research Department, Permanente, Calif.
Division of Metallurgical Research, Spokane, Wash.
Keokuk Electro-Metals Company, Keokuk, Iowa
Libbey-Owens-Ford Glass Company, Toledo, Ohio
P. R. Mallory & Company, Indianapolis, Ind.
McGean Chemical Company, Cleveland, Ohio
Merck & Company, Inc., Rahway, N. J.
Metal & Thermit Corporation, Detroit, Mich.
Minnesota Mining & Manufacturing Company, St. Paul, Minn.
Monsanto Chemical Company, St. Louis, Mo.
Motorola, Inc., Chicago, Ill.
National Cash Register Company, Dayton, Ohio
National Lead Company, New York, N. Y.
National Research Corporation, Cambridge, Mass.
Norton Company, Worcester, Mass.
Olin Mathieson Chemical Corporation, Niagara Falls, N. Y.
High Energy Fuels Organization (2 memberships)
Pennsalt Chemicals Corporation, Philadelphia, Pa.
Philips Laboratories, Inc., Irvington-on-Hudson, N. Y.
Pittsburgh Metallurgical Company, Inc., Niagara Falls, N. Y.
Poor & Company, Promat Division, Waukegan, Ill.
Potash Company of America, Carlsbad, N. Mex.
Radio Corporation of America, Harrison, N. J.
Ray-O-Vac Company, Madison, Wis.
Raytheon Manufacturing Company, Waltham, Mass.
Reynolds Metals Company, Richmond, Va. (2 memberships)
Schering Foundation, Inc., Bloomfield, N. J.
Shawinigan Chemicals Ltd., Montreal, Que., Canada
Speer Carbon Company
International Graphite & Electrode Division, St. Marys, Pa. (2 memberships)
Sprague Electric Company, North Adams, Mass.
Stackpole Carbon Company, St. Marys, Pa. (2 memberships)
Stauffer Chemical Company, Henderson, Nev., and New York, N. Y. (2 memberships)
Sumner Chemical Company, Division of Miles Laboratories, Inc., Elkhart, Ind.
Superior Tube Company, Norristown, Pa.
Sylvania Electric Products Inc., Bayside, N. Y. (2 memberships)
Sarkes Tarzian, Inc., Bloomington, Ind.
Tennessee Products & Chemical Corporation, Nashville, Tenn.
Texas Instruments, Inc., Dallas, Texas
Titanium Metals Corporation of America, Henderson, Nev.
Udylite Corporation, Detroit, Mich. (4 memberships)
Upjohn Company, Kalamazoo, Mich.
Victor Chemical Works, Chicago, Ill.
Wagner Brothers, Inc., Detroit, Mich.
Weirton Steel Company, Weirton, W. Va.
Western Electric Company, Inc., Chicago, Ill.
Wyandotte Chemicals Corporation, Wyandotte, Mich.
Yardney Electric Corporation, New York, N. Y.

How to make metal blackening an exact science: What metal do you have to blacken? Steel, copper, brass, zinc? There are seven Ebonol® compounds in Enthone's specially developed series of blackeners for you to call on for jet blackness, maximum wear resistance and adhesion. Enthone is exceptionally well equipped and qualified to assist you in all phases of metal finishing. Years of practical experience, extensive research and service laboratory facilities manned by a team of specialists in the finishing field are at your service. Write us about your needs or problems. Send a sample of your product in question, if possible. Enthone, Inc., 442 Elm St., New Haven 11, Conn.

ENTHONE

ENTHONE, INC. IS A SUBSIDIARY OF AMERICAN SMELTING AND REFINING COMPANY